Quantification of short term interactions between soil and fungi.

A thesis submitted in partial fulfilment of the requirements of the University of Abertay Dundee for the degree of Doctor of Philosophy

by

Radoslaw Pajor

University of Abertay Dundee

School of Contemporary Sciences

March 2012

I certify that this thesis is the true and accurate version of the thesis approved by examiners.

Signed…… …. Date……
(Director of Studies)

Declaration

I hereby declare that this thesis has been composed by myself and that it was not accepted in any previous applications for the degree. The work, of which it is a record, is my own unless otherwise stated. All verbatims have been distinguished by quotation marks and sources of information specifically acknowledged by means of references.

Radoslaw Pajor

Acknowledgments

Even if I would write a separate chapter I would not be able to acknowledge all the help and support I received during my PhD.

First I would like express my sincere thanks to University of Abertay Dundee, for providing the funding for my study.

I would like to thank my supervisory team: Professor Wilfred Otten, Drs Ruth Falconer and Dmitri/y Grinev, for the guidance and motivation for my work. Especially I would like to acknowledge Professor Wilfred Otten for looking after my development throughout the whole period of my study.

I would also like to thank the SIMBIOS team, people from Urban Water Centre, STAiR, SAGES Graduate School and all my friends for creating a great atmosphere and making my time in Dundee unforgettable.

Finally I would like to thank my parents and my wife, Anna, for the unconditional love, trust and support.

Abstract

This thesis evaluates protocols to visualise and quantify short-term interactions between soil-borne fungi and soil. The quantification captures interactions between the ubiquitous soil saprotroph and plant pathogen *Rhizoctonia solani*, and a sandy loam soil, over a period of five days. The literature review provides evidence of mutual interactions between soil and fungi and highlights the lack of understanding about processes occurring at short time scales, which are crucial for modelling the complexity of soil environment.

The first part of the thesis merges X-ray microtomography, image analysis and laboratory measurements to investigate the impact of short term incubation of fungi on soil water retention and soil structure at macro (whole microcosm) and micro (individual aggregate) scales. Part Two quantifies the effect of experimental variables such as aggregate-size and soil bulk-density on key descriptors of the soil pore network. Finally, a fungal growth model was used to quantify to what extent soil structure mediated by bulk-density affected fungal growth dynamics.

The experimental work showed that despite high fungal biomass content there was no effect of fungal colonisation on soil structure and hydraulic properties after short-term incubation. However, it was possible to alter the geometry of soil pore space and thus influence fungal growth dynamics. This was achieved by manipulating the initial conditions of re-packed soil microcosms through variation of aggregate size and bulk density.

Table of Contents

Table of Figures

Table of Tables

CHAPTER 1

INTRODUCTION

1.1. SOIL CHARACTERISTICS

Soil is a natural material covering the outer surface of Earth, and plays a crucial yet underestimated role in sustaining life on the planet. It provides a wide range of services including water supply, food and fiber production, carbon storage and many others valued for over $33T per year (Costanza *et al.* 1997). However due to intensive exploitation and pollution of this ecosystem the top layer of soil is disappearing at a rate of 1 % percent of volume per year (Baveye *et al.* 2011). This alarming situation has resulted in more research focusing on improving strategies of land management by deepening our understanding of soil ecosystems and linking processes occurring at micro-scale to field conditions.

Soil, the top layer of lithosphere which evolved over time as an outcome of interacting physical, chemical and biological processes which influence decomposition and alteration of rock materials. Soil consists of three phases: a solid phase (comprising mineral, organic and clay), gas and liquid (Koorevaar *et al.* 1983). The solid phase in most cases is in majority and creates a skeleton or soil structure which constrains the other phases. The structure of the solid phase of soil can be described in terms of hierarchy of its structural elements (Dexter 1988). A widely accepted concept is based on aggregate hierarchy developed by Tisdall and Oades (1982). The process of aggregate formation, known as aggregation starts from free primary mineral particles, clay platelets (1-2 µm), which, when aligned, create flexible stacks (quasi-crystals), rigid platy particles (domains) or blocky particles (assemblage). 2-20 µm sized clusters of these particles combined together by a range of physical and biological forces form microaggregates (20-250 µm) (Dexter 1988). Macroaggregates sized >250 µm are formed by microaggregates bound together physically by fungal hyphae or chemically bound with the products of decomposition of organic matter (Bossuyt *et al.* 2001).

The level of compaction of such aggregates determines the bulk density and this is influenced by tillage operations. Osunbitan *et al.* (2005) observed a decrease in bulk density during tillage and an increase of bulk density with increasing time from period of tillage. Bulk density (ρ_b) of soil samples is expressed as mass of soil per volume:

$$\rho_b = M/V \quad [1.1]$$

Where:

M = the mass of a sample (kg)

V = the volume of the sample (m^3)

The bulk density of the whole sample should not to be confused with the particle density (γ_s), which is expressed as the mass of a given phase divided by its volume:

$$\gamma_s = M_s / V_s \quad [1.2]$$

Compaction of material has an impact on the structure of the pore space. With increasing density there is a decline of porosity and pore size (Harris *et al.* 2003, Pajor *et al.* 2010). Porosity (ε) is defined as the volume of pores per volume sample.

$$\varepsilon = V_{pores} / V_{sample} \quad [1.3]$$

If the bulk density of sample and particle density are known, then the porosity can be calculated according:

$$\varepsilon = 1 - (\rho_b / \gamma_s) \quad [1.4]$$

Where:

ρ_b = bulk density of sample (g/cm^3),

γ_s = soil particle density (g/cm^3).

The porosity is commonly expressed as a percentage or decimal fraction. Since the presence of the other phases (liquid and gas) is limited to the porespace, porosity can be expressed as the sum of volumes of these phases.

$$V_{pores} = V_{gas} + V_{liquid} \quad [1.5]$$

For soil biological and transport processes it is not only the total volume of pores that is significant but their three-dimensional geometry. It is crucial how the pores are connected, as this will dictate preferential pathways for spread of microorganisms, flow of water and gas. There are two common concepts of connectivity of the pore networks. Perret (1999) defined the connectivity as the number of independent pathways between the two surfaces. Such defined connectivity is subjective to the size of the analysed sample and void diameter. Considering the soil packed with the same porosity values, connectivity will increase with a decline in the sample size and pore size (Luo *et al.* 2010a). Another approach to define the connectivity is expressing it as a fraction of pores that are connected into the largest cluster (Vogel 1997). This approach does not restrict the analysis only to the surface connected voids however it is related to the pore size distribution.

Pore size distribution describes the fraction of pores according to the pore diameters. The size of pores defines the maximum size of organisms which can explore a given space and can influence the water conductivity and gas diffusion (Holtham *et al.* 2007). However pore size distribution does not provide the information of the spatial distribution and the tortuosity of the pore networks.

Both structural descriptors, the connectivity and pore size distribution will influence the tortuosity of the pore networks. Tortuosity is a measure of spatial organization of pore networks. It was defined as the true length between two point in the void (geodesic length) and the shortest, straight line connecting those two points known as Euclidean distance (Armatas 2006, Prado *et al.* 2009).

The combination of the structural descriptors such as porosity, pore connectivity, pore size distribution and tortuosity defined above, will be hereafter referred to as pore network geometry.

The gaseous phase of soil is a mixture of gases including oxygen, nitrogen, carbon dioxide and water vapour. The composition of the gaseous phase diffuses through the structure of soil and controls biological activity, degradation of organic matter and soil aeration processes. The liquid phase, which is also crucial for biological activity in soil contains dissolved compounds including microelements such as Na^+, K^+, Ca^{2+}, Mg^{2+}, Cl^-, NO_3^-, SO_4^{2-}; soluble organic compounds (including microbial derived ones) and dissolved gases. Water in soil may occur as a thin water film surrounding soil particles or a residue present in contact points between soil particles at unsaturated condition or fill pores completely at the point of saturation (Koorevaar *et al.* 1983, Or *et al.* 2007). The amount of water present in a soil is therefore a critical characteristic. The volumetric water content of a soil (θ) is defined as ratio of the volume of the liquid phase and the volume of the sample.

$$\theta = V_{liquid} / V, \qquad [1.6]$$

or

$$\theta = (M_{ws} - M_{ds}) / \rho_w V_s, \qquad [1.7]$$

where:

M_{ws} = the mass of wet soil (kg),

M_d = the mass of dry soil (kg),

ρ_w = the density of water (kg/m^3),

V_s = the volume of the soil sample (m^3).

Water in soil is subjected to several force fields such as those originating from the presence of the solid phase and its structure, from dissolved salts, from external gas pressure (if present) and from gravity. These forces combined determine the energy that is required to extract water from soil as well as determine the direction of flow of water

through soil. For example, the drier the soil the lower the potential and the more plants will struggle to extract water. The potential is defined relative to the same mass of free water at the same temperature and elevation. The total potential of the liquid phase can be expressed as:

$$\Psi_t = \Psi_m + \Psi_g + \Psi_o + \Psi_a, \quad [1.8]$$

Where:

Ψ_t = total potential of liquid phase,

Ψ_m = matric potential,

Ψ_g = gravitational potential,

Ψ_o = osmotic potential,

Ψ_a = pneumatic potential.

Potentials by definition are expressed in J/kg, but these can also be expressed as psi, kPa, bars. Hydrologists often express the potential in terms of matric heads (m), which is height of a water column, in equilibrium with water in soil or pF values (potential free energy) which are a $\log_{10}$ of matric head (Wojcik 2005). Plant scientists prefer to express this in Bars or Pa, units more commonly used to describe the energy status of water within plan roots.

The ability of soil to retain water is an effect of various mechanisms working antagonistically to gravity, evaporation, plants uptake etc. This ability to hold water as a function of its relative energy status is commonly known as water retention relationship. The soil water retention curve describes the relationship between the water content and the range of negative pressures. Hence the shape of retention curve is dictated by the geometry of pore space in the given soil sample. In order to empty the pores filled with water, there is a need to achieve negative pressures which will gradually fill pores with

air while water is being sucked out. The smaller the pore is the lower the pressure required to empty it (Klute 1986). The relation between the pore diameter and pressure required to empty or fill it is represented by equation (Nimmo *et al.* 2004):

$r = (-2\sigma (\cos\alpha)) / P,$ [1.9]

Where:

r = pore radius (m),

P = pressure (N/m^2),

α = contact angle of water in capillary,

σ = surface tension of water (N/m).

The influence of simple pore geometry on the pressure required to empty it can be explained if two samples are considered with the same porosity (pore volume), the pore size distribution (PSD) and connectivity, but a different pore geometry like depicted in Fig.1.1. If we assume that air enters the sample from above, the diameter of the top pore will have major impact on the pressure value that is required for air entry. The pore on the top (Fig.1.1.a) of the sample requires high negative pressure to fill the smallest pore with air. At the point when this pressure is achieved all pores drain completely and immediately, as the smallest pore requires the highest negative value of pressure. Therefore all other pores will drain at the same pressure, as visualised by sample 1 (blue retention curve in Fig.1.2): there is almost no change in water content till very low pressures corresponding to the value of air entry of the smallest pore on top and once this is reached it causes a sudden and complete drainage of pore networks.

In the sample shown in Fig.1.1.b, the situation is different, since the largest pore is on the top of the network and with gradual decrease of pore diameter with depth, the network will drain stepwise when air enters from above, and when the critical pressure

is met for each radius. Sample 2 (red line in Fig.1.2) represents qualitatively the water retention relationship for such a structure. Each water loss corresponds to a negative pressure achieved for a given radius of pore. The biggest loss of water is at the lowest negative pressure required to drain the pore with the biggest radius on top of the sample.

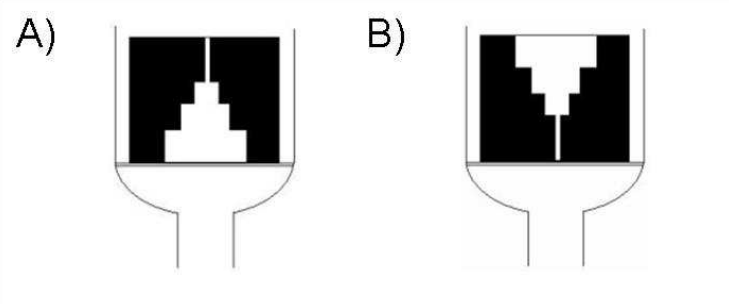

Fig.1.1. The schematic examples of two pore networks, having the same pore volume and size distribution but different geometry of pores, affecting the shape of water retention properties.

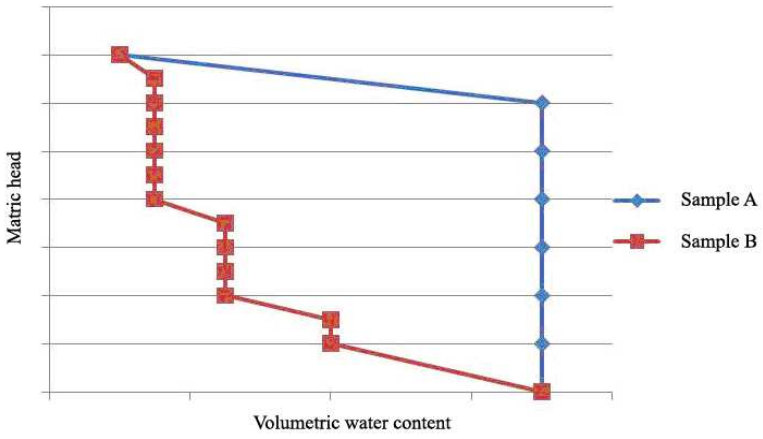

Fig.1.2. Schematic retention curves of samples A and B, shown in Fig. 1.1. Differently shaped retention curves of samples with the same pore volume reflect the have different air-entry value reflected in the different shapes of drying curves.

The geometry of the pore space hence defines the shape of the water retention curve. To empty pores filled with water, a negative pressure needs to be achieved low enough to drain the smallest diameter within a complex geometry. There is however a difference

between desorption and absorption of water by soil which is known as hysteresis. It is linked with irregularities of pore network geometry, changes in contact angle, entrapped air during saturation or clay content (Koorevaar *et al.* 1983). Such a macroscopic behavior is directly related to the microscopic heterogeneity of the pores in soil.

A traditional method of measuring water retention relies on equilibrating soil with water at a known potential (Klute 1986). This can be done for example by equilibrating the soil sample with a porous medium in which the negative pressure is controlled, or alternatively by applying a positive pressure on the sample relative to a pressure at the bottom which will be maintained at a controlled value (e.g. pressure plates). The hanging water column method, or another method where soils are equilibrated on for example a sand or clay table, is a widely used method as it is cheap, widely accessible and reliable for conditions relating to the wet end of the relationship. All the above methods provide information for the average water content of the sample, and they do not offer insight on how this water is distributed within the sample. Bayer *et al*. (2004) used X-ray microtomography to measure the water content at known pressures range in soil sample based on differences in X-ray adsorption. This method limited the size of the samples to fit them into CT system and required the custom built miniature of Heines apparatus. Such setup would be an advantage in study quantifying the water distribution at the different matric potentials.

Since the soil water retention is related to simple geometries, it is possible to predict water retention from pore size distribution. For this reason, soil has often been simplified and presented as a 'bundle of capillary tubes'. It can be achieved by deriving the pore diameter for each equilibrium (negative pressure).

$$2r = 4\sigma \times (\rho_l \times g \times |h_m|)^{-1} \qquad [2.0]$$

Where:

σ = surface tension of liquid (N/m),

ρ_l = density of the liquid (kg/m^3),

g = gravitational acceleration (m/s^2),

h_m = matric head (m).

Unfortunately, such an oversimplification only works for well defined geometries. For more realistic geometries, such as that of pore space, it is often impossible to know the geometry in sufficient detail to do such calculations. However, should the geometry be known, it is possible.

Soil water retention is not just affected by pore geometry. Another factor strongly influencing soil water retention is soil repellency. Repellency is defined as the decrease of the affinity of soil to the water and as a resulting in the periodical resistance of soil to wetting (Doerr and Thomas 2000). Water repellent soil may cause reduction in water infiltration, formation of preferential flowpaths for water, increased surface run-off, which can result in nutrient leeching, and increased soil erosion (Doerr *et al.* 2000). However, repellency can also cause an increase of water stable soil aggregates by preventing their degradation (Rillig 2005). There are various factors influencing the degree of soil repellency, such as soil texture (Wallis and Horne 1992) and microbial products of soil organic matter decomposition (Hallett and Young 1999). There has been a strong focus on fungal activity producing glycoproteins such as glomalin (Steinberg and Rillig 2003). However, Feeney (Feeney *et al.* 2006a) showed the increase of repellency induced by microbial activity, however was unable to correlate this with the structure of the microbial community.

In the development of suitable experimental systems to study soil processes the complexity and heterogeneity of the soil is a challenge. There is a need to create a model soil environment that allows for control over structural, chemical and biological

properties and provides the reproducible and representative surrogates of soil structure. A solution commonly used is repacked soil microcosms with the use of pre-treated soil, at known initial conditions such as bulk density and aggregate size. Typical pre-treatment of soil used for production of re-packed soil microcosms includes the following stages: air-drying, sieving, sterilisation and packing. However the main drawback of soil pre-treatment procedures is the loss of the natural heterogeneity of the soil structure. Sieving creates aggregates which are artificial components of soil structure, removes plant residue and soil organic matter (Young *et al.* 2001). Packing the aggregates with uniform structure also introduces the homogeneity of the pore network geometry.

1.2. SOIL-BORNE ORGANISMS

The type of soil-borne microbial activity and biomass is driven partly by the type of soil and soil management practices that strongly impact on the pore network (Young and Ritz 2000). Soil rich in organic matter which is not subject to extensive physical disruptions such as tillage is dominated by fungi whereas soil regularly tilled with high content of non-organic based fertilizers have a higher bacterial content (Schulten *et al.* 1990). This infers that alteration of soil structure will result in control over microbial habitats. However it is crucial to adjust the scale at which the structural conditions can be changed as different groups of organisms will react differently. At the field scale it is much easier to disturb extensive fungal networks than bacterial communities which occupy smaller niches according to their pH preference, O_2, water and SOM availability (Nunan *et al.* 2003). Obviously changes to the pore network structure also influence the distribution of nutrients and water. The presence of water films and residues in thin pores and valleys will influence the flow of soil gases because gas diffusion in water is

significantly slower than in air-filled pores. Hence this process will influence the nature of microbial processes, affecting the balance between anaerobic and aerobic organisms (Young and Ritz 2000). Additionally some groups of organisms, such as nematodes, protozoa and bacteria, are completely dependant on water in terms of motility and sourcing the nutrients. Fungi are less affected by this occurrence because of the nature of their hyphal form of growth. Fungi have the ability to translocate nutrients and water through hyphal networks (see Fig.1.3) which allows them to sparsely explore the available, connected pore space of soil and to bridge air gaps in soil (Griffin 1978). However the growth through the pores with low nutrient and water content are demanding in terms of energy, and sparse networks also create higher risk to mechanical disruptions (Ritz and Young 2004). On the other hand colonization limited to the small environmental niches such as thin valleys and pores can provide a physical protection from predators, if the diameter of occupied pore is smaller than that of the predator (Powlson 1980).

Soil-borne organisms and plant roots also have a significant influence on the structure itself. Actively growing plant roots can cause a direct increase in the soil compaction around the roots, and in this phase they are likely to attract symbiotic organisms like myccorhizal fungi and bacteria (Eldridge and Freudenberger 2005). However once the roots reach stage of decomposition there is an increasing number of saprotrophic organisms observed (Dorioz *et al.* 1993).

Fig.1.3. Soil-borne fungi *Rhizoctonia solani* grows onto the edge of Petri dish plate. Fungi are not restricted to water meniscus and can readily bridge airgaps between the structures.

Bacteria and fungi have a significant role in stabilisation of soil structure, although their effect can be observed at different scales. Bacteria are known to affect stabilisation of microaggregates, smaller than 250 µm (Dexter 1988, Beare and Bruce 1993) whereas fungi are known to influence stability of macroaggregates, bigger than > 250 µm and sand slopes (Meadows *et al.* 1994). Earthworms although more common in soils with no tillage (Fraser *et al.* 1994) also play a significant role in creating macropores by burrowing (Drees *et al.* 1994) and soil aggregation by forming cast (Brown *et al.* 2000). Earthworms are also strongly linked with stabilisation of soil C content by increasing the number of stable aggregates (Six *et al.* 2004). However there are reasons to investigate the effect of soil characteristics on fungal dynamics. Fungi are ubiquitous soil organisms and the subject of studies as saprotrophs, plant pathogens, biocontrol and symbionts. The discovery of *Armillaria bulbosa*, a single fungal colony occupying an area exceeding 15 hectares and being genetically stable for the period of time exceeding 15 centuries, placed fungi amongst the largest and oldest organisms living on the planet (Smith *et al.* 1992). In addition fungi are engineers of soil structure (Tisdall *et al.* 1997). The role of fungi in soil structure dynamics can be considered at

two spatial scales. At the microscale fungal hyphae are likely to change the alignment of primary soil particles such as clay platelets (Ritz and Young 2004). Soil borne fungi are also considered to be a significant binding agent increasing the stability of soil structure. There are several mechanisms of fungal soil stabilization, one of them is surrounding soil particles or microaggregates with hyphal network, which has been described as 'sticky string bag' (Bossuyt *et al.* 2001). This activity promotes macroaggregate creation and also enhances the resistance of aggregates to physical disruptive forces. Fungi also produce a wide range of binding substrates that cement soil particles together (Wright *et al.* 2006). One of the most studied fungal exudates in this context is glomalin, which is an insoluble and hydrophobic proteinaceus substance counteracting aggregate break down induced by water. The significance of glomalin has been proved by numerous studies quantifying the relation between the presence of glomalin and the amount of water stable soil aggregates. The increase in glomalin correlates with an increased number of stable soil aggregates contributing to the stability of soil structure (Wright and Upadhyaya 1998). Enhancement of the stability of the soil structure was detected and quantified by analysis of sand slopes. Samples colonised with fungi showed significantly increased stability and the fungal network was clearly visible after the sand slope collapsed subject to physical disturbances (Meadows *et al.* 1994). The degree of increase in stability depends on several factors influencing the strength of fungal network, such as the age of the hyphal network and the rate of colonisation which correlates with the nutritional status and availability of water (Li *et al.* 2002). Also fungal influence on soil structure is not reflected by the quantity of fungal biomass but activity (Degens 1997). The fungal exudates which act as structural stabilizators, i.e. polysaccharides, glycoprotein based melanins and enzymes, can also impact on the hydraulic properties of soils. The best characterised glycoprotein is glomalin, a

characteristic for arbuscular mycorrhizal fungi and described for the first time in 1996 (Wright and Upadhyaya 1996). Glomalin is ubiquitous in tropical forest soils to the extent that C and N from Glomalin have been estimated to be 5 % of the total pool (Rillig *et al.* 2001). Glomalin is one of the exudates that influences the soil hydraulic properties by increasing hydrophobicity (Hallett *et al.* 2001). Such interactions will have an affect on soil sorptivity and water retention. In addition to chemically changing the soil structures by fungal exudates, fungi have been hypothesised to alter soil hydraulic properties by structural changes to soil.

The effects of myccorhizal fungi on soil water retention were shown by Auge (2001) and Bearden (2000). Both studies examined the impact of fungal colonisation after long term incubation, required for the growth of roots. Mycorrhizal soil appeared to start loosing water at lower h_m than controls (they were breaking at lower negative pressure values). However there appears to be fewer studies investigating influence of fungi colonization on soil water retention in relation to structural changes. Crawford *et al.* (2011) showed the increased porosity by 50 % in samples inoculated with fungi. Crawford *et al.* (2011) created a link between the structural changes and hydraulic properties using the lattice Boltzman model to quantify the hydraulic conductivity. Soils inoculated with *R. solani* showed higher conductivity values of 1.52 cm/d compared to 0.52 cm/d for the control samples. Also increased hydraulic conductivity infers enhanced connectivity of the porespace providing additional evidence of fungal effect on the soil structure.

In order to alter the soil properties, fungi would have to spread through it first. The way soil fungi colonize soil depends on geometry of soil pore networks (Harris *et al.* 2003, Otten *et al.* 2004). This makes it plausible to assume that the initial conditions ultimately also determine the dynamics of the fungal colonization. Harris *et al.* (2003)

proved that bulk density and porosity have a significant effect on fungal growth dynamics and spatial organization of fungi in soil. Patchy and sparse growth have been identified for soils packed at low bulk densities with high porosity in contrast to organised and dense colonies at more compacted soil. There was also an increase in fungal biomass per gram of soil with increase of soil compaction. Although this phenomena is linked to the ability of fungi to create small but dense colonies in situations where further exploration is blocked by water filled pores (Otten *et al.* 1999). A number of studies have focused on the influence of pore connectivity and tortuosity on fungal growth (Otten and Gilligan 1998, Otten *et al.* 2004). These studies concluded that fungi spread preferentially, along the well connected macropores. Such behaviour allows fast and sparse exploration of pore space for nutrients and easy branching required for growth (Otten *et al.* 1999). Although hyphae have the ability to bridge the air gaps, surface growth is the preferred form as it is the most efficient way to maintain in contact with material and nutrients when available (Otten *et al.* 2004).

Fungal visualisation and quantification in soil has been a focus of research for many decades due to the importance of fungi in ecosystem processes. The most suitable method used to date that is used to visualise hyphae in relation to soil pore networks is the analysis of 2D cross sections of resin impregnated soils containing stained fungal hyphal networks. This procedure although revealing insights (Harris *et al.* 2003, Nunan *et al.* 2006) disregards the complexity of soils in three-dimensions. Recent rapid development of commercial microtomography paired with image analysis and mathematical modelling is a promising way forward. However to date fungal colonies are not able to be visualised in soil with the use of X-ray tomography. This is due to the differences in a density between heterogeneous soil material and hyphae although

Bulcke *et al.* (2009) showed that is possible to visualise fungi in wood at a high resolution.

1.2.1 Biology and taxonomy of *Rhizoctonia solani*

The fungus selected as a model organism in this thesis, *Rhizoctonia solani* AG4, belongs to the division of *Basidiomycota* (class: *Agaricomycetes*, order: *Agaricales*, family: *Cirticiaceae*, genus: *Rhizoctonia*) (Parmeter 1970). *Rhizoctonia* is a complex genus of fungi, which is classified based on a set of common and characteristic features, such as septated, multinucleated hyphae, coloured from light brown to black, branching at right angles from the main hyphae, hyphal constriction at the branch origin, presence of moniloid cells forming the sclerotia and lack of asexual spores (Garcia *et al.* 2006). Sexual forms, teleomorphs, occur very rarely and were recently classified as genera *Ceratobasidium*. Thus, all characterisation and studies are commonly carried out on, so called sterile hyphae isolated from the plant or soil material. The *R. solani* species is divided further into anastomosis groups (AG), based on genetical similarities and ability to fuse hyphae between isolates (anastomosis). This classification distinguishes between binucleate isolates (AG from 1-13 and BI) and multinucleate isolates (AG labelled from A to U) (Garcia *et al.* 2006).

Isolates belonging to *R. solani* are ubiquitous soil saprotrophs and common destructive plant pathogens with a wide range of host plants. *R. solani* causes rot of stem and plant organs intact with soil material and damping-off in seedlings and foliar lesions (Kucharek 2000). The colonization of the target plant with *R. Solani* can be described as four main processes: adhesion, penetration, colonisation and host reaction (Garcia *et al.* 2006). The colonisation usually starts with fast, directional growth of unbranched hyphae (runner hyphae) on the surface of the host plant. At the latter stage

runner hyphae start to repetitively branch. Subject to isolate and the type of host, branching hyphae can directly penetrate host tissues or alternatively aggregate hyphae and form penetrating structures (cushions). Cushions produce pegs which penetrate the cuticle and epidermal cell walls. Penetration and colonisation processes are accompanied by high enzymatic activity of fungi producing a range of pectinolytic, cellulolytic and hydrolytic enzymes which degrade the plant cell walls (Bertagnolli *et al.* 1996). In later stages of colonisation the fungi induce cytological changes leading to the death of cells of infected tissues. The secreted enzymes penetrate plant material, damaging the cellular structure in advance of fungal spread. This phenomenon classifies *R. solani* behaviour as a necrophytic pathogens.

If the growth conditions are favourable, with temperature between 18 to 30 ^{o}C and 40 to 100 % of humidity, *R. solani* spreads between the plants through the growth of hyphae or by creating the sexual spores (Parmeter 1970). Spores form on structures known as basidia, each basidium produces 4 basidiospores. In moist conditions basidiospores disperse and germinate, the new hyphal spores fuse in the process of somatogamy (no fusion of nuclei) to create multinucleate hyphea ready to colonise another plant. In stressful conditions associated with low temperatures or insufficient moisture, *R. solani* creates survival forms, known as sclerotia, which are resistant to adverse environmental conditions. Sclerotia are irregularly shaped, usually <1 mm in diameter and consist of compacted monilioid cells. In the lack of presence of the compatible host plant *R. solani* acts as a strong saprotroph decomposing soil organic matter (Garcia *et al.* 2006).

1.3. VISUALISATION AND QUANTIFICFATION OF SOIL STRUCTURE

There is a range of destructive methods available for investigating the internal structures of soils. An efficient method is thin sectioning (Harris *et al.* 2003) based on microscopic observations of 2D these sections derived from resin – impregnated soil samples. However, this method is very time consuming (impregnation with resin, cutting soil in few micrometers thick slices) and provides information only for 2D. Serial sectioning of soils (Lymberopoulos and Payatakes 1992) works under the same principle of a stepwise removal of layers of material. However, this involves imaging at high resolution the each surface of impregnated sample at each step. The 3D volume of the porous material can be then obtained by stacking the high resolution images (Vogel and Roth 2001). Again this method is time consuming allowing up to 20 slices per hour to be visualised and to recreate the connectivity of the structures there is a need to apply statistical methods with ability to predict the neighbourhood connectivity patterns (Vogel and Roth 2001).

Pseudo 3D data with optical quality can be obtained by confocal laser scanning microscopy. This method derives a set of high resolution images with ability to in-depth focus, which can be reconstructed into representative 3D volume with surface characteristics. The biggest disadvantage of this method is the limitations of depth that can be examined in this sample (Fredrich *et al.* 1995).

All above methods of visualisation and quantification of soil structure are destructive. This means there is no possibility of continuous use of samples, or monitoring certain structural changes during experiments. Although characterisation of fungal colonies by CT scanning is still a challenging but not an impossible task, quantification of soil structure by X-ray microtomography is fairly routine with some interpretational challenges. X-ray microtomography is a non - invasive method allowing

reasonably fast, visualisation and quantification of inner structures of samples at high resolutions in 3D without interrupting their structure. Resolutions of microns can be routinely obtained with laboratory systems. Although the technique is not novel, it is due to the development of commercial benchtop systems and their availability that the range of applications in science rapidly expands into new areas.

1.4. DEVELOPMENT OF X-RAY MICROTOMOGRAPHY

The history of Computed Tomography (CT) began in 1940, with a patent granted to Gabriel Frank who described the basics of tomographic data acquisition and optical reconstruction. The patent included schemes of equipment aiming to create linear representation of measurements (sinographs) and description of possible optical backprojection techniques of reconstructing the image (Hsieh 2009). In 1961 W. H. Oldendorf performed a series of experiments using a simple setup consisting of the source (collimated radioiodine) generating beam towards detector in form of sodium iodine scintillation crystal paired with photomultiplier. The sample was placed on a model train moving slowly on rotating turntable. Only one radiograph was produced for the line of centre of rotation and successfully detected the two metal nails in the phantom. The foundations of CT were established by A.M. Cormack who created a mathematical theory for image reconstruction in 1963. Cormack developed his work while experimenting in Groote Schuur Hospital and aimed to develop a method which enables reconstruction of attenuation coefficient (Intensity of X-rays which passed through the sample). Independently from the work of Cormack, G. N. Hounsfield in EMI laboratories in England started development of the first clinical CT scanner. In 1979 the Nobel Prize in Physiology and Medicine was shared between the pioneers: A. M. Cormack, and G.N. Hounsfield for their discoveries in CT systems.

The very first laboratory scanner was developed in 1967, equipped with a low intensity source and it would produce an image after 9 days of scanning. Improvements in the reconstruction method and X-ray source led to development of first clinically available CT scanner (first generation scanner or EMI scanner), based in Atkinson – Morley Hospital in London in 1971 (Hsieh 2009).

With the 40 years of development tomography evolved into a very powerful, fast and reliable tool that paired with image analysis techniques allows visualisation and quantification of the internal structure of objects. Tomography nowadays is not restricted to medical use; it has a growing range of applications in engineering, food technology and biophysics. In soil science microtomography is used for quantification of soil structure at various scales from the a microcosm or typical soil sampling core (Kim *et al.* 2010, Pajor *et al.* 2010, Crawford *et al.* 2011, Schluter *et al.* 2011) to an individual aggregates (De Gryze *et al.* 2006, Kravchenko *et al.* 2011b). CT systems are also used for visualisation and quantification of complexity of plant root systems (Pierret *et al.* 1999, Nunan *et al.* 2006, Hopmans 2010, Tracy *et al.* 2010, Davey *et al.* 2011). Combined with other techniques, i.e. Positron Emission Tomography this can deliver information about metabolic processes in plants (Garbout *et al.* 2011). CT systems are also used to measure soil water content based on the changes in greyscale values (Bayer *et al.* 2004) quantifying the preferential flow of water (Luo *et al.* 2008).

Commercial CT scanners evolved from clinical systems, with the major difference that in commercial 'benchtop' systems the X-ray source and detector are static while the sample is mounted on rotating turntable. However the basic operational principles remain the same as described below. The modern commercial CT microtomographs use a heated cathode system to generate an electron beam. In the X-ray tube (gun) an electron beam is accelerated by an operating voltage through an anode

ring towards the target via a focus coil. The coil passes the current and aids to focus it on a micro focal spot on the target. X-rays are being emitted by sudden deceleration of electrons colliding with focal spot on target material. The size of the focal spot is also determined by the length of the filament. The type of target material determines the nature of this occurrence and as an effect the characteristics of the X-ray beam. The intensity of X-ray beam is proportional to the atomic number of the target material and difference in potentials between anode and cathode. Voltage defines the energy (acceleration rate) of electrons; the number of X-rays generated is independent of the voltage and can be controlled by the current. However only 1% of the energy is converted into emission of X-rays, the remaining 99 % turns into heat and hence an appropriate cooling system is crucial (Fig.1.4).

The X-ray beam passes through the sample and is being captured by the detector. The reduced intensity of the detected beams transmitted through a material is measured and known as the attenuation coefficient.

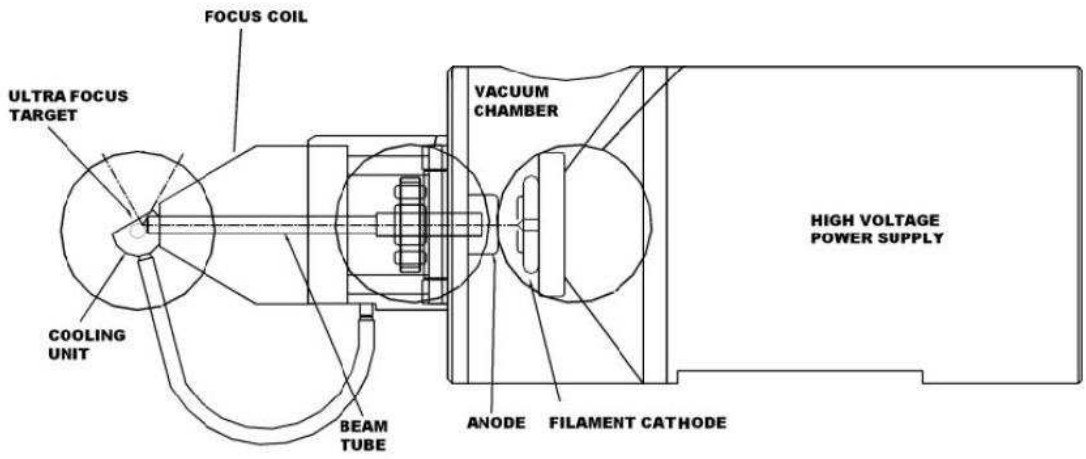

Fig.1.4. Scheme of typical X-Ray X-tek gun with fixed focal spot (one length of filament) (X-tek manual – modified).

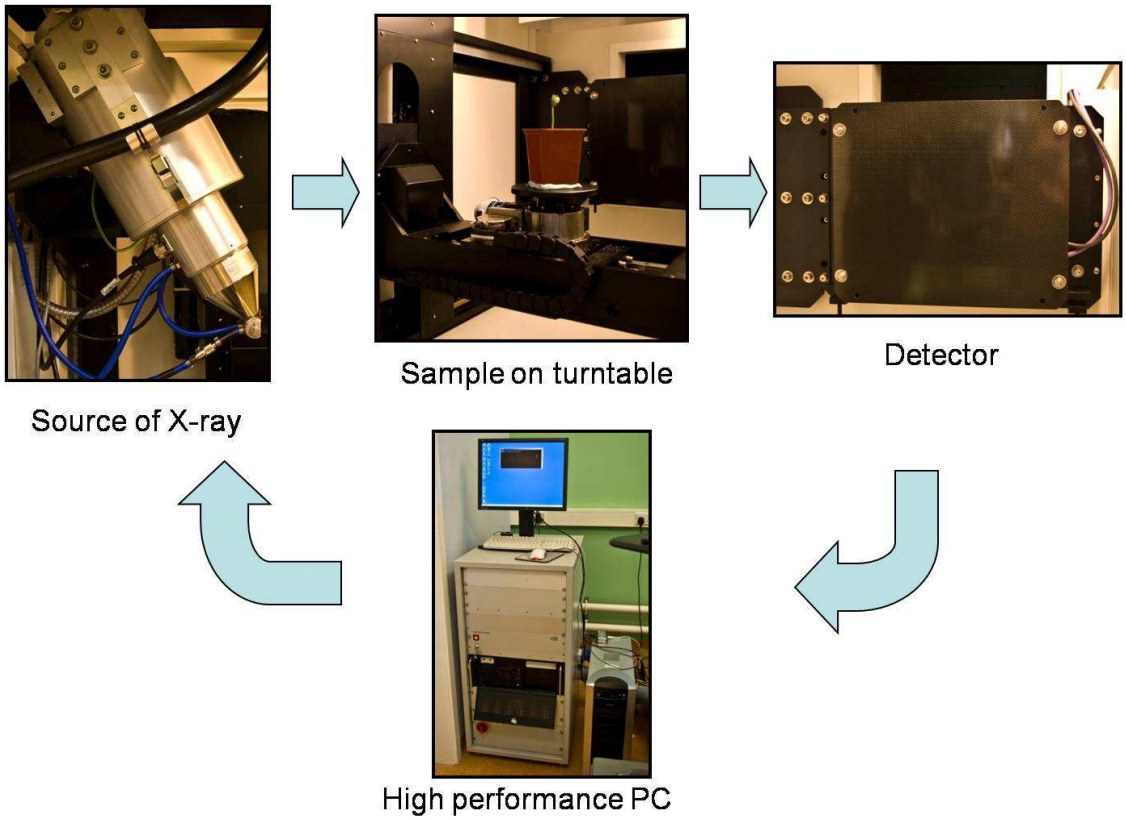

Fig.1.5. The principle of scanning procedure (image acquisition). The high performance computer governs the conditions of the scan and monitors the status of the whole system. X-ray source produces the X-ray beam which passes through the sample. The X-ray beam transmitted through the sample is detected by detector, which converts the signal to a 2D cross section of the sample and sends it to the computer.

The sum of the attenuation data allows reconstruction of CT image which is a 2D cross section of given object being sent to the computer controlling the whole process (Hsieh 2009) (Fig.1.5.).

The commercial tomography units generate a polychromatic X-ray beam. This means that operator can control the maximum energy of the X-rays. However the actual beam has wide spectrum of energy levels with only a percentage of those with highest specified value. The X-rays which are lower in energy than specified, so called softer X-rays can be scattered, or cause insufficient penetration and as a result noise and artefacts appear in the data. Monochromatic beam alleviates some of these issues and is

achieved with synchrotons, where thanks to a special optic systems the one to million part of the beam can be selected at specified energy and used for scanning. There are such facilities placed in France (European Synchrotron Radiation Facility), Japan (Super Photon Ring) and United States (Argonne National Laboratories). The history of the Advanced Photon Source (APS), used in this work dates back to the first reactor built at University of Chicago known as Chicago Pile 1 (CP-1) after short test has been relocated near Argonne in 1946. The research complex developed over the years into interdisciplinary center with a very limited and restricted access, operated by the University of Chicago and U.S. Department of Energy. At present the center comprises of 1.1 km in circumference, circular synchrotron (APS), with adjacent complex of facilities accommodating 2900 employees (Rivers *et al.* 1999, Rivers *et al.* 2004, Rivers *et al.* 2006). At the synchrotron the beam of electrons is emitted by cathode to heated 1100° C. The beam is then accelerated by high-voltage alternating electric fields and injected into the booster synchrotron which is an oval ring of electromagnets. The beam of electrons is then accelerated to the 99,999 % of speed of light and let into the storage ring (1104 m in circumference). In the storage ring electrons are focused to create narrow beam by electromagnets and can be injected into research station situated along the ring. System of crystal and mirror optics allows adjusting the beam according to the characteristics of analysed material (http://www.anl.gov/).

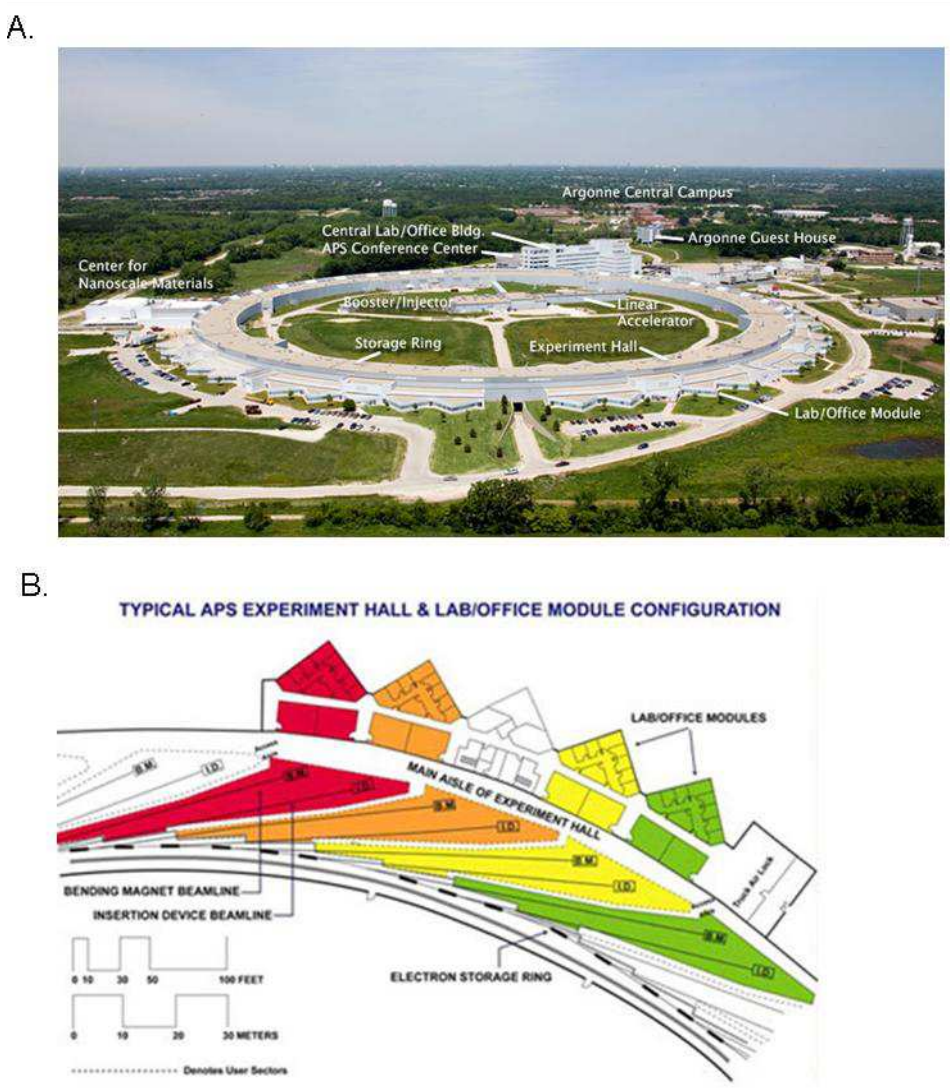

Fig. 1.6. Aerial photo of APS with specified facilities (A) and a schematic view of the beam stations and associated facilities (B) (http://www.aps.anl.gov).

1.5. THE STAGES OF IMAGE PROCESSING

The process of typical CT data acquisition and analysis consists of four stages: (i) image acquisition, (ii) reconstruction of the 3D structure of the volume of interest, (iii) rendering of the 3D sample and converting it to the form required for analysis software, (iv) binarization (thresholding) and further analysis.

The image acquisition process is usually governed by complex software package which allows adjustment of the scan conditions, monitoring, calibration and basic diagnostics of the CT system.

Reconstruction of the CT volumes is based on filtered backprojection. This method projects the information collected at each angle adding the contribution from each voxel (pixel in 3D) and counteracting the radial blurring by Fourier transformation, filtering and inverse transformation. This process removes blurring but might introduce high frequency noise (Hsieh 2009). Reconstruction can be repeated with different options (range of digital filters, centre of rotation, ROI).

In the next stages reconstructed volumes are read into software packages such as VGStudiomax 2.1 (VGSM 2.1, http://www.volumegraphics.com). The 3D reconstructed volumes are visualised, converting these into image stacks, segmentation of structures according to gray-scale values, volume analysis and creating 3D animations, an example of the software is VGSM 2.1.

One of the most important steps in the image analysis of a soil samples is thresholding or segmentation which is the process of defining the boundary of pores and solids. There is a number of ready to use algorithms for thresholding, such as histogram based methods, adaptive thresholds However because of heterogeneity of soil material there is no universal thresholding method for soil data. Baveye *et al*. (2010) showed how user-dependant existing methods are. The most accurate method from the range of compared approaches was the manual choice of a single global threshold value being an average of values set for 5 random slices within the volume of interest, but overall the work demonstrated that unacceptable inaccuracy is introduced by unstandardised thresholding methods. Sezgin (2004) compared 40 different algorithms on ultrasonic images of the samples and text documents. The comparison was performed only on 2D

images (ultrasonic images and images with text) only one method (clustering algorithm by Kittler and Illingworth (Sezgin and Sankur 2004)) produced the most accurate output for both types of images. However all these methods were unsuitable for multithresholding of 3D datasets. Thresholding is still a developing area of image analysis with new algorithms emerging frequently.

Further stages of image analysis involve quantifying ecologically relevant characteristics of soil structure such as pore connectivity, volume, pore size distribution and pore surface area. Quantification of these soil characteristics can be carried out with the use of various software packages or their combination depending on the requirements of analysis. There are readily available software packages such as Volume Graphics Studio Max (Tracy *et al.* 2012), Avizo (Luo *et al.* 2010a), AMIRA (Luo *et al.* 2008), 3DMA (Kravchenko *et al.* 2011b), ImageJ (Deurer *et al.* 2009, Pajor *et al.* 2010, Crawford *et al.* 2011). In addition some groups prefer to implement the algorithms themselves to suit the analysis requirements (De Gryze *et al.* 2006, Schluter *et al.* 2011).

CT scanning combined with image analysis techniques allows relatively fast non-destructive visualisation of internal structure of objects at high resolution and quantification of their structural properties. Datasets obtained by the scanner can be applied in a wide range of mathematical models which are extending the analysis using CT derived soil structure as the environment in which the flow or spread of fungi can be investigated.

1.6. CONCLUSIONS AND OBJECTIVES

There is extensive evidence in the literature that soil is a heterogeneous and dynamic ecosystem. However there are fewer studies bringing together the interactions amongst

soil structure, hydraulic properties and soil-borne organisms which better captures the sheer complexity of this ecosystem. This thesis addresses this gap in the knowledge by investigating the effects of short term interactions between soil and fungus *R. solani*. It is clear a combination of techniques and methods will be required to elucidate the impact of fungal growth on soil and hydraulic properties.

The first part of this thesis involves the development of protocols for quantifying in experimental or theoretical manner the link between soil structure and colony dynamics. The first objective is to develop a protocol allowing producing representative and replicable soil microcosms, suitable for investigating fungal colonisation and water retention measurements within soil samples with known ranges of structural properties. The next step involves quantification of the impact of fungus *Rhizoctonia solani* on the soil water retention and soil structure. Soil physical structure will be characterised with the use of X-ray microtomography combined with image analysis as cutting-edge, non-invasive techniques to quantify and visualise the fungi-induced structural changes to the soil microcosms.

The second part of the thesis determines the impact of factors such as bulk density and aggregate size used for constructing soil microcosms on the geometry of pore networks. Additionally merging the CT scanning with mathematical modelling allows quantifying the effect of the soil structure on dynamics of fungal colonisation.

CHAPTER 2

Development and evaluation of protocols to prepare, maintain and quantify structural heterogeneity in soil microcosms

2.1. INTRODUCTION

Soil experiments are best performed on undisturbed soil sampled from a field, as the material would preserve its natural structure. Such structures are often too heterogeneous to obtain replicable, representative samples which can be used to compare different treatments (i.e. interactions between soil structure and soil-borne organisms). However, it is possible to exert control over some bulk properties when microcosms are prepared. For example, repacked soil microcosms may lose natural soil heterogeneity, but allow for control of factors such as bulk density, aggregate size, and water content and thus, make inoculations with given microorganisms easier to control. This chapter describes development of protocols for packing soil microcosms and methods used to ensure uniformity of soil structure. This is followed by a description of inoculation methods of these microcosms and a description of X-ray CT systems and protocols used throughout my thesis.

2.2. SOIL AND SOIL TREATMENT

For all laboratory work in this thesis the same type of soil was used. This soil was collected from the James Hutton Institute's (JHI, formerly Scottish Crop Research Institute) experimental site, referred to as Bullion Field. The soil is an arable sandy loam: organic matter, 2.6 %, sand, 71 %; silt, 19 %; clay, 10 %; pH 6.2 with particle density of 2.52 Mg/m^3 (Toyota *et al.* 1996). Soil was air-dried in a glass house at JHI, sieved into three fractions of aggregates sized <1 mm, 1-2 mm and 2-4 mm, and then stored in a cold-room (4^oC) in the dark till it was used.

For all experiments, sieved soil was sterilized by autoclaving (moist heat) in plastic beakers covered with silver foil with holding time of one hour @ 121^{o}C. To ensure successful autoclaving, it was repeated after 48 h (Trevors 1996).

Before packing soil at the selected bulk-density, sterile soil was wetted up to a water content of 0.19 cm^3/g and left for 48 hours to equilibrate and to avoid the initial rapid flush of microbial activity (Kieft *et al.* 1987, Harris *et al.* 2003). Such prepared soil was packed into pvc rings with a diameter and height of 4 cm at a specified density as determined by the experimental design. Further details are given in the specific chapters.

2.3. DEVELOPMENT OF UNIFORM STRUCTURE OF SOIL MICROCOSMS AT EACH BULK DENSITY AND AGGREGATE SIZE

The methodology of packing soil microcosms was verified to ensure the uniformity of density throughout the sample. Any variability occurring in the density at the scale of microcosms could have an effect on the distribution of microbial biomass and on the measurements of hydraulic properties of soil. We used the Nikon Benchtop X-ray micro-tomography system to visualise and quantify the structure of these microcosms. The details of this system are given in section 2.5. There was no need to perform the full 3D scan as the variability could be readily identified on 2D transects (radiographs) of the samples. With increasing density of the objects the grayscale values were declining resulting in darker areas of the images. Radiographs were generated with the same settings for all microcosms: 120 kV, 109 µA and with the use of an 0.25 mm Al filter.

The first microcosm (Fig.2.1) was prepared by packing three layers of soil approximately 1.33 cm thick at a density of 1.3 g/cm^3, with 1-2 mm aggregate size. Each layer was compressed with the flat surface of 15 ml centrifuge tube's

(Fisherbrand) screw cap (diameter of approximately 2 cm). Radiograph of this microcosm showed visible density gradients in regions where the surfaces of layers of soil were in contact with each other. Additionally it revealed that the thicknesses of layers were compressed more in the centre than near the edges of microcosm. However this could be also an artefact of X-ray beam absorption caused by cylindrical shape of soil microcosms. The thickness of microcosms on the edges was smaller than in the centre of the sample. Increasing the distance for X-rays to travel through an object, results in a decrease of intensity of the beam. The thicker or denser the sample material is, the more X-rays are absorbed by the sample (attenuated).

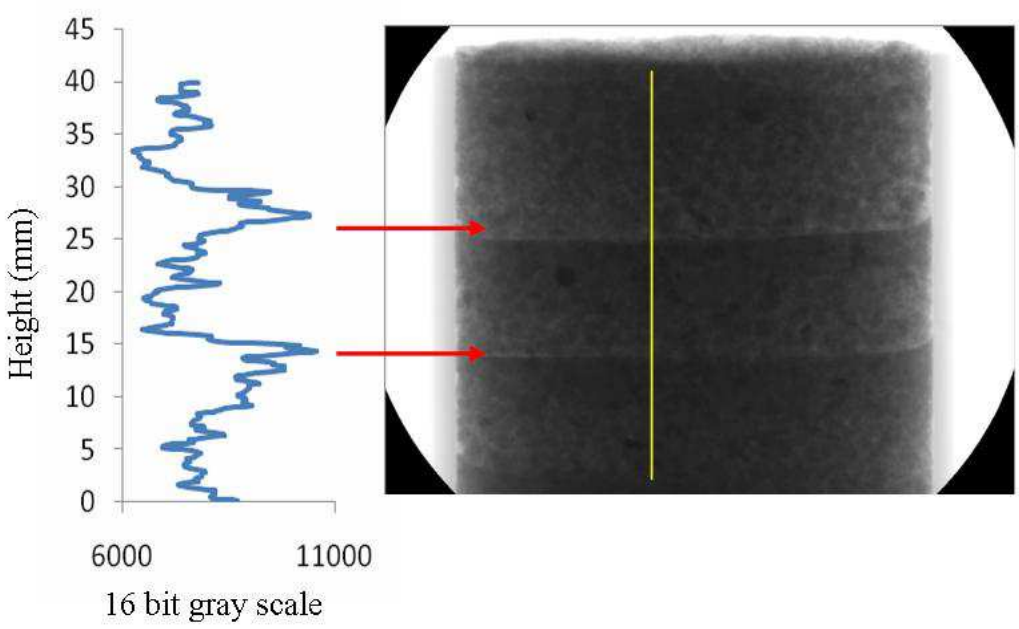

Fig. 2.1. Non uniform packing of soil material results in inconsistency of density, confirmed by gray scale histogram derived for vertical transect in the centre of the sample (left).

Surface plots of greyscale values reflecting the levels of compaction were created with ImageJ (http://rsbweb.nih.gov/ij/) for a line in the centre of microcosm. The function 'surface plots' within ImageJ was used to create a histogram of the

distribution of grayscale values within the selected area. The denser the object is the higher the greyscale value will be. Histograms confirmed the visual judgement by showing significant peaks in less dense material conforming to the areas of contact between layers of soil.

In order to reduce these structural artefacts the effect of thickness of the layers during the preparation of microcosms was tested. For this, another set of microcosms was prepared at the same bulk-density and with the same aggregate size as the previous one. Soil was compacted in layers either 1 cm or 0.5 cm thick and this was compared with the entire volume compressed in one go (Fig.2.2). A new larger piston, comprising a screw cap with a diameter of 3.7 mm of a large 50 ml Fisherbrand centrifuge tube, was used in an attempt to improve compression and to eliminate differences in compaction near the edges of the rings. Special care was taken to avoid rotation or tilt of the piston to reduce deformations of soil layers. Radiographs of these microcosms showed that the most uniform structure was obtained with compression of the whole volume in one go, evidenced by absence of layers of lower density within the sample (Fig.2.2.). However this method also produced density gradients as the packing of the soil on the top of the microcosm where the piston was used was denser than the soil in the bottom part. In addition this method of compression would require a different inoculation method for fungi because the method preferred in this thesis places poppy seeds colonised by fungi on top of each layer of soil to ensure more homogeneous colonisation of soil from multiple sites of inoculation (see Chapter 2.4.1).

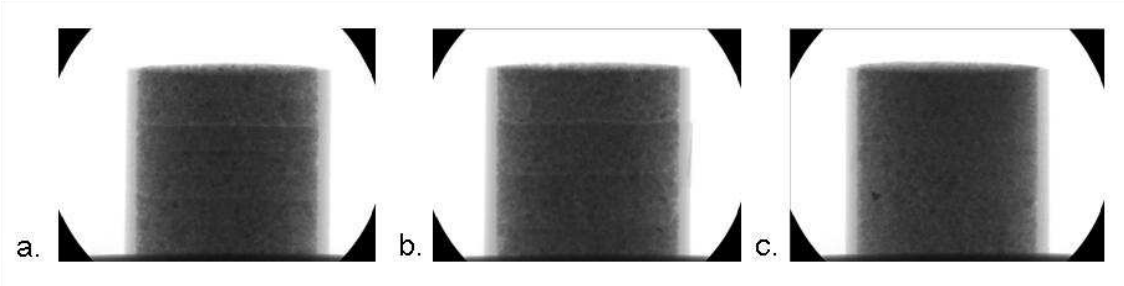

Fig.2.2. Attempt to reduce the inconsistency in soil structure - microcosms with soil packed into PVC rings, 4 cm high and 4 cm diameter with use of 0.5 cm layers of soil (a), 1cm layers (b) and with the whole volume of soil compressed.

Regions of lower density were possibly created between two packed layers because of the flat surface of the piston which could create a flat layer of compacted material. This caused insufficient contact between the compressed soil and material from the layer above. This issue was resolved by gently loosening the top surface of each layer with a scalpel before loading and compressing the material for next layer. The final result was a more uniformly packed microcosm without significant changes in density (Fig.2.3). The plot of greyscale values did no longer show any significant peak values.

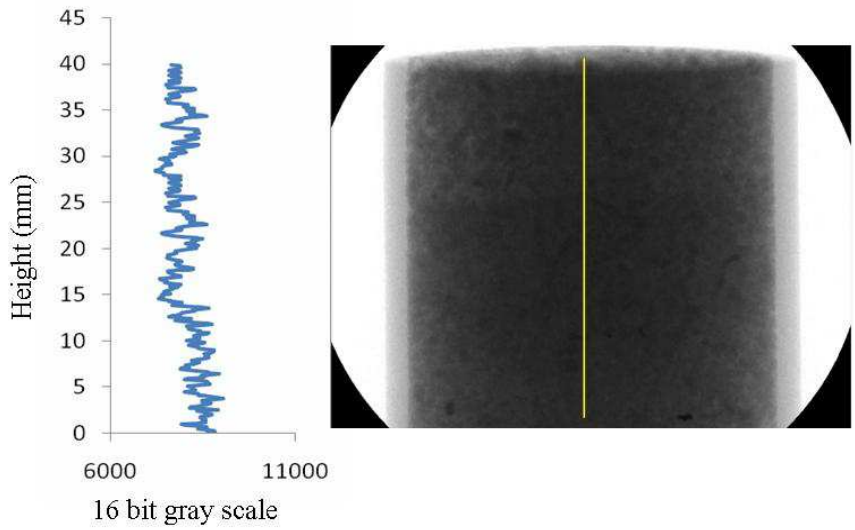

Fig.2.3. Microcosm with a uniform structure obtained by improving the contact between the layers of soil.

2.4. FUNGI IN SOIL

2.4.1. Fungal inoculum

We used the ubiquitous soil plant pathogen *Rhizoctonia solani* R3 Kühn AG group 4 (IMI 385768) as a saprotrophic fungus representative for other saprotrophic fungi (Otten *et al.* 2001, Crawford *et al.* 2011). Fungal colonies were maintained on weekly basis on PDA petri dish plates (OXOID Potato Dextrose Agar 39 g/l of tap water) or on PDA slopes in vials stored in fridge and renewed every month to minimize the risk of contamination or loss of stock cultures on plates.

R. solani was introduced to repacked soil microcosms as colonized poppy seeds (*Papaver somniferum* L.). Poppy seeds were chosen to act as inoculum instead of small agar cores, as they are a richer source of nutrients and carbon and they are not so easily available for bacteria. Before colonization with fungi, 10 g of poppy seeds with addition of 200 ml of water were autoclaved twice with 48 h interval. Sterile poppy seeds were stored in fridge till further use. Fungal inoculum in the form of a 0.7 mm core from the growing edge of a colony was placed on a PDA plate and incubated at 23^{o}C for 3 days (Harris *et al.* 2003). After this period of time poppy seeds were sprinkled over the surface of the PDA plate with the actively growing fungal colony and placed in the incubator for another 3 days at 23^{o}C. During this period *R. solani* colonized the poppy seeds. During packing of soil microcosms three poppy seeds were placed on top of each surface of compressed soil, apart from the bottom and very top one. These soil microcosms were then incubated for 5 days in an incubator in the dark at 23^{o}C.

2.4.2. X-ray effect on fungal colonies

To quantify the effect of fungal growth on soil physical structure X-ray microtomography was used. Hence it was necessary to quantify the effect of X-ray dosage on the radial colony growth of soil-borne fungi as *R. solani*. For this work we used two isolates, namely AG 2-1 (referred to as R5) and AG 4 (referred to as R3).

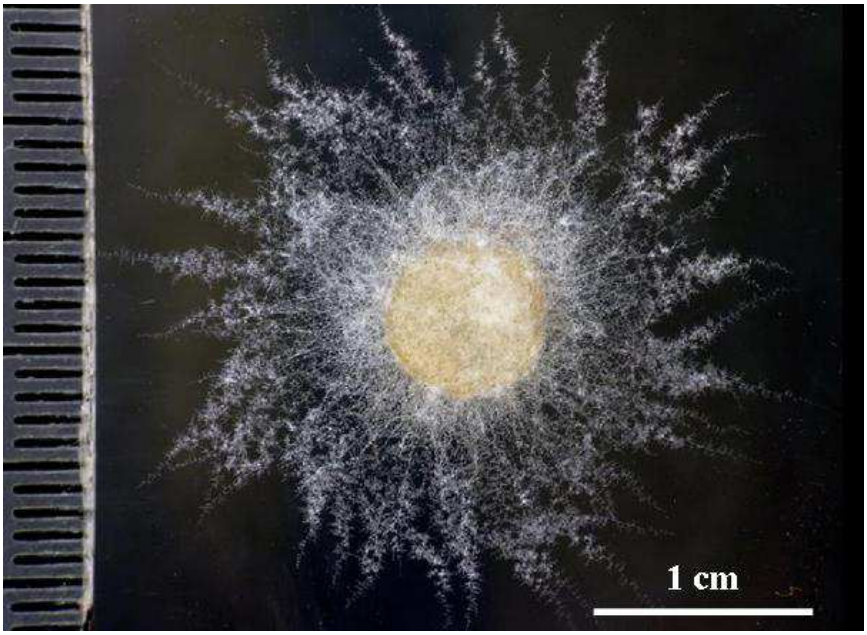

Fig. 2.4. Measurement of fungal colony diameter on Petri dish with Potato Dextrose Agar (PDA).

A 0.7 mm core from the growing edge of 4 day old fungal colony was placed on a PDA plate and incubated at 23^{o}C in the dark. After 24 h of growth, the plates were exposed to radiation in the Benchtop system for 60 minutes at settings 95 kV and 70 µA. For each fungal isolate, there were 13 replicates and the colony diameter was measured before exposure, and from then onwards measurements were taken twice a day. Because colonies were growing fats the overnight period was leaving too large gap between measurements. Therefore the experiment was repeated with decreased amount

of nutrients in PDA to 10 % (3.9 g of PDA per 1l of tap water), and the experiment was repeated as above.

There was no visible difference in fungal growth and no significant differences in the colony radius after 4 days from exposure to radiation (Fig.2.5.).

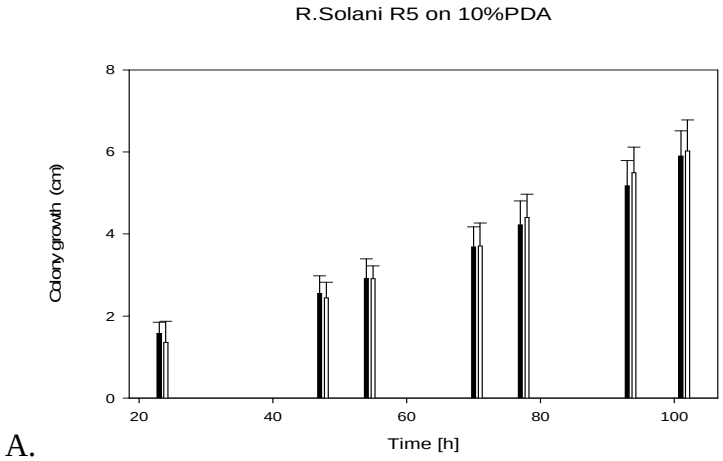

A.

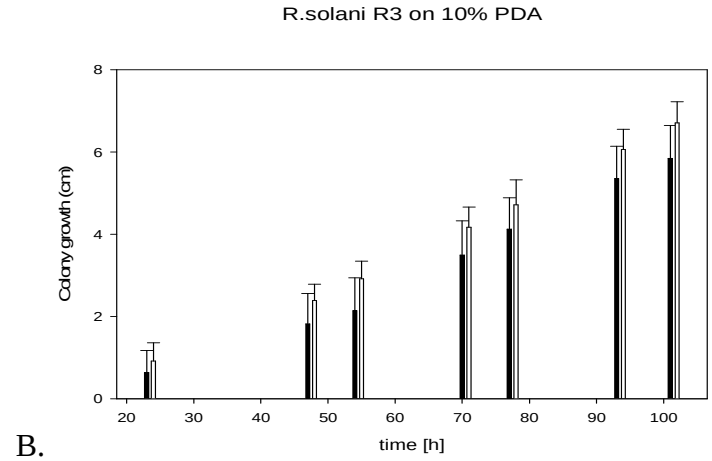

B.

Fig. 2.5. Diameter of fungal colonies exposed to X-ray radiation for A. *R. solani* R5 and B. *R. solani* R3 on 10% Potato Dextrose Agar (PDA) Black corresponds to colonies exposed to radiation, white to control samples. Average values of 13 replicates per treatment and standard errors are represented.

2.4.3. Quantification of fungal biomass.

Upon local inoculation it was essential that the fungus colonizes the entire soil microcosms. To test this, we quantified how well microcosms became colonized with fungi. Two destructive methods were used for this assay:

1) Ergosterol assay – a measure of fungal biomass
2) Colony forming units from aggregates – quantifying the fraction of aggregates colonised by fungi.

Details of these assays are given below.

2.4.3.1. Evaluation of biomass by Ergosterol assay

Ergosterol is a compound which is characteristic for fungi and some microalgae. Ergosterol can be found in the phospholipid layer of cell membrane and is not species specific (Montgomery *et al.* 2000). The measurement was carried out for 4 microcosms (2 inoculated with fungi, incubated for 5 days and 2 controls). Each was divided into 3 parts (top, middle, bottom). There were five replicates for each soil layer. Extraction of ergosterol from the soil samples was performed following Ruzicka (1995).

In the first step of this method, 0.2 g of glass beads were weighed and placed into 2 ml microcentrifuge tubes, one for each sample. Then 0.2 g of soil and 400 µl of methanol : ethanol (4:1) were added to each tube and incubated for 2 hours at 4 °C (samples were stored in the fridge). After incubation the samples were placed in a container with ice to maintain low temperatures, and 1 ml of iso–hexane : Propan-2-ol (98 : 2) was added to each sample. The sample was homogenised with the use of a Mini BeadBeater 8 (Biospec Products), at the high power setting for 1 minute. The appliance shakes and rotates the samples to break down soil particles and mix with chemical

compounds. After homogenisation the samples were allowed to settle on ice for 15 minutes and then centrifuged for 2 minutes at 13000 RPM and 4 °C (Eppendorf Centrifuge 5451 R). As the result the samples contained three phases: soil material at the bottom of the tube and two phases of liquid. The very top phase contains the solution of ergosterol and this layer was carefully removed with a syringe. The content was filtered through 0.2 μm PTFE microfilter (Whatman) into a screw–cap tube. In this form samples were stored in the freezer (-20 °C) until the HPLC analysis. Ergosterol standards (Sigma-Aldrich) of 0.25, 0.5, 1, 1.5, 2 ppm (parts per million) were used as reference to calculate the ergosterol content in soil samples. The results were divided by dry mass of soil used for extraction and expressed as the ppmor μg of ergosterol per 1 g of soil. Erogosterol content was over 8 times higher for inoculated samples than for controls (sterile soil without fungal inoculum) (Table 2.1.) suggesting successful fungal colonisation.

Sample	**Ergosterol (ppm) ±se**	**ppm/g of soil**
Inoculated	2.15 (0.13)	13.43
Control	0.26 (0.05)	1.62

Table 2.1. Ergosterol content for the soil inoculated with *R. solani* and controls.

The ergosterol content in samples inoculated with *R. solani* of 13.43 μg per 1 g of soil was significantly higher than the ergosterol contents of 0.38 to 0.46 μg of ergosterol per 1 g of soil, quantified by Stefani (2010) for natural myccorhizal soils. Control samples were not free from ergosterol, containing 1.62 μg of ergosterol per 1 g of soil and were also higher than values reported for natural myccorhizal soils. However this method of biomass evaluation determines the total amount of ergosterol and does not distinguish between fungal species or between alive and dead hyphea. Therefore despite the

sterilization of soil and lack of fungal inoculum there were still traces of ergosterol in control samples.

2.4.3.1. Evaluation of biomass by Colony forming Units

A second method to evaluate fungal colonization of the soil was quantification of colony forming units. This method allowed a measure of the number of successfully colonized soil aggregates to be estimated by using a semi selective medium to quantify the colonisation for each aggregate placed on it. The aggregates were obtained by breaking and sieving microcosms through a sieve with a 2 mm diameter. Aggregates were plated onto semi selective medium for *R. solani* with 5 replicates per treatment (n = 9 aggregates per plate). This media was prepared by dissolving 2 g of $NaNO_3$, 1 g of KH_2PO_4, 0.5 g $MgSO_4$. 7 H_2O, 0.5g KCl, 0.01 g $FeSO_4$ .7 H_2O (prepared as 0.1 g of $FeSO_4$ dissolved in 10 ml of H_2O just before use), 12 g of agar (if the medium will be poured into plates) in 1 l of tap water. This was followed by sterilisation by autoclaving with a 15 minutes hold time and subsequently cooling down to room temperature. The preparation consists of two stages because compounds added in the second stage are sensitive to temperature and would not retain their ability after autoclaving. The final stage consists of addition of 50 mg of chloramphenicol, 50 mg of streptomycin sulphate, 1.38 ml of diluted 'Filex' (prepared as 1 : 72000, Filex : H_2O) and 0.4 g of gallic acid. The last compound, gallic acid is the component which makes it semi selective for *R. solani*, as this is one of the species that can use it as carbon source. Change of colour of the medium from clear to brown indicates the presence of colonies of *R. solani* (Fig.2.6.). After 3 days of incubation almost 100% of aggregates were colonized for samples from soils inoculated with *R. solani* compared to 11 % of CFU for control microcosms (Table 2.2.).

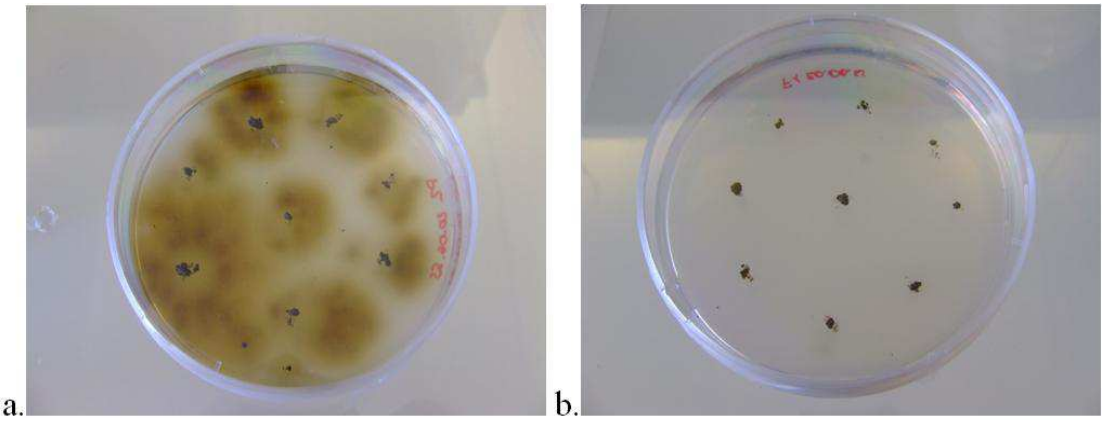

Fig. 2.6. Aggregates plated on semi selective medium after 3 days of incubation. Colonized soil (a) changes colour to brown in presence of *R. solani*. Aggregates from non-colonized soil (b) don't show activity of *R. solani*.

Colonised aggregates from microcosms inoculated with fungi (%)					
Top layer	100	100	100	100	89
Middle layer	100	100	100	100	100
Bottom Layer	100	100	100	100	100
Colonised aggregates from control microcosms (%)					
Top layer	22	11	0	33	22
Middle layer	0	0	11	0	22
Bottom Layer	0	33	11	11	0

Table 2.2. Colony forming units showed successful colonisation of microcosms with *R. solani* with almost 100% of aggregates creating colony forming units.

2.5. X-RAY MICROTOMOGRAPHY SYSTEMS USED IN THIS STUDY.

For non-destructive visualisation and quantification of the internal soil structure X-ray microtomography (computerised tomography – CT) was used. The SIMBIOS centre has currently two of X-ray CT systems, both supplied by NIKON metrology: a Benchtop and HMX 225 (http://www.nikonmetrology.com). General background to X-ray and lab-based systems was given in Chapter 1. Here the specific details of equipment and methods used in this study are given.

The Benchtop CT system is equipped with an X-ray source capable of generating a cone beam with a maximum energy of 160 kV, with a current range 0 - 1000 µA. The X-ray gun in this system has a 5 µm focal spot reflection target, with a single material (Molybdenum). The detector of this system is based on a CCD chip, with a maximum field of view of 20 x 20 cm and geometrical magnification up to 100x.

The HMX unit is capable of generating an X-ray beam with a higher energy – up to 225 kV, with a current between 0 - 2000 µA. Similarly to Benchtop, the X-ray gun has a 5 µm focal spot reflection target, but with a choice of target material between Molybdenum, Copper, Silver and Tungsten. The more powerful energy gun results in the ability to penetrate denser objects and different target materials. This system is equipped with a different detector type: a Varian 2520 which is a 14 – bit amorphous silicon flat panel allowing scanning objects with a maximum size of 25 x 20 cm and a magnification up to 160x (very close to the X-ray source). Unlike the Benchtop system, the HMX unit has a built in air-conditioning system that helps to reduce the effect of heat generated during scanning inside the machine (http://www.xtekxray.com).

2.5.1. Image acquisition.

Both CT systems use InspectX (http://www.nikonmetrology.com/products/x-ray_and_ct_inspection/x-ray_and_ct_inspection_software) software for controlling the process of image acquisition. The latest version of this software suite (Metris XT 1.6, version 1.60.3509.26893) was used in this thesis. It covers all steps of image acquisition from setting the initial parameters of the scan, capturing radiographs to reconstruction of 3D volumes of the scanned object.

Choosing the correct settings for each material is a complex process. When adjusting the CT scan settings, the operator has to take into consideration individual characteristics of the sample material and find the balance between the desired quality of data and amount of time available. The first step in image acquisition is positioning the sample. This defines the resolution of the scan and path of X-rays penetrating the object. There is a trade off between resolution and magnification: the further samples will be placed from the radiation source the smaller the magnification and higher the resolution will be. On the other hand moving objects towards the X-ray gun will result in an increase of magnification and resolution of the scan. The operator needs to ensure that the object will stay in the field of view throughout the scan as the sample rotates 360^{o} during the scan. Especially at high magnifications the object needs to be placed as central on the holder as possible to avoid blurred details of the image. In case of irregular shapes it is also desired to manipulate the position of the object on the holder to reduce differences in length of volume being penetrated by the beam to avoid the noise and artefacts caused by insufficient or different penetration of the sample with X-rays.

Once the sample has been positioned, the characteristics of the X-ray beam need to be selected. Adjusting the energy of the X-rays defines the characteristics of the generated beam. The voltage defines the penetrating power of the beam whereas the current defines the number of X-rays passing through the sample. It is important to ensure that the beam has enough energy to penetrate the longest path through the volume of the sample and is captured by detector, while avoiding over-saturating the image. The operator can control these settings by observing changes in gray scales presented on a histogram during live viewing of the radiograph of the sample. The gray scales in the darkest point of the specimen should be higher than the gray scale value for

black by at least 15 % of the gray scale values assigned to the brightest area (white) of the field of view (Hsieh 2009).

Both available CT systems are generating a polychromatic beam. This means that only the maximum energy of the beam can be specified, and that the generated beam has a wide spectrum of energies. The chosen voltage is the energy used to accelerate electrons from the heated filament through an anode ring along the beam tube to finally hit material of the target. During this sudden deceleration, X-rays are being generated, and the nature of this interaction with the target defines the energy of each X-ray produced.

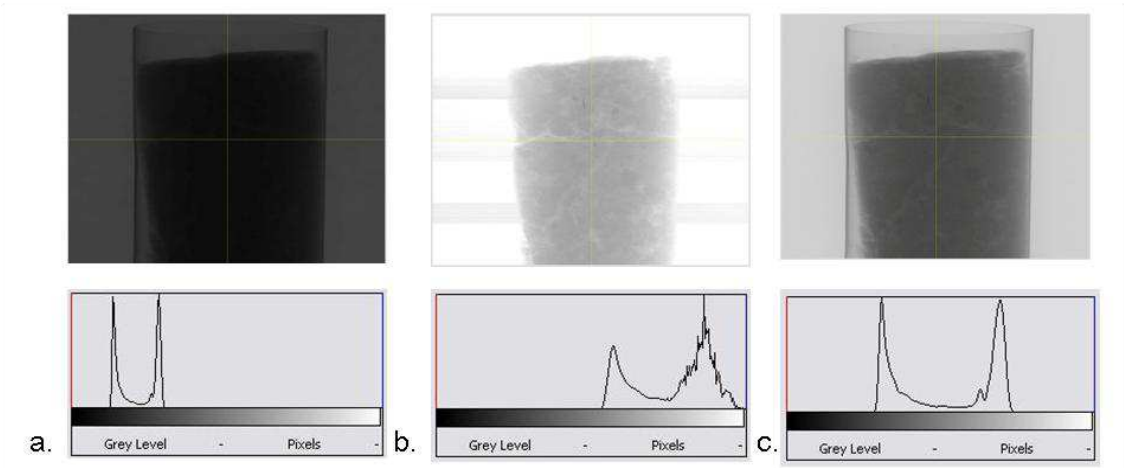

Fig. 2.7. Soil sample in live view with gray-scale histograms at different settings, adequately: (a) low energy of X-rays (60 kV), insufficient penetration of sample, many dark voxels (b) saturated conditions, high energy levels (180 kV), and many bright voxels, (c) correct distribution of gray-scale peaks in the histogram (115 kV). Gray scale is based on 16 bits.

X-rays with different energy levels interact differently with given materials. Lower energy X-rays are more likely to be absorbed by dense objects as they are stopped more efficiently than the high energy ones. However reconstruction algorithms assume that all X-rays generated have the same energy, and use the decrease in X-ray intensity at all angles to calculate the density of an object and length of path.

Insufficient penetration by low energy X-rays leads to the increase in mean energy of X-rays passing through the sample (attenuated). As a result of this the reconstructed volume will contain fake differences in material density, an effect known as beam hardening. This can be reduced by the use of suitable filters, which mounted in front of X-ray source reduces the flux in the energy spectrum of the beam. By using the Aluminium filters with different thickness, it was possible to cut off the low energy X-rays, filters decrease the differences in contrast between transmitted and attenuated X-rays. Generally the choice of filter type depends on the material of the sample that is scanned. It is preferred that a filter has similar material characteristics to the object scanned. The thickness of the filter should be adjusted to avoid saturation of background with X-rays which are not going through the sample but are directly absorbed by detector (unimpeded).

In order to achieve sufficient levels of detail at the desired resolution, it is important to acquire the correct number of radiographs (projections). To prevent interpolation of data in edge voxels, the required number of projections needs to be adequate to generate volumes with angular increment not larger than 1 voxel. The minimum number of projections is subject to the size of specimen and can be calculated according to equation:

$$X = N \times \pi/2 \qquad [2.1]$$

where N stands for the size of image of the sample in voxels in horizontal plane. Choosing a higher number of projections will not introduce more details, but will improve signal to noise ratio in the reconstructed 3D volume. It is also possible to increase the number of frames per projection (2 FPP by default), which reduces the

noise by averaging the gray scale values over the acquired number of frames corrected for black and white referencing images. Finally the exposure time can be adjusted by selecting the number of frames per second (FPS). Reducing the number of frames per second (1 FPS by default) is recommended for operations with use of low energy X-rays, increasing the exposure of the sample to X-rays also improves signal to noise ratio.

For the reconstruction the centre of rotation needs to be determined. The centre of rotation defines the axis about which the whole sample rotates during acquisition. This is a crucial parameter of the reconstruction algorithm. Centre of rotation is defined during the scan set-up procedure in Inspect-X software automatically, calculated for a slice of choice or calibrated from a rod replacing the sample prior to scanning. The latter is recommended for irregular shapes and small samples. It can also be controlled manually or corrected during the reconstruction process with use of CT-Pro reconstruction software (Inspect X user manual, Ramsey 2005). This is sometimes required if identical scans need to be performed for the same sample.

The last step of the acquisition involves defining the volume which can be automatically reconstructed after completed scan. Two images of the specimen are being collected, at 0^o and at 90^o, by adjusting the boundaries of a region of interest. This has no influence on the resolution. Reconstruction of 3D representatives of samples starts automatically after each scan, unless specified differently, and generates input volume files which can be imported into Volume Graphics Studio Max (VGSM) for further analysis. The size of the volume depends on the sample size and number of projections but can be approximately 0.5 – 15 GB for the Benchtop and HMX respectively.

2.6. IMAGE ANALYSIS

The sections below describe the various methods that have been used in this thesis in more general terms. For each of those methods specific selections and setting often need to be made for specific samples. Where appropriate such setting and selections are described in subsequent chapter. This section contains broader description of principles and generic steps commonly used in X-ray CT of soil samples and the results of initial tests of these methods.

2.6.1. Quality assessment and preparation of image stacks

Reconstructed 3D datasets scanned by the CT system were opened or imported by dedicated software Volume Graphics Studio Max (VGSM, current version 2.1.). Opening the volume file will set default settings, whereas importing the volumes, which is the preferred and used in this work, allows specifying the exact resolution (voxel size) of the volume and the range of grayscales based on the histogram. VGSM is sophisticated software allowing visualisation, segmentation and quantification of samples in 3D. It is capable of working with volume files generated by reconstruction software or with stacks of images which can be imported and re - combined into 3D structures.

In the first step of the image analysis process, VGSM is used for visualisation of scanned and reconstructed volumes to examine the quality of scan. In case a scan met the requirements, 3D volumes were converted into image stacks for further processing with software packages not compatible with large volume files such as thresholding algorithms specifically developed for soil samples or java based plugins for ImageJ analysis tools to quantify soil samples. 3D volumes can be sliced in one of the three perspectives, with specified size of the image (in pixels), saved as stacks of image files

in one of available formats (with the most frequently used: *.tiff, *.bmp, *.JPEG) (http://www.volumegraphics.com, Heidelberg - Germany).

2.6.2. Defining the image method for thresholding soil samples.

Characterisation of soil properties often requires thresholded (binarized) images. Thresholding is the crucial step of image analysis and probably most uncertain one as it is the process of deciding upon values of gray scales which distinguish between pore space and solids. There are a number of ready-made algorithms for thresholding, however none of them were designed specifically for handling such heterogeneous material as soil, hence there is no uniform and robust method accepted worldwide (Baveye *et al.* 2010). There was however a need to select a consistent method of thresholding samples for the purpose of the work carried out in this thesis. The desired thresholding method should be able to produce reliable and consistent outcomes in relatively short time. The test of a range of available thresholding methods was performed in order to select the most suitable one for this work.

The methods considered to be used in this thesis are the selection from available and commonly used approaches at the time the work in thesis was conducted. As time progressed and newer methods became available,the method of analysis was accordingly adapted so that the most up-to-date methods required and suitable to analyse my samples were used throughout the thesis when possible. The approaches used could be divided into three groups: manual, histogram based algorithms and adaptive thresholding methods (Sezgin and Sankur 2004). They are briefly presented below:

1) Manual thresholding: This requires most input from the operator, hence is the most subjective method. The user-defined choice of a threshold values is based on visual comparison of the non-thresholded sample in gray scale and the sample being thresholded. This is done by every operator in a different way. In this thesis the following procedure was applied: the threshold value finally applied is an average of 5 values set individually for 5 different slices within the image stack (Baveye *et al.* 2010).

2) Histogram based algorithms: these include fully automated selections of thresholding values from analysis of the image or stack histogram. Two algorithms were selected for the tests, both running as plug-in extensions in ImageJ and successfully used in previous research.

a) Isodata – an iterative calculation, primarily dividing the histogram into two parts using a value of half the maximum dynamic range followed by a calculation of mean values of voxels corresponding to pore space, and separately to the solid. The threshold value is an average of these two means. The process is repeated until the final and starting threshold values are the same (Ridler and Calvard 1978).

b) Li algorithm – based on analysis of gray scale histogram, uses the one-point iteration scheme to minimize cross entropy between the thresholded and non thresholded image (Li and Lee 1993).

3) Adaptive threshold – these algorithms divide datasets into segments and set the threshold value for the segment depending on the gray scale values of voxels in the neighbourhood with user defined input parameters (such as offset, global neighbourhood size). Global threshold values (applied for the whole dataset) use a mean

value of values for segments. A macro written to run under Karl Zeiss KS300/400 software (originally for microscopy images processing purposes) was used for the purpose of this tests. This macro was developed specifically for a very noisy data set, one of the first datasets acquired at Argonne Photon Source. Therefore the original code contained a lot of image pre-processing procedures aiming to reduce noise including low pass and sigma smoothing procedures. However datasets acquired for the test were of far better quality with a minimum of noise hence the pre-processing part was removed, preserving just a code required for stepwise calculations of threshold value (Nunan *et al.* 2006).

All thresholding methods were tested on the same dataset representative for samples in my study. The image stack (300 x 300 x 300 pixels) of microcosms with known density within a range between 1.2 – 1.6 g/cm^3, were scanned on the HMX system and reconstructed at a resolution of 29.4 µm. Expected porosity values were known from previous analysis of these samples by Harris *et al.* (2003). However these values were estimated from this sections and include pores with diameter below the scanning resolution. The performance of various thresholding methods was based on comparison of the porosity values derived with the use of ImageJ for each thresholded dataset with the real porosity as well as the expected trend with increasing bulk density.

The manual method was the most time-consuming and the most subjective approach. However, it was the most consistent one and samples thresholded manually produced porosity values closest to the expected data (Fig.2.8.), and shared a trend in agreement with data from Harris *et al*. (2003).

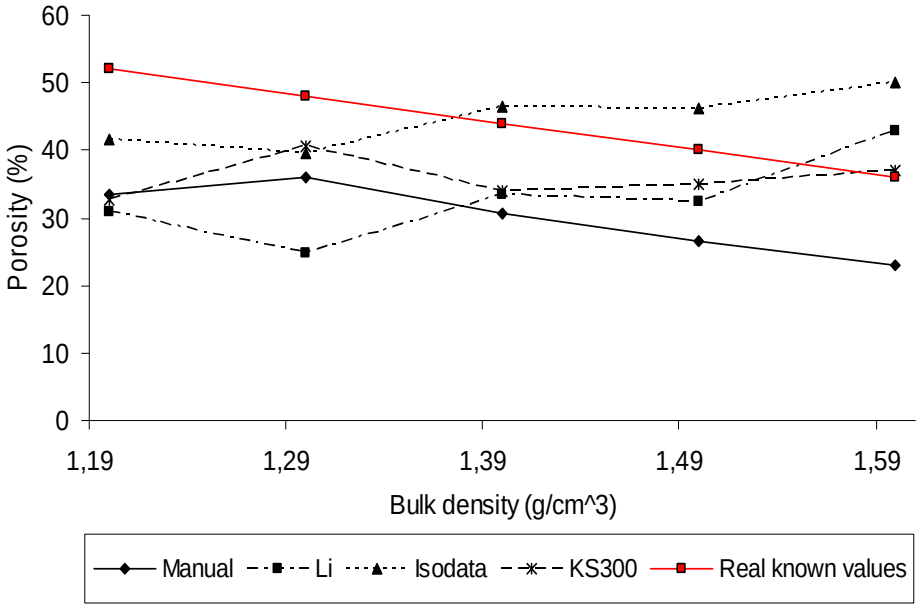

Fig. 2.8. Porosity evaluation for each bulk density treatment with 4 different threshold methods applied. Known data are taken from Harris *et al*. (2003).

Li and Isodata algorithms were the fastest ones and did not require any user input but failed to produce thresholded datasets which would follow the trend of real porosity values.

KS300 method was the most accurate, partly automated approach. Porosity values of datasets were very close to real data and trends of porosity values almost follow those of the manual thresholding. Slight variation might have been caused by the fact that for the test purposes only one offset value (the difference between values corresponding to pore and solid) was selected, which could be set individually for each treatment (density in our case). The only downside of this method is that because of software limitations it does not allow to set neighbourhood size to larger than 255 pixels and the software had issues with importing some of the images from the stack turning them into 100% pore space or all solid which corrupted the analysis. However for those data sets for which it worked, it produced consistent datasets with reasonable porosity

values, and it detected small pores and thin valleys better than any other method tested (Fig.2.9.)

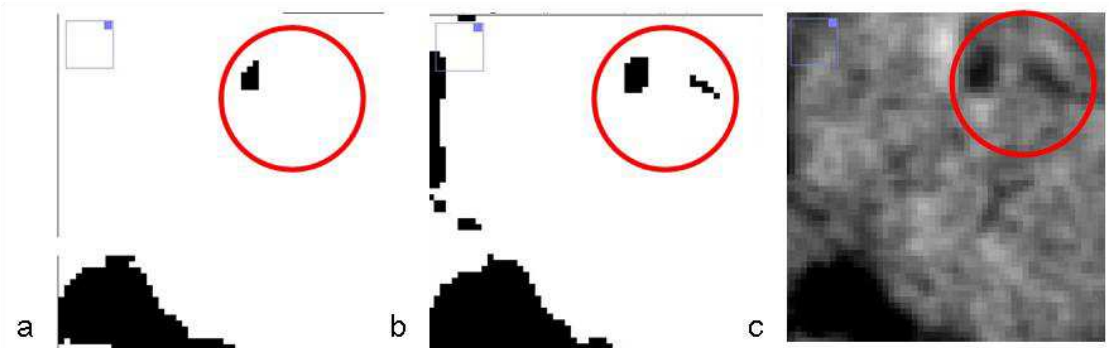

Fig. 2.9. Detection of thin valleys and small pores structures is better by KS300 than by any other tested algorithm. From the left respectively: a) poor detection of small pores by manual threshold, b) an example of KS300, c) non thresholded original gray-scale image.

Upon these result of the comparison of various thresholding algorithms it was initially decided to use manual threshold for the analysis in this thesis despite the well understood shortcomings for that method. It produced the most consistent results despite being the most subjective method. Manual method was also proven to be a reliable method in the study by Baveye *et al.* (2010), who compared threshold methods from various experts worldwide. Effectively the manual thresholding was used to binarize datasets in Chapter 4 and 7.

In parallel to the progress in the experimental work new methods of thresholding have been developed both in SIMBIOS and other groups. One of them was an automated method based on edge detection, using gradient masks defined as regions of interest for determining the threshold values. Since this method focused on the soild/pore interface it also applied median filtering as an aid to identify transition of phases (Schluter *et al.* 2010). It was decided to repeat the evaluation of threshold algorithms, also to check how the manual thresholding changed over the time, as the

perception of what is and what isn't pore could have changed over time and with the experience gained in image analysis methods. Comparison included manual threshold, isodata algorithm (built in to ImageJ) and the new in-house developed method using gradient masks. Thresholding was carried out on the same set of the samples, packed at different bulk densities ranging between 1.2 – 1.6 g/cm^3. There were two significant outcomes of that experiment. First was that the manual method proved again to be subjective to user. The same datasets, thresholded manually by the same operator after 2 years of experience in image analysis had similar trend in porosity values over densities range. However the porosity values (resulting from the thresholded data) differed from the ones generated for samples in previous experiment. Schluter *et al.* (2010) algorithm produced consistent results, closely reflecting the trend of control porosity values (known porosity values in the soil microcosms) (Fig.2.10.). Since this algorithm is fully automated and doesn't require any user input it replaced the manual method in the remaining analysis in Chapter 6.

This resulted in the use of two different thresholding methods in this thesis. Analysis of an early scanned datasets is based on manual thresholding, whereas the others were binarized by automated method when it became available. Effectively the manual threshold was applied in Chapters 4 and 7, whereas Shluter algorithm was used to binarize datasets analysed in Chapter 6.

However all these algorithms mentioned above were limited to analysis of regular, cubic samples. In Chapter 5 of this thesis we looked at structural characteristics of the whole soil aggregates thus there was a need for thresholding method coping with irregular shapes. For this purpose we adapted the protocol for segmentation of 3D volumes in VGSM 2.1 (www.volumegraphics.com, please see Chapter 5 for details) to act as a thresholding method.

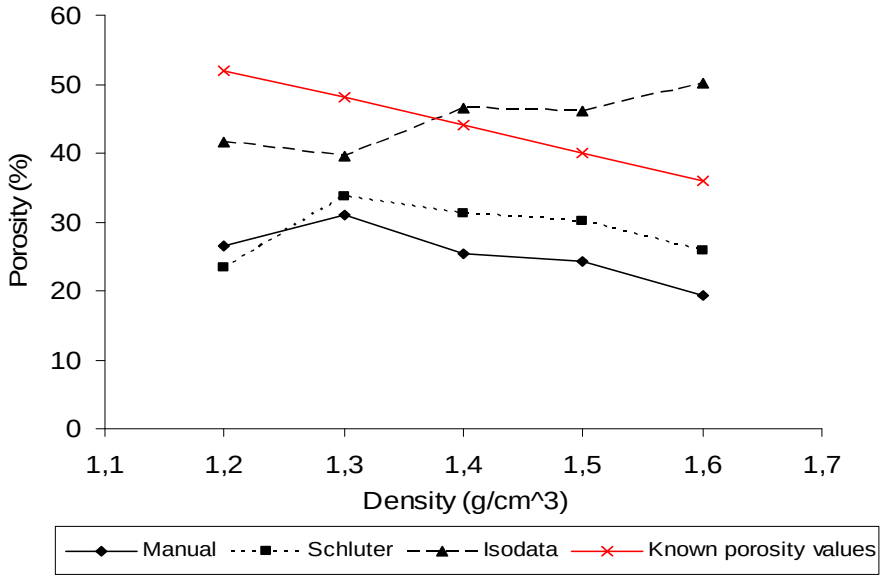

Fig. 2.10. Total porosity values for soils packed at different bulk densities, derived from image stacks thresholded with 3 different algorithms. Known data are taken from Harris *et al*. (2003).

2.6.3. Volume segmentation in 3D using VG Studio Max 2.1

Segmentation of the chosen features from the volume of soil samples according to their gray scale values is also possible with use of VGSM. The method of segmenting out the volume of interest and its analysis with the use of VGSM 2.1 is described here for an example of pore network extraction and characterisation. Already thresholded (binarized) samples (sized 300 x 300 x 300 voxels) were used in this experiment. Binary image stacks were imported into the VGSM and the physical size of the voxels (29.4 µm) was specified to ensure the output will be presented in a correct units. The first step to segmenting out the pore space was to create a border which prevents the selection tool from including the background. A rectangular selection tool was used, to create the cube surrounding the sample volume to create the border between the analysed object

and the outer space. A square covering each face of the sample was applied 1 slice under the surface (square regions of interest at slice 1 and 298 at every orientation).

Within such a closed volume, the region grower was used as a selection tool. It was set to avoid other regions of interest to prevent selections expanding to the outside of the analysed area. Region grower tool uses a flooding algorithm to create a selection starting from a picked voxel. The selection grows within connected voxels if their gray scale values fall within the user determined tolerance in relation to value in the starting point. To select the total pore space and not only the largest connected pore cluster, solid phase was selected first as it's most likely to be 100% connected. A new region of interest (ROI) was then created. Inverting this selection created the new ROI consisting of the total pore space of the soil sample. The new ROI was then extracted into a new 3D object ready for further analysis.

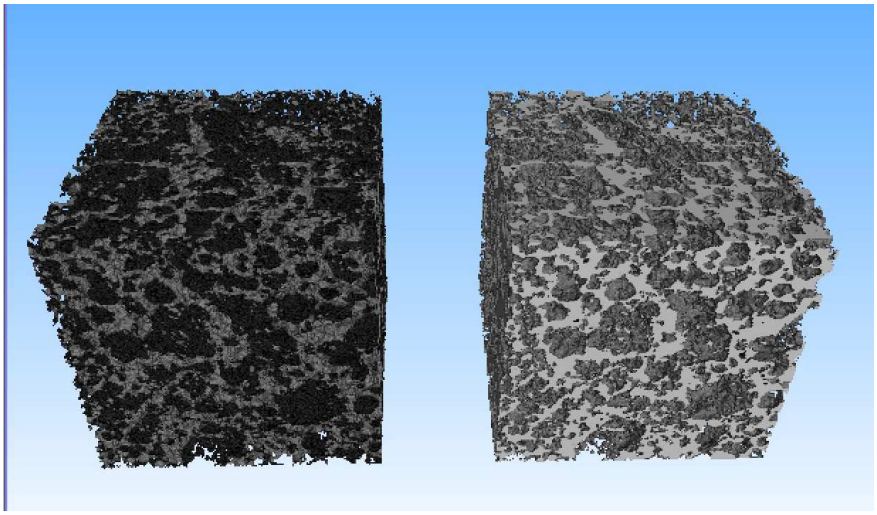

Fig. 2.11. Segmented and visualised – solid phase of soil microcosm (left) and pore space (right) – ready for quantification.

2.6.4. Quantification of physical properties of soil structure

3D volumes converted to image stacks and subsequently thresholded were used in further steps of image analysis. We quantified descriptive factors such as total porosity, pore connectivity, pore size distribution, surface area and volume of pores. There is a wide range of software packages which are adapted for quantification of soil structure (Chapter 1.5 for details), with the following ones selected for the purpose of this work: ImageJ, VGSM and an in-house developed script based on Minkowsky Functionals (Schluter *et al.* 2011, Falconer *et al.* 2012).

One of the programs dedicated for image analysis is freely available ImageJ (rsbweb.nih.gov/ij). In its basic form ImageJ offers a wide range of standard image analysis tools such as various modes of selecting and cropping image stacks to a region of interest, standard measurement tools (length, angles, and surface area in 2D) and basic adjustments of contrast/brightness. However the reason for choosing ImageJ is that it is also equipped with a built-in range of noise reduction filters, thresholding algorithms and can be extended by Java based plugins such as in house developed SCAMP, dedicated for characterisation of soil properties (Pajor *et al.* 2010, Crawford *et al.* 2011). This plug-in quantifies the following physical properties of 3D porous media:

- Porosity – as the total number of voxels identified as pores divided by total volume of the sample. This represents the total volume of pores in a soil sample within which all biological processes take place.
- Pore space connectivity – it makes use of a burning algorithm to check if directly neighbouring voxels belong to the same connected pore volume. Individual pore clusters are then analysed if they are connected with each other. This function allows also separating the largest connected pore volume to a separate image stack.

- Pore sizes distribution – calculates pore radius by simulating a growing sphere at every voxel of pore space till it reaches the boundary with solid phase, then interprets the result as the distribution of the radii of the spheres.

VGSM has a built in volume analyser tool which can be used to quantify the physical properties of a volume of interest such as segmented out pore space or a solid phase of soil sample. Connected component analysis is part of the volume analyser and is based on defect detection in VGSM. It detects and analyses connected objects within selected area at specified grayscale values. The output is presented as a table listing all detected objects together with their properties, according to the size of the objects. The analysed features include: total volume of object in mm^3 (interpreted as volume of pores), voxel count of a given object and total surface. This output is saved to a VGSM report or copied to an excel spread sheet.

Additional pore network characteristics such as material porosity, surface density, mean curvature, total curvature and Euler number were derived as Minkowski functionals with the use of in house developed software (Falconer *et al.* 2012). Minkowski functionals are known to be a range of geometrical descriptors of 3-D structures presented as binary datasets. Surface area is proportional to a number of transitions between solid phase and pore. This number was quantified by an algorithm which first finds pores, defines their direction and derives surface characteristics based on radius of spheres fitted in the given pore (Vogel *et al.* 2010).

2.6.5. Visualisation of the 3D volume – creating an animation.

Rendered and segmented volumes were also saved as animations, in particular to aid visual interpretation as well a presentation of results. Creating an animation requires defining the trajectory of the camera in 3D, time and number of frames used to render

animation. All these features can be adjusted by switching to the animation tools and keyframer mode in VGSM. By default the camera performs simple 'fly', divided into 4 timesteps around the sample (Fig. 2.13).

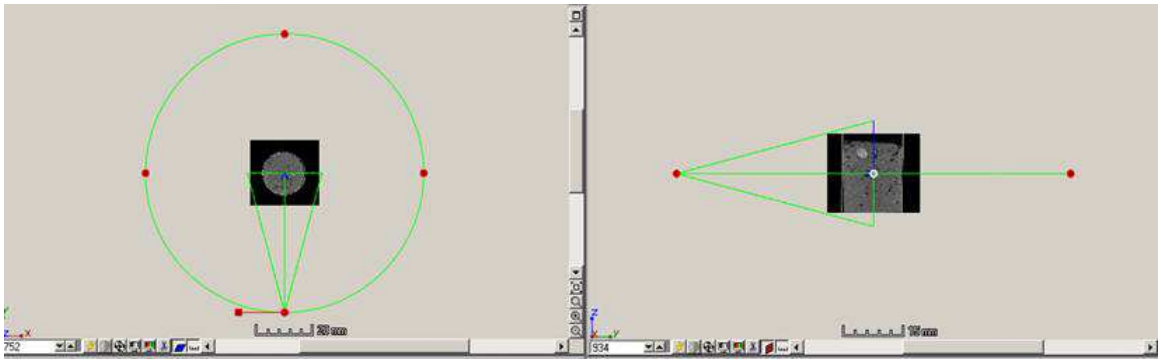

Fig. 2.12. Default camera trajectory (VGSM 2.1.) for circular fly around the 3D representative for soil microcosm, view from top (left) and side (right). Green line corresponds to the movement of the camera, red dots represent timesteps.

The operator can define the total length of an animation and the speed of the camera movement independently from the number of timesteps. The number of timesteps can be increased or decreased upon requirements and allow adjusting the trajectory of camera (if not using one of the standard built-in movements) and the displayed volume(s).

At each timestep independently one can change transparency of a volume of interest, its intensity and assign colours to given grayscale values for improved contrast of selected features. Once satisfied with the camera trajectory and properties of the rendered volumes at each timestep the animation can be saved using built into VGSM video codecs or custom imported ones. It is also required to specify the number of frames per second (FPS). With increasing FPS, the time of rendering the window also increases, but the animation has a better quality and runs smoother.

CHAPTER 3:

The influence of fungi on hydraulic properties of soil

3.1. INTRODUCTION

Fungi are ubiquitous soil organisms involved in many processes affecting soil structure, such as forming and stabilizing aggregates, decomposing organic matter and they are involved in many interactions with plant roots (Ritz and Young 2004). Fungi were described as 'engineers of soil structure' because of their ability to surround soil particles with hyphal network (Degens 1997) and glue them together with polysaccharides and gums secreted during the process of decomposition of organic matter (Schlecht-Pietsch *et al.* 1994). Ritz and Young (2004) also stated that fungi could change soil structure to the extent that they alter the path of water flow. Crawford *et al.* (2011) in their study combined experimental and modelling approaches and showed that colonisation of the soil-borne fungus *R. solani* increased the volume of pores and improved connectivity of the soil pore network. Crawford *et al*. (2011) also linked structural changes with enhanced hydraulic conductivity of soil microcosms inoculated with fungi. Hydraulic conductivity is the measure of water flow dynamics through porous material. Conductivity relies on permeability of the material which reflects structural characteristics such as porosity, pore-size distribution and pore connectivity. Crawford *et al.* (2011) used the a lattice Boltzman model (Zhang *et al.* 2005) to quantify the hydraulic conductivity of soil samples.

Fungi were identified as the main group of organisms that contribute to soil water repellence (Feeney *et al.* 2006c). Soil-borne fungi produce hydrophobic surfactants and exudates that could induce changes to soil hydraulic properties of by making soil more water repellent (Hallett and Young 1999). This can affect water run-off and accelerate the drainage of the soil. Hallet *et al.* (2001) used an experimental set-up in which they inhibited fungal growth selectively in a sandy soil, and they observed a decrease of water repellency in relation to decline in fungal biomass content. The same

trend was observed with bacteria. Feeney *et al.* (2006c) conducted a similar experiment showing that microbial activity enhanced stability of soil structure and increased water repellence. However they were unable to relate these effects with the structure of the microbial community. The effect of soil-borne fungi on soil water retention was also quantified. These measurements relate to the size, connectivity and geometry of the pore networks as well as to hydrophobicity. The water retention curve informs about the ability of soil to retain the water under the negative pressure.

Auge *et al.* (2001) and Bearden and Petersen (2000) showed that a mycorrhizal fungus, *Glomus* spp. had a significant effect on water retention. Both these papers showed that samples inoculated with mycorrhizal fungi started to drain faster than those that were not colonised. Drainage of soil at lower pressures suggested a higher number of large pores, a higher conductivity, an increased hydrophobicity or all these effects combined. Microcosms colonised with mycorrhizal fungi also showed increased soil stability. Soil samples colonised with *Glomus* spp. were more resistant to fast wetting cycles, showing fewer new cracks appearing due to fast wetting-drying cycles (Bearden and Petersen 2000). The studies by Auge *et al.* (2001) and Bearden and Petersen (2000) examined large pot samples with plant roots and mycorrhizal fungi after a long-term incubation period of 7 months and 10 weeks, respectively.

The findings of Auge *et al.* (2001) and Bearden and Petersen (2000) support the main findings by Crawford *et al.* (2011), that fungi could increase the amount of macropores and enhance the connectivity of a pore network. All three studies quantified the effect of fungal colonization after long-term incubation, typically much longer than the time it takes for fungi to colonize soil, although the effect of fungal hydrophobins on soil repellence was quantified in just 10 days of incubation (Feeney *et al.* 2006c). Studies quantifying the dynamics and the form of fungal growth in soil by Harris *et al.*

(2003) and Otten *et al.* (2004) showed sufficient colonisation in a relatively short time (5 days). The rapid growth was also confirmed for *R. solani* in microcosms studies used in this thesis (Chapter 2.4.3). There is therefore a lack of information about the link between short time fungal colonisation and changes to structural and hydraulic properties of soil.

Therefore the main aim of this chapter and the related Chapter 4 is to quantify changes in soil structure caused by short-term fungal activity, and its impact on soil water retention. First a set of replicable microcosms were created, representative of the field conditions, at the beginning of the season when there is a high biological activity. Using a developed protocol (as in Chapter 2) the microcosms were inoculated with, *R. solani*. Subsequently water retention measurements were conducted. Additional measurements were made to capture the effect of wetting and drying cycles on water retention and how this effect is mediated by fungi.

This work is followed-up in Chapters 4 and 5 where the aim is to quantify the structural changes occurring in microcosms in order to explain possible changes in water retention measured in this chapter.

3.1.1. Hypotheses

1. Short-term colonisation of soil microcosms with the soil-borne fungus *Rhizoctonia solani* will increase the volumetric water content at saturation.

2. Soils colonised by *R. solani* will have a lower air-entry point and as a result start draining quicker than samples without fungi.

3. Fungal colonisation affects the degree at which soil water retention properties are affected by a wetting and drying cycle.

3.2. MATERIALS AND METHODS

This section outlines the experimental protocols that were used to detect and quantify the influence of fungi on soil water retention. The experimental design starts with the pre-treatment of the soil followed by ways to manipulate the structure and initial conditions for repacked soil microcosms. Then the method used to measure the soil water retention is described.

3.2.1. Preparation of soil

For all experiments in this work the same type of soil was used: an arable sandy loam collected from an experimental site (Bullion Field) at the James Hutton Institute (formerly Scottish Crop Research Institute), Dundee, UK. Soil was air-dried and sieved into three fractions of aggregates sized: <1 mm, 1-2 mm and 2- 4 mm. The sieved soil was sterilized by double autoclaving (1 h hold time at 120^{o}C) with 48 h interval. The sterile soil was wetted to obtain a 30 % air filled porosity (Chapter 2.2), and left for 48 h at 23^{o}C to equilibrate before packing to avoid the impact of sudden increase of biological activity on colonization of the microcosms by *Rhizoctonia solani* (Harris *et al.* 2003).

3.2.2. Determining the microcosm setup

In order to conduct measurements which reflect the conditions occurring in undisturbed fields, we estimated the desired bulk density of the repacked microcosms. Undisturbed soil was sampled using a metal rings sized 6 cm high and 6 cm in diameter from the same field site as described above (see 2.2.1.). The samples were taken from three different locations in the field corresponding to a range of densities from 1.3 g/cm^3 for

sample taken from ploughed and tilled part of the field to 1.6 g/cm^3 corresponding to samples from the areas that were not ploughed and which were compacted under heavy farm machines after harvesting (Fig.3.1).

Sample representing the ploughed part of the field corresponding to the bulk density of 1.3 g/cm^{3}was selected to be the reference point for the re-packed microcosms design Sample from the ploughed part of the field showed the highest volumetric water content at the saturation point of 0.45 (cm^3/cm^3), and lost the largest amount of water (22.2 g) during the measurement (Appendix 1.1). These results showed that the sample from a ploughed part of the field was the most porous with well connected pores among the tested samples.

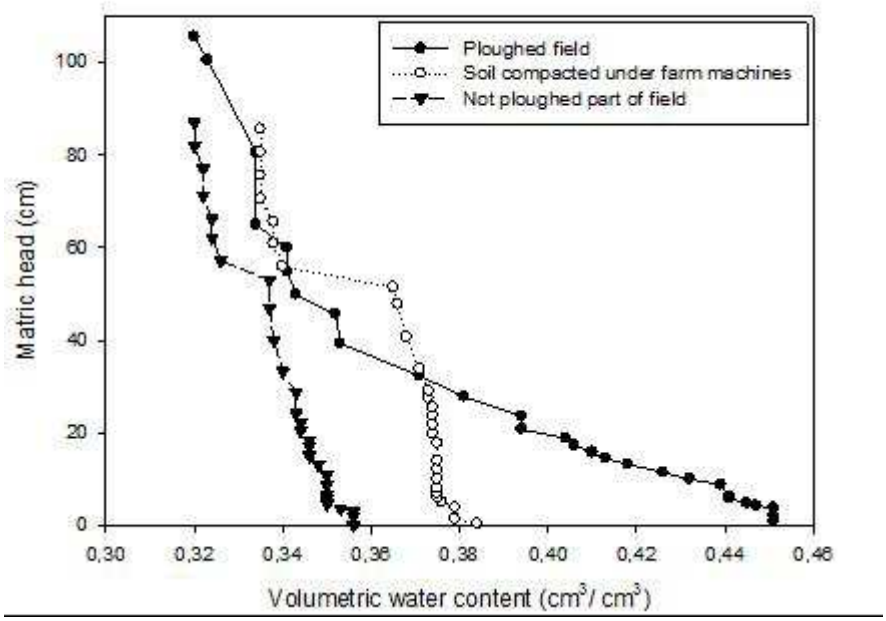

Fig. 3.1. Water retention curves of undisturbed soil sampled from the areas at different tillage stages on experimental site of Bullion Field at James Hutton Institute.

3.2.3. Preparation of fungal inoculum

Poppy seeds colonised with *Rhizoctonia solani* were used as fungal inoculum (See Chapter 2.4 for details). The soil microcosms were packed in layers which allowed

placing three inoculated poppy seeds on top of each 1cm thick layer of soil apart from the very top one. Such prepared microcosms were then incubated for 5 days in 23^{o}C to allow sufficient colonisation (Harris *et al.* 2003).

3.2.4. Water retention measurements

Water retention was measured with the hanging water column method (Fig.3.2.). Limitations of measurements with the use of this method is that matric head values can only be realized between 0 – -1000 cm of water, depending on the characteristics of the porous plates (size of pores) (Klute 1986).

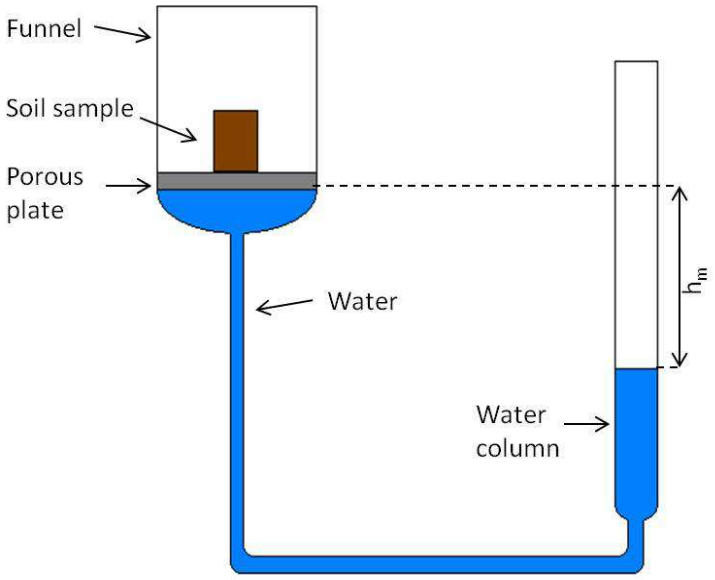

Fig. 3.2. The schematic representation of Heines apparatus set-up used in experimental work to measure water retention. Matric head (h_m) expresses the negative pressure causing water outflow from the soil sample on the porous plate.

In the hanging water column method, soil samples are placed at the top of a porous ceramic plate. After saturation the sample is equilibrated to a matric head of zero

at the bottom of the soil sample (level of the porous plate). To obtain the desired values of negative pressure, a burette was lowered slowly and stepwise with sufficient time intervals allowing for equilibration of the soil sample to the negative pressures. The matric head of the sample was then calculated as the difference in height between the water level in the burette and the porous plate.

After each equilibration the outflow of water from the soil sample, the weight of the sample and the height of water column was recorded. At the end of the experiment, soil samples were weighed and then placed in the oven at 105^{o}C for 48h to obtain the dry weight of the soil samples. These data were then used in the equation below, which determines the water content of samples for each step (Kosugi and Nakayama 1997).

$$\theta = [(M_w + M_o) - M_d] / \rho_w V_s , \qquad [4.1]$$

where:

θ - water content ($cm^3\ cm^{-3}$),

M_w – mass of wet soil (g),

M_o – mass of water flown out of sample (g),

M_d – mass of dry soil (g),

ρ_w – water density ($g\ cm^{-3}$),

V_s – volume of sample (cm^3).

Water content values were plotted against the difference in the height of water level in the burette (based on burette readings or measurements from the ground level to the meniscus) starting from the zero point (equilibrium at the level of the porous plate) (Koorevaar *et al.* 1983).

3.2.5. Experimental design of water retention measurements

To develop the most optimized set up to quantify the influence of fungal activity on soil water retention water retention measurements are described in four experiments:

Experiment 1 – test of experimental design.

The first water retention measurements were performed on re-packed microcosms to test the method of packing and inoculation with fungi. Repacked soil microcosms with four replicates per treatment were used (n=4 samples inoculated with fungi and n=4 controls). All microcosms were prepared as in 4.2.2 i.e. by packing soil in 1 cm layers in to 6 cm height and 6 cm diameter stainless steel rings. These rings were typically used for soil sampling and measurements of soil physical properties. A fine mesh was attached to the bottom to prevent loss of soil particles while weighing microcosms. Five Heines apparatus were used, 4 small (∅ = 13 cm) which were able to accommodate only one microcosm, and one large one (∅ = 20 cm) with space for 4 microcosms.

Experiment 2 – changed microcosm design

For analysis and comparison of the measurements there was a need to increase the number of replicates and use uniform equipment. These requirements led to the development of smaller soil microcosms, using PVC rings of 4 cm in height and diameter (see Chapter 2.3 for details). The change of the ring material was done to allow for visualisation and quantification of soil structure with X-ray CT systems (Chapters 4 and 5). The thick layer of stainless steel would have otherwise introduced artefacts in scanning (Chapter 1.4 for details).

The second water retention experiment was carried out with a higher number of replicates (n = 11 of inoculated and n = 11 controls) distributed over seven small funnels. The microcosms were not weighed individually after achieving equilibrium in order to reduce the disruptions in soil-water contact. Instead, the differences in soil water content were calculated based on water outflow read from the burettes. As the effect the water retention curves were presented for each funnel, only average values over three microcosms in each funnel could be calculated this way. The only exception was one of the funnels which accommodated two microcosms inoculated with *R. solani,* and two controls. In this case samples were weighed at each equilibrium. The odd number of equipment made this somewhat unusual usage of the seventh system the most optimal way.

Experiment 3 – impact of drying and wetting cycle on water retention

In this experiment an additional effect of drying and wetting cycles was investigated and the impact it had on soil water retention. It is known that wetting and drying cycles can cause swelling of soil during wetting and shrinkage during drying (Dexter 1988). Thus a new experimental protocol was applied including two water retention measurements with air-drying for a two week period in between. The same total number of microcosms with n=8 replicates per treatment and the same size and material of the rings was used as in Experiment 2.

Experiment 4 – decreasing the variability within the treatments.

The final experiment aimed to reduce variability within treatments, and to confirm the effect of a drying and wetting cycle on retention curve. Water retention measurements were repeated with the following conditions: four pressure plates were used,

accommodating 16 microcosms in total. Eight microcosms were inoculated with *R. solani* and eight microcosms were without fungi, hereafter referred to as controls. Water retention measurements included the influence of a drying – wetting cycle. In the interval between water retention measurements, the soil microcosms were slowly air-dried for three weeks. Also X-ray microtomography scans were performed during three stages: i) after inoculation and incubation of fungi, ii) after the first water retention but before air-drying, iii) after the second water retention measurement but before oven-drying. The X-ray CT scanning results are presented in Chapter 4.

3.2.6. Statistical analysis

The van Genuchten model (Porebska *et al.* 2006) was used to summarize the retention curves. Van Genuchten model is based on equation [4.2] and characterises the typical shape of water retention curve. The relationship is given by:

$$\theta = \theta_r + ((\theta_s - \theta_r)/(1+(\alpha h)^n)^m) \quad [4.2]$$

Where:

θ - effective water content (cm^3/ cm^3),

θ_r - residual water content (cm^3/ cm^3),

θ_s - water content at saturation (cm^3/ cm^3),

h - matric head (cm),

α - air entry suction (cm^{-1}),

n, m – parameters related to pore size distribution, where m = 1 – 1/n (dimensionless).

Parameters for the van Genuchten equation were estimated in SigmaPlot 10.0.1. The curve fitting based on maximum-likelihood estimation (Hollenbeck *et al.* 2000),

was applied on data from the second and third experiments only. However, the relationship only poorly described the data. Hence it was decided that it was not appropriate to use parallel curve analysis to determine an effect of fungi on water retention.

Thus to statistically quantify the effects of fungal growth on soil water retention, volumetric water content was compared at (i) the point of saturation, at (ii) the lowest pressure and (iii) the water loss over the full range between saturation and the lowest pressure allowing to obtain data for (calculated on basis of the weight difference between the wet and dry microcosm). To compare the means of the above parameters independent sample t-test was used with 95% confidence interval of the difference. Due to minor differences in outflow of water from the samples the exact matric head wasn't exactly the same at each point of comparison but this difference was judged to be not significant enough to prevent comparison ($p>0.05$).

3.3. RESULTS

Experiment 1 – test of experimental design

The first experimental data (Fig.3.3) did not show any effect of fungal colonisation on hydraulic properties.

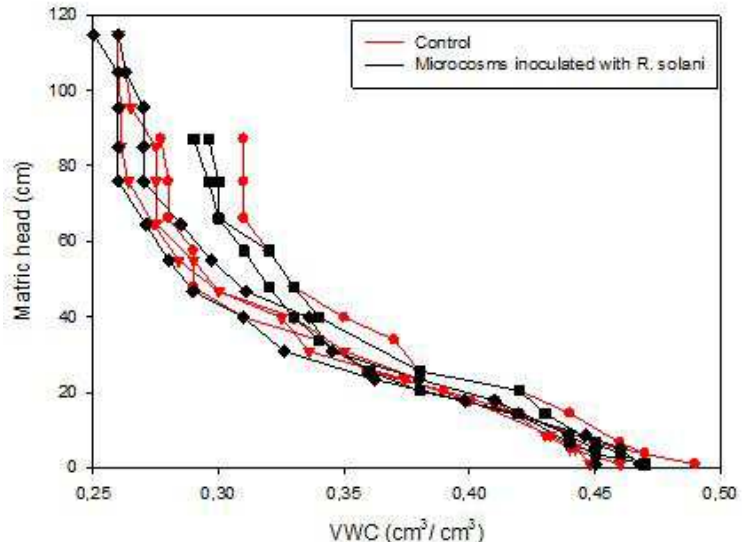

Fig. 3.3. First water retention experiment, using re-packed soil microcosms describing the relationship between volumetric water content and matric head. There is a notable difference in the range of pressures achieved during measurement, as an effect of using two types of funnels.

Average volumetric water content at the point of saturation were between 0.45 cm^3/ cm^3 and 0.49 cm^3/ cm^3 (Table 3.1) and the volumetric water content at the lowest achieved pressure ranged from 0.25 cm^3/ cm^3 to 0.31 cm^3/ cm^3. The retention curves of both inoculated and control microcosms had similar evolutions.

Samples inoculated with *R. solani*			**Controls**		
VWC at saturation (cm^3/cm^3)	**VWC at highest pressure (cm^3/cm^3)**	**Lost of water (g)**	**VWC at saturation (cm^3/cm^3)**	**VWC at highest pressure (cm^3/cm^3)**	**Lost of water (g)**
0.47	0.30	29.5	0.45	0.26	36.1
0.47	0.29	30.5	046	0.26	30.6
0.45	0.26	32.3	0.49	0.27	31.9
0.47	0.25	36.9	0.49	0.31	33.8

Table 3.1. Individual measurements for the water outflow, volumetric water content at the saturation point and the lowest pressure for Experiment 1 showing high variability within each treatment (samples inoculated and controls) and no significant effect of the growth of *R. solani*.

There was a lack of a typical 'S' shape as the samples started to drain from the lowest pressures applied. There was also a significant difference in the range of measurements between the – 115 cm for the samples on the large funnel and – 85 cm for the rest of microcosms. However within the 85 cm range the samples lost on average 32.7 g of water. For the record of individual measurements please see Appendix 1.2. Variability increased with larger negative pressure.

Experiment 2 – changed microcosm design

Changes to the protocol (see section 3.2.5 for details) including the use of uniform sizes of funnels and limiting the disturbance in soil/water contact increased the measurement range up to 130 cm (Appendix 1.3). However similarly to Experiment 1 there was no effect of fungal colonisation on the soil water retention. The water content at the point of saturation varied between 0.39 (cm^3/cm^3)and 0.41 (cm^3/cm^3)with an average value for inoculated soils of 0.4 cm^3/cm^3 and 0.41 cm^3/cm^3 for controls. The average water loss per funnel was 20.2 g and 20 g respectively (Table 3.2).

Samples inoculated			**Controls**		
VWC at saturation (cm^3/cm^3)	**VWCat highest pressure (cm^3/cm^3)**	**Lost of water (g)**	**VWCat saturation (cm^3/cm^3)**	**VWCat highest pressure (cm^3/cm^3)**	**Lost of water (g)**
0.41	0.28	20.0	0.39	0.28	18.0
0.40	0.27	20.8	0.41	0.27	18.0
0.41	0.30	20.0	0.40	0.29	21.0
-	-	-	0.40	0.30	22.8

Table 3.2. Individual measurements for the water outflow, volumetric water content at the saturation point and the lowest pressure for samples inoculated with *R. solani* and controls, measured in Experiment 2.

One of the funnels which contained samples that were inoculated with fungi had to be discarded as an outlier. These soil microcosms had somehow gained water rather than loosing it. This set of samples is not included in the analysis (Fig.3.4).

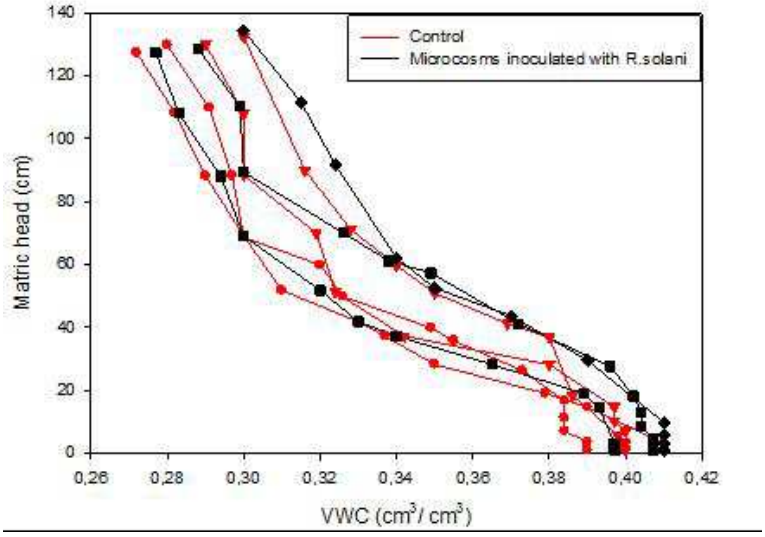

Fig. 3.4. Water retention measeurements for the samples inoculated with *R. solani* and controls, collected in the Experiment 2. The curves were constructed per funnel rather than for individual microcosms to reduce the disturbance to the soil-water contact.

The data did not display the expected typical 'S' shape of the retention curve, and the Van Genuchten curve did not capture the data well (Fig. 3.5). It lacked the characteristic air entry value that breaks the desorption curve, describing the pressure at which soil sample starts loosing water until it reaches the residual water content value. Fitted curves showed that samples immediately started draining, from the beginning of measurement. The poor fit can be explained by variability of measurements within the treatments, the lack of information about the residual water content, or by the presence of a large number of large, well connected pores with a relatively low air entry value (Fredlund *et al.* 1994, Eldridge and Freudenberger 2005, Porebska *et al.* 2006).

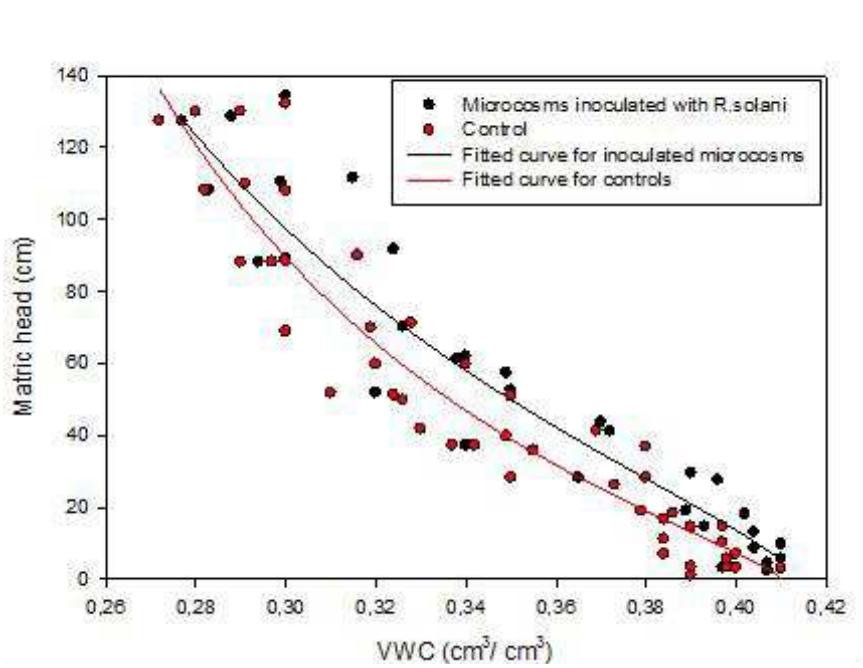

Fig. 3.5. Van Genuchten curves fitted on the water retention data measured in Experiment 2. High variability within the treatments and low range of measurements caused very poor fitment.

Experiment 3 – impact of drying and wetting cycle on water retention

In both water retention measurements the volumetric water content at saturation point significantly differed between the samples inoculated with fungi and controls ($p = 0.04$ for the first measurement and $p < 0.001$ for the second one). This difference could be a result of fungal growth increasing the porosity or connectivity of pore networks and as a result increasing the volumetric water content values at the point of saturation. However volumetric water content values at the point of saturation significantly differed between the individual samples within the treatments in both water retention measurements (single sample t-test with $p < 0.001$). The variability between the samples of the same treatment suggests that the microcosms were not representative. However there was also a difference in the water loss during drying between inoculated samples and controls ($p = 0.049$), although here too a high variability within treatments was observed ($p < 0.001$) (Table 3.3).

Samples inoculated			Controls		
VWC at saturation (cm^3/cm^3)	**VWC at highest pressure (cm^3/cm^3)**	**Lost of water (g)**	**VWC at saturation (cm^3/cm^3)**	**VWC at highest pressure (cm^3/cm^3)**	**Lost of water (g)**
First water retention measurement					
0.40	0.29	3.7	0.39	0.30	3.9
0.40	0.30	4.0	0.39	0.29	4.3
0.39	0.27	4.6	0.38	0.30	3.7
0.39	0.29	4.9	0.38	0.29	4.1
0.41	0.27	6.1	0.40	029	4.5
0.39	0.30	3.9	0.39	0.30	2.8
0.39	0.29	4.2	0.38	0.31	3.9
0.40	0.28	4.7	0.39	0.28	4.2
Second water retention measurement					
0.40	0.25	6.3	0.36	0.25	4.7
0.38	0.25	5.5	0.36	0.25	4.8
0.38	0.25	7.0	0.37	0.25	5.4
0.38	0.25	5.7	0.37	0.24	4.3
0.40	0.24	5.8	0.37	0.25	5.2
0.37	0.24	5.5	0.36	0.26	4.9
0.37	0.26	4.9	0.36	0.25	5.4
0.38	0.26	5.4	0.38	0.24	5.7

Table 3.3. Individual measurements for the water outflow, volumetric water content at the saturation point and the lowest pressure for samples inoculated with *R. solani* and controls, recorded for two water retention measurements in Experiment 3.

There were also differences between the first and the second water retention measurements. This demonstrates an impact of drying and wetting cycle on water retention (Fig.3.6.).

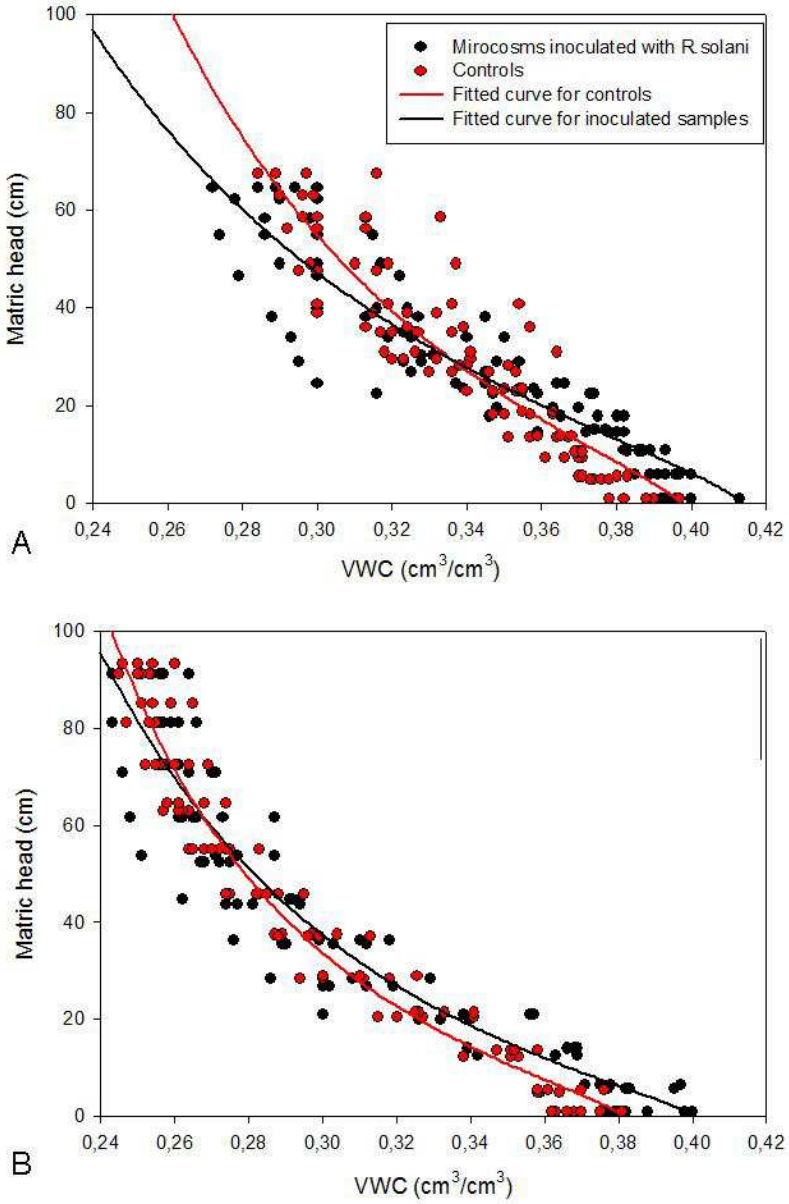

Fig. 3.6. Water retention measurements for soils inoculated with *R. solani* and controls, including the effect of DW cycle: A – first measurement, B – the measurement after air drying of the samples. Van Genuchten model was used to fit the predicted curves to allow the comparison between the treatments.

Samples during the first draining cycle had a slightly higher water content at saturation ranging from 0.38 to 0.42; after drying and re-wetting the range was lower: 0.36 – 0.4 ($p < 0.001$). A similar trend was preserved in the volumetric water content at the lowest pressure achieved, which in the first draining cycle varied between 0.27 to

0.31 and in the second measurement was between 0.24 – 0.26 ($p<0.001$) (Table 3.3). The variability between the treatments decreased in the second cycle during which we were able to obtain lower matric heads, namely -91 cm in comparison with -63 cm in the first approach (for individual measurements please refer to Appendix 1.4 a and b).

Experiment 4 – decreasing the variability within the treatments

The measurements of soil water retention properties showed no significant effect of fungal colonisation on soil water retention. Although there were four soil microcosms on each porous plate, the weight was recorded for each microcosm individually (for detailed records please see Appendix 1.5 a and b. This setup allows presenting data as retention curves as means of four microcosms representing one funnel (Fig.3.7) or individually (Fig.3.8).

The individual water retention curves of microcosms plotted separately for inoculated and control microcosms (Fig.3.8.) showed low variability within treatments. Statistical comparison showed no significant differences in the volumetric water content at the saturation point between the soil microcosms inoculated with *R. solani* and controls (in the first water retention measurement $p = 0.6$, in the second measurement $p = 0.38$). There was also lack of differences in the overall water loss during both of the water retention measurements between the inoculated samples and the controls ($p > 0.05$) (Table 3.4).

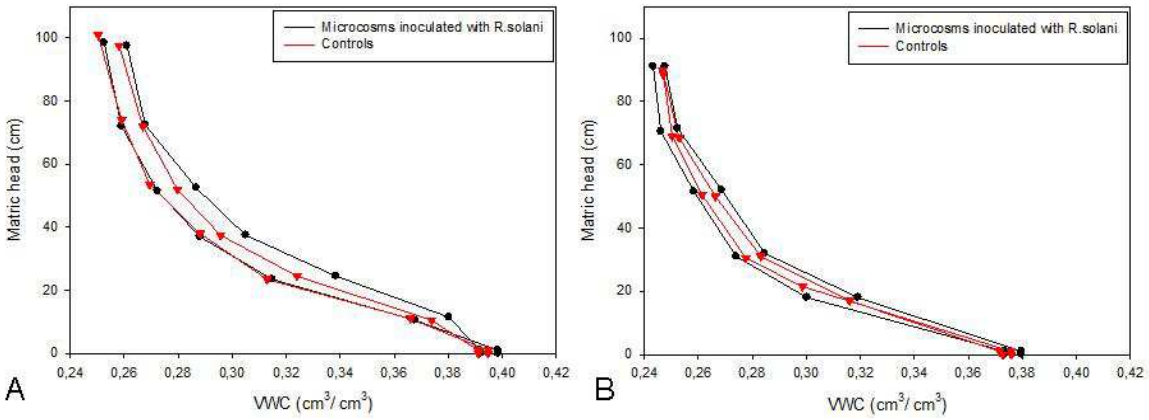

Fig. 3.7. Water retention curves of samples inoculated with *R. solani* and controls. The measurements are presented per funnel where each curve represents mean water content values of four microcosms. The Experiment 4 included two measurements before (A) and after air drying (B).

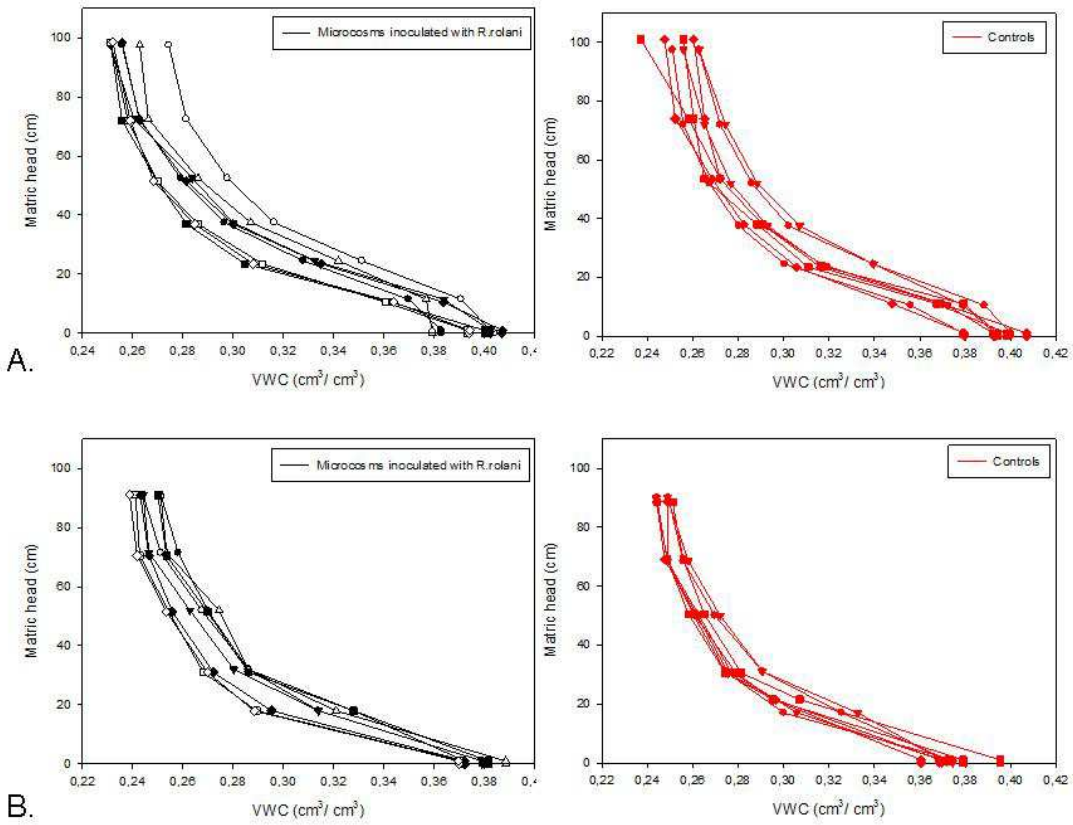

Fig. 3.8. Water retention curves of samples inoculated with *R. solani* (black) and controls (red) quantified in Experiment 4. The measurements are presented for individual microcosms in two measurements before (A) and after air drying (B).

However there was a significant effect of a DW cycle. There was a significant difference between the two water retention measurements in volumetric water content of microcosms at saturation. In the first retention cycle the mean water content for all samples, inoculated and controls, was 0.39 (s.e. 0.004). During the second water retention cycle the water content at saturation was 0.38 (s.e. 0.002) for inoculated samples and 0.37 (s.e. 0.003) for the controls. Although this difference was significant ($p = 0.001$) such a small effect has little ecological value.

The two water retention experiments were not performed with the same negative pressure values; hence it was difficult to test the effect of DW on water retention measurements formally, although there was one common point with identical matric head for both retention experiments, at h_m = - 50 cm. The mean volumetric water content at this point differed significantly between the two measurements for inoculated samples ($p = 0.002$) and controls ($p = 0.001$). However there are no significant differences within the treatments in the amount of water released from 0 to -50 cm pressure in both water retention measurements. Samples inoculated with fungi released on average 5 g (s.e. = 0.2) of water during the first measurement and 4.8 g (s.e. = 0.06) during the second one ($p = 0.55$, after a DW cycle) whereas controls lost 5 g (s.e. = 0.15) and 4.8 g (s.e. = 0.16) ($p = 0.2$) (Table 3.4).

The statistical analyses confirmed that there was no significant influence of short-term fungal colonisation on soil retention properties. There is however evidence of an effect of a DW cycle, which didn't appear to alter the trend (shape) of the water retention curve but did significantly change the volumetric water content (introducing more or less a shift of the curves).

Samples inoculated			Controls		
VWC at saturation (cm^3/cm^3)	**VWCat highest pressure (cm^3/cm^3)**	**Lost of water (g)**	**VWCat saturation (cm^3/cm^3)**	**VWC at highest pressure (cm^3/cm^3)**	**Lost of water (g)**
First water retention measurement					
0.38	0.25	5.4	0.38	0.25	5.5
0.4	0.27	5.6	0.4	0.26	5.9
0.4	0.25	6.5	0.39	0.25	5.9
0.38	0.26	5	0.39	0.26	5.6
0.4	0.25	6.4	0.39	0.24	6.8
0.39	0.25	6.1	0.4	0.25	6.1
0.4	0.25	6.5	0.38	0.24	5.7
0.39	0.25	6.1	0.4	0.26	6.3
Second water retention measurement					
0.38	0.25	5.5	0.37	0.25	5.3
0.37	0.24	5.5	0.37	0.24	5.6
0.38	0.24	5.8	0.37	0.25	5.2
0.39	0.25	5.9	0.37	0.24	5.6
0.38	0.25	5.7	0.39	0.25	6.2
0.37	0.24	5.6	0.38	0.24	5.8
0.37	0.24	5.5	0.37	0.24	5.4
0.37	0.24	5.6	0.36	0.25	4.8

Table 3.4. Individual measurements for the water outflow, volumetric water content at the saturation point and the lowest pressure for samples inoculated with *R. solani* and controls, recorded for two water retention measurements in Experiment 4. The data showed reduced variability within the treatments and no effect of fungal colonisation on the water retention measurements.

3.4. DISCUSSION

Water retention was not significantly affected by fungal colonization. There may have been a trend in one of the measurements but overall no substantial differences were observed that could have ecological value or would be expected to substantially alter soil functioning. However, we did observe a high variability within treatments despite the use of controlled structures, even though the experiment was repeated several times trying to reduce this as much as possible. The result of repeated experiment still inferred that there was no impact of *R. solani* on soil water retention. This work continues in the next chapters of the thesis as the internal structure of soil microcosms was visualised

and quantified at various stages of water retention measurements. We quantified retention properties within the range of matric heads up to -120 cm, which corresponds to the resolution of the X-ray microtomography scans performed on microcosms to quantify and visualise possible changes to the soil structure induced by fungal activity, and described in Chapter 4.

In the experiments we observed increased variability between retention curves at high pressure values. These differences suggest that changes to the soil structure may occur within smaller pores which drain at lower pressures. It could also be an artefact caused by frequent disturbance of the soil-water contact while lifting the microcosms after each equilibrium to quantify the weight of microcosms to determine its water loss. This could break-up contact between soil water and the plate, preventing it from draining. The increased variability can also be caused by biomass filling the porous material of pressure plate and clogging the flow of the water at the latest stages of experiment. Samples were placed on pressure plates up to 2 weeks time which is ample time for bacteria to grow and clock pores. The error in measurements would then accumulate at the lower pressures (coinciding with an increase in time) thereby potentially increasing the variability within the treatments.

The time scale at which the effects of fungal activity were quantified was one of the factors which could have potentially limited the results. We incubated the samples for five days, which was enough for fungi to colonise the available pore space (see 2.4.3). Auge *et al*. (2001), Bearden and Petersen (2000), and Crawford *et al*. (2011) investigated the effect of fungal presence in soil colonized by mycorrhizal on its hydraulic properties, and found a difference after 25 days of incubation. This could suggest that longer experiments are required to observe changes in water retention. However, Hallet *et al*. (2001) showed that by adjusting fungal biomass in sandy soils

the effects in hydraulic properties are already significant after 10 days confirming shorter timescales like those used in this study.

Fungi were stated as the main factors causing repellence of soil by producing hydrophobic exudates. One of the most studied exudates is hydrophobic glomalin, a substance produced by fungal hyphae and accumulated in soil (Rillig and Steinberg 2002, Feeney *et al.* 2004). These exudates are not only substances that enhance the stability of aggregates and soil structure (Wright *et al.* 1999) but also change the contact angle between soil and water (Hallett *et al.* 2001). Glomalin is referred to as the soil glue which increases stability of soil structure and as a result could make soil more resistant to damage caused by drying and wetting cycles. According to these facts we would have expected to see a quicker drainage of the samples inoculated with fungi. However changes to the soils microstructure could obscure these increases in hydrophobicity induced by drying and wetting cycles.

3.5. CONCLUSIONS

The analysis and comparison of water retention properties did not show a significant impact of the growth (estimated by analysis of ergosterol content) of *R. solani* on water retention. Despite the carefully designed protocol to pack representative microcosms with a uniform structure, there was still a high variability in water retention within each treatment. There was also a significant effect of a DW cycle on water retention, which significantly ($p=0.002$) reduced the volumetric water content at saturation. It was concluded that *R. solani* did not induce measurable changes to water retention during colonization of the soil sample. This contradicted previous finding possibly as they considered longer time scales indicating that effects previously reported may not have resulted from fungal growth but were possibly mediated by processes at later stages.

This chapter was the first chapter of a series of three to quantify the effect of the colonisation of soil with soil-borne fungi. Water retention measurements in Chapter 3 are followed by analysis of soil structure in Chapters 4 and 5.

CHAPTER 4

The effect of fungal growth on soil structure: analysis at microcosm scale

4.1. INTRODUCTION

Soil is an extremely heterogeneous material with physical, biological and chemical processes varying across a huge range of spatial scales. Quantifying soil structure has long been a problem which has hampered quantitative insight into factors that may alter soil structure. The processes involved in changing soil structure are also inter-linked. For example, the structure changes over time scales due to numerous physical (e.g. tillage operations or drying and wetting cycles) and biological factors. The pore space of soil, which is one of the most important characteristics of soil structure, creates environmental niches for micro-organisms (Ritz and Young 2004). The properties of pore networks, such as the volume available, the connectivity of the pore volume, size distribution of pores, and the tortuosity of pathways within this volume are crucial factors that have a major impact on life in soil by controlling for example the spatial distribution of water and nutrients, as well as the movement of some organisms. On the other hand soil-borne organisms, such as earthworms (Lubbers *et al.* 2010) bacteria (Feeney *et al.* 2006b) and fungi (Crawford *et al.* 2011), and plant roots (Eldridge and Freudenberger 2005) are not just affected by soil structure in the way they explore soil, but also have a significant influence on soil structure. This makes soil a complex ecosystem where the soil structure defines niches for organisms, but is at the same time also shaped by soil organisms. This leads to the introduction of soil as a self-organised system by Crawford *et al*. (2005, 2011).

In Chapter 3 the impact of fungal colonisation on soil hydraulic properties was assessed and quantified. The experiments did not confirm any significant influence of fungal activity on water retention. This result was perhaps surprising, as there is sufficient literature that has presented evidence that soil fungi affect soil structure (Crawford *et al.* 2011), and consequently would be expected to affect water retention,

which is to a large extent determined by pore geometry. As discussed in Chapter 3, this might have been due to the time-scales used in this study being relatively short. Although microorganisms were shown to have affected the soil hydraulic properties within equally short time scales (Feeney *et al.* 2006a). It is possible that various processes affecting water retention work together or possibly cancel each other out. This thought is strengthened by the fact that the overwhelming evidence exists that fungi affect soil structure (Ritz and Young 2004). It is therefore important to assess the impact fungal growth had on soil structure independently of the water retention measurements described in Chapter 3. Work in this chapter was therefore carried out in parallel to the water retention measurements to quantify if fungal colonization or processes associated with drying and wetting cycles induced any changes to the structure of the soil microcosms.

There are specific reasons to look at the relation between soil characteristics and the presence of fungal colonies. Fungi are ubiquitous and ecologically important organisms in soil. They are known as saprotrophs, plant pathogens, biocontrol agents and mycorrhiza. Fungi are highly effective in colonizing heterogeneous soil environments due to unique growth form (Ritz and Young 2004). Colony expansion is based on branching and extension of vegetative hyphae, which allows for sparse spreading through available, connected pore networks (Otten *et al.* 2004). Because a fungal colony is very well connected through the hyphal network, nutrients and water can be translocated within the hyphal network (Bailey *et al.* 2000, Olsson and Wilhelmsson 2000, Boddy *et al.* 2009). This interconnectivity is a fundamental difference from other organisms which means that fungi are not restricted to a water meniscus (as is the case for bacteria) or areas rich in nutrients (Young and Crawford 2004).

Fungi are considered as engineers of soil structure (Tisdall *et al.* 1997). The effect of fungi on soil structure dynamics can be considered at least at two spatial scales. At the micro-scale, fungal hyphae are likely to change the alignment of primary soil particles such as clay platelets to create narrow channels (Ritz and Young 2004). These channels might have an influence on water flow or water holding capacity, carbon storage and microbial activity when (Dorioz *et al.* 1993). At large scales fungi act as a significant binding agent increasing the stability of soil structure. There are several mechanisms by which fungal stabilize soil. One is by surrounding soil particles or micro-aggregates with a hyphal network, which physically holds the micro-aggregates together (Bossuyt *et al.* 2001). This activity promotes creating macro-aggregates (see chapter 5) (Dexter 1988). Fungi also produce a wide range of surfactants and exudates that cement particles together (Hallett and Young 1999, Wright *et al.* 2006). These compounds influence the hydrophobicity of soil (Hallett *et al.* 2001, Feeney *et al.* 2006b). Structure enhancement has quantified for sand slopes where samples colonised with fungi showing significant increase in stability (Meadows *et al.* 1994). The degree of enhancement depends on several factors such as the age of a hyphal network and the rate of colonisation which correlates with nutritional status and availability of water (Li *et al.* 2002). Little is known of the role of soil structure on these processes even though this hugely affects fungal colonization. This gap in our knowledge is mainly the result of our inability to quantify soil structure non-destructively.

Chapter 3 gave a detailed description of the experimental design of water retention measurements consisting of two sets of measurements relating to drying and wetting cycles (DW). This chapter aims to detect and quantify with the use of X-ray microtomography the structural changes of these microcosms due to fungal colonisation

and drying and wetting cycles. The CT scans were performed at three different stages of the water retention measurement in order to capture and distinguish between differences in soil structure caused by fungal colonisation and those caused by the DW cycles. DW cycles can cause swelling (wetting) and shrinkage (drying) of soil material leading to rearrangement of soil particles that can result in changes in pore geometry and connectivity (Li *et al.* 2004). Also, especially sudden changes in water content may build up hydraulic stresses leading to crack formation in weak planes of soil. Such cracks can define the initial surface and boundaries for macro-aggregate formation. These mechanisms can be used to restore structure of non-aggregate soil (Dexter 1988, Rajaram and Erbach 1999). In addition, the drying process shifts microbial balances towards the advantage of fungi which are less restricted to water rich areas (Yao *et al.* 2011) and because of fungal preference to spread rapidly through macro pores and cracks (Otten *et al.* 2004). Therefore there is strong evidence that structural changes will occur in soil microcosms.

There are various views regarding the timescales at which these structural changes can occur. Auge *et al.* (2001) found differences in hydraulic properties of myccorhizal incubated soil after 7 months of incubation. However this length of time was necessary to allow the roots to grow. Crawford *et al*. (2011) were able to detect structural changes caused by microbial colonization after 25 days of incubation. In this work fungal colonisation occurred over just 5 days. This short term colonisation was proven to be sufficient as evidenced by the degree of colonisation of aggregates and the ergosterol content (see Chapter 2.4.3.). Also if we are interested to understand if feedbacks occur between fungal colonization and re-shaping of the soil structure it is essential that both processes are understood at identical time scales. Therefore, it was

decided to test if soil structure was affected within the time scale it took for fungi to colonize the soil.

This chapter describes the use of a non-invasive method, X-ray micro-tomography combined with image analysis techniques in order to:

1) detect and quantify the effects of fungal colonisation on soil structure,

2) capture and quantify the changes to the soil structure induced by DW cycle for samples with and without fungi.

Whereas structural aspects have been investigated previously, this is the first study in which X-ray CT is used to quantify pore geometry and use this to asses the impact of soil fungi at the same short time scales that fungi take to grow through soil and on samples for which water retention data are also available. As such it is also a test to see if X-ray CT can be used in combination with microcosms in this way.

4.1.1. Hypotheses

1. Short-term colonisation of soil microcosms with the soil-borne fungus *Rhizoctonia solani* will increase the soil porosity.

2. A wetting and drying cycle can alter pore geometry of repacked soil microcosms.

3. Fungal colonisation affects soil structure during a drying and wetting cycle.

4.2. MATERIALS AND METHODS

4.2.1. Soil Microcosms

Microcosms used in this part of the work are the same as those described in the Chapter 3. In brief, samples consisted of a sandy loam soil, with aggregates of a diameter of 1-2 mm packed at a density of 1.3 g/cm^3 into PVC rings, 4 cm high and 4 cm in diameter.

There were 16 microcosms in total, n=8 controls and n=8 inoculated with fungi. *Rhizoctonia solani* was introduced to these soil microcosms via inoculated poppy seeds (Harris *et al.* 2003). The fungus was allowed to spread through the soil microcosms for 5 days, which was enough to ensure sufficient colonisation (see Chapter 2.4). All these soil microcosms were used in two water retention measurements including one full drying/wetting cycle.

4.2.2. Micro CT data acquisition

A Nikon Metrics HMX225 micro X-ray CT system was used to characterise the internal structure of microcosms. Scans were performed at an energy level of 120 kV, a 75 µA current, and with a 0.25 mm Al filter. These settings were saved into a profile to allow all samples to be scanned at the same energy levels and to be placed in the same position, ensuring all scans were done with the same resolution.

The quantification of fungal growth on soil structure in this chapter supplements the data of the soil water retention in Chapter 3. The CT scans were performed on microcosm at different stages of two water retention measurements (Fig.4.1.). The first CT scan was performed after incubation of microcosms with fungi, e.g the microcosms were approximately one week old at this stage. At this stage the aim was to detect and quantify differences caused by fungal colonisation in soil structure between control and inoculated samples. The second scan took place at the end of the first water retention, with all samples at the h_m = -120 cm. This aimed to visualise and quantify any changes in soil structure of microcosms caused by water retention measurement, which reduced the water content of the sample and to asses the structural differences between treatments (with and without fungi). The third CT scan was performed after a second water retention measurement. At this stage the samples had undergone a full drying and

wetting cycle before returning to the same state as the second scan. The analysis focused on the influence of drying and wetting cycle on the structure of soil in microcosms by comparing with the results of the second scan and also to test if any difference resulting from wetting and drying would be affected by differences between the treatments.

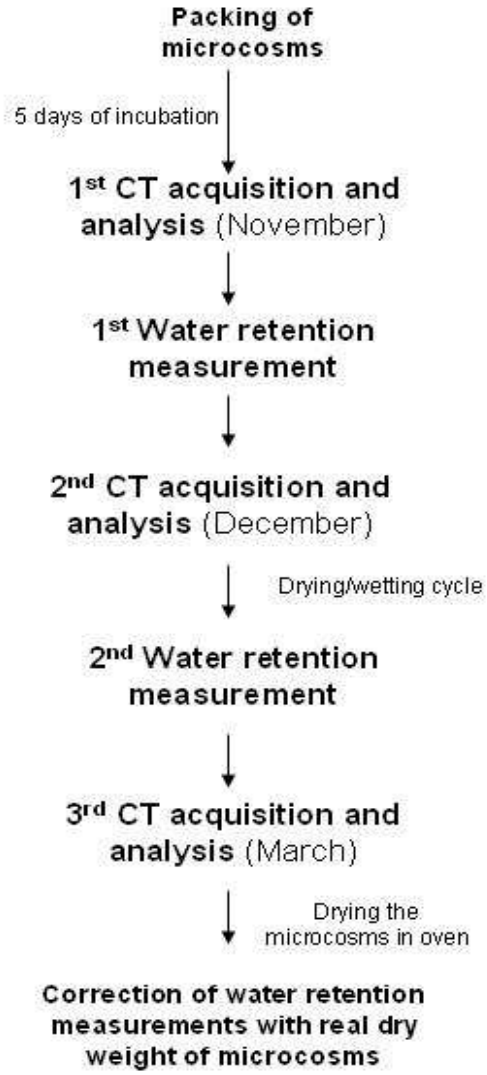

Fig.4.1. Diagram showing the stages of the experiment during which the structure of soil was quantified in 3D (the schedule is replicated here from Chapter 3 for clarity and ease of reading this chapter).

4.2.3. Image analysis

2D radiographs collected with X-ray CT were reconstructed into 3D volumes in CT Pro (www.nikonmetrology.com) at the resolution (voxel size) of approximately 30 µm. In the next stage they were rendered and converted into stacks of *.bmp images with VG Studiomax 2.1 (http://www.volumegraphics.com). These image stacks were imported into ImageJ and cropped to a region of interest sized 440 x 440 x 1000 voxels (l x w x h) for further analysis. The size of the volume was limited by computational constraints, but also aimed to include a region of the sample as large as possible whilst excluding the areas with noise, beam hardening and edge effects related to the sampling ring. Then the datasets were binarized via manual thresholding. The choice of threshold value was based on the visual analysis of the histogram corresponding to boundary between pores and solids in pores of different shapes and sizes (Falconer *et al.* 2011). A single threshold value for each dataset was computed from the average of 5 randomly selected slices per sample as described in Section 2.6.2 (Manual thresholding).

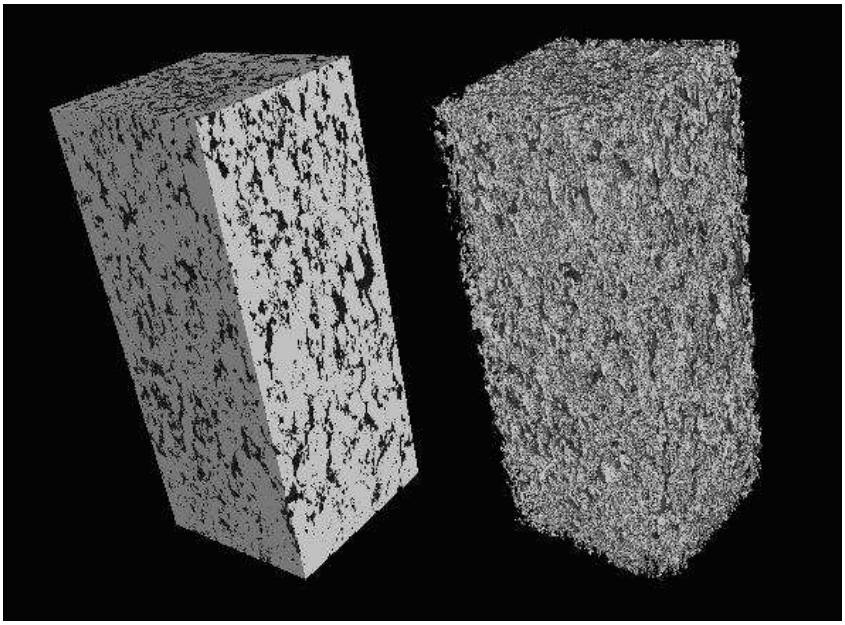

Fig.4.2. Extraction of pore volume from binarized region of interest (sized 440 x 440 x 1000 voxels) cropped from the whole microcosm (thresholded image stack on the left, extracted pore volume on the right).

The quantification of physical descriptors of soil structure such as connectivity and porosity was carried out with in house developed software (Houston, personal communication, also see Chapter 2.6.3.). Further calculations, including the surface area of the pore-solid interface, were performed in VGStudiomax. The region grower tool was used to segment out the solids (see Chapter 2 for details of the procedure). In order to select all pore space instead of just the largest connected cluster the region grower was applied to the solid phase. This was then extracted into a new ROI, and the selection was subsequently inverted to select the pore volume (Fig.4.2). The surface area and the volume of segmented out porespace was quantified by volume analysis tool in VGStudiomax (Chapter 2.6.3.).

4.2.4. Statistical analysis

Means and standard errors were computed and analysed in SPSS using an independent sample t-test. Significance was determined at 5% level of confidence. 2-D boxplots were used to visualise the distribution of the data including the means and standard errors.

4.3. RESULTS

The internal structure of all soil microcosms could be visualised and quantified. These quantifications were done three times during the water retention measurements. The first scan was performed immediately after fungal colonization and prior to the water retention measurements the second one after completing of the first drying cycle, and the third and last measurement after completion of the second drying cycle (with a full drying and wetting cycle between the second and third scan). The resolution at which

these data were scanned and analysed excluded pores smaller than 30 µm. However, this resolution corresponds to the pore sizes that are expected to drain during the water retention measurement (as explained in Chapter 1).

Analysis of the samples showed that despite the tight control and the use of repacked sieved soil, the porosity for individual measurements ranged from 20.5% to 30.1% for replicated samples, and the connectivity values ranged from 89.5% to 97.4% for the largest pore cluster (Table 4.1).

	1st analysis		**2nd analysis**		**3rd analysis**	
	Porosity (%)	**Connectivity (%)**	**Porosity (%)**	**Connectivity (%)**	**Porosity (%)**	**Connectivity (%)**
Control	20.5	92.4	28.1	92.1	29.1	97.2
	30.1	89.9	27.7	92.9	27.8	96.8
	25.5	90.4	26.2	89.5	25.6	94.9
	27.8	91.6	29.1	91.9	29.5	97.4
	29.1	91.2	29.9	92.5	27.5	97.1
	25.9	89.8	27.5	91.9	29.1	97.4
	25.7	90.3	26.8	91.5	27.1	96.7
	25.8	90.3	26.9	90.9	25.3	96.5
Inocul-ated	26.2	91.1	26.4	91.4	25.6	94.5
	28.3	92.0	28.7	91.2	27.9	96.5
	29.7	91.6	27.2	91.9	28.4	97.3
	26.4	93.3	29.2	92.6	28.7	97.4
	27.7	91.6	30.1	92.8	27.3	96.7
	26.1	90.4	27.3	90.8	29.7	96.9
	23.7	91.5	30.3	93.2	27.0	96.1
	25.4	91.3	27.1	91.0	28.0	91.0

Table 4.1. Individual results of structural analysis for soil samples inoculated with fungi and controls. Quantification was performed for all three CT acquisitions: 1st after incubation of microcosms, 2nd after first water retention measurement and 3rd after second water retention measurement (see Fig.4.1.).

The mean porosity values ranged from 26.8% to 28.6% for samples inoculated with fungi and between 26.5% and 27.6% for controls. All pore space in those samples is well connected with connectivity values all above 90% for all samples (Table 4.2).

Sample name		Porosity (%)		Connectivity (%)	
		Average	**Std. error**	**Average**	**Std. error**
1st analysis	**Control**	27.5	0.4	91.6	0.4
	Inoculated	28.6	0.5	91.9	0.3
2nd analysis	**Control**	26.5	1.0	90.7	0.5
	Inoculated	26.8	0.8	91.7	0.5
3rd analysis	**Control**	27.6	0.6	96.7	0.3
	Inoculated	28.1	0.4	96.8	0.2

Table 4.2. The summary of mean pore characteristics such as porosity and connectivity characterising soil microcosms for both: control and inoculated samples. Quantification was performed at different stages of water retention measurement (Fig. 4.1.).

Consistently, for all three parts of the analysis (1st, 2nd and 3rd scan, see Section 4.2.2. for details), the porosity and connectivity values of control samples (those not inoculated with fungi) were higher than those for samples colonized by fungus (Fig.4.3.). Nevertheless these differences were not found significant with 'p' values for porosity: p1= 0.7, p2=0.3, p3=0.4, and the p-values for connectivity of: p1= 0.1, p2=0.6, p3=0.8 (subsequently for 1st, 2nd and 3rd analysis). Porosity and connectivity values compared within the treatments between the 3 stages of analysis were also found to be not significant ($p>0.05$).

The volume of pores varied from 1322 mm^3 to 1422 mm^3, and the surface area ranged from 57690 mm^2 to 67713 mm^2 (Table 4.3). The values of the control samples (no fungal inoculation) were slightly higher than those of the inoculated samples. This is consistent with the trends in porosity analysed previously (Table 4.2). However, also these differences between the treatments were not significant in each of the three measurements, with p values ranging from 0.1 to 0.9.

1) 1st analysis

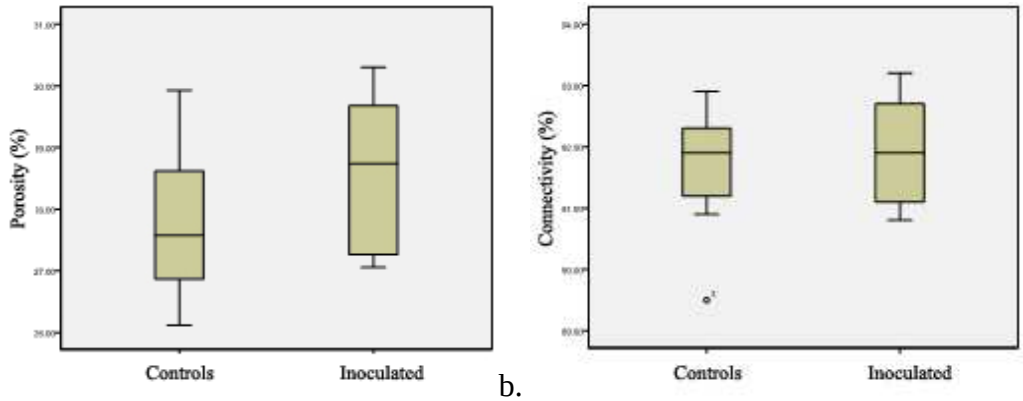

a. b.

2) 2nd analysis

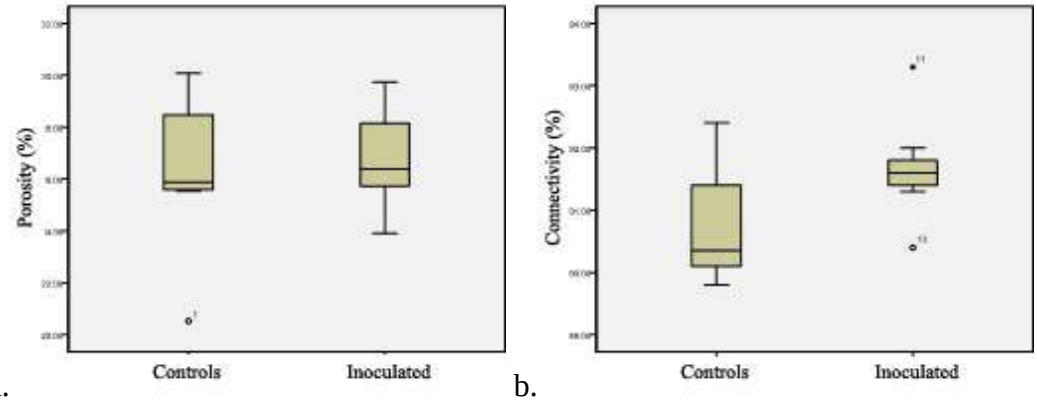

a. b.

3) 3rd analysis

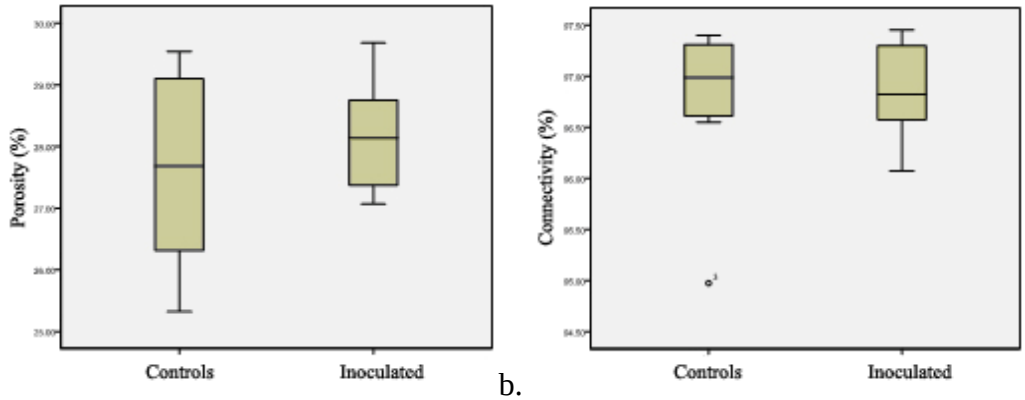

a. b.

Fig.4.3. Boxplots showing the distribution of the following data: a – porosity and b – connectivity, for all steps of analysis carried out in three different stages of water retention measurement (Fig. 4.1.).

Sample name		Volume of pores (mm^3)		Surface (mm^2)	
		Average	**Std. error**	**Average**	**Std. error**
1st analysis	**Control**	1322.0	70.0	60419.0	3771.6
	Inoculated	1388.0	27.0	57690.0	1091.4
2nd analysis	**Control**	1357.0	26.6	60350.0	2683.0
	Inoculated	1400.0	21.6	65013.0	2131.3
3rd analysis	**Control**	1367.0	26.6	64035.0	2683.0
	Inoculated	1422.0	21.6	67713.0	2131.3

Table 4.3. Summary of pore volume and surface area for control and inoculated samples quantified at three different stages of water retention measurement (Fig.4.1).

4.4. DISCUSSION

The measurements showed no significant differences, in any of the quantitative measures of soil structure applied here, between the soil samples with fungal growth and those without. Also no differences were found as a result of the drying-wetting cycle. There was a trend at each scanning time that samples that had been inoculated with fungi had a higher volume of pore space and that this pore space was also better connected and had a higher surface area, but none of these data proved significantly different

It was expected that we would demonstrate evidence of fungal induced changes to the soil structure. However, the outcome of analysis is contradictory to the general statement referring to fungi as '*engineers of soil structure'* (Tisdall *et al*. 1997) or at least that these changes do not occur for investigated fungal species and within short time scales. Measurements did not show any significant differences in soil structure caused by fungal colonisation nor by the effect of drying and wetting cycles. The latter was not unexpected for this soil type, but it was essential to test this within the experimental design and it had not been shown previously. Nevertheless, fungi have been reported to have a wide range of mechanisms that can affect the structure and

stability of soils, ranging from re-arrangement of primary soil particles, enmeshment of soil particles and small aggregates, resulting in the formation of soil macro-aggregates. They can also increase the amount of water stable aggregates leading to a higher resistance of soil structure to physical disruption (Dexter 1988). Soil stability can also be enhanced by exudates, such as polysaccharides and protein–based mucilages, which often are adhesive and can act as binding factors cementing the soil particles together (Schlecht-Pietsch *et al.* 1994).

The drying and wetting cycle was included into the experimental protocol as an additional factor to test if it would change the soil structure. There is an extensive amount of research showing the effect of multiple drying and wetting cycles results in crack formation in soils, aggregate formation and impact on the tensile strength of aggregates (Rajaram and Erbach 1999). According to Yao *et al.* (2011) DW cycles can also affect the rate of soil organic matter decomposition and induce a shift in the soil balance between fungal and bacterial biomass. Multiple DW cycles promote fungal colonization as the way fungi grow makes them less affected by drying processes as the network of hyphae is able to translocate water and nutrients (Otten and Gilligan 1998). In addition DW can induce cracks and as a result large pores which can act as preferential growth patterns for fungi. These cracks may play less significant roles in microcosm based experiments as uniformly packed soil samples do not include such large pores nor cracks (Young and Ritz 2000). Fungi generally have a preference for spread through macro-pores or cracks, as they grow faster along surfaces than tortuous pores and can span air gaps (Otten *et al.* 2004). The lack of significant differences between samples with and without fungi could be caused by using just one DW cycle in experimental design instead of a series of them. The DW impact was an additional factor to exclude the possibility that any detected changes in soil structure or water

retention curves were the effect of DW cycles and not the fungi or that a DW cycle was required before any effect on water retention could be detected (see Chapter 3).

The X-ray microtomography setup allowed data acquisition at a resolution of 30 µm (voxel size), which conforms to the range of pore sizes expected to be drained by the water retention equipment used in this experiment (see Chapter 3). As a result the smallest pores that could be detected would in theory be a single voxel sized thin valley with diameter of 30 µm. Although in practise it is likely to be higher as single voxels would be difficult to distinguish from random noise. Therefore, such single voxel sized pores and valleys are extremely difficult to detect and segment-out during thresholding of the image (Falconer *et al.* 2012). The thresholding method we used in this study is operator dependant, yet proven to be consistent for these type of samples (Baveye *et al.* 2010) Image binarization was performed by setting single global threshold value (see 4.2.3). Such a thresholding method often underestimates these small pores or classifies it as noise (see Chapter 2). Overlooking small pores and thin valleys could be a reason for not finding differences between treatments. Crawford *et al*. (2011) in their work on soil-microbe systems successfully performed similar experiments. They were able to quantify the effect of fungal colonisation on soil physical properties such as porosity and connectivity. They found this effect at a higher resolution of 9 µm, whereas no differences were reported at a resolution of 53 µm. In order to investigate the scale at which the fungi can possibly have induced changes we analysed the soil structure at the level of individual aggregates to obtain a resolution of 5.5 µm (see Chapter 5).

4.5. CONCLUSIONS

This chapter aimed to quantify and visualise changes to soil structure induced by the soil-borne fungus *R. solani*. With the use of CT systems and image analysis, the inner

structure of soil microcosms was visualised and quantified at three different stages of water retention measurements. Soil structure was characterised by descriptors such as porosity, connectivity of the pore space and the surface of the pore network. However, there was also no significant impact of the growth of *R. solani* on any of these structural measures. The lack of fungal growth induced changes to soil structure could be due to the relatively short time scale of fungal inubation or due to the spatial scale at which the pore geometry was quantified. Soil structure was quantified and visualised at a resolution of 30 µm. Such diameters correspond to the smallest pores expected to drain by the range over which water retention was measured in Chapter 3. In order to eliminate that the absence of an effect was the result of the fact that smaller pores were omitted from the analysis. Thus the next chapter aims to quantify the impact of *R. solani* on soil structure and pore geometry within individual aggregates.

CHAPTER 5

The effect of fungal growth on soil structure: analysis at the scale of individual aggregates

5.1. INTRODUCTION

The work in Chapter 4 investigated if pore geometry was affected for pores sized 30 µm and above. However, no evidence was found to support the hypotheses that fungi would alter soil structure. This chapter investigates this further by analysing soil aggregates at a much higher resolution of approximately 5 µm. The concept of aggregates as units upon which measurements can be conducted is debatable, but it is still the most widely used element of soil structure for analysis (Young *et al.* 2001). Soil structure can be defined at various spatial scales according to a hierarchy of its structural elements (Dexter 1988). The acknowledged scheme of aggregate hierarchy and formation (aggregation) has been developed by Tisdall and Oades in 1982 with very significant corrections in 1984 (Oades 1984, Six *et al.* 2004). The aggregate hierarchy theory is widely accepted event though abilities to test these have been very limited.

At the foundations of the theory of aggregate hierarchy are free primary mineral particles such as clay platelets (1-2 µm). These can be combined into aligned, flexible stacks (quasi-crystals), rigid platy particles (domains) or blocky particles with <10% of surface contact between primary particles (assemblage). 2-20 µm sized clusters of these particles can combine together by a range of physical and biological forces to form micro-aggregates (20-250 µm) (Dexter 1988). Macro-aggregates sized >250 µm are formed by micro-aggregates bound together physically by fungal hyphae, plant roots or chemically by polysaccharide binding agents of microbial or plant origin (Bossuyt *et al.* 2001). This theory of evolution from clay particle to macro-aggregate has been supplemented by Oades (1984) who introduced the theory of micro-aggregates within macro-aggregates. The breakdown of aggregates can be caused by soil stress caused by hydraulic activity (i.e. drying and wetting cycles) or mechanical disruption. Water has been identified as one of the major disruptive factors, and quick changes of water

content, especially rapid wetting, can build-up air pressure causing high levels of stress in weak planes (cracks defining initial surface of macro-aggregates) (Dexter 1988). Based on these examples I expect that wetting and drying cycles as well as fungal growth can potentially affect the structure of aggregates.

Aggregate dynamics can be described in three following stages: (i) formation, (ii) stabilisation and (iii) breakdown (De Gryze *et al.* 2005). The first two stages (formation and stabilisation) are mainly subject to microbial activity and soil organic matter (Bossuyt *et al.* 2001). Bacteria are considered to be involved mainly in inception of microaggregates, whereas fungal activity is mostly associated with formation of macroaggregates (De Gryze *et al.* 2005). Both groups of microorganisms take part in processes related to decomposition of soil organic matter, which leads to production of polysaccharide-based binding compounds. Thus, the influence of microorganisms on soil structure does not depend on the quantity of living organisms, but is rather a measure of their activity (Degens 1997).

For the purpose of this thesis the focus is on fungal activity. Fungi were described as '*engineers of soil structure*' (Tisdall *et al.* 1997). One of the main mechanisms inducing aggregation is that hyphal networks are able to surround soil particles (microaggregates) like a '*sticky string bag*' clustering them together (Bossuyt *et al.* 2001). This mechanism also enhances the resistance of aggregates to physical disruptive forces. Fungi also produce a range of organic exudates acting as a particle binding agents. One of most studied fungal exudates in this context is glomalin, an insoluble and hydrophobic proteinaceus substance counteracting the aggregates break down induced by water. The significance of glomalin has been demonstrated by numerous studies quantifying the relation between the presence of this substance and the amount of water stable soil aggregates (Wright *et al.* 1998, Wright *et al.* 2006).

However, in all cases, precise investigation of the internal structure of aggregates and quantification of soil structure characteristics (total porosity, connectivity, void size distribution, etc.) was not possible. More traditional methods for studying structure *in situ* such as 'thin sections' are destructive, time consuming and provide limited information based on microscopic investigation of cross sections. X-ray microtomography combined with image analysis offers a way forward.

Recent developments in X-ray microtomography cause a rapid increase in the number of studies applying this technique to soil science. De Gryze *et al.* (2006) in their study showed an impact of soil organic matter decomposition on the structure of aggregates. De Gryze *et al.* (2006) quantified the structural characteristics of aggregates sized 6 – 8 mm at a resolution of 13.4 µm after 21 days of incubation. There was an increase in total porosity values and pore morphology (newly formed cracks) in aggregates with organic matter in comparison with controls, being so called 'native' aggregates samples from the field. De Gryze *et al.* (2006) related structural changes to daily drying – wetting cycles during incubation and microbial activity.

Crawford *et al.* (2011) showed that the structure of microbial activity influences the structural changes of aggregates. Crawford *et al*. (2011) in their study quantified the structure of individual aggregates inoculated for 25 days with bacteria, bacteria and fungi and fungi on their own. Analysis with X-ray tomography, at the resolution of 9 µm showed that there was a significant effect only in case of aggregates incubated with soil-borne fungi (*R. solani*). Aggregates colonised by fungi showed an increase in porosity by 50 % on average. Also a modelling approach used in Crawford *et al*. (2011) showed significantly increased hydraulic conductivity from 0.27 cm/d for sterile soil to 1.5 cm/d for structures colonised by fungi, suggesting enhanced connectivity of pore network.

Another study quantified the effect of long term tillage effects on the structure and stability of soil aggregates. Kravchenko (2011b) used the same facilities at Advanced Photon Source in USA as was used to quantify the structure of aggregates in this chapter. Kravchenko (2011b) compared aggregates derived from soils sampled from field with no tillage, natural succession and conventionally tilled. The analysis at the resolution of 14.6 µm showed that the highest porosity was observed in soils with natural succession, which were also the most heterogeneously structured aggregates. Kravchenko (2011b) links the result with the decomposition of plant roots which could have increased the macroporosity of aggregates as was also shown by studies by De Gryze *et al.* (2006) and Crawford *et al*. (2011).

This chapter links closely to the quantification of the effect of colonisation with fungus *R. solani* on water retention (Chapter 3) and soil structure at the scale of the entire microcosm (referred to as macroscale in Chapter 4). Quantification of the impact of fungal growth on soil structure at the macroscale was performed with CT systems available in the SIMBIOS Centre and this showed no effect of the *R. solani* on soil structure. This part of the thesis focuses on the effect of fungal colonisation on individual aggregates (microscale) and characterisation of the structure of aggregates. For the best quality and highest resolution of CT data, samples have been scanned at Argonne Photon Source (APS) and subsequently analysed with software developed in SIMBIOS Centre and described in Chapter 2.

Access to the Advanced Photon Source is limited and constrained by conditions related to importing of foreign soils in the US. It was therefore not possible to analyse the aggregates at all sampling times. As no additional effect of the DW cycles was found in the previous chapter, only one cycle is compared in this chapter to analyse the effect of fungal colonization on the shape and internal structures of aggregates.

5.1.1. Hypotheses

1. Colonisation of soil microcosms by *Rhizoctonia solani* results in larger aggregates.

2. Colonisation of soil microcosms by *Rhizoctonia solani* will increase the porosity and connectivity of the pore space within soil aggregates.

5.2. MATERIALS AND METHODS

5.2.1. Soil Microcosms

Sandy loam soil sampled from the Bullion Field at an experimental site of James Hutton Institute (formerly Scottish Crop Research Institute) in Dundee (UK) was used to prepare the soil microcosms. Soil was air-dried and sieved to obtain aggregates sized 1-2 mm, as described in Chapter 2.1. Then the soil was sterilized by double autoclaving for 60 min with 48 hours interval. Sterilized soil was wetted up to a volumetric water content of 0.186 cm^3/g of soil (as set in chapter 2.1), and packed to PVC rings (4cm high and 4 cm diameter) at a same bulk density of 1.3 g/ cm^3. Half of microcosms (n=8) were inoculated with *Rhizoctonia solani* R5 fungi (as in chapter 2), the remaining microcosms were treated as controls (no fungal growth) and incubated for 5 days. The microcosms were then sterilized as previously by double autoclaving with 48 hours of interval as requirement prior shipping soil samples to Advanced Photon Source (APS) in Argonne. In the APS sample preparation room, the microcosms were destructively sampled. Only large (2-4 mm), intact aggregates were picked and glued with the use of superglue (Boliglue.com), to a toothpick for scanning purposes.

5.2.2. Quantifying the structure of aggregates

The quality of the data derived from X-ray tomographs relies on the contrast between different densities of material. The most optimal contrast can be obtained with the use of monochromatic beam generated by synchrotron instead of polychromatic beam common for commercial X-ray microtomographs. Hence, the approved beam time on research Beamline Station 13-BM-D at the Advanced Photon Source (Argonne National Laboratory, USA), operated by GeoSoilEnvironCARS (GSECARS) of the University of Chicago, was used in order to acquire 3-D datasets to characterize the inner structure of the aggregates.

Datasets were acquired with a monochromatic X-ray beam at the energy level of 20keV with 720 projections and an exposure time of 1s. Radiographs were reconstructed into 3-D volume at a resolution of 5.54 µm and sliced into image stacks (520 tiff images per aggregate) with the use of software developed in house at the APS. Further image analysis was carried out in the SIMBIOS Centre.

5.2.4. Image analysis – quantification of aggregate's physical properties and morphology in 3-D.

The analysis aimed to describe physical characteristics of aggregate structure as well as the morphology of aggregates. Thus the range of quantified characteristics of whole aggregates included descriptors such as porosity, pore network surface as well as the outer surface and total volume of aggregates. Image stacks of aggregates obtained from APS were first visually examined using ImageJ software to discard datasets, which contained stones or very fine particles held only by glue, as they would not be representative for physical characterization of aggregates.

In the next stage image stacks were imported in to VG Studio Max 2.1 which allows specifying of the voxel size and rendering of datasets in 3D. The first task was to segment aggregates from the glue surrounding it or the glue residue at the bottom of sample (Fig.5.1.). The region grower in VGStudiomax was used for that purpose because its algorithm selects voxels of interest with gray scale values within a specified range from the values of selected voxel. The selection of the region of interest was adjusted by an erode and dilate function (erode reduces the Region Of Interest (ROI), whereas dilate expands selection) to ensure that the segmented ROI included also all voxels belonging to internal porosity of aggregates.

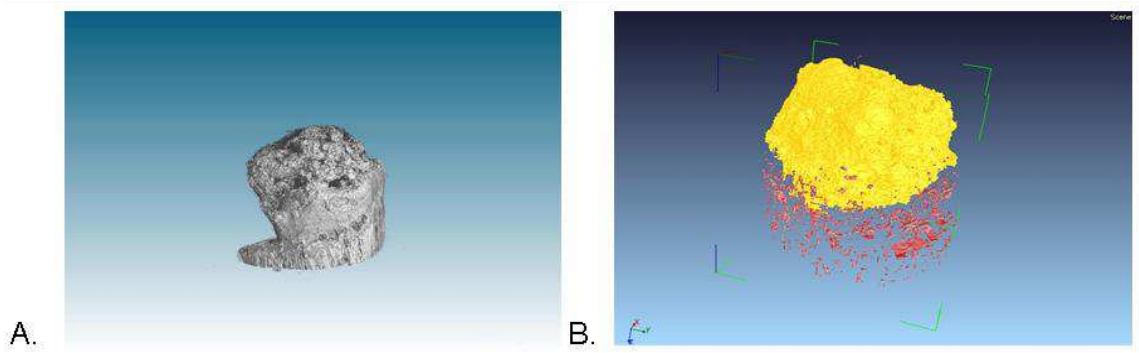

Fig.5.1. Segmentation – separating soil aggregate from the glue and parts of wooden toothpick: 3-D view of aggregate before segmentation (A) and the aggregate after removing residual glue (B), in yellow – larges connected volume, red – dense particles of toothpick or loose soil particles trapped by the glue that are not included in analysis.

Such selected regions of interest (formally the volume representing aggregates to be analyzed) were extracted to create a separate object, which was investigated independently from original volume which consisted of the aggregate and the glue.

The final stage for characterizing the morphology of aggregates was the quantification of physical properties of the volume of interest (whole aggregate). For this Volume Analyzer tool within VGStudiomax was used. This function calculates and

presents parameters such as volume of an object (in voxels and in physical units specified when importing the data) and their outer surface area.

The next stage of the analysis aimed to quantify the internal pore-space of aggregate. This required segmenting the volume once again to separate pore volumes from the solids. The first step was to create a border which prevents the selection tool from including the background, in this case the air and glue surrounding the aggregate. However, since the aggregates have already been separated from the background its surface area acted as such boundary. The region grower was used to select all internal pore space of the aggregates. The region grower tool was set to avoid other ROIs (e.g. only grayscale values within certain limits and belonging to the same volume are considered). This allowed the selection of a ROI only within the boundaries of the volume of aggregate. Segmented pore networks were saved as a new volume and characterized by the Volume Analyzer tool.

5.2.5. Image analysis – quantification of aggregate's physical properties based on subsamples

The second part of the quantification of the physical properties was carried out on cubical ROIs. Sub-sampled volumes characterised soil aggregates at microscales, but they don't reflect any possible morphological differences between aggregates of the two treatments. Image stacks were first imported to ImageJ and cropped to subsamples sized 128 x 128 x 128 voxels for further analysis. Images were not cropped around one fixed point. Selection of region of interest was done to avoid areas with visible glue, cracks and stones (Fig.5.2.).

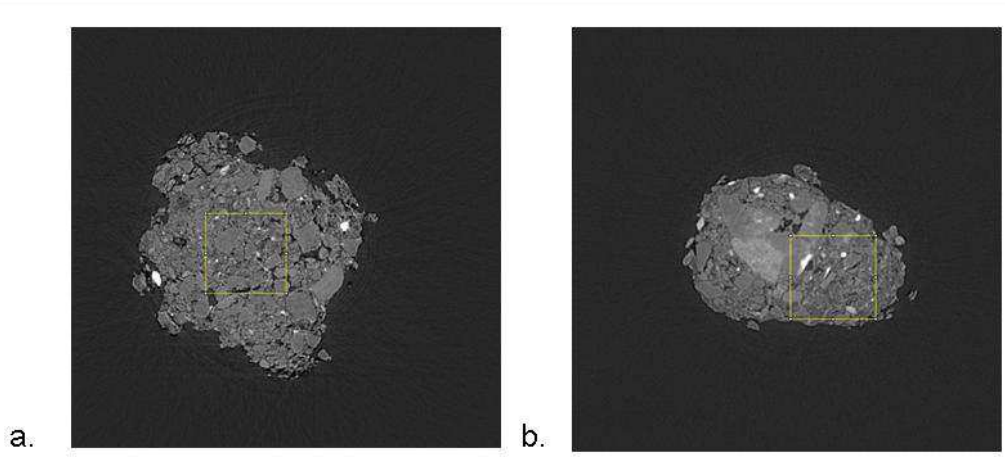

Fig. 5.2. Selection of region of interest sized 128 x 128 x 128 voxels avoiding areas with glue and large stones. Yellow square defines the selection of ROI.

In the next step, image stacks of the ROIs were imported to VGSM 2.1. Segmentation of the pore-space and quantification of structural characteristics including porosity, pore connectivity and the surface area of pore networks was carried out in VGSM following the procedure for the whole aggregates (Section 5.2.4.).

5.2.6. Statistical analysis

Means were derived and compared in SPSS package with the use of independent samples t-test. Significance was determined at 5% level of confidence. In the next step statistical summary of the data was generated. From the summary 2-D Boxplots were then used to visualise the distribution of the data paired with means and standard errors.

5.3. RESULTS

After selection of aggregates (see 5.2.1.) there were 30 aggregates left for image analysis (half of them inoculated and the other half controls). The quantification of physical characteristics of subsamples (128 x 128 x 128 voxels) showed that there are no significant differences between the treatments.

Sample name		Pore volume (voxels)	Volume of largest connected cluster (voxels)	Pore surface area (mm^2)	Connectivity (%)	Porosity (%)
Controls	C1	388395	355037	25.6	91.4	18.4
	C2	482560	469988	23.7	97.4	22.8
	C3	481324	471024	22.9	97.8	22.7
	C4	458479	448479	20.6	97.8	21.7
	C6	512997	493901	20.7	96.2	24.2
	C7	390275	372246	21.1	95.3	18.5
	C8	445790	431075	19.7	96.7	21.0
	C9	419099	379960	20.7	90.6	19.8
	C10	474070	464889	21.3	98.0	22.4
	C12	508194	473877	30.7	93.2	24.0
	C17	496007	448936	30.1	90.5	23.5
	C21	494665	469413	32.0	94.9	23.4
	C22	488445	467437	27.8	95.7	23.1
	C23	405175	375843	23.0	92.7	19.7
	C25	475022	447681	31.8	94.2	22.5
Soil inoculated with *R. solani*	F3	305848	292582	16.0	95.6	14.5
	F4	523702	489961	23.5	93.5	24.8
	F5	551316	545754	25.0	98.9	26.0
	F7	554922	522104	25.2	94.0	26.3
	F8	507872	471122	25.7	92.7	24.0
	F10	454307	422115	27.1	92.9	21.5
	F12	403143	371805	21.4	92.2	19.0
	F14	450344	410397	30.7	91.1	21.3
	F15	459258	421397	29.9	91.8	21.7
	F18	522653	493719	33.2	94.4	24.7
	F19	528005	478197	32.5	90.6	24.9
	F20	490074	457294	30.0	93.3	23.2
	F21	597695	560064	31.6	93.7	28.3
	F24	581401	548010	30.9	94.3	27.2
	F25	433079	401634	30.4	92.7	20.5

Table 5.1. The results of measurements of the structural characteristics for individual cubic ROIs, cropped from aggregates inoculated with *R. solani* and controls.

Both treatments had an inter-aggregate pore space volume which was very well connected (p = 0.1), with over 90% of total internal porosity belonging to the largest connected cluster (Table 5.1). Also in both cases the porosity values were similar (p = 0.2), with mean values of 23.2% for aggregates inoculated with *R. solani* and 21.9% for controls (Table 5.2). There was a trend showing larger mean pore surface area for ROIs cropped from aggregates colonized with *R. solani* than in controls, with mean values of 27.5 mm^2 and 24.8 mm^2 respectively. However, statistical analysis showed that this difference was not significant (p = 0.11).

	Porosity (%)	**s.e.**	**Connectivity (%)**	**s.e.**	**Pore surface area (mm^2)**	**s.e.**
Control	21.80	0.01	94.80	0.01	24.70	1.10
Fungal	23.20	0.01	93.40	0.01	27.50	1.20

Table 5.2. Mean values of physical descriptors of soil structure quantified on region of interest (sized 128 x 128 x 128 voxels) with the use of ImageJ. Mean values and standard errors represent n = 15 replicates per treatment.

The basic descriptive factors derived from artificially selected subsamples didn't show any significant differences between inoculated microcosms and controls hence whole aggregates were analysed to enable more descriptive factors related to shape and size (Table 5.3).

The additional measurements showed that aggregates sampled from control microcosms (without fungi) had insignificantly (p = 0.7) smaller volume of 3.3 mm^3 in comparison to ones inoculated with fungi which had a mean value of 3.4 mm^3 (Fig.5.3). The outer surface of control aggregates was also smaller 23.8 mm^2 than the surface of aggregates inoculated with fungi 28.4 mm^2 (p = 0.07), similarly the surface of internal pores in controls was smaller 133.2 mm^2 than for inoculated samples (164.2 mm^2) (p =

0.2) (Table 5.4). However, statistical analysis showed that the differences between treatments are not significant (p values >0.05).

Sample name		Aggregate volume (mm^3)	Surface of aggregates (mm^3)	Volume of pores (mm^3)	Pore surface area (mm^2)	Porosity (%)
Controls	C1	3.6	25.1	0.8	192.8	21.6
	C2	2.3	15.8	0.3	100.5	12.9
	C3	2.1	16.7	0.2	88.9	12.3
	C4	2.2	15.7	0.2	69.8	9.6
	C6	3.5	21.2	0.7	99.9	18.7
	C7	2.9	23.1	0.9	183.2	23.4
	C8	3.2	30.6	0.5	132.4	13.9
	C9	3.8	24.5	0.4	77.5	7.3
	C10	3.6	28.8	0.3	112.0	9.7
	C12	2.9	21.1	0.2	80.0	7.6
	C17	2.4	18.6	0.4	157.7	17.1
	C21	4.9	32.0	0.7	195.0	13.6
	C22	3.2	25.0	0.3	142.6	10.0
	C23	3.9	26.0	0.6	164.2	14.4
	C25	3.8	36.8	0.6	220.0	14.7
Soil inoculated with *R. solani*	F3	2.0	22.5	0.4	126.4	21.3
	F4	4.4	26.0	0.9	234.8	19.8
	F5	2.5	22.4	0.2	58.2	7.5
	F7	5.3	37.8	1.0	314.6	19.1
	F8	4.9	28.0	0.7	144.3	15
	F10	3.1	22.5	0.6	230.7	17.7
	F12	7.7	25.5	0.9	270.6	25.9
	F14	3.2	25.0	0.3	122.5	9.0
	F15	3.6	31.0	0.4	152.8	10.0
	F18	3.3	24.5	0.6	240.0	16.8
	F19	2.4	28.0	0.3	117.3	13.3
	F20	3.0	22.7	0.3	117.5	9.3
	F21	3.6	24.0	0.2	108.7	6.9
	F24	2.0	46.3	0.2	73.0	8.3
	F25	3.9	40.3	0.3	151.3	8.5

Table 5.3. The results of measurements of the physical and morphological characteristics for individual aggregates inoculated with *R. solani* and controls.

Treatment	Volume of aggregates (mm^3)	s.e.	Outer surface of aggregates (mm^2)	s.e.	Surface of pores (mm^2)	s.e.	Porosity of aggregates (%)	s.e.
Control	3.3	0.2	23.8	1.4	133.2	12.5	13.8	1.2
Inoculated	3.4	0.2	28.4	1.9	164.2	19.5	13.9	1.5

Table 5.4. Mean values of physical descriptors of soil structure quantified on whole aggregates with the use of VG Studio Max 2.1. Mean values and standard errors represent n = 15 replicates per treatment.

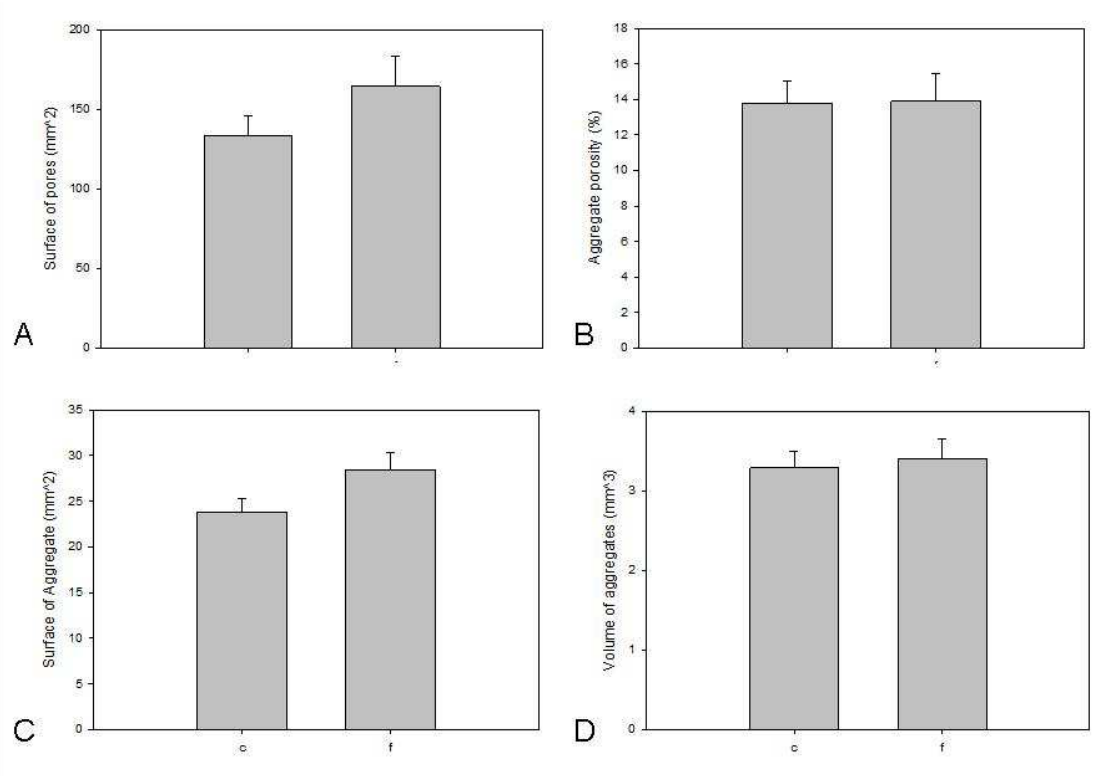

Fig.5.3. Mean values and standard errors of physical and morphological properties: surface of pores (A), porosity (B), outer surface of aggregates (C) and volume of aggregates (D) quantified on whole aggregates. There are differences between surface of aggregates (A) and surface of pore networks (C). However, these were found to be insignificant ($p > 0.05$).

The difference in aggregate size (volume) could have been caused by subjective sampling of aggregates. To exclude that this would affect the output of analysis, the aggregates structure (Table 5.3.) was corrected for the volume of aggregates by looking at relative values (Table 5.5). Despite no significant differences in porosity values between 13.8% for control samples and 14% for those inoculated with fungi ($p = 1$) there was a difference in outer surface of aggregates and the surface of internal pores. However, comparison of means with independent samples t-test showed that these differences were not significant (P value for outer surface of aggregates was 0.1 and for surface of pores $p = 0.2$). Aggregates from samples colonised by fungi were more variable than controls (Fig. 5.4.)

Treatment	Outer surface of aggregates (mm^2)	Surface of pores (mm^2)	Porosity of aggregates (%)
Control	7.3	40.9	13.8
Inoculated	9.0	47.9	14.0

Table 5.5. Quantification of aggregates characteristics, corrected for the volume of aggregates.

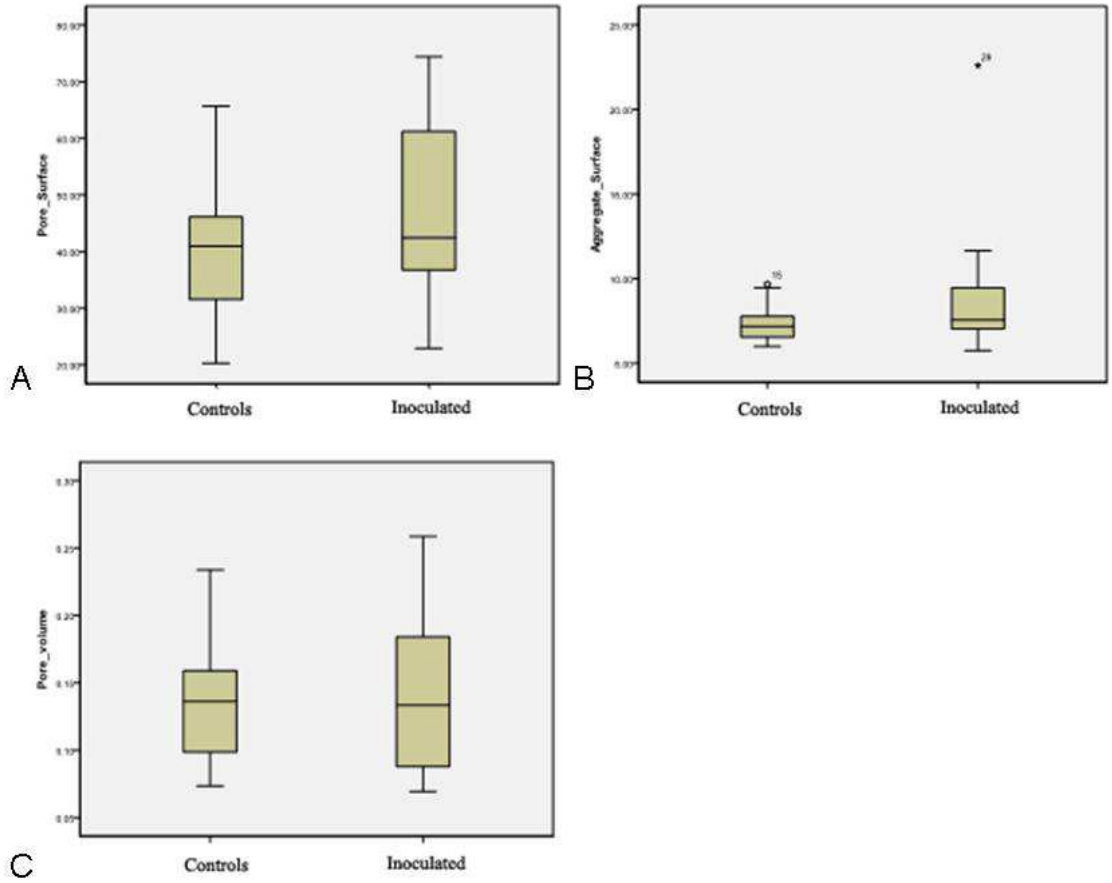

Fig. 5.4. Box plots showing the distribution of the data and mean values for aggregate characteristics corrected in respect to volume: A - the pore network surface, B – outer surface of aggregate and C the pore volume. Mean values and standard errors represent n = 15 replicates per treatment.

5.4. DISCUSSION

Analysis of the datasets generated at the APS was done with the use of two methods: physical characteristics of whole aggregates and analysis of selected regions of interest sampled from the aggregate. Analysis of such subsamples sized 128 x 128 x 128 voxels focused on physical description of internal structures of aggregates using descriptive factors such as porosity, pore network connectivity and pore surface area. Cutting the

cubical ROI from the datasets aimed to capture structural characteristics, which are not biased by the morphology of the aggregates. Also it was reported that internal pore structure of aggregates differed from the surface of aggregates and as a result the pore networks between the aggregates was different. These differences occur in the size and structures of the microbial community (Drazkiewicz 1994, Drazkiewicz 1996, Blackwood and Paul 2003) affecting the rates of microbial respiration contributing to the storage and decomposition of soil organic matter like Phosphorus and Nitrogen (Santos *et al.* 1997, Smucker *et al.* 2007) .

The analysis of whole aggregates included additional morphological factors like the volume of aggregates, surface area of pores and aggregates. The output of the analyses for the whole aggregates was corrected for differences in the volume of aggregates to avoid the artefacts in the data caused by subjective selection of aggregates. Due to the variability in the data, the comparison of means in both cases showed that these differences were not significant. Box plots (Fig.5.4.) showed that the range of data corresponding to samples inoculated with fungi was wider than that for controls.

Statistical analysis showed significant differences in porosity values between the two methods of analysis. Cubical regions of interest had mean values of 21.8 % for control samples and 23.2 % for those inoculated with fungus, whereas analysis of whole aggregates provided significantly smaller means of 13.8 % for controls and 13.9 for fungal samples. The difference in porosity values could possibly be explained by the method of selecting cubical subsamples from the aggregates. As previously stated (Section 5.2.1.) the aggregates were sampled destructively from the larger microcosms (cylindrical samples 4 x 4 cm), and some of them were discarded prior to analysis as they contained large stone with only few soil particles surrounding it or the samples

consisted of small soil particles held together by glue residues. However, many aggregates still contained stones, cracks or some glue residues. The cubical subsamples have been carefully selected to avoid such areas and as much as possible contain only soil particles. During the analysis of whole aggregates the glue had been segmented out and discarded however it included stones within aggregates, which may have caused the aforementioned differences. De Gryze *et al.* (2006) overcame that problem by analysis of artificial, secondary aggregates formed from fine (<250 µm) soil particles, packed and incubated with addition of organic matter.

This chapter exhibits the advantage of up to date analysis methods that allow the non-invasive quantification of internal structure of porous materials in 3-D. X-ray microtomography combined with image analysis that replaced 2-D thin sectioning is less time consuming, more accurate and non-destructive. The advantages allow increased number of replicates and for the possibility to track the changes in various stages of the processes (multiple scanning).

The statistical comparison of means did not show any differences between the treatments. Also it was impossible to see any fungal colonies in our samples due to the differences in the density between soil material and fungal hyphea. Fungal colonies have been visualised to date in sub-micron scans of wood samples (Van den Bulcke *et al.* 2009). Soil material is much more dense and heterogeneous than wood which could result in insufficient density contrast between soil particles and fungal hyphae. In addition fungal biomass could be damaged as samples analyzed in this chapter had to be sterilized before dispatch to the United States (Carter *et al.* 2007) – a condition imposed by US customs. It is also speculative if fungi could penetrate inner pore space of aggregates (Ritz and Young 2004). Fungi are generally known to prefer well connected macropores (space between aggregates) where they can freely branch, or at least pores

not smaller than the diameter of fungal hyphea (Otten *et al.* 2004). Also the most common mechanism of fungal input to improve stability of macro-aggregates is surrounding the soil particles with hyphae and grouping micro-aggregates and small particles into macro-aggregates (Bossuyt *et al.* 2001).

Recent studies (De Gryze *et al.* 2006, Crawford *et al.* 2011, Kravchenko *et al.* 2011b) showed an impact of fungal growth on the structure and morphology of pore networks in aggregates. The lack of significant differences quantified in this thesis could be related to the short term incubation of *R. solani* in soil. De Gryze *et al.* (2006) observed structural changes after 21 days of incubation, Kravchenko *et al.* (2011b) quantified the structure of aggregates from different tillage methods applied on the site for the last 24 years and Crawford *et al.* (2011) using the same type of fungus (*R. solani*) showed structural differences after 25 days of incubation. Thus there was missing information about the short term effects of fungal growth on soil structure quantified in this chapter. *R. solani* was incubated for only 5 days but this was proved to be sufficient for growth (Chapter 2). The lack of significant structural differences could be also related to the treatment of aggregates prior sending them overseas. Whole soil microcosms from which analyzed aggregates were sampled had to be autoclaved (shipment license requirements) twice at 120^{o}C with 60 min holding time and with 24 h interval. This process could interfere with changes to the soil structure (Wolf 1994, Lotrario *et al.* 1995). It is also possible that the scale at which we quantify the properties of soil structure after short time incubation with *R. solani* is still too large.

5.5. CONCLUSIONS:

The structure of individual aggregates was visualised and quantified at the Argonne Photon Source at a resolution of 5.54 µm. Protocols were developed to analyse the

shape and internal structure of individual aggregates. This analysis complements the analysis in Chapter 4 where the impact of the growth of *R. solani* on soil structure was quantified at a resolution of 30 µm which will predominantly include pores between aggregates. Aggregates of soil inoculated with *R. solani* had a larger volume and surface area of pore networks. However, statistical analysis proved that these observations were not significant. Therefore similarly to the findings in Chapter 4, the quantification did not find any significant effects of fungal colonization on the total porosity values and the pore network connectivity.

CHAPTER 6

Manipulation of pore geometry in repacked soil microcosms

This work is part of a publication in preparation and some of the work has been done in combination with another PhD student derived networks from the same data and used network properties as additional quantitative measures of pore geometry. The outcome of that part of the study is described in the PhD thesis of Dr Amin Garbout, *'3D quantification of soil structure and functioning based on PET and CT scanning techniques'*.

6.1. INTRODUCTION

In a natural environment one of the basic mechanisms determining soil structure is aggregation. Soil particles are joined and compacted by various physical forces such as drying and wetting cycles, freeze and thaw cycles or tillage operations. The outcome is the combination of processes is a very heterogeneous material, with its three phases solid, liquid and gas constantly changing with time (Tisdall and Oades 1982). Physical characteristics of soil structure can be quantified by a number of destructive laboratory experiments. Aggregate size and stability can be determined by sieving and sedimentation of the solid phase material, porosity can be quantified with the use of a gas pycnometer, mercury intrusion or approximated by water desorption methods which also informs about pore size distribution of the soil (Klute 1986). Other methods for visualisation of soil structure which operate at smaller spatial scales include thin sectioning (Harris *et al.* 2003, Nunan *et al.* 2003) but these involve disrupting the microcosms. More recently, the evolution of CT microtomography is becoming a more popular, readily available and non destructive tool in soil imaging and analysis (as described in chapter 2.3).

It is widely recognized that soil structure is the key driver of biological and physical processes underpinning ecosystem services and the role of soil structure and soil physical conditions is increasingly receiving interest (Nunan *et al.* 2006). The difficulty to capture the structural heterogeneity in microcosms means that we typically disrupt all physical structure when collecting soils. Often this process is followed by a process of drying and sieving, thereby exerting physical forces upon soil to disrupt the structure. We then use surrogate measures of soil structure such as aggregate size distribution and bulk density, in an attempt to recreate conditions encountered in the

field. These bulk-measures are too crude and do not describe the heterogeneity at microscopic scales where microorganisms operate.

The geometry of pores and the surface area of soils are key characteristics that would be expected to affect microbial interactions. The complex pore geometry can offer refuge for microbes (Young *et al.* 2008) determine pathways for interaction and preferential pathways for fungal spread (Otten *et al.* 2004) and water flow and provide surfaces for bacterial attachments, access to food sources and nutrient adsorption (Young *et al.* 2008). Recent advances in the use of X-ray CT in soils research means that these characteristics can be readily quantified (Vogel *et al.* 2010), and various papers in recent years have described the impact of management strategies and physical forces on soil structural characteristics (Peth *et al.* 2010, Kravchenko *et al.* 2011b, Schluter *et al.* 2011). Given the importance it is perhaps surprising that the impact of the key experimental control factors that are used in the preparation of microcosms, namely aggregate size distribution and bulk density, on the pore geometry remains un-quantified to date beyond readily measurable porosity. Therefore we have little insight in the loss of naturally occurring structural characteristics when we prepare soil microcosms, nor in the possibility to manipulate and control these in a pre-described manner.

Although the construction of microcosms is important for a variety of studies, the emphasis of this thesis is on the role of fungi hence the work focused on factors that control pore geometry that is expected to have an impact on fungal growth dynamics. It is known that fungal growth is not limited to water films (like bacteria) as they have ability to translocate nutrients within hyphal network (Ritz and Young 2004). Also fungal spread is not random through a soil structure and hyphea tend to follow preferential pathways through soil. Otten *et al*. (2004) proved that fungi are more likely

to select the large connected pores to actively avoid more complicated networks with small pores. However the smallest colonized pores must be larger in diameter than a fungal hyphea and connected with other pores to allow branching of hyphea.

The impact of different bulk densities of soil on fungal colonisation were previously studied by Harris *et al*. (2003) who used 2-D cross sections that showed different growth behaviour according to changes in density. For low bulk-densities the fungal colonies were sparse and patchy, whereas with an increase of density colonies were more compacted and dense. Chapter 7of this thesis showed that increase in bulk soil density significantly slowed down the colonisation of the pore networks. There was also a decline in the amount of fungal biomass with an increase in density which links to changes in amount of pores available for colonisation.

The aim of the current chapter is to visualise and quantify pore geometry of soil microcosms prepared with commonly used surrogate experimental measures of soil structure. Specifically to quantify how variable replicated microcosms are in pore geometry and which characteristics of pore geometry are most affected by bulk-density (BD) and aggregate–size distribution (ASD) as the two most commonly used empirical surrogates of soil structure. We address these questions by quantifying the pore space of replicated soil microcosms with X-ray CT and use porosity, connectivity, pore size distribution and surface area as quantitative parameters.

6.1.1. Hypotheses

1. The properties of soil pore networks can be manipulated in a replicable way for re-packed soil microcosms with bulk-density mainly affecting pore volume and aggregate-size mainly affecting pore geometry.

2. An increase in bulk-density of soil microcosms reduces the total porosity and decreases the amount large pores in the re-packed soil microcosm.

3. The increase in diameter of aggregates used to pack soil microcosm does not affect the total porosity values but increases the number of large pores.

6.2. MATERIALS AND METHODS

6.2.1. Preparation of soil samples

Two series of packed microcosms were examined in this study. For all samples were obtained from a sandy loam soil sampled from an experimental site, Bullion Field, situated at the James Hutton Institute, Dundee Scotland (formerly known as the Scottish Crop Research Institute). Further description of the soil can be found in Chapter 2.

In order to quantify the effect of aggregate sizes in soil microcosms, soil was air dried and sieved to obtain three fractions of aggregates: <1 mm, 1-2 mm, 2-4 mm. From these fractions we created two additional mixtures, one comprising 50% (w/w) of aggregates <1 mm and 50% (w/w) of 1-2 mm, hereafter referred to as <2 mm, and the other comprising 50% (w/w) of 1-2 mm and 50% (w/w) of 2-4 mm, hereafter referred to as 1-4 mm. All fractions were wetted up to a volumetric water content of 0.186 g/g, and packed in PVC rings (4 cm high and 4 cm diameter) at a density of 1.3 g/cm^3, a representative density for field conditions for this type of soil. There were 4 replicates for each treatment.

For quantification of the impact of different soil bulk densities on the soil structure, we selected samples from a previous study that used resin impregnated soils to look at the effect of soil structure on fungal growth Harris *et al.* (2003). These samples were from the same soil type as described above but sampled at a different time. The samples were sieved to obtain a fraction of 1-2 mm and packed at densities of 1.3 (n = 2), 1.4 (n = 3), 1.5 (n = 4), and 1.6 (n = 2) g/cm^{-3}. These densities reflect

conditions for this soil type ranging from just after ploughing to very dense soil conditions such as those found under wheel tracks.

Quantification of soil structure with X-ray CT

An X-ray microtomography system, HMX225, was used to characterise and visualise the internal soil structure (NIKON, http://www.nikonmetrology.com/). All microcosms used to quantify the effect of aggregate sizes were scanned at 120 keV, 125 µA, 2979 angular projections with 2 frames per second and a 0.1 mm aluminium filter. Radiographs were reconstructed into 3-D volumes using CT-Pro (NIKON, Tring, UK) at a resolution of 29.4 µm. Data were imported into VGStudiomax (Volumegraphics, Heidelberg, Germany, www.volumegraphics.com) and converted into stacks of voxel-thick, 8-bit gray scale bmp images. All image stacks were cropped around a fixed central point to a cuboid sized 300 x 300 x 900 voxels. Because of computational limitations of image analysis software packages used to calculate the geometric characteristics, datasets had to be sub-divided into 3 samples sized 300 x 300 x 300 voxels each. These subsamples were treated as pseudo-replicates in the analysis.

The samples that we used to quantify the effect of bulk density were scanned at 160 keV, 202 µA, 2855 angular projections with 2 frames per second and 0.1 mm Aluminium filter. For the rest data handling, reconstruction and resolution of the final data set was as described above with cubed samples 300 x 300 x 300 produced from each sample.

Quantification of soil pore geometry

Segmentation of pores from the grey-scale was done with an algorithm based on a segmentation method developed by Schluter *et al*. (2010) (Houston, personal

communication). The method applies edge detection and uses gradient masks, which are regions of interest around the soil-pore interface, for the determination of threshold values. As edge detection and thresholding methods are sensitive to noise (Schluter *et al.* 2010) a median filter with a radius of 2 was applied in ImageJ (http://rsbweb.nih.gov) prior to data processing.

Geometric characterization (porosity, connectivity, pore-size-distribution and surface area) was performed within ImageJ (Pajor *et al.* 2010, Crawford *et al.* 2011). In brief, porosity was calculated as the percentage of voxels corresponding to pores in relation to the total number of voxels representing solids and pores. Pore size distribution was obtained with the use of a growing sphere algorithm, by computing for each voxel the spheres of maximum diameter whilst excluding the pore space which has been previously covered by another sphere. Connectivity was calculated as the percentage of connected pore space in respect to the total porosity with pores classified as belonging to the same cluster if directly neighbouring voxels are both classified as pore. Finally the surface area which is proportional to a number of transitions between solid phase and pore within a volume was quantified, and expressed as a unitless ratio relative to the surface area of a side of the cube (Vogel *et al.* 2010, Falconer *et al.* 2012).

6.2.2. Statistical analysis

In the treatment quantifying the impact of different aggregate sizes on soil structure every size class had 4 replicates. Each microcosm was divided into 3 subsamples (pseudo-replicates). For the comparison of the structural characteristics between these microcosms, each pseudo-replicate was considered as an independent sample. The

significance of structural differences between the treatments was tested with use of independent samples t-test with 5 % confidence interval.

6.3. RESULTS

6.3.1. The effect of various aggregate sizes on pore network structure.

Visual comparison of selected representative 2-D slices (Fig.6.1) indicated that soil structure was affected by the use of various aggregate sizes during packing of microcosms. There were clearly visible differences in the sizes of pores which increased with the diameter of aggregates used to create the microcosms. Different sizes of aggregates that were used to prepare the microcosms were still easy to recognize. Prior to analysis however a noise filter needed to be applied (Fig.6.1.).

Examination of pore space in 3-D showed that all samples had very well connected pore networks, all of them with more than 90 % of the pores linked into the largest cluster (Table 6.2). The average values even were 98 % or more (Table 6.1.). The soil bulk-density of 1.3 g/cm^3 was used for the analysed microcosms. This density was identified as the most representative for the experimental field from where the soil was sourced (Chapter 3) and samples packed at similar initial physical conditions have been analysed (Chapters 4).

Because the microcosms were packed at the same density it was expected to achieve the same volume of pores across treatments. Although there were visible variations of porosity values amongst the subsamples (Table 6.2.) the mean values derived for the treatments (Table 6.1., Fig.6.1.) showed very similar values between the treatments varying from 27.5 % for aggregate size class 2 - 4 mm to the value of 29.1 % for aggregates sized <2 mm ($p = 0.868$ between the extreme treatments).

The most significant differences were detected in the surface area of the pores. There was a decline in mean pore network surface with increasing size of aggregates. The highest value of 44.2 (unitless) was noted for the microcosms built with the smallest aggregate size (<2 mm), and the values decrease to 29.6 for microcosms with aggregates sized between 2-4 mm ($p = 0.01$).

There was a noticeable increase in mean median pore size class (classes are multiplication of the resolution of the datasets) from 149.5 µm for microcosms prepared with aggregate sizes smaller than 2 mm to 156.8 µm for samples with an aggregate size range of 2-4 mm (Table 6.1).

Treatment	**Porosity (%)**	**s.e.**	**Connectivity (%)**	**s.e**	**Surface area**	**s.e**	**Mean median pore size (µm)**	**s.e.**
<2 mm	29.1	1.4	98.7	0.2	44.2	1.66	149.5	2.4
1-2 mm	28.1	1.2	98.8	0.1	35.7	0.85	151.9	3.3
1-4 mm	28.6	1	98.9	0.1	32.4	0.93	154.3	3.8
2-4 mm	27.5	2	98.1	0.4	29.6	0.64	156.8	4.1

Table 6.1. Mean estimates for physical properties of microcosms used for investigating the impact of aggregate size on pore networks. Mean values and standard errors represent 12 replicates per treatment.

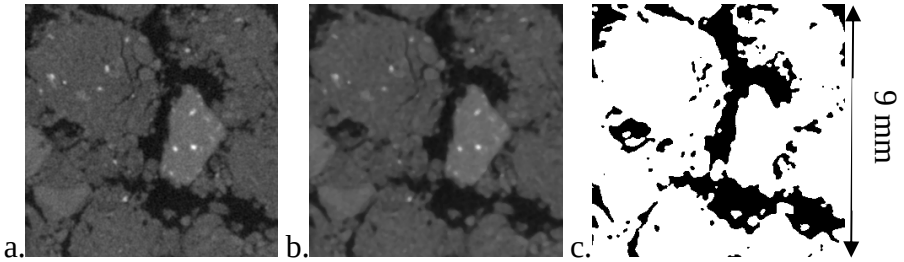

1-4 mm

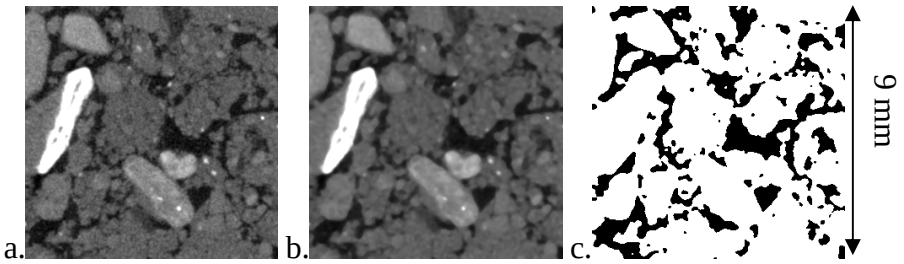

1-2 mm

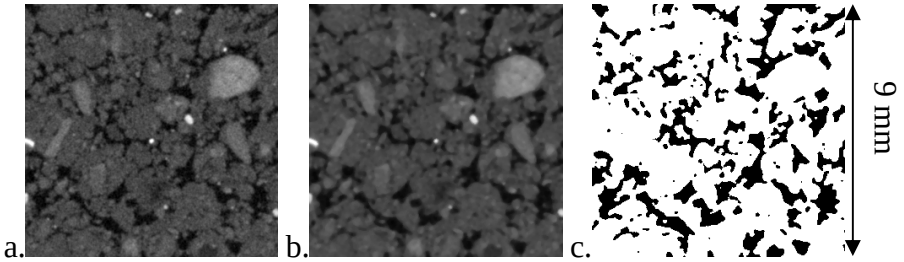

<2 mm

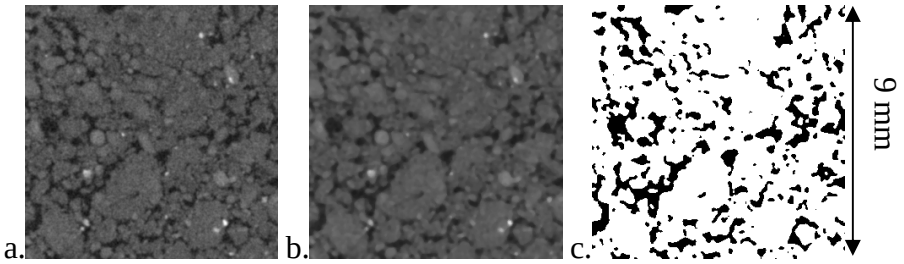

Fig. 6.1. Visual comparison of microcosms prepared with different aggregate sizes at various stages of image analysis: a – gray scale image, b – g/s after applying filter, c – binarized dataset.

Aggregate size	Sample number	Subsample	Porosity (%)	Connectivity (%)	Surface area
1-2 mm	1	A	27.4	98.9	36.6
		B	25.5	97.6	30.8
		C	35.3	99.4	35.9
	2	A	26.7	98.7	37.1
		B	25.0	98.7	36.8
		C	32.9	99.4	41.7
	3	A	26.2	98.9	36.6
		B	24.6	98.5	34.4
		C	33.4	99.5	37.1
	4	A	24.9	98.3	33.0
		B	23.0	97.5	31.2
		C	32.8	99.5	37.3
1-4 mm	1	A	28.3	98.5	34.6
		B	25.1	98.3	28.3
		C	35.0	99.1	30.4
	2	A	25.6	98.7	31.2
		B	22.4	98.4	28.6
		C	30.9	99.2	31.9
	3	A	27.2	98.5	27.9
		B	28.4	98.9	32.4
		C	29.2	99.2	35.9
	4	A	30.8	99.1	35.5
		B	27.8	98.9	35.4
		C	32.8	99.3	37.1
<2 mm	1	A	21.3	97.6	35.1
		B	21.7	97.6	36.5
		C	28.8	99.0	37.0
	2	A	32.6	99.5	44.1
		B	29.2	98.8	41.2
		C	26.8	99.0	43.5
	3	A	29.7	99.2	45.7
		B	34.3	99.6	49.6
		C	38.7	99.8	52.2
	4	A	27.8	99.1	47.2
		B	33.0	99.5	49.4
		C	26.4	98.7	49.5

Table 6.2. The physical characteristics of microcosms packed with use of various aggregate size classes at a density of 1.3 g/cm^3. Surface area is expressed as the ratio without units (Section 6.2.1 for details).

Aggregate size	Sample number	Subsample	Porosity (%)	Connectivity (%)	Surface area
	1	**A**	22.6	97.9	25.0
		B	24.4	98.3	27.8
		C	33.3	99.4	28.1
	2	**A**	25.8	98.7	30.8
		B	24.5	98.2	29.1
		C	39.2	99.4	31.8
	3	**A**	19.1	94.3	28.7
		B	24.9	98.3	31.4
		C	39.3	99.5	33.6
	4	**A**	21.6	97.2	30.1
		B	21.1	97.2	28.8
2-4 mm		**C**	34.0	98.7	30.2

Table 6.2. Table continued from p.148.

Further analysis of the pore size distribution confirmed that the microcosms prepared with aggregates sized <2 mm and 1 – 2 mm had the largest number of pores belonging to size classes between 58.8 µm to 205.8 µm (Fig.6.2). From the point with pores of a diameter higher than 250 µm (macropores) the curves for mean pore size distribution crossed showing that microcosms build with aggregates sized above 2 mm had the highest number of macro-pores.

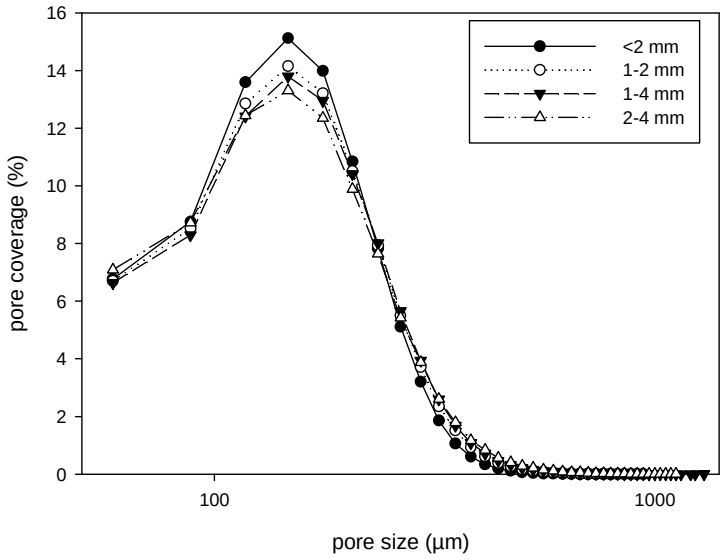

Fig. 6.2. Mean pore size distribution of microcosms prepared with various aggregate size range.

6.3.2. The effect of different bulk soil densities on pore network structure.

Bulk-density had a significant impact on the characteristics of the pore network. Even visual inspection of 2-D slices (Fig.6.3) showed that with increasing soil bulk-density there was a reduction in the bulk-porosity. The only samples that were outliers are microcosms packed at a density of 1.2 g/cm^3, which seemed to have a relatively low number of pores for such loose material. If these data were omitted from the analysis, a noticeable decrease in the amount of large pores with increasing bulk-density was found with small pores and thin valleys gradually substituting larger pores.

Image analysis showed that all datasets apart from the treatment of 1.2 g/cm^3 had more than 90% of pore space connected into the largest cluster (Table 6.3). Also quantification of physical structure confirmed the trend observed in Fig.6.3. of a decrease in porosity with an increase in bulk-density.

The lowest porosity values were found for the treatment with a density of 1.2 g/cm^3 with values of 18.7 %. This treatment had also the lowest connectivity value of 81.9 %, a mean median pore size (117.6 µm) and surprisingly the lowest pore surface area (22.03). From this point onwards this sample is being treated as an outlier.

The highest bulk porosity value of 30.1 % was found for the treatment with a density of 1.3 g/cm^3 and from then on the values significantly decreased ($p = 0.03$) with increasing bulk density to a porosity of 22.6 % for samples packed at a density of 1.6 g/cm^3 (Table 6.4). Mean surface area values increased with increasing bulk density from 26.0 for a density of 1.3 g/cm^3 to 38.1 for a density of 1.6 g/cm^3 ($p = 0.04$). Increasing surface area suggested an increase in fine pores and thin valleys with increasing bulk-density. The mean median pore size declined with in the increasing soil

compaction. The most densely packed material showed the mean median pore size of 132.3 µm, whereas in the most loosely packed soil it was 147 µm.

Treatment	Sample	Porosity (%)	Connectivity (%)	Surface area
1.2	**A**	23.7	93.6	29.2
	B	17.3	74.8	19.5
	C	15.1	77.4	17.2
1.3	**A**	31.3	98.1	24.6
	B	28.9	97.2	27.3
1.4	**A**	29.8	98.7	35.4
	B	29.6	98.6	33.4
	C	27.7	97.4	36.8
1.5	**A**	24.7	96.9	37.8
	B	27.4	98.1	38.9
	C	27.2	98.3	39.4
	D	27.4	97.5	26.5
1.6	**A**	22.1	96.6	37.9
	B	19.7	93.9	34.8

Table 6.3. The physical characteristics of microcosms packed at different bulk density values and aggregate size of 1 – 2 mm. Surface area measurements are expressed as unitless ratio.

Treatment	Porosity (%)	s.e.	Connectivity (%)	s.e	Surface area	s.e	Mean median (µm)	s.e.
1.2 g/cm^3	18.7	2.56	81.9	5.88	22.1	3.69	117.6	0
1.3 g/cm^3	30.1	1.19	97.6	0.45	26.0	1.34	147	0
1.4 g/cm^3	29.0	0.68	98.2	0.42	35.3	0.98	147	0
1.5 g/cm^3	26.7	0.67	97.7	0.31	35.6	3.06	147	0
1.6 g/cm^3	22.6	1.23	96.2	1.35	38.1	1.58	132.3	14.7

Table 6.4. Mean values for structural descriptive factors of microcosms prepared with different bulk soil densities and aggregate size of 1 – 2 mm. Mean values and standard errors represent three replicates for densities 1.2 g/cm^3, 1,4 g/cm^3, two for densities 1.3 g/cm^3, 1.5 g/cm^3 and one for microcosms packed at density of 1.6 g/cm^3.

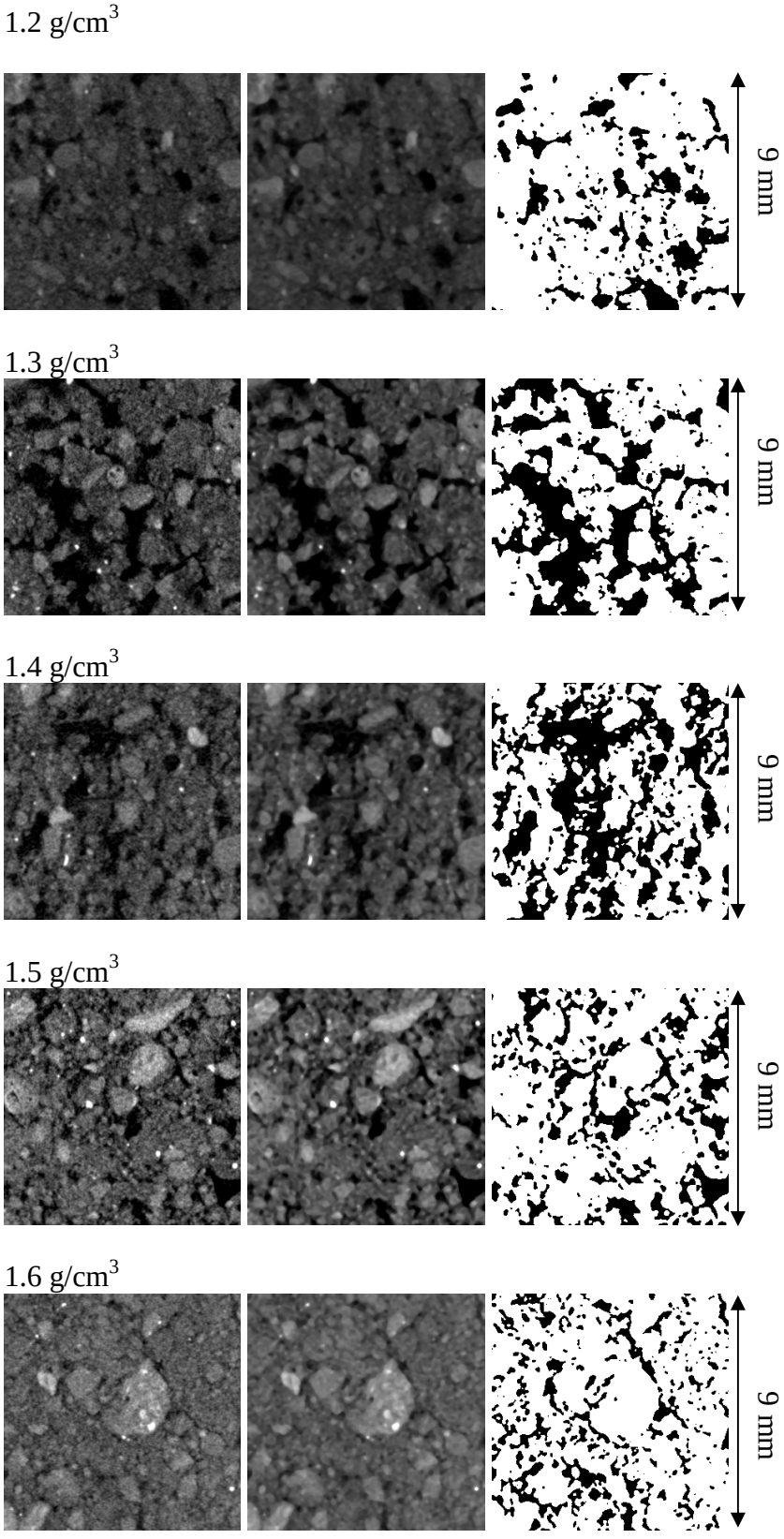

Fig. 6.3. Visual comparison of microcosms prepared with different bulk densities at various stages of image analysis: a – gray scale image, b – g/s after applying filter, c – binarized dataset.

Further analysis of mean pore size distribution curves, again omitting the treatment with a density of 1.2 g/cm^3, showed that the most densely packed material had the highest percentage of small pores (58.8 – 205.8 µm) followed by a decrease in the number of macro-pores. The most loosely packed microcosms (density 1.3 g/cm^3 and 1.4 g/cm^3) had the highest share of macropores and the lowest percentage of micropores (Fig.6.4).

The outlier treatment (1.2 g/cm^3) had the highest amount of pores with sizes ranging from 58.8 to 88.2 µm. This peak was followed by a rapid decline in the number of pores with increasing pore size till the diameter reached value of 294 µm when it produced another peak.

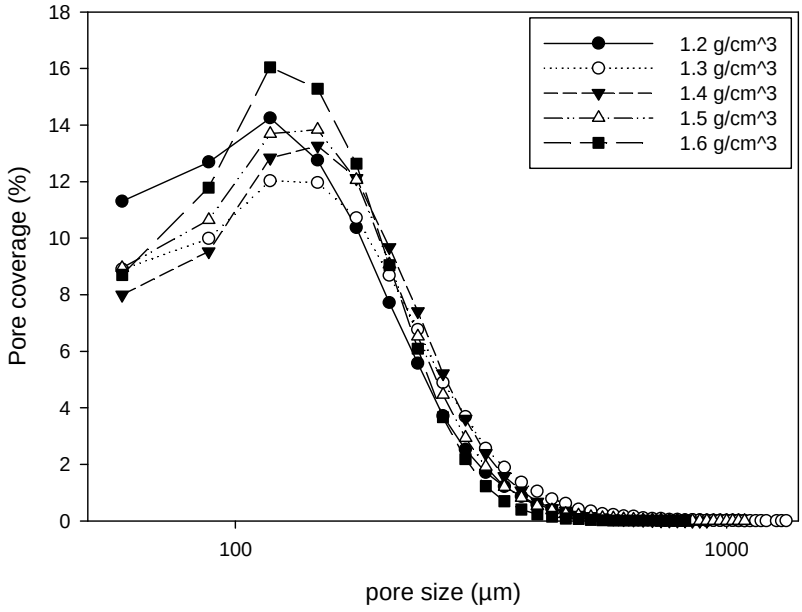

Fig. 6.4. Mean pore size distribution for microcosms build with different bulk densities.

6.4. DISCUSSION

This chapter showed that it is possible to alter physical characteristics of soil structure with the use of various initial conditions. Increasing aggregate size at the same density will lead to formation of pore networks with a majority of macro-pores and will also

decrease surface area of pores. On the other hand increasing the density of material consisting of aggregates with the same size reduced the volume of the porespace. Also the more compacted the soil was the more likely aggregates will have been broken thereby creating pores with a smaller diameter which increased the surface are of the pore-solid interface.

Soil packed with different aggregate sizes, but at the same bulk density of 1.3 g/cm^3 aimed to achieve the same total porosity values but different geometries. Mean porosity values varied for treatments from the maximum of 29.1 % for microcosms created with aggregates sized <2 mm to the smallest amount of 27.5 % for samples prepared with the largest aggregate size group (2-4 mm). However, statistical comparison of the means showed that the difference in porosity observed for the pore space have been larger than 29.4 µm (resolution) was not significant.

Porosity values were also closely related to the bulk soil density. As expected there was a decrease of porosity values with increasing density of soil (Harris *et al.* 2003, Pajor *et al.* 2010) from 30.1 % for samples with bulk density of 1.3 g/cm^3 to 22.2 % for soil at bulk density of 1.6 g/cm^3. That decreasing trend excluded microcosms with soil packed at density 1.2 g/cm^3, which has the lowest porosity, connectivity and mean median pore size values from the whole range of treatments (Table 6.4.). The difference could be identified even by visual comparison of representative 2D slices (Fig. 6.7.). This could be explained by the activity of the median filter, which was applied in the image pre-processing and which removed the noise such as most isolated – single voxel pores, but which would also affect the solid – air interface in macropores. Mean pore size distribution curves indicated that there was a peak of pores 58.2 - 88.2 µm and then another one for pores larger than 294 µm. A high number of macropores agrees with the relatively low pore surface area quantified for that treatment. As expected all

microcosms had a very highly connected pore space, with almost all microcosms with more than 90% of the total pore-space connected into one large pore cluster.

Larger aggregates (2-4 mm fraction) increased the number of pores larger than 200 µm and decreased the number of smaller pores. The same trend of increasing number of macropores was noticed with decreasing bulk-density. Changes to pore size were correlated with surface area of pore networks. With an increasing pore size related to more loosely packed material or use of larger aggregates, the pore surface area declined significantly ($p<0.05$).

The volume of available pore networks and their characteristics have a major impact on a wide range of biological, chemical and physical processes. Well connected macropores are preferential paths of fungal colony spread followed by exploration of smaller connected pores and thin valleys (Otten *et al.* 2004, Pajor *et al.* 2010). On the other hand meso- and micropores, where water menisci hold for longer period of time under negative pressure, are more suited for organisms that require instant access to water like bacteria (Ritz and Young 2004). Pore size is a key determinant of the shape of the water retention curve: micropores have a higher air entry value than macropores so there is a need of a higher negative pressure to drain them (Klute 1986). Macropores are the main pathways for the flow of water which has a direct impact on transport of water soluble nutrients (Luo *et al.* 2010a, Luo *et al.* 2010b). A reduction in pore surface area may reduce the rate of evaporation (Witkowska-Walczak 2000) and limit ion exchange processes (Lipiec *et al.* 2007). Such processes have a significant impact on plant nutrient availability and oxygen exchange (Horn *et al.* 1995).

Between the two considered treatments (different aggregate size and different bulk density) one batch of microcosms was prepared with the same settings – aggregate size of 1-2 mm packed at bulk density of 1.3 g/cm^3. In both cases analysis showed

similar porosity values ($p = 0.533$) and connectivity ($p = 0.58$) values. The only significant difference ($p = 0.01$) was detected for the pore surface area. However, the differences in physical characteristics between overlapping settings in both treatments could be explained by the fact that the samples from two considered treatments had different requirements for CT acquisition and image analysis. As described in Chapter 2 the microcosms packed at different bulk density values had been resin impregnated whereas the microcosms prepared with the use of various aggregate sizes were fresh soil samples (soil prepared as in 7.2.1.). Resin impregnated samples require higher energy for CT scans and increase the noise on images introducing the possibility of artefacts (ie. loose particles in porespace) and partial volume effect. Moreover, it is possible that although the same aggregate size range was used, that the composition and distribution within that range was slightly different for both series. Both reasons could have contributed to a difference in pore-solid surface area, even though good agreement was achieved in the other bulk characteristics.

The most difficult task was the choice of an appropriate thresholding method which was consistent and could produce realistic binary volumes taking into account the different characteristics of the data. Three different thresholding methods had been compared: manual, isodata, and Schluter *et al.* (2010). As a reference point for comparison, soil physical characteristics published in previous work on resin impregnated samples (Harris *et al.* 2003) were used. It was taken into consideration that the measurements might differ as a result of different quantification method (2D thin section and analysis of 3D volume) and different resolution (in this case only pores larger than resolution of 29.4 µm could be seen). Hence, the comparison of the output focused mainly on the trends between treatments rather than exact values. The most consistent and objective method for all datasets turned out to be a method based on

Schluter (2010) algorithm. All microcosms showed a significant peak in the percentage of single voxel pores (29 µm). According to Vogel (Vogel *et al.* 2010)data points close to the resolution are estimations which can be affected by noise and partial volume effect.

6.5. CONCLUSIONS

This chapter combined X-ray tomography and image analysis to show the influence of the various parameters commonly used to pack microcosms on soil structure and pore-geometry. The analysis quantified the impact of soil compaction between the density range of 1.2 - 1.6 g/cm^3 and the use of various fractions of aggregate sizes (<2 mm, 1 - 2 mm, 2 - 4 mm and 1 - 4 mm). Analysis of the data with X-ray micro-tomography proved that, with increased aggregate size at the same bulk density, both the fraction of macro-pores and the surface area of pores reduced. On the other hand increasing the density of soil with aggregates of the same size reduced the total volume of pore networks. The more compacted the material the more likely aggregates broke down thereby likely to have created pores with a smaller diameter. Despite packing the microcosms with the specified initial conditions there was still high variability within the treatments. This underpins the heterogeneity of soil structure occurring even in re-packed samples, with the same structural parameters such as bulk density, aggregate size, and wetness.

The changes to the pore network mediated by bulk-density and aggregate-size, as demonstrated in this chapter would be expected to have a substantial impact on soil hydraulic properties, oxygen and nutrients gradient. Soil structure would also be expected to affect the dynamics and spatial organisation of soil-borne fungi. This effect is tested in Chapter 7, where the effect of the soil bulk-density on fungal invasion was quantified and visualised.

CHAPTER 7

Modelling and quantifying the effect of heterogeneity in soil physical conditions on fungal growth

This chapter is adapted from work published as: Pajor, R., Falconer, R., Hapca, S., Otten, W. 2010. Modelling and quantifying the effect of heterogeneity in soil physical conditions on fungal growth. *Biogeosciences*, **7**, 3731-3740. DOI: 10.5194/gb-7-3731-2010

7.1. INTRODUCTION

The pivotal role of fungi in ecosystem functioning is now widely accepted and soil management strategies that support fungal diversity are to be encouraged (Young and Crawford 2004). Fungi are ubiquitous microorganisms in soil (0.8 – 16 km of hyphae per 1g of soil (Finlay 2006)) and they have a significant influence on aggregation and stabilisation of soil particles (Tisdall 1991, Bossuyt *et al.* 2001), nutrient and carbon dynamics (Wilkinson *et al.* 2002), and many soil-borne diseases (Otten *et al.* 2004). Their unique mycelial form of growth makes them particularly suited for exploration of heterogeneous environments such as soil (Otten and Gilligan 1998, Boswell *et al.* 2002). Whether or not they are capable of doing so depends on their ability to translocate carbon and nutrients combined with the ability to explore the soil environment and negotiate the complex pore geometry (Olsson and Wilhelmsson 2000). However, very little work has looked at how fungi colonize soil and how microscopic heterogeneity affects the colony morphology, and a theoretical framework of species interaction in a 3D heterogeneous soil environment is still lacking.

Soil provides an environment within which interactions between plants, biota and soil microorganisms take place, and it is one of the most complex ecosystems to study and understand. Soils are heterogeneous at spatial scales ranging from the μm (reflecting the pores within which microbial interactions take place) to km (where heterogeneity may results from different parental materials). Whereas, the heterogeneity of soils at larger scales has received considerable attention (Lark 2005), the microscopic heterogeneity has been largely ignored (Finlay 2006). This approach has changed recently by linking the dynamics of ecosystems occurring in macro-scale to the mechanisms at the micro-scale level (Ritz and Young 2004). Pore networks in soil create spatially separated niches for various microorganisms which affects the

interactions between them (Falconer *et al.* 2007). The structure creates preferential pathways through which microorganisms can move either autonomously or via convective transport with water. The opacity of soils and a lack of non-invasive quantitative techniques to study growth dynamics of microorganisms *in situ* make it difficult to understand how the microscopic heterogeneity of soils affects microbial dynamics and contributes to soil biodiversity. Nevertheless, it appears reasonable to hypothesize that the pathways that are provided by the soil physical environment play a crucial role in the movement and interaction of microorganisms, determining the outcome of many ecologically important processes, such as nutrient dynamics, colonization of roots by mycorrhizae or the invasion of fungal plant pathogens (Ritz and Young 2004). In this chapter, novel techniques to quantify the soil physical environment *in situ* and described in previous chapters are combined with mathematical modelling to study the impact of soil structure on fungal invasion.

As demonstrated in previous chapters, notably Chapter 6, X-ray micro-tomography provides insight into 3-D soil structure at scales relevant to microorganisms (Vogel 2002, Hsieh 2009, Baveye *et al.* 2010). However, current capabilities of X-ray microtomography systems still do not allow visualisation and quantification the dynamics of fungi in soils. Some progress was made to visualise fungi in wood (Van den Bulcke *et al.* 2009), but to date it has not been possible to visualise them in soil. Neither are there currently other techniques that can quantify the spatial distribution of fungi within a 3-D heterogeneous structure at microscopic scales and certainly not those that will allow following growth over time. However, the use of mathematical modelling offers a way forward. There are a number of fungal growth models, which consider fungal growth dynamics at different spatial scales: the colony (cm) or the hyphal scale (µm). The most recent models merge both scales which is important to

predict colony dynamics from interactions between hyphae and the environment. Most models are based on earlier work by Edelstein (1982) who considered fungal spread at colony scales. Boswel *et al*. (2002) extended these models by including directional growth and bidirectional translocation mechanisms. Stacey *et al*. (2001) developed a model to scale-up from hyphae to the colony level. This work was used to investigate transmission rates of plant pathogens between the plants. Vectorial-based model (Meskauskas *et al.* 2004) moved analysis from 2-D to 3-D with the possibility to model fruiting bodies. The model used in this chapter is a fungal growth model developed by Falconer *et al.* (2005), which enables modelling fungal spread in 3-D, and can be combined with the X-ray CT data providing characteristics of the pore geometry. This is the first time that this model will be applied to a range of pore geometries that result from different bulk-densities.

The main aim of this chapter is to establish a protocol that will enable us to quantify and visualise the effect of the internal structure of soil on fungal growth dynamics and colonization efficiency in 3-D. At first the influence of bulk density was on the pore geometry at microscopic scales was investigated. The next step was to quantify the effect of pore geometry on fungal colonization.

7.1.1. Hypotheses

1. Bulk-density affects microscopic heterogeneity of pore geometry which impacts upon fungal colonisation

2. Progression of a fungal invasion front is determined by pore geometry.

3. Fungal colonization is predominantly affected by pore volume but pore connectivity and geometry also have a significant impact.

4. Fungal invasions occur in first instance through larger connected pore volumes followed by colonization of smaller pores behind the invasion front.

5. A decrease in porosity and connectivity causes a decline in the colonisation rate.

7.2. MATERIALS AND METHODS

7.2.1. Preparation of soil microcosms

A sandy loam soil sampled from an experimental site (Bullion field) of the James Hutton Institute (formerly Scottish Crop Research Institute UK) was used to create soil microcosms. The soil was air-dried and sieved to obtain aggregates sized 1-2 mm. Soil was packed into the PVC rings at densities of 1.2 g/cm^3 (n=3), 1.3 g/cm^3 (n=2), 1.4 g/cm^3 (n=3), 1.5 g/cm^3 (n=4) and 1.6g/cm^3 (n=2) as described in Chapter 6. Here the samples are analysed at smaller spatial scales to test within and between treatment variability and it's impact on fungal invasion These soils were used in a previous study where the invasion of fungi into soil was investigated in thin sections from these samples (Harris *et al.* 2003), for which the samples were resin impregnated. The aim was to produce samples that differed in pore geometry to test its effect on fungal colonization.

7.2.2. Quantification of soil structure

A Metris X-Tek X-ray micro-tomography system was used for quantification and visualisation of the inner pore space of the soil microcosms. All soil microcosms were scanned at 160 kV, 201 µA and 3003 angular projection, 4 frames per second and a 0.1 mm Al filter. Radiographs were reconstructed as described previously in Chapter 6 at a resolution of 30 µm (voxel size).

The reconstructed volumes were cropped to obtain equally sized volumes for all samples of 300 x 300 x 300 voxels (9 mm x 9 mm x 9 mm). This sample volume was

selected as it was the largest volume that we were able to obtain from all samples. A single global threshold value was set for each of these samples. Binary data sets were created by thresholding the greyscale image stacks in ImageJ. The choice of threshold value was based on the histogram region corresponding with the pore-solid interface, taking into account variation of grey scale values in pores of different shapes and sizes.

To allow for analysis of the effect of pore geometry on fungal growth, the thresholded (binary) datasets were further divided into eight subsamples (pseudo replicates) with dimensions of 128 x 128 x 128 voxels (see Fig.7.1). This division was necessary due to computational limitations of the fungal growth model in a 3-D space. In this work replicates of each treatment (density, n=2-4) will be referred to as the samples, and datasets sized 128^3 will be called subsamples. Quantification of soil properties included descriptors such as total porosity, pore connectivity and pore size distribution (see Chapter 2 for details) as these are in particular hypothesized to have an impact on fungal colonization.

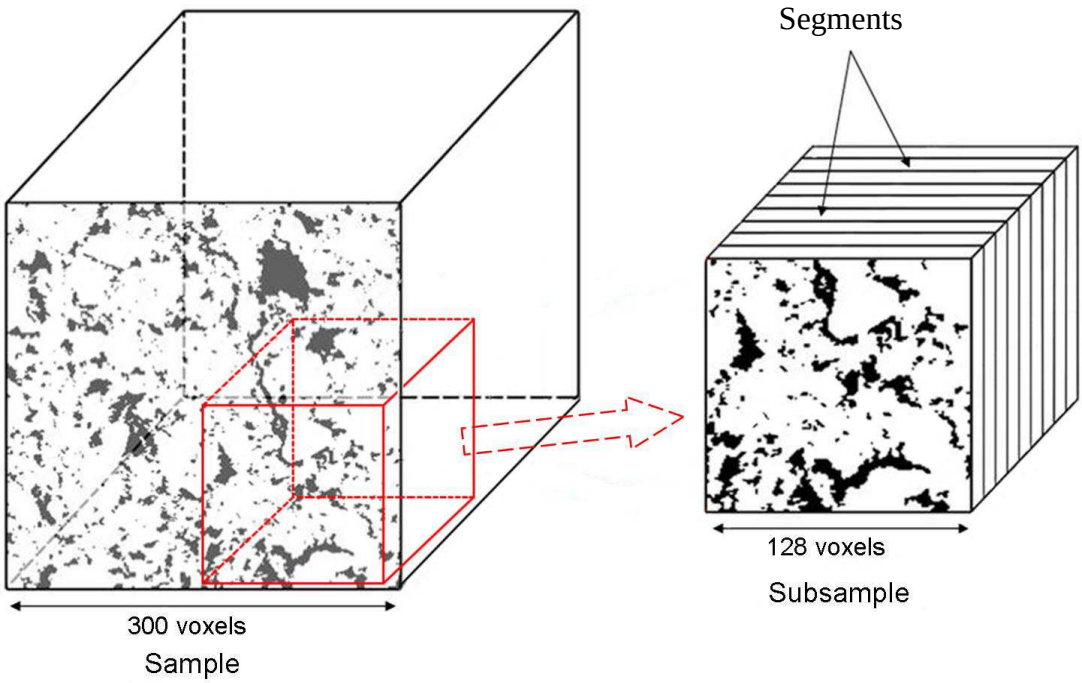

Fig. 7.1. 3-D spatial arrangement of the data structure. Microcosms were represented by cubical ROIs, divided into subsamples. Structure of the subsamples was divided into 8 segments to allow quantification of fungal colonisation.

7.2.3. Fungal growth model

Fungal growth was modelled using the framework developed by Falconer *et al*. (2005). This model is parsimonious in construction and reduces the biological complexity capturing the minimal set of physiological processes required to reproduce observed ranges in phenotypic responses (Falconer *et al.* 2005). It was shown that the model can capture fungal growth dynamics in homogeneous as well as in nutritionally heterogeneous environments (Falconer *et al.* 2007). The model is based on five physiological processes**:** uptake, redistribution of biomass, remobilisation of biomass, inhibitor production, and growth. These processes control and divide the fungal biomass into mobile, insulated, immobilised and non insulated (Fig.7.2.).

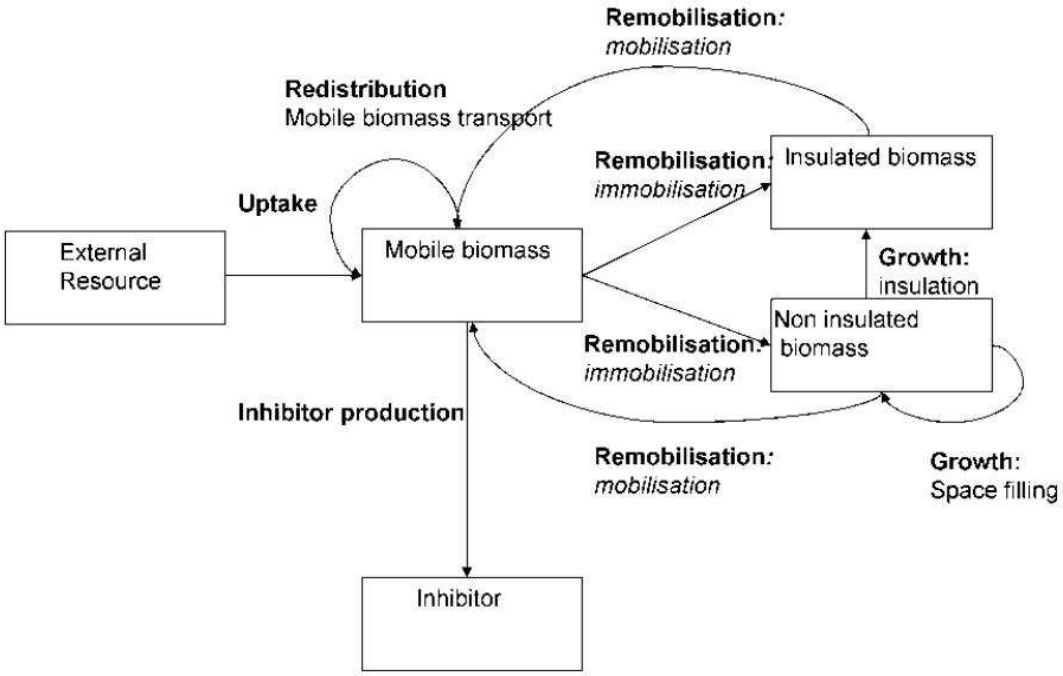

Fig. 7.2. Flow chart illustrating the processes of biomass in Falconer fungal growth model (Kravchenko *et al.* 2011a). Fungal biomass is governed by 5 processes: uptake of resources, growth, redistribution of biomass, remobilisation of biomass and production of inhibitors.

Spread of biomass through the soil structure is effectively described by a diffusive process. This basically assumes growth in random directions according to density gradients, a form of models which has shown to be able to model fungal growth. All of physiological processes are known to be important for vegetative growth of fungi but have not been collectively described in any other modelling framework (Falconer *et al.* 2005). The model can simulate growth in a 3-D pore space, which enables analysis of the effect of pore geometry on fungal development. As the objective of this study was to analyse the effect of pore geometry and not for example explore the effect of all fungal traits, parameters for only one fungal species were used. The selected parameters have previously been identified as those resulting in most effective colonisation of heterogeneous environments (Falconer *et al.* 2008). Simplified assumptions were also made with respect to the nutritional heterogeneity of the soil environment. Carbon was assumed to be homogeneously distributed throughout the pore volume. This is the most uniform case which will allow us to investigate the effect of structure by comparing different samples. The effect of a high (100, C units per voxel) and low (10, C units per voxel) carbon content on fungal growth dynamics were compared to test if the results were dominated by the availability of resources. For example, we would anticipate that for high C content it would be easier for a fungus to explore the entire soil volume. At the start of the simulation, fungal biomass was placed only in a unit-thick voxel vertical plane on one side of the sample (Fig.7.2). Fungal spread was initiated from this plane and followed throughout the sample. The simulations were terminated when a threshold value of total biomass (10^{-6}) reached the opposite edge of the subvolume. The time when that point was reached we refer to as break through time.

7.2.4. Interpretation of output from the model

This work makes use of a pre-developed fungal growth model (Falconer *et al.* 2005), see 7.2.3.). The model generates output in the form of structure file describing the volume of the sample where 0 refers to solids and 1 to pore-space. For each time step of fungal colonisation the model also generates files with information about the density of fungal biomass in connected pore-space of a sample expressed by a number, and 0 values corresponding to solids, not connected or not yet colonised pores.

An additional program code was written in R (http://www.r-project.org/) to analyse the output files and interpret them in context of ecologically relevant relationships between soil structure and fungal growth dynamics. To enable comparison of fungal invasion between treatments and to capture the dynamics and spatial distribution of fungal invasion each subsample was divided into nine segments that were perpendicular to the direction of fungal growth and parallel to the plane of inoculation (Fig.7.1.). Segmenting the 128^3 voxel cube into 9 equal segments was possible because first and last images from the stack were used as a boundaries for model framework. The R script required two input files generated by the model:

- Input 1 – a text file of binarized structure of the soil sample with dimensions of 128 x 128 x 128 voxels. Each of the 128 slices from the stack of the 128 binarized images was translated into a paragraph with 128^2 characters corresponding to individual voxels, where 0 referred to solid, and 1 corresponded to pore-space. As the result the structural file contained 128 paragraphs with 128^2 characters each.
- Input 2 – a text files structured in the same way as input 1, however this one contained information about the fungal biomass, with 0 representing the solids

and uncolonised pore space, and numbers specifying fungal biomass density in pore space colonised by fungi.

The R script was developed to focus on ecologically significant relationships, defined for each time-step:

- Porosity within each segment – this quantified the fraction of pore space per segment at specified distances from the plane of inoculation. This was calculated from the structural data (input one), and expressed as fraction of the volume of the segment. The differences between all segments in the sample provide a measure of the variability in the pore volume available for fungal spread at microscopic scales.
- Biomass per segment – this quantified (based on input 2) the amount of biomass per segment at specified distances from the site of inoculation at each time step. The total biomass value was a measure of the ability of fungi to invade the soil structure.
- Fraction of pore volume, and segment volume occupied by fungal biomass – the fraction of biomass-occupied-pores required to combine the data on the porosity within each segment with the biomass per segment to calculate for each time-step the fraction of pores that are filled with biomass. The volume fraction of biomass was expressed as the number of pore-voxels occupied with biomass, divided by the total number of segments. This measure enabled characterization of the efficiency at which the pore volume was colonised by fungi.

The form of the output changed with different versions of the script. The output from version 1 (Appendix 2.1) was presented in form of graphs generated for each time

step optionally saved as *.tiff files. Graphs were generated at each time step for total biomass over segments, number and fraction of pores occupied with biomass, the porosity and biomass and the porosity and total biomass values over the segments (Fig.7.3). In addition to the graphical output, a table with data was generated at each time step with the key values like total porosity, biomass, fraction of occupied pores and volume for each segment.

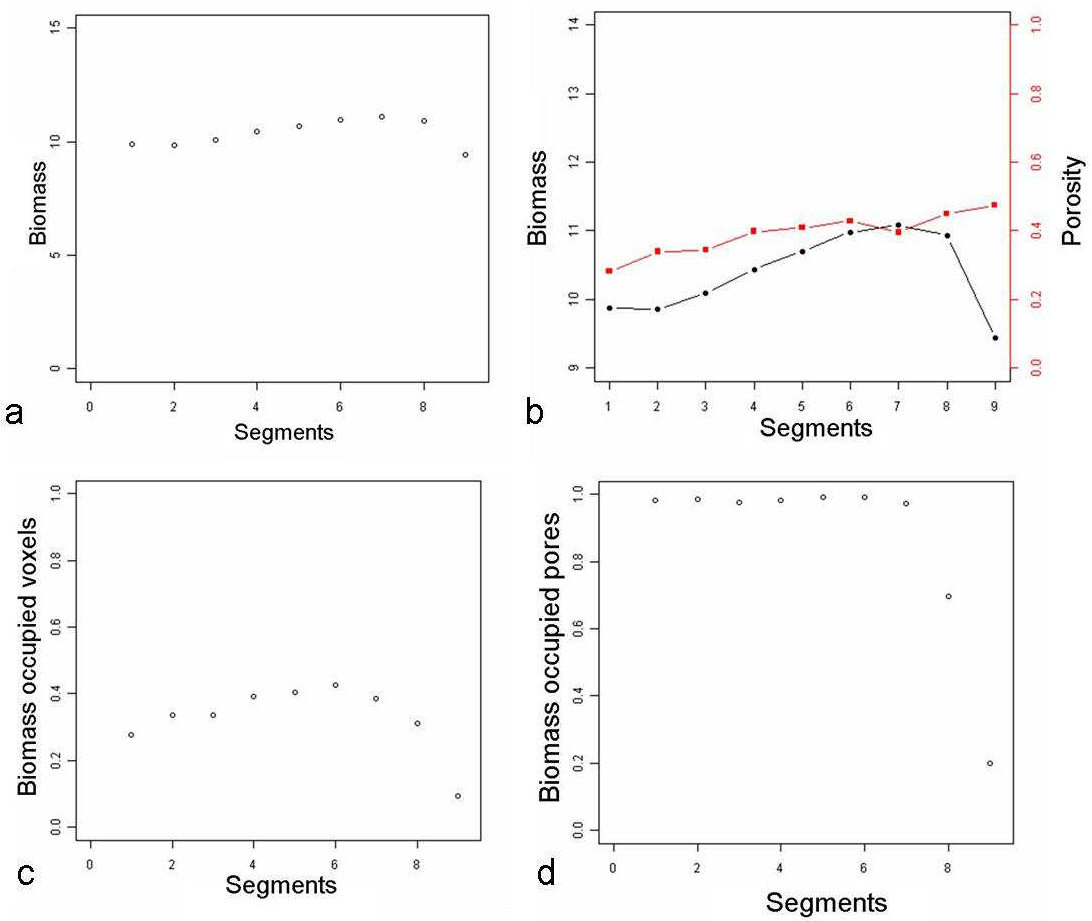

Fig. 7.3. Example of graphical form of output from R script interpreting the final time step of the simulation, showing the biomass values over the segments of the segments of the sample (a), relationship between biomass and porosity (b), number of voxels occupied by fungal biomass (c) and the fraction of colonised pores (d).

In total there were 50 time steps requiring the analysis. In order to make the analysis automated in first instance the code was copied 50 times with manual input of 50 different output names. If the model generated less than 50 time-steps (as the fungal

colony had reached the edge and the simulation was stopped) the script automatically stopped after analysis of the last available input file. In version 2 of the script (Appendix 2.2) the calculation was looped, so that the analysis of the model output is repeated for user-specified number of time steps and the code generated the output in the form of a summary table with the results.

7.2.5. Statistical Analysis

To test for the effect of the bulk-density on soil porosity, medium pore size and measures of connectivity, a nested ANOVA model was used with bulk-density as fixed factor (with levels 1.2, 1.3, 1.4, 1.5, 1.6) and the samples as nested factors within the different bulk-density levels. Bonferroni post-hoc pair-wise comparison tests were carried out to determine significant differences among means (Hardin and Hilbe 2003).

A Generalized Estimation Equations (GEEs) model was used with normal errors and first order auto-regressive correlation structure to test for an effect of bulk-density and distance from the site of inoculation on fungal biomass densities within each subsample. The variables were defined as bulk-density (with five levels), distance (with nine levels (segments) corresponding to the distance from the inoculation point), and sub-samples that were nested with the different bulk-density levels. More specifically, bulk-density was introduced as a between subjects factor, while distance was treated either as within subject covariate or as a factor, as indicated by the Quasi Likelihood under Independence model selection criterion (QIC). An interaction term between factors bulk-density and distance was also accommodated in the model and Bonferroni post-hoc pair wise comparison tests were carried out to determine significant differences among means of the different factor levels at a significant level of 0.05. All the statistical analyses were carried out in SPSS v.17 (Hardin and Hilbe 2003).

7.3. RESULTS

7.3.1. Effect of density on physical properties

The 3-D geometry of the pore space was substantially affected by the density at which the samples were packed (Fig.7.4.). Visual examination of the pore volumes in 3-D showed decrease in the total pore space with increasing density of packed soil. The majority of pores was connected and belonged to a single large cluster. In addition, for soil packed at higher densities the pore volume appeared to be connected via smaller valleys, additionally the largest connected cluster was always in contact with all sides (Fig.7.4.k-o).

Porosity was calculated for subsamples (which is the volume through which fungal growth was modelled) and for segments within the subsamples (which reflects smaller scale heterogeneity within each sample through which fungal growth was simulated). No significant interactions between the different treatment densities ($p=0.269$) nor between individual segments within each sample ($p=0.15$) were found. However the mean porosity was very strongly affected by the density ($p < 0.001$) ranging from 0.38 for density 1.3 g/cm^3 to 0.21 for samples at 1.6 g/cm^3 density (Table 7.1).

There was a decline in the median pore size with bulk-density (Table 7.1.) but only the median pore diameter at a density of 1.6 g/cm^3 was significantly different from those packed at 1.2 g/cm^3 and 1.3 g/cm^3 ($p < 0.04$). The changes in porosity and pore diameter show that when soils were packed at higher densities the overall pore volume declined and mainly the larger pores were reduced. However, for all samples the mean pore diameter remained an order of magnitude larger than a typical fungal diameter of 1-50 µm (Finlay 2006). No significant differences were found for porosity and median pore diameter between replicated samples at this scale.

1.2 g/cm^3

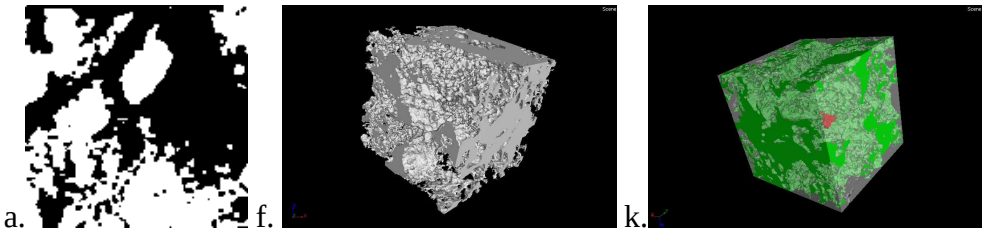

1.3 g/cm^3

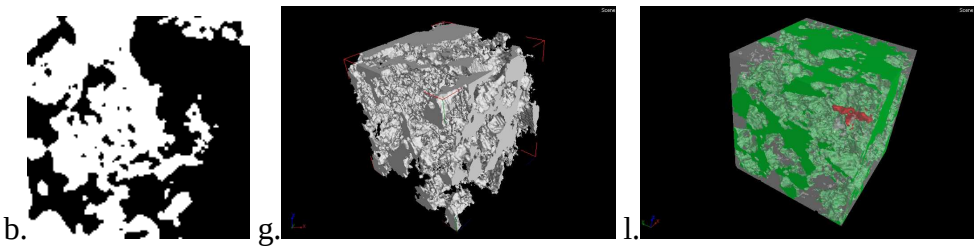

1.4 g/cm^3

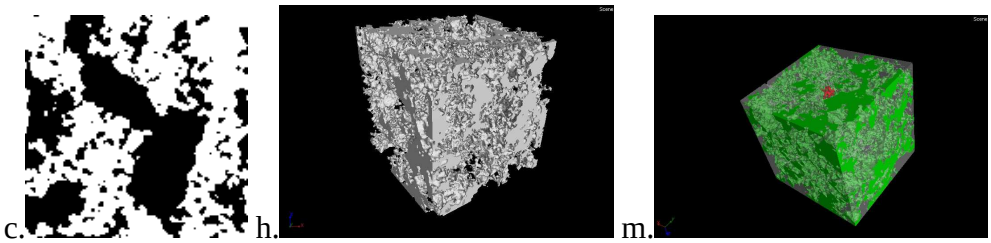

1.5 g/cm^3

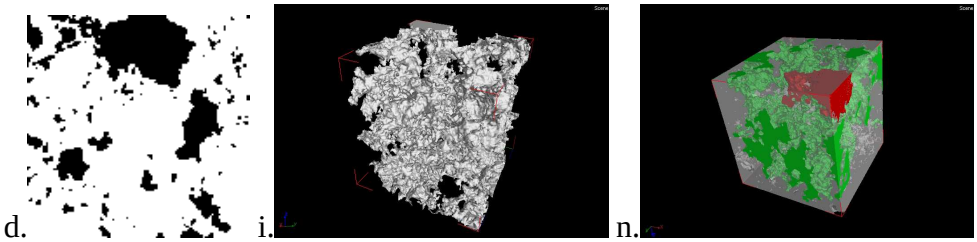

1.6 g/cm^3

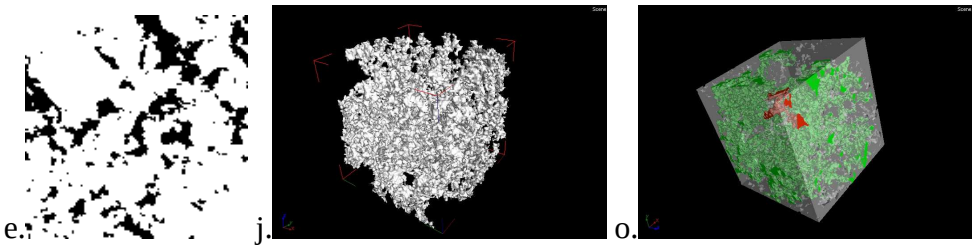

Fig. 7.4. Pore space visualisation – a-e) thresholded 2-D slice of subsample (white-solid, black-pore), f-j) extracted whole pore space in 3-D, k-o) 3-D view of subsample with largest connected pore (green), second largest connected pore (red) and the remaining pore space (bright gray).

All subsamples had highly connected pore volumes with a minimum of 90% of the pore volume connected to a single large cluster for all densities. There were significant differences in connectivity between replicates at all densities ($p<0.001$) indicating high variability of this parameter at this scale. In particular, the connectivity was significantly lower for the samples at higher densities i.e. 95% for 1.5 g/cm^3 ($p<0.015$) and 90% for 1.6 g/cm^3 ($p<0.001$), as compared to lower densities 97% for 1.2 g/cm^3, 1.3 g/cm^3 and 1,4 g/cm^3 soil bulk density.

Sample density (g/cm^3)	**Mean porosity (%)**	**Standard error**	**Mean connectivity (%)**	**Standard error**	**Median of pore size (μm)**	**Standard error**
1.2	33	0.01	96.5	0.5	370.1	22.63
1.3	38	0.02	97.0	0.3	374.9	24.27
1.4	31	0.01	97.0	0.4	347.8	22.88
1.5	26	0.01	95.1	0.2	333.6	11.45
1.6	21	0.01	90.0	0.6	308.7	12.99

Table 7.1. Mean values of bulk physical characteristics for soil microcosms used as the environment for fungal growth model. Mean values and standard errors represent three replicates for densities 1.2 g/cm^3, 1,4 g/cm^3, two for densities 1.3 g/cm^3, 1.5 g/cm^3 and one for microcosms packed at density of 1.6 g/cm^3.

7.3.2. Effect of the physical characteristics on fungal invasion

Due to the high connectivity of the pore space, the amount of biomass following fungal invasion displayed trends similar to those found for the porosity, with significant differences between treatments ($p<0.001$) (Fig.7.5B). As expected, biomass content decreased as porosity decreased, and the sample with the highest porosity also had the highest biomass after fungal invasion. The soil with the lowest porosity had an average biomass colonization of only 54% of the value for the sample with the highest porosity (Fig.7.5B). This difference is comparable with the difference in the porosity which

demonstrates the overriding importance of the total pore volume for fungal invasion. There was a noticeable drop ($p < 0.001$) in biomass content at distances further than approximately 2.5 mm from the site of inoculation. The drop in biomass content characterized the front of colony growth.

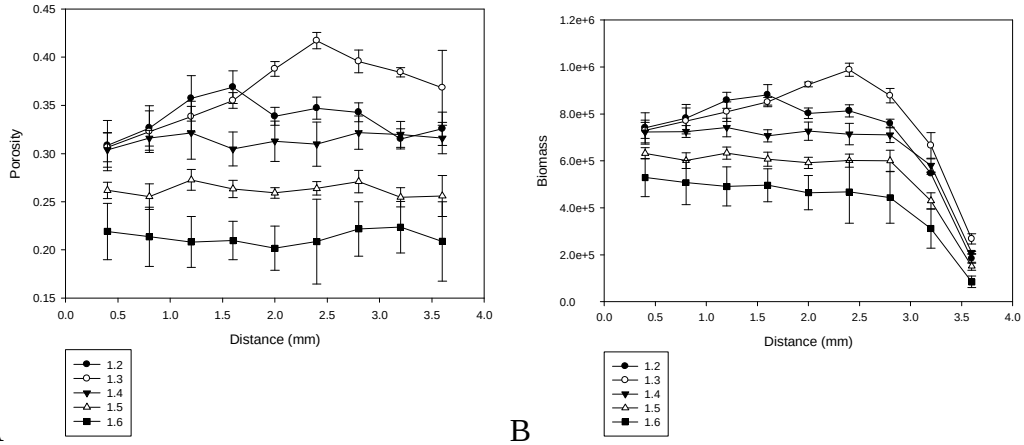

A B

Fig. 7.5. Porosity profiles (A) and biomass distribution over the distance from the inoculation site at the final time-step of simulation (B). Porosity is expressed as the fraction whereas biomass as unitless measure of density per voxel.

The amount of biomass per sample did not provide information about the spatial distribution of the biomass. In order to obtain a quantitative measure of the spatial colonization, the fraction of the pore space that became colonized was quantified. With increasing distance from the site of inoculation, the fraction of pores occupied by biomass declined steeply (Fig.7.6.). At distance <2.5 mm, nearly all of the pore space was occupied by fungal biomass. This reflects the high connectivity of the pore space for all samples. The drop in biomass at larger distances coincided with a drop in the fraction of pores that were occupied (Fig.7.6.).

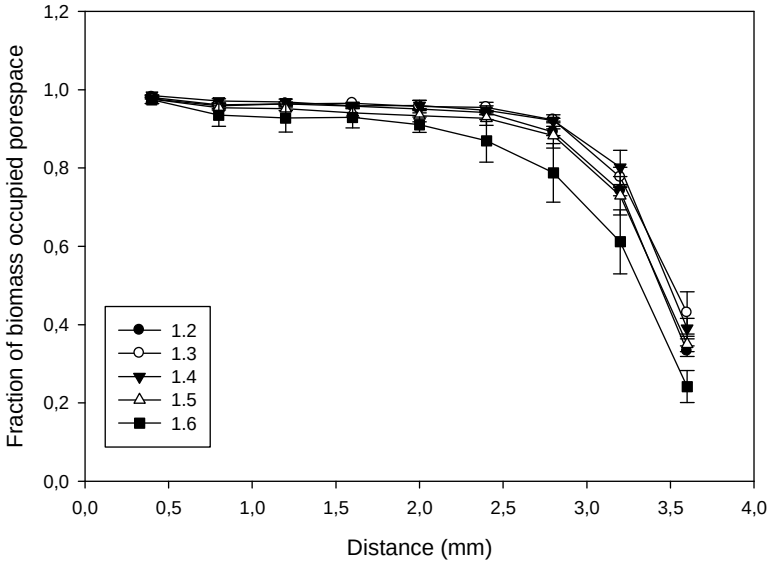

Fig. 7.6. The fraction of biomass occupied pore space at the final time step of simulation. Mean values and standard errors represent three replicates for densities 1.2 g/cm^3, 1,4 g/cm^3, two for densities 1.3 g/cm^3, 1.5 g/cm^3 and one for microcosms packed at density of 1.6 g/cm^3.

Soil packed at a density of 1.6 g/cm^3 (the most densely packed material) showed an earlier decline in the fraction of pores colonized with distance ($p<0.001$). As the porosity did not change with distance for these samples (Fig.7.5A) it is most likely a consequence of the lower connectivity for this sample (Table 7.1.). As a fungal colony spread into a soil sample, the larger pores got colonized first (as they were typically well connected, Fig.7.7 a) and this was followed by colonization of the smaller pores (Fig.7.7 b), and the invasion typically followed a sharp colony front (Fig.7.7 d and e).

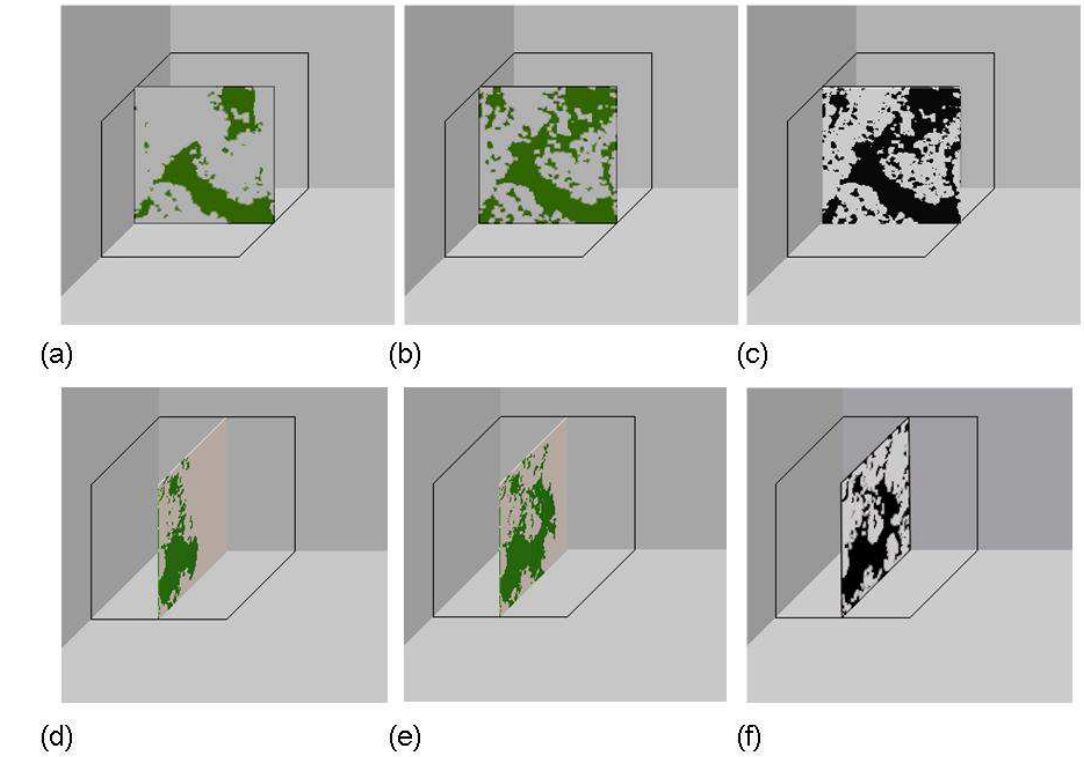

Fig. 7.7. 2-D slices through the z axis (a-c) and x axis (d-f) showing biomass occupancy at t=8 (a, d), t=12 (b, e), and corresponding pore space (c, f) where solid –brown, pore space – gray.

7.3.3. Carbon level and dynamics of fungal invasion.

Differences in the dynamics of fungal invasion were investigated on the single, middle segment (5^{th}) of the volume of the sample. For this segment fungal colonization over time was characterised. All treatments had a similar characteristic shape for the dynamics. Initially, for t<8, the biomass was absent till the edge of a fungal colony had progressed sufficiently far into the soil sample. Once the edge of a colony reached a specified distance from the site of inoculation (here shown for 2.5 mm in Fig.7.8.) then the pore volume at that distance becomes rapidly colonized for all densities. However, the rate of colonization differed per treatment with the highest rates (sharpest increase) for the lower density samples. As expected, in a better connected sample (lower density soil) fungal biomass moved through the volume rapidly, almost as a steep front over

time filling all available pore space. For the more densely packed soil, fungal invasion progressed slower (shown by the lower rate of increase) and the final level of fungal biomass was lower.

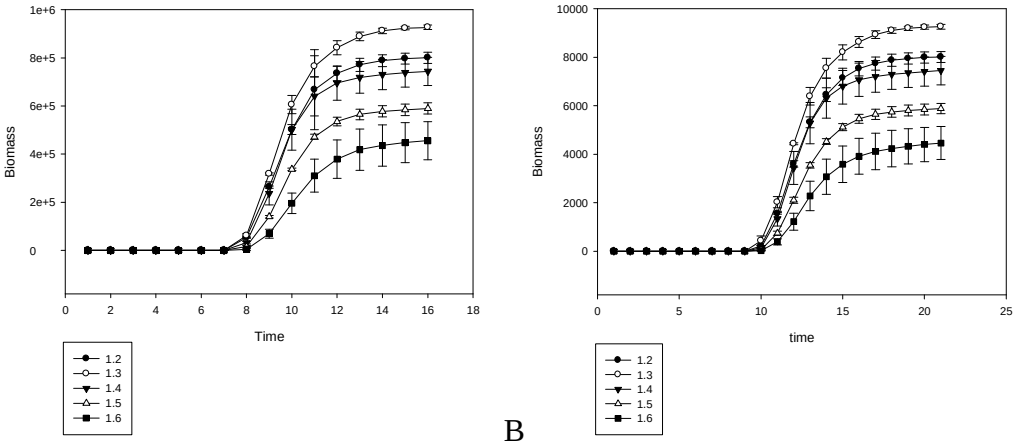

A B

Fig. 7.8. The dynamics of biomass over the time of simulation for middle segment (5th) of subsamples with 'unlimited' (A) and limited (B) resource. Time and biomass values are unitless, relative output from the model.

The dynamics of fungal invasion were also determined by the availability of Carbon in the soil (Fig.7.8 B). Although the trends for fungal invasion were qualitatively similar for both resource levels (Fig.7.8.A,B), the limitation of carbon radically affected biomass content reducing the final level of biomass following invasion to 1%. As expected, this reduction reflects the lower amount of C available for fungal growth. Limitation of C level also affected the rate of invasion. With unlimited resources colonization at a distance of 2.5 mm from the site of inoculation started at t = 7, but the starting point for microcosms with limited resources was delayed to t =10. Overall it also took longer for soils with a lower resource level for the fungal colony to spread through the entire soil volume. At high resource levels this took on average 17 time units, whereas at lower resource levels this increased to 22 time units.

7.4. DISCUSSION

Quantification of physical descriptors of soil structure at the scale of subsamples showed that with increase of soil bulk density there is a decrease in porosity, pore connectivity and pore size distribution. These results confirmed the trends characterised in Chapter 6, observed for the same samples but at larger scale. Additionally, modelling fungal growth through these 3-D volumes showed that the extent and rate of the invasion of fungi subjects to the volume of connected pores in the soil microcosm. Also the larger pores are colonized first (as they are better connected) and the smaller pores are colonized behind the invading front.

As the fungal invasion is expressed by diffusive spread, all connected pore space would be expected to be colonized eventually in the model simulations. Close to the site of inoculation nearly all pores became indeed colonized, as they belonged to one large connected cluster. However, with decreasing pore connectivity, the amount of pore space that was available for colonization also decreased (biomass spreads only through a connected network) causing less similarities between trends of biomass distribution and porosity over the segments of volumes with increasing distance from the source of inoculation. Although simulations showed that fungal invasion occurred in first instance in the larger connected pore volume, the model appeared to overestimate the colonization of smaller pores as experimental data showed that one would expect a greater preference for larger connected pores in these samples (Otten *et al.* 2004). Diffusive spread will allow for invasion of all pores including those that would be too narrow for fungal hyphae. Future work may need to address this in more detail where it would be possible to extend the modelling approach by including mechanisms that enhance spread through larger pores.

For all treatments, we observed steep declines in biomass density and percentage of colonized pores at the colony growing front. For loosely packed soil a steeper front was being observed, which is characteristic for a fast and homogeneous colonisation. This is consistent with experimental work by Otten *et al.* (2004) who showed steeper colonization profiles for *Rhizoctonia solani* in denser soils. A less steep growing front was found for soils packed at higher densities with a smaller amount of available pore space, less connectivity and with smaller median pore size (Table 7.1.). This is in agreement with experimental results reported by Harris *et al.* (2003) and Ritz *et al.* (2004) where it was shown that fungi spread faster through large pores with a high percentage of air-filled spaces. Fungi in volumes with small, poorly connected pores grow slower but colonies tend to have denser biomass (Harris *et al.* 2003). Whereas the differences appear to be small, it should be noted that such small differences can have a significant impact larger scale invasive spread of fungi (Kleczkowski *et al.* 1997, Bailey *et al.* 2000).

In natural soils nutrients and carbon are located heterogeneously and it is part of the heterogeneity of soil. Availability of nutrients and carbon influences colony growth. Studies in 2-D showed that in nutrient rich medium fungal colonies have a circular shape and have high concentration of biomass. However, in environments with a low content of nutrients fungi grow very sparsely searching for nutrient sources. Aggregated mycelia (cords) can connect dispersed rich niches of nutrient sources creating a large (up to few hectares) robust colonies (Boddy *et al.* 2009). In this study nutrient or carbon was placed ubiquitously and the only variance we introduced was the total amount available for fungal growth, and not the way it is distributed. Quantification of the impact of different nutrient distributions on fungal growth was not the key subject of

this chapter hence it was not introduced into the parameterisation of model, but it is likely to have a major impact on fungal colonization (Falconer *et al.* 2008).

One of the biggest challenges in X-ray microtomography is finding the balance between the sample size and resolution (voxel size) – with the resolution declining with an increase in sample size. The disadvantage of a lower resolution is loss of information about micropores, which has impact on connectivity of the pore space. Whereas, with available systems it is possible to obtain resolutions smaller than typical fungal diameters, this would require restrictions of the sample size below meaningful for fungal colonisation. The resolution used in this work is believed to be appropriate to study fungal invasion as the spread through a pore network is not just determined by a hyphal diameter, but depends on the ability of fungal hyphae to branch within such a network (Otten and Gilligan 1998). Another bias in the results related to image analysis can be caused by thresholding, which is the most crucial yet the most subjective step in image processing, when an operator differentiates between solid material and pore-space. Hovever the method used to binarize data for this work has been proved to be the most accurate by Baveye (2010, Chapter 2).

7.5. CONCLUSIONS

This chapter developed a theoretical framework that links soil management strategies with fungal ecology. X-ray computed tomography was used to quantify and characterize the pore geometry of samples with bulk-densities ranging from 1.2–1.6 g/cm^3. Structural data acquired with CT systems created the framework for the fungal growth model comprising a minimum set of physiological processes. X-ray micro-tomography and mathematical modelling was used to analyse the effect of the pore structure on fungal invasion. The degree and rate of fungal invasion was affected mainly by pore-

volume and pore-connectivity. With an increase in sample bulk-density there was a decrease in biomass reflecting a decline in pore space available for colonisation. Reduced connectivity and pore-sizes resulted in a delay in progression of the fungal colonisation, which otherwise progressed through the volume as a steep front of biomass.

This work leads to better understanding of the relation between soil structure and fungal colonisation. However further development is still required to identify how colonization efficacy relates to fungal traits and heterogeneity in the availability of carbon.

CHAPTER 8

GENERAL DISCUSSION

8.1. INTRODUCTION

This thesis focused on the relation between fungal colonisation, soil structure and water retention. Existing literature identifies a number of approaches to capture, quantify and visualise the effects of microorganisms and physicochemical factors on soil structure (Chapter 1). This thesis is a unique mix of methods and approaches to better capture the complexity of soil ecosystem by investigating multiple factors and their interactions, i.e. interactions amongst soil structure, soil hydraulic properties and soil-borne fungi. Another novelty of this study is the quantification of these interactions, at multiple scales (macro and micro) of the soil microcosm and with short incubation times (5 days). This thesis applies the use of an emerging technology, X-ray micro-tomography and combines it with image analysis and mathematical modelling and investigates how fungal spread is affected by soil physical properties and at the same time scales how fungal spreads can alter soil physical characteristics. As such it showed the potential of feedback loops in the soil-fungal system, a crucial first step to test the concept of self-organisation of soil.

The results from both, the characterisation of the physical structure and the water retention measurements are contradictory with the hypotheses. There was no effect of fungal growth on soil water retention or on soil structure. However, it was shown that soil structure had an effect on the rate of fungal colonisation. Despite clear visual differences in soil structure, the effect of manipulation of soil structure with the use of different bulk-densities and various aggregates sizes on quantitative descriptors of soil structure was not as extensive as expected. The treatments had small yet significant differences, most notable for structural descriptors such as pore size distribution, pore surface area and total porosity for microcosms packed at different densities.

There is evidence of an impact of fungal activity on soil structure. Crawford *et al*. (2011) combined the effect of fungi on soil structure and predicted hydraulic properties (hydraulic conductivity) in their study and published this work after the experimental part of this thesis was completed. Crawford *et al*. (2011) showed that fungi have a significant impact on soil structure, by increasing the porosity values by 4% in comparison to other samples inoculated with bacteria, bacteria and fungi and controls. They also used mathematical modelling approach to predict hydraulic conductivity at saturation. In their study soil samples inoculated with fungi had a significantly higher conductivity than the other treatments. They concluded that fungi-induced structural changes include increased connectivity.

Crawford *et al*. (2011) in their work used the same species of fungi as used in this thesis, namely *R. solani*. However, the soil used in Crawford's study contained a higher content of clay. This may have affected the effect of fungi on soil structure as one mechanism of fungal activity is that hyphae have an ability to rearrange clay platelets (Ritz and Young 2004). They quantified structural characteristics after 25 days of incubation and at two spatial scales, namely at 54 µm and 9 µm. The samples were cropped to regions of interest 140 x 140 x 200 voxels, and binarized using algorithms built-in to SCAMP (see section 2.6.4.). This thresholding algorithm is a variation of the Isodata algorithm which was found to be inconsistent in this thesis and also found to be underestimating the pore-space in the comparison with other available methods (see section 2.6.2. for details). The effect of fungi on structural and hydraulical properties of soil was detected and quantified only in case of samples scanned at the higher resolution of 9 µm. This means that the effects occurred on a sub-aggregate scale, which clearly implies that fungi cannot be responsible for the changes as typical fungal hyphae diameter is (5-12 µm) (Otten *et al.* 1999).

Other studies report increasing the stability of the aggregates both in field and microcosm scale (Tisdall and Oades 1980, Schreiner *et al.* 1997, Bearden and Petersen 2000), stability of soil slopes (Meadows *et al.* 1994) and also increase in porosity (Crawford *et al.* 2011). Such structural changes would have an impact on soil hydraulic properties. Bearden *et al*. (2000) and Auge *et al*. (2001) reported significant changes in water retention caused by mycorrhizal fungi. Bearden *et al*. (2000) showed enhanced aggregate stability and resistance to breakdown during fast wetting with water. In addition both studies reported that mycorrhizal fungi increased the amount of meso- and macro-pores. This resulted in faster drainage of soils with fungi at low pressure values than control samples with soil which was not inoculated.

In addition to affecting the hydraulic properties of soil by changing the structure, fungi also produce a wide range of hydrophobic compounds. Fungi, especially myccorhizal species are reported as the main factors causing soil repellency (Czarnes *et al.* 2000, Doerr *et al.* 2000, Hallett *et al.* 2001, Feeney *et al.* 2006c). Repellency caused by changes in water contact angle, will affect the preferential flow paths and as a result nutrient distribution and structural stability (Hallett *et al.* 2001). One of the most widely analysed and reported compunds is the glycoprotein glomalin (Rosier *et al.* 2006). Based on the above evidence of fungal activity it was expected that there would be a noticeable and significant effect of fungal colonisation on structure and water retention. The results of this study, which mostly question these conclusions, can be explained by the temporal and spatial scale at which fungal effects were quantified or by the methods used.

8.2. TEMPORAL SCALE

The lack of impact of growth of *R. solani* on soil water retention and structural characteristics could be related to the spatial (please see Chapter 8.3 for details) or temporal scales at which the soil characteristics were quantified. In this thesis all analysis was performed within 5-7 days from the inoculation. This is a short time-scale compared with other reports. Auge *et al*. (2001) reported changes in water retention measurements occurring after 7 months, whereas Bearden *et al*. (2000) allowed 10 weeks of incubation of the samples before measurements. Both studies involved water retention measurements for large samples with plant roots which required therefore longer incubation times. Also both studies used the same fungus, *Glomus* spp. from the largest genus of mycorrhizal fungi (Kirk *et al.* 2008). For the changes in repellency caused by fungi, Feeney *et al*. (2006c) allowed 8 – 10 days of sample incubation. Crawford *et al*. (2011) observed increases in porosity of samples inoculated with fungi in comparison with controls after 25 days since inoculation of microcosms.

However, the period of 5 days used in this work was found to be sufficient for studies of the impact of bulk-density on fungal spatial organisation (Harris *et al.* 2003). The rate of fungal growth depends on the source of inoculation and of all reported studies this thesis is the only study that also provided data on colonization efficiency and growth dynamics. Harris *et al*. (2003) quantified the spatial characteristics of growth of the same fungal species (*R. solani*) in the same type of soil (the sandy loam) as this thesis. Otten *et al*. (2004) in their study showed that after 5 days of incubation fungi reach the maximum efficiency of colonisation. Also the quantification of fungal biomass used in the experiments showed successful and nearly complete colonisation after 5 days since inoculation (see Chapter 2.4.3. for details).

In this study plant roots were not used, as they require longer incubation period and there are no reports of fungal effects on soil structure or hydraulic properties at short time scales for these interactions. Thus, quantification of the possible influence of fungal colonisation on soil hydraulic and structural characteristics was a novel approach.

8.3. SPATIAL SCALES

The spatial scale at which the structural changes caused by fungal colonisation can be visualised and quantified within soil was one of the key unknowns in this project. There are no standards for the size of the typical soil microcosm and the size is dictated by the research questions being addressed. The structural characteristics can be quantified for individual aggregates (De Gryze *et al.* 2006, Kravchenko *et al.* 2011b), see also Chapter 5) as well as for whole microcosms (Crawford *et al.* 2011, Garbout *et al.* 2011, Schluter *et al.* 2011), see Chapter 4). When using the commercial CT systems to quantify the structural characteristics, the key limitation is the minimum size of pores and particles that can be visualised.

The level of details in the datasets scanned with the use of X-ray micro-tomography systems depends on the resolution at which the data were reconstructed and scanned. Resolution corresponds to the physical size of the voxel (3D pixel). There is always a trade off between the sample size and resolution (voxel size), with increasing sample size causing a decline in the resolution. The disadvantage of a lower resolution is the loss of information about micro-pores, which could have a significant impact on the connectivity of the pore space. Whereas, with available systems it is possible to obtain resolutions smaller than typical fungal diameters, this would require restrictions

of the sample size below those meaningful for fungal colonisation, dimensions arguably more related to the size of a fungal colony (cm).

Resolution of 30 µm for whole microcosms and 5.5 µm for aggregates, used in this thesis were believed to be appropriate to study fungal invasion. The spread through a pore network is not just determined by a hyphal diameter (for *R. solani* typically 3 – 17 µm (Otten *et al.* 2001), but also depends on the ability of fungal hyphae to branch within such a network (Otten and Gilligan 1998). Crawford *et al*. (2011) carried out similar quantifications of changes to soil structure caused by microbial activity, and used two spatial scales: the whole microcosm, scanned at resolution of 53 µm and randomly picked aggregates at a resolution of 9 µm. The only significant difference quantified in this work was caused by fungus (*R. solani*), at the higher resolution (9 µm). This would ensure that the scanning protocol in this thesis has the potential of capturing the structural changes to soil samples as those found in the study by Crawford *et al*. (2011).

The resolution of 30 µm used in this study matched the radius of the smallest pores detected by the range of water retention measurements. The water retention curves show the relation between the volumetric water content and the matric potential which is equivalent of the pore size (Bearden and Petersen 2000). Thus the volume of water lost by soil microcosms from the zero pressure point to the maximum negative pressure value applied to the sample equals the volume of porosity of pores larger than the size expected to drain at that pressure. This allows a comparison of porosity values quantified with the use of two methods, the water retention measurements and image analysis of data acquired with the use of CT systems. The average porosity value derived from water retention curves for control samples (without fungal inoculum) equalled 13.3 % (s.e. = 0.2) and for microcosms inoculated with fungi it was 13.5 %

(s.e. = 0.3). The mean porosity values for the same microcosms derived by image analysis of CT datasets were twice higher, for the controls 27.2 % (s.e. = 0.3, n=8) and for the inoculated samples porosity of 27.8 % (s.e. = 0.5, n=8). The factor 2 difference can be explained because the water retention gives an indication of only connected pore space whereas image analysis takes into account the total porosity. Considering this hypothesis there would be a difference expected in the results from both methods however further image analysis showed that the pore networks are well connected. The connectivity values expressed as the fraction of total porosity connected into the largest cluster (see Chapter 2.6.3. for details) were all above 90 %. A second explanation for the difference could be that the water retention measurement starts from the 'zero' pressure equilibrated for the bottom of the sample. The water content value at this point is already lowered becuase of the potential gradient associated with the sample height. As many large pores exist in repacked sieved soil, such a potential gradient can mean that at the point identified as 'zero' a large fraction of the pore space has already drained (Klute 1986). Finally, air entrapment can mean that the samples were not fully saturated at the start of the water retention measurments. All these factors cause that the porosity values derived from the retention curve should be treated as a lower estimate for the connected pore network only and that the pore volume determined with X-ray CT is always expected to be higher.

8.4. MICROCOSM DESIGN AND FUNGAL COLONISATION

Soil structure is an outcome of a complicated interactions between the range of structure forming and decaying processes (Schluter *et al.* 2011). It is the soil pore network that creates environmental niches hosting soil-borne organisms. All changes to the pore geometry will have a significant impact on water distribution, availability of nutrients

and oxygen gradients (Crawford *et al.* 2005). These factors will affect the biology and fungal spread characteristics (Harris *et al.* 2003). Although Young and Ritz (2000) claimed in their review that typical changes to soil structure caused by tillage will not affect fungal colony dynamics at small scales, Bailey *et al.* (2000) showed the importance of changes to pore networks at microscale as they can differentiate between invasive and non-invasive fungal colonisation.

This thesis also examined to what extent in re-packed microcosms one could manipulate the pore network by changing the initial conditions like various aggregate sizes and compaction of soil to obtain different bulk densities and how that can influence fungal activity. As expected increasing the bulk-density reduced the total porosity value and reduced the number of macro-pores in favour of small pores and thin valleys (see Chapter 6 for details). This aligns with the hypothesis that during soil compaction aggregates may move, degrade or deform influencing the pore geometry and volume (Assouline 2006). Increasing aggregate size caused a decline in pore surface area and an increase in the amount of larger pores. The analysis was focussed on soil structure characteristics rather than stability as this information was more relevant to the study of the fungal growth. Stability, despite being the most widely used descriptor of soil structure, was described as unreliable and highly subjective to sampling methods, with methods specific for each soil type (Schluter *et al.* 2011).

In order to quantify the environmental significance of the structural differences between pre-packed soil microcosms, a simulation approach was used as it is still not possible to visualise fungal biomass in soils at the 5.5 and 30 micron scale. Falconer's fungal dynamics model (Falconer *et al.* 2005) was used to asses the impact of the soil structure on fungal colonisation (Pajor *et al.* 2010). The model was used on the samples representing different bulk densities. Samples with various bulk-densities significantly

varied in the amount of pore networks available for fungal colonisation (see Chapter 6). In addition Harris *et al*. (2003) showed the impact of bulk-densities on the organisation of fungal growth. Simulations in experimental part of this thesis showed that although fungal colonies were moving efficiently through the pore space as a steep growing front, the increase of bulk-density delayed the colonisation rate. This outcome conforms to work by Harris *et al*. (2003), Otten *et al*. (2001) and Ritz and Young (2004) who proved that soil-borne fungi spread faster through well-connected structures with larger pores. However, at the higher densities where the amount of pores is limited and the connectivity is reduced the colonisation process is slower but colonies have a denser biomass (Harris *et al.* 2003).

In order to achieve representative results there is a need to introduce sample replication. This study showed high variability in soil structure within the replicates for a given treatment. This reflects the heterogeneity of soil structure (Crawford *et al.* 2011) and highlights that it is impossible to create identical soil samples even when using the same initial conditions (bulk density, aggregate size, moisture content).

Otten *et al*. (2012) proposed the concept of producing replicable soil microcosms at the scale suitable for the research purpose. The concept is based on the real soil microcosm being scanned by a CT system and binarized. Such prepared digital representatives can be arbitrarily scaled and processed by a 3D printer. This procedure results in replicable 3D volumes of soil structure which can be used in various experiments overcoming the variability within the treatments but retaining some of the soil's natural structural heterogeneity (Fig. 8.1.).

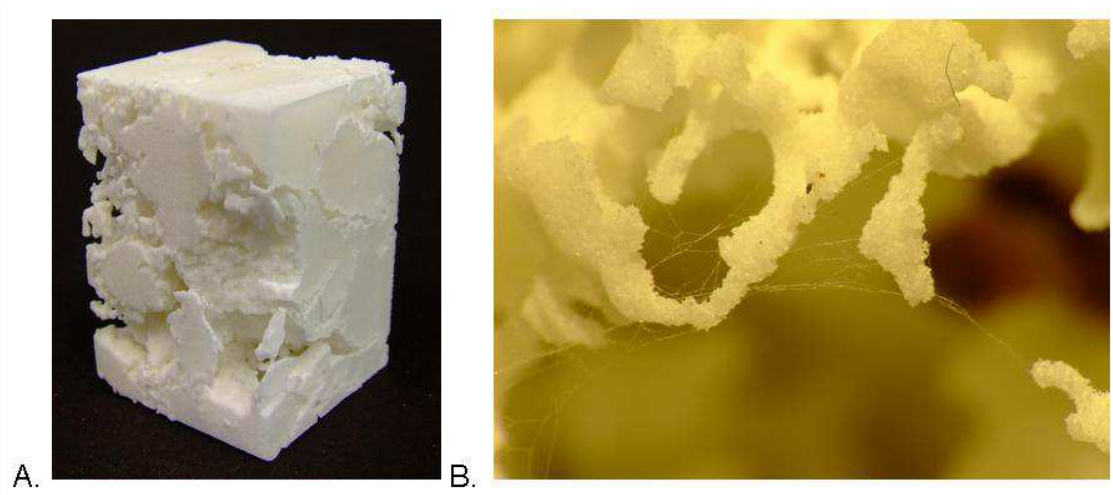

Fig. 8.1. The 3D printed surrogate of undisturbed soil sample (A) reflecting the sample scanned at 30 µm and the example of application to research (B) with fungal spread through the pore space visible at close up (Otten *et al.* 2012).

8.5. X-RAY MICROTOMOGRAPHY AND IMAGE ANALYSIS

Another bias in the results related to image analysis can be caused by thresholding, which is the most crucial yet the most subjective step in image processing when an operator has to differentiate between solid material and pore-space (see Chapter 2.6.2. for details). So far there is no uniform and universal method which copes with binarization of different materials and datasets from different acquisition systems. Even in this thesis, there were two different systems used to visualise and quantify the soil structure at different scales. Lab-based CT system at the SIMBIOS centre was used to analyse the whole soil microcosms at resolution of 30 µm, whereas a synchrotron was used to analyse individual soil aggregates at 5.5 µm. The facilities at APS apart from being capable of scans at higher resolution also use a monochromatic beam which at least in theory results in better contrast of the images and signal to noise ratio (Hsieh 2009).

There are three different thresholding methods used in this thesis: a manual threshold (Baveye *et al.* 2010), a fully automated approach based on an algorithm

proposed by Schluter *et al*. (2010) and a segmentation tool in VG Studio Max 2.1 (www.volumegraphics.com). For consistency, thresholding methods were always applied in separate chapters thus they do not overlap and allow comparison of the results within a chapter. The use of three different methods across the thesis reflects the progress of development of thresholding algorithms for soil science as well as the limits in applications.

The manual method was used on initial datasets. The comparison of the methods available at the time showed that despite this method being the most user–dependant and the most subjective, it produced the accurate and consistent results within one sample series (see Chapter 2.6.2). In comparison with the other methods used worldwide for thresholding, it also proved to be in agreement with the expected values (Baveye *et al.* 2010). Since the start of this project new methods were developed, including the threshold algorithms based on the gradient masks (see Chapter 2.6.2. for details). This fully automated user independent method excludes the input from an operator and produced very consistent results. However this algorithm was designed to analyse cubical regions of interest and is not adapted to work with samples of irregular shapes such as soil aggregates. For the analysis of soil aggregates such as those scanned at APS in Chicago (see Chapter 5), the pore space was segmented out and quantified with the use of VGSM 2.1. For consistency the same method was used to derive the characteristics of soil structure of the cubical regions of interest. This shows that thresholding is still a developing yet very crucial part of image analysis. There is no universal method, compatible with datasets of various samples acquired by different types of CT Scanners.

8.6. CONCLUSIONS AND FUTURE DIRECTIONS

This thesis combines a novel mix of methods e.g. X-ray microtomography, image analysis and modelling to quantify the relations between fungal colonisation and soil physical properties. Analysis included quantifying the effect of manipulations of the initial conditions for packing microcosms, like different bulk-densities and various aggregate sizes, on soil pore geometry and on fungal colonisation dynamics.

In this study it was shown that the short-term incubation of fungi in soil microcosms did not lead to structural changes. This outcome applies to the scale of a whole microcosm as well as individual soil aggregates (see Chapters 4 and 5). There was also no effect of fungal colonisation on water retention. These results are valuable information which guide the design of mathematical models reflecting soil heterogeneity, dynamics and self-organisation (Falconer *et al.* 2011).

It was also shown that it is possible to alter physical properties during packing of soil microcosms (Chapter 6). Increasing soil-bulk density caused a decline in porosity values, pore-size distribution and pore-surface area. Similarly when packing the microcosms at the same bulk-density but with different aggregate sizes, with the use of larger aggregates there is a shift in pore-size distribution increasing the amount of macropores and decreasing the surface area of the pore-space. Knowledge of how to manipulate soil conditions using these initial conditions will enable creating microcosms with desired properties, as the structure and geometry of pores regulates the hydraulic properties of soil and has an impact on the environmental niches. The effect was shown with the use of data acquired with the use of CT systems of samples packed at different bulk-densities and applied fungal growth models to them (see Chapter 7 for details). An increase in soil density reduced the amount of pore space available for colonisation, thus there was a reduction in the rate of colonisation and the amount of

fungal biomass. These differences can distinguish between the invasive an non-invasive fungal spread strategies, which are significant for fungal epidemiology (Bailey *et al.* 2000).

By extending the work in the future there would be a need to perform measurements of structural and hydraulic characteristics of soil, with methods developed and successfully tested in this thesis on different soil types. In this study only one type of sandy loam was considered. It is however, a common soil type in the Angus area and arable soils are known to be suitable for quantification of fungal growth (Harris *et al.* 2003). . Additionally the interactions between soil and fungi were quantified with use of only one fungal species, *R. solani*. Although *R. solani* is known as the ubiquitous soil-borne saprotroph, facultative parasite and mycorrhizal fungus (Otten *et al.* 2001) further work should consider other soil-borne fungi.

In case of fungal modelling, again only one phenotype was considered. The analysed fungus was described as the most fit by the Falconer *et al*. (2005) thus was suitable for quantification of the effect of structure on the fungal colony spread dynamics. The direction for the future work would be to introduce more than one fungal species to quantify the effect of soil structure on the interactions between the two competing strains. In addition the modelling framework could be extended into a three phase model, acknowledging the effect of water on the connectivity. Such a framework has already been build (Falconer *et al.* 2012) and is ready for further experimental validation.

REFERENCES

Armatas, G. S. 2006. Determination of the effects of the pore size distribution and pore connectivity distribution on the pore tortuosity and diffusive transport in model porous networks. *Chemical Engineering Science*. 61(14): pp.4662-4675.

Assouline, S. 2006. Modelling the relationship between soil bulk density and the water retention curve. *Soil Science Society of America Journal*. 5 pp.554 - 563.

Auge, R. M., Stodola, A. J. W., Tims, J. E. and Saxton, A. M. 2001. Moisture retention properties of a mycorrhizal soil. *Plant and Soil*. 230(1): pp.87-97.

Bailey, D. J., Otten, W. and Gilligan, C. A. 2000. Saprotrophic invasion by the soil-borne fungal plant pathogen Rhizoctonia solani and percolation thresholds. *New Phytologist*. 146(3): pp.535-544.

Baveye, P. C., Laba, M., Otten, W., Grinev, D. V., Bouckaert, L., Dello Starpaio, P., Goswami, R. R., Hu, Y., Liu, J., Mooney, S., Pajor, R., Sleutel, S., Tarquis, A., Wang, W., Wei, Q. and Sezgin, M. 2010. Observer-dependent variability of the thresholding step in the quantitative analysis of soil images and X-ray microtomography data. Geoderma. *Geoderma*.

Baveye, P. C., Rangel, D., Jacobson, A. R., Laba, M., Darnault, C., Otten, W., Radulovich, R. and Camargo, F. A. O. 2011. Fomr dust bowl to dust bowl: Soils still a frontier of science. *CSA News*. pp.4-11.

Bayer, A., Vogel, H. J. and Roth, K. 2004. Direct measurement of the soil water retention curve using X-ray absorption. *Hydrology and Earth System Sciences*. 8(1): pp.2-7.

Bearden, B. N. and Petersen, L. 2000. Influence of arbuscular mycorrhizal fungi on soil structure and aggregate stability of a vertisol. *Plant and Soil*. 218(1-2): pp.173-183.

Beare, M. H. and Bruce, R. R. 1993. A Comparison of Methods for Measuring Water-Stable Aggregates - Implications for Determining Environmental-Effects on Soil Structure. *Geoderma*. 56(1-4): pp.87-104.

Bertagnolli, B. L., Dal Soglio, F. K. and Sinclair, J. B. 1996. Extracellular enzyme profiles of the fungal pathogen *Rhizoctonia solani* isolate 2b-12 and two antagonists, *Bacillus megaterium* strain B153-2-2 and *Trichoderma harzianum* isolate Th00.I. Possible correlations with inhibition of growth and biocontrol. *Physiology Molecular Plant Pathology*. 48 pp.145-160.

Blackwood, C. B. and Paul, E. A. 2003. Eubacterial community structure and population size within the soil light fraction, rhizosphere, and heavy fraction of several agricultural systems. *Soil Biology & Biochemistry*. 35(9): pp.1245-1255.

Boddy, L., Hynes, J., Bebber, D. P. and Fricker, M. D. 2009. Saprotrophic cord systems: dispersal mechanisms in space and time. *Mycoscience*. 50(1): pp.9-19.

Bossuyt, H., Denef, K., Six, J., Frey, S. D., Merckx, R. and Paustian, K. 2001. Influence of microbial populations and residue quality on aggregate stability. *Applied Soil Ecology*. 16(3): pp.195-208.

Boswell, G. P., Jacobs, H., Davidson, F. A., Gadd, G. M. and Ritz, K. 2002. Functional consequences of nutrient translocation in mycelial fungi. *Journal of Theoretical Biology*. 217(4): pp.459-477.

Brown, G. G., Barois, I. and Lavelle, P. 2000. Regulation of soil organic matter dynamics and microbial activity in the drilosphere and the role of interactions with other edaphic functional domains. *European Journal of Soil Biology*. 36(3-4): pp.177-198.

Carter, D. O., Yellowlees, D. and Tibbett, M. 2007. Autoclaving kills soil microbes yet soil enzymes remain active. *Pedobiologia*. 51(4): pp.295-299.

Costanza, R., dArge, R., deGroot, R., Farber, S., Grasso, M., Hannon, B., Limburg, K., Naeem, S., Oneill, R. V., Paruelo, J., Raskin, R. G., Sutton, P. and vandenBelt, M. 1997. The value of the world's ecosystem services and natural capital. *Nature*. 387(6630): pp.253-260.

Crawford, J. W., Deacon, L. J., Grinev, D. V., Harris, J., Ritz, K., Singh, B. K. and Young, I. M. 2011. Microbial diversity affects self-organization of the soil-microbe system with consequences for function. *Journal of The Royal Society*.

Crawford, J. W., Harris, J. A., Ritz, K. and Young, I. M. 2005. Towards an evolutionary ecology of life in soil. *Trends in Ecology & Evolution*. 20(2): pp.81-87.

Czarnes, S., Hallett, P. D., Bengough, A. G. and Young, I. M. 2000. Root- and microbial-derived mucilages affect soil structure and water transport. *European Journal of Soil Science*. 51(3): pp.435-443.

Davey, E., Wigand, C., Johnson, R., Sundberg, K., Morris, J. and Roman, C. T. 2011. Use of computed tomography imaging for quantifying coarse roots, rhizomes, peat, and particle densities in marsh soils. *Ecological Applications*. 21(6): pp.2156-2171.

De Gryze, S., Jassogne, L., Six, J., Bossuyt, H., Wevers, M. and MerckX, R. 2006. Pore structure changes during decomposition of fresh residue: X-ray tomography analyses. *Geoderma*. 134(1-2): pp.82-96.

De Gryze, S., Six, J., Brits, C. and Merckx, R. 2005. A quantification of short-term macroaggregate dynamics: influences of wheat residue input and texture. *Soil Biology & Biochemistry*. 37(1): pp.55-66.

Degens, B. P. 1997. Macro-aggregation of soils by biological bonding and binding mechanisms and the factors affecting these: A review. *Australian Journal of Soil Research*. 35(3): pp.431-459.

Deurer, M., Grinev, D. V., Young, I. M., Clothier, B. E. and Muller, K. 2009. The impact of soil carbon management on soil macro-pore structure: a comparison of two apple orchard systems in New Zealand. *European Journal of Soil Science*.

Dexter, A. R. 1988. Advances in Characterization of Soil Structure. *Soil & Tillage Research*. 11(3-4): pp.199-238.

Doerr, S. H., Shakesby, R. A. and Walsh, R. P. D. 2000. Soil water repellency: its causes, characteristics and hydro-geomorphological significance. *Earth-Science Reviews*. 51(1-4): pp.33-65.

Doerr, S. H. and Thomas, A. D. 2000. The role of soil moisture in controlling water repellency: new evidence from forest soils in Portugal. *Journal of Hydrology*. 231 pp.134-147.

Dorioz, J. M., Robert, M. and Chenu, C. 1993. The Role of Roots, Fungi and Bacteria on Clay Particle Organization - an Experimental Approach. *Geoderma*. 56(1-4): pp.179-194.

Drazkiewicz, M. 1994. Distribution of Microorganisms in Soil Aggregates - Effect of Aggregate Size. *Folia Microbiologica*. 39(4): pp.276-282.

Drazkiewicz, M. 1996. Generic composition of fungi in soil aggregates. *Folia Microbiologica*. 41(3): pp.272-276.

Drees, L. R., Karathanasis, A. D., Wilding, L. P. and Blevins, R. L. 1994. Micromorphological Characteristics of Long-Term No-Till and Conventionally Tilled Soils. *Soil Science Society of America Journal*. 58(2): pp.508-517.

Edelstein, L. 1982. The Propagation of Fungal Colonies - a Model for Tissue-Growth. *Journal of Theoretical Biology*. 98(4): pp.679-701.

Eldridge, D. J. and Freudenberger, D. 2005. Ecosystem wicks: Woodland trees enhance water infiltration in a fragmented agricultural landscape in eastern Australia. *Austral Ecology*. 30(3): pp.336-347.

Falconer, R. E., Bown, J. L., White, N. A. and Crawford, J. W. 2005. Biomass recycling and the origin of phenotype in fungal mycelia. *Proceedings of the Royal Society B-Biological Sciences*. 272(1573): pp.1727-1734.

Falconer, R. E., Bown, J. L., White, N. A. and Crawford, J. W. 2007. Biomass recycling: a key to efficient foraging by fungal colonies. *Oikos*. 116(9): pp.1558-1568.

Falconer, R. E., Bown, J. L., White, N. A. and Crawford, J. W. 2008. Modelling interactions in fungi. *Journal of the Royal Society Interface*. 5(23): pp.603-615.

Falconer, R. E., Houston, A. N., Otten, W. and Baveye, P. C. 2011. Emergent behaviour of soil fungal dynamics: Influence of soil architecture and moisture distribution. *Soil Science, accepted*.

Falconer, R. E., Houston, A. N., Otten, W. and Baveye, P. C. 2012. Emergent behaviour of fungal dynamics: influence of soil architecture and water distribution. *Soil Science*. 177(2): pp.111-119.

Feeney, D. S., Bengough, A. G., Hallett, P. D., Rodger, S., White, N. and Young, I. M. 2006a. Assessing the impact of biological exudates associated with soil water repellency. *Soil Management for Sustainability*. 38 pp.475-483.

Feeney, D. S., Crawford, J. W., Daniell, T., Hallett, P. D., Nunan, N., Ritz, K., Rivers, M. and Young, I. M. 2006b. Three-dimensional microorganization of the soil-root-microbe system. *Microbial Ecology*. 52(1): pp.151-158.

Feeney, D. S., Daniell, T., Hallett, P. D., Illian, J., Ritz, K. and Young, I. M. 2004. Does the presence of glomalin relate to reduced water infiltration through hydrophobicity? *Canadian Journal of Soil Science*. 84(4): pp.365-372.

Feeney, D. S., Hallett, P. D., Rodger, S., Bengough, A. G., White, N. A. and Young, L. M. 2006c. Impact of fungal and bacterial biocides on microbial induced water repellency in arable soil. *Geoderma*. 135 pp.72-80.

Finlay, R. D. ed. 2006. *The fungi in Soil*. CRC Press.

Fraser, P. M., Haynes, R. J. and Williams, P. H. 1994. Effects of Pasture Improvement and Intensive Cultivation on Microbial Biomass, Enzyme-Activities, and Composition and Size of Earthworm Populations. *Biology and Fertility of Soils*. 17(3): pp.185-190.

Fredlund, D. G., Xing, A. Q. and Huang, S. Y. 1994. Predicting the Permeability Function for Unsaturated Soils Using the Soil-Water Characteristic Curve. *Canadian Geotechnical Journal*. 31(4): pp.533-546.

Fredrich, J. T., Menendez, B. and Wong, T. F. 1995. Imaging the Pore Structure of Geomaterials. *Science*. 268(5208): pp.276-279.

Garbout, A., Munkholm, L. J., Hansen, S. B., Petersen, B. M., Munk, O. L. and Pajor, R. 2011. The use of PET/CT scanning techniques for 3D visualisation and quantification of real-time soil/plant interactions. *Plant and Soil*.

Garcia, V. G., Potal Onco, M. A. and Susan, V. R. 2006. Review. Biology and systematics of the form genus *Rhizoctonia*. *Spanish Journal of Agricultural Research*. 4(1): pp.55-79.

Griffin, D. M. ed. 1978. *Effect of Soil Moisture on Survival and Spread of Pathogens*.
Hallett, P. D., Ritz, K. and Wheatley, R. E. 2001. Microbial derived water repellency in golf course soil. *International Turfgrass Society Research Journal*. 9 pp.518-524.

Hallett, P. D. and Young, I. M. 1999. Changes to water repellence of soil aggregates caused by substrate-induced microbial activity. *European Journal of Soil Science*. 50(1): pp.35-40.

Hardin, J. W. and Hilbe, J. M. 2003. Generalized estimating equations. *Stata Corporation*.

Harris, K., Young, I. M., Gilligan, C. A., Otten, W. and Ritz, K. 2003. Effect of bulk density on the spatial organisation of the fungus Rhizoctonia solani in soil. *FEMS Microbiology Ecology*. 44(1): pp.45-56.

Hollenbeck, K. J., Simunek, J. and van Genuchten, M. T. 2000. RETMCL: Incorporating maximum-likelihood estimation principles in the RETC soil hydraulic parameter estimation code. *Computers & Geosciences*. 26(3): pp.319-327.

Holtham, D. A. L., Matthews, G. P. and Scholefield, D. S. 2007. Measurement and simulation of void structure and hydraulic changes caused by root-induced soil structuring under white clover compared to ryegrass. *Geoderma*. 142(1-2): pp.142-151.

Hopmans, J. 2010. Tomography of soil-root-water processes. *Geochimica Et Cosmochimica Acta*. 74(12): pp.A416-A416.

Horn, R., Domzzal, H., Slowinska-Jurkiewicz, A. and Van Ouenwerkerk, C. 1995. Soil compaction processes and their effects on the structure of arable soils and the environment. *Soil and Tillage Research*. 35(1-2): pp.23-36.

Hsieh, J. 2009. *Computed Tomography Principles, Design, Artifacts, and Recent Advances*. Second edition ed.: John Wiley & Sons

Kieft, T. L., Soroker, E. and Firestone, M. K. 1987. Microbial Biomass Response to a Rapid Increase in Water Potential When Dry Soil Is Wetted. *Soil Biology & Biochemistry*. 19(2): pp.119-126.

Kim, H., Anderson, S. H., Motavalli, P. P. and Gantzer, C. J. 2010. Compaction effects on soil macropore geometry and related parameters for an arable field. *Geoderma*. 160(2): pp.244-251.

Kirk, P. M., Cannon, P. F., Minter, D. W. and Stalpers, J. A. 2008. *Dictionary of the Fungi*. 10 ed. Wallingford: CABI Publishing

Kleczkowski, A., Gilligan, C. A. and Bailey, D. J. 1997. Scaling and spatial dynamics in plant-pathogen systems: From individuals to populations. *Proceedings of the Royal Society of London Series B-Biological Sciences*. 264(1384): pp.979-984.

Klute, A. 1986. *Methods of soil analysis. Part1. Physical and Mineralogical Methods.* Madison, WI, USA: ASA - SSSa Inc.

Koorevaar, P., Menelik, G. and Dirksen, H. 1983. *Elements of soil physics.*: Elsevier

Kosugi, K. and Nakayama, Y. 1997. A method for estimating unsaturated hydraulic properties of vertically heterogeneous soils from transient capillary pressure profiles. *Agricultural and Forest Meteorology*. 84(1-2): pp.37-50.

Kravchenko, A., Falconer, R. E., Grinev, D. V. and Otten, W. 2011a. Fungal colonization in soils of contrasting managements: modelling fungal growth in 3D pore volumes of undisturbed soil samples. *Ecological Applications*. 21.4 pp.1202-1210.

Kravchenko, A., Wang, W., Smucker, A. and Rivers, M. 2011b. Long-term differences in tillage and land use affect intra-aggregate pore heterogeneity. *soil Science Society of America Journal*. 75(5): pp.1658-1666.

Kucharek, T. 2000. *Rhizoctonia* diseases in aboveground plant parts of agronomic and vegetable crops. *Plant pathology fact sheet*. p.41.

Lark, R. M. 2005. Exploring scale-dependent correlation of soil properties by nested sampling. *European Journal of Soil Science*. 56(3): pp.307-317.

Li, C. H. and Lee, C. K. 1993. Minimum Cross Entropy Thresholding. *Pattern Recognition*. 26(4): pp.617-625.

Li, D. C., Velde, B. and Zhang, T. L. 2004. Observations of pores and aggregates during aggregation in some clay-rich agricultural soils as seen in 2D image analysis. *Geoderma*. 118(3-4): pp.191-207.

Li, Z. J., Shukla, V., Wenger, K., Fordyce, A., Pedersen, A. G. and Marten, M. 2002. Estimation of hyphal tensile strength in production-scale *Aspergillus oryzae* fungal fermentations. *Biotechnology and Bioengineering*. 77(6): pp.601-613.

Lipiec, J., Walczak, R., Witkowska-Walczak, B., Nosalewicz, A., Slowinska-Jurkiewicz, A. and Slawinski, C. 2007. The effect of aggregate size on water retention and pore structure of two silt loam soils of different genesis. *Soil & Tillage Research*. 97(2): pp.239-246.

Lotrario, J. B., Stuart, B. J., Lam, T., Arands, R. R., Oconnor, O. A. and Kosson, D. S. 1995. Effects of Sterilization Methods on the Physical Characteristics of Soil - Implications for Sorption Isotherm Analyses. *Bulletin of Environmental Contamination and Toxicology*. 54(5): pp.668-675.

Lubbers, I. M., Brussaard, L., Otten, W. and van Groenigen, J. W. 2010. Earthworm-induced N mineralization in fertilized grassland increases both N(2)O emission and crop-N uptake. *European Journal of Soil Science*. 62(1): pp.152-161.

Luo, L., Lin, H. and Halleck, P. 2008. Quantifying soil structure and preferential flow in intact soil using x-ray computed tomography. *Soil Science Society of America Journal*. 72(4): pp.1058-1069.

Luo, L., Lin, H. and Li, S. 2010a. Quantification of 3-D soil macropore networks in different soil types and land uses using computed tomography. *Journal of Hydrology*. 393(1-2): pp.53-64.

Luo, L. F., Lin, H. and Schmidt, J. 2010b. Quantitative Relationships between Soil Macropore Characteristics and Preferential Flow and Transport. *Soil Science Society of America Journal*. 74(6): pp.1929-1937.

Lymberopoulos, D. P. and Payatakes, A. C. 1992. Derivation of Topological, Geometrical, and Correlational Properties of Porous-Media from Pore-Chart Analysis of Serial Section Data. *Journal of Colloid and Interface Science*. 150(1): pp.61-80.

Meadows, A., Meadows, P. S., Wood, D. M. and Murray, J. M. H. 1994. Microbiological Effects on Slope Stability - an Experimental-Analysis. *Sedimentology*. 41(3): pp.423-435.

Meskauskas, A., Fricker, M. D. and Moore, D. 2004. Simulating colonial growth of fungi with the Neighbour-Sensing model of hyphal growth. *Mycological Research*. 108 pp.1241-1256.

Montgomery, H. J., Monreal, C. M., Young, J. C. and Seifert, K. A. 2000. Determination of soil fungal biomass from soil ergosterol analyses. *Soil Biology & Biochemistry*. 32(8-9): pp.1207-1217.

Nimmo, J. R., Rousseau, J. P., Perkins, K. S., Stollenwerk, K. G., Glynn, P. D., Bartholomay, R. C. and Knobel, L. L. 2004. Hydraulic and geochemical framework of the Idaho National Engineering and Environmental Laboratory vadose zone. *Vadose Zone Journal*. 3(1): pp.6-34.

Nunan, N., Ritz, K., Rivers, M., Feeney, D. S. and Young, I. M. 2006. Investigating microbial micro-habitat structure using X-ray computed tomography. *Geoderma*. 133(3-4): pp.398-407.

Nunan, N., Wu, K. J., Young, I. M., Crawford, J. W. and Ritz, K. 2003. Spatial distribution of bacterial communities and their relationships with the micro-architecture of soil. *FEMS Microbiology Ecology*. 44(2): pp.203-215.

Oades, J. M. 1984. Soil Organic-Matter and Structural Stability - Mechanisms and Implications for Management. *Plant and Soil*. 76(1-3): pp.319-337.

Olsson, P. A. and Wilhelmsson, P. 2000. The growth of external AM fungal mycelium in sand dunes and in experimental systems. *Plant and Soil*. 226(2): pp.161-169.

Or, D., Smets, B. F., Wraith, J. M., Dechesne, A. and Friedman, S. P. 2007. Physical constraints affecting bacterial habitats and activity in unsaturated porous media - a review. *Advances in Water Resources*. 30(6-7): pp.1505-1527.

Osunbitan, J. A., Oyedele, D. J. and Adekalu, K. O. 2005. Tillage effects on bulk density, hydraulic conductivity and strength of a loamy sand soil in southwestern Nigeria. *Soil & Tillage Research*. 82(1): pp.57-64.

Otten, W. and Gilligan, C. A. 1998. Effect of physical conditions on the spatial and temporal dynamics of the soil-borne fungal pathogen Rhizoctonia solani. *New Phytologist*. 138(4): pp.629-637.

Otten, W., Gilligan, C. A., Watts, C. W., Dexter, A. R. and Hall, D. 1999. Continuity of air-filled pores and invasion thresholds for a soilborne fungal plant pathogen, Rhizoctonia solani. *Soil Biology & Biochemistry*. 31(13): pp.1803-1810.

Otten, W., Hall, D., Harris, K., Ritz, K., Young, I. M. and Gilligan, C. A. 2001. Soil physics, fungal epidemiology and the spread of Rhizoctonia solani. *New Phytologist*. 151(2): pp.459-468.

Otten, W., Harris, K., Young, I. M., Ritz, K. and Gilligan, C. A. 2004. Preferential spread of the pathogenic fungus Rhizoctonia solani through structured soil. *Soil Biology & Biochemistry*. 36(2): pp.203-210.

Otten, W., Pajor, R., Schmidt, S., Baveye, P. C., Hague, R. and Falconer, R. E. 2012. Combining X-ray CT and 3D printing technology to produce microcosms with replicable, complex pore geometries. *Soil Biology & Biochemistry*. 51 pp.53-55.

Pajor, R., Falconer, R. E., Hapca, S. and Otten, W. 2010. Modelling and quantifying the effect of heterogeneity in soil physical conditions on fungal growth. *Biogeosciences*. 7 pp.3731 - 3740.

Parmeter, J. R. 1970. *Rhizoctonia solani, biology and pathology*. University of California Press

Perret, J., Prasher, S. O., Kantzas, A. and Langford, C. 1999. Three-dimensional quantification of macropore networks in undisturbed soil cores. *Soil Science Society of America Journal*. 63(6): pp.1530-1543.

Peth, S., Nellesen, J., Fischer, G. and Horn, R. 2010. Non-invasive 3D analysis of local soil deformation under mechanical and hydraulic stresses by mu CT and digital image correlation. *Soil & Tillage Research*. 111(1): pp.3-18.

Pierret, A., Capowiez, Y., Moran, C. J. and Kretzschmar, A. 1999. X-ray computed tomography to quantify tree rooting spatial distributions. *Geoderma*. 90(3-4): pp.307-326.

Porebska, D., Slawinski, C., Lamorski, K. and Walczak, R. T. 2006. Relationship between van Genuchten's parameters of the retention curve equation and physical properties of soil solid phase. *International Agrophysics*. 20 pp.153-159.

Powlson, D. S. 1980. The Effects of Grinding on Microbial and Non-Microbial Organic-Matter in Soil. *Journal of Soil Science*. 31(1): pp.77-85.

Prado, B., Duwig, C., Marquez, J., Delmas, P., Morales, P., James, J. and Etchevers, J. 2009. Image processing-based study of soil porosity and its effect on water movement through Andosol intact columns. *Agricultural Water Management*. 96(10): pp.1377-1386.

Rajaram, G. and Erbach, D. C. 1999. Effect of wetting and drying on soil physical properties. *Journal of Terramechanics*. 36(1): pp.39-49.

Ridler, T. W. and Calvard, S. 1978. Picture Thresholding Using an Iterative Selection Method. *IEEE Transactions on Systems Man and Cybernetics*. 8(8): pp.630-632.

Rillig, M. C. 2005. A connection between fungal hydrophobins and soil water repellency? *Pedobiologia*. 49(5): pp.395-399.

Rillig, M. C. and Steinberg, P. D. 2002. Glomalin production by an arbuscular mycorrhizal fungus: a mechanism of habitat modification? *Soil Biology & Biochemistry*. 34(9): pp.1371-1374.

Rillig, M. C., Wright, S. F., Kimball, B. A., Pinter, P. J., Wall, G. W., Ottman, M. J. and Leavitt, S. W. 2001. Elevated carbon dioxide and irrigation effects on water stable aggregates in a Sorghum field: a possible role for arbuscular mycorrhizal fungi. *Global Change Biology*. 7(3): pp.333-337.

Ritz, K. and Young, I. M. 2004. Interactions between soil structure and fungi. *Mycologist*. 18.

Rivers, M. L., Citron, D. T. and Wang, Y. eds. 2006. *Recent developments in computed tomography at GSECARS*.

Rivers, M. L., Sutton, S. R. and Eng, P. eds. 1999. *Geoscience applications of x-ray computed microtomography*.

Rivers, M. L., Wang, Y. B. and Uchida, T. eds. 2004. *Microtomography at GeoSoilEnviroCARS*.

Rosier, C. L., Hoye, A. T. and Rillig, M. C. 2006. Glomalin-related soil protein: Assessment of current detection and quantification tools. *Soil Biology & Biochemistry*. 38(8): pp.2205-2211.

Ruzicka, S., Norman, M. D. P. and Harris, J. A. 1995. Rapid Ultrasonication Method to Determine Ergosterol Concentration in Soil. *Soil Biology & Biochemistry*. 27(9): pp.1215-1217.

Santos, D., Murphy, S. L. S., Taubner, H., Smucker, A. J. M. and Horn, R. 1997. Uniform separation of concentric surface layers from soil aggregates. *Soil Science Society of America Journal*. 61(3): pp.720-724.

Schlecht-Pietsch, S., Wagner, U. and Anderson, T. H. 1994. Changes in composition of soil polysaccharide and aggregate stability after carbon amendments to different textured soils. *Applied Soil Ecology*. 1 pp.145-154.

Schluter, S., Weller, U. and Vogel, H.-J. 2011. Soil-structure development including seasonal dynamics in a long-term fertilization experiment. *Journal of Plant Nutrition and Soil Science*. 174(3): pp.395-403.

Schluter, S., Weller, U. and Vogel, H. J. 2010. Segmentation of X-ray microtomography images of soil using gradient masks. *Computers & Geosciences*. 36(10): pp.1246-1251.

Schreiner, R. P., Mihara, K. L., McDaniel, H. and Bethlenfalvay, G. J. 1997. Mycorrhizal fungi influence plant and soil functions and interactions. *Plant and Soil*. 188(2): pp.199-209.

Schulten, H. R., Hempfling, R., Haider, K., Groblinghoff, F. F., Ludemann, H. D. and Frund, R. 1990. Characterization of Cultivation Effects on Soil Organic-Matter. *Zeitschrift Fur Pflanzenernahrung Und Bodenkunde*. 153(2): pp.97-105.

Sezgin, M. and Sankur, B. 2004. Survey over image thresholding techniques and quantitative performance evaluation. *Journal of Electronic Imaging*. 13(1): pp.146-168.

Six, J., Bossuyt, H., Degryze, S. and Denef, K. 2004. A history of research on the link between (micro)aggregates, soil biota, and soil organic matter dynamics. *Soil & Tillage Research*. 79(1): pp.7-31.

Smith, M. L., Bruhn, J. N. and Anderson, J. B. 1992. The Fungus *Armillaria bulbosa* is among the Largest and Oldest Living Organisms. *Nature*. 356(6368): pp.428-431.

Smucker, A. J. M., Park, E.-J., Dorner, J. and Horn, R. 2007. Soil micropore development and contributions to soluble carbon transport within macroaggregates. *Vadose Zone Journal*. 6(2): pp.282-290.

Stacey, A. J., Truscott, J. E. and Gilligan, C. A. 2001. Soil-borne fungal pathogens: scaling-up from hyphal to colony behaviour and the probability of disease transmission. *New Phytologist*. 150(1): pp.169-177.

Stefani, F. O. P., Tanguay, P., Pelletier, G., Piche, Y. and Hamelin, R. C. 2010. Impact of Endochitinase-Transformed White Spruce on Soil Fungal Biomass and Ectendomycorrhizal Symbiosis. *Applied and Environmental Microbiology*. 76(8): pp.2607-2614.

Steinberg, P. D. and Rillig, M. C. 2003. Differential decomposition of arbuscular mycorrhizal fungal hyphae and glomalin. *Soil Biology & Biochemistry*. 35(1): pp.191-194.

Tisdall, J. M. 1991. Fungal Hyphae and Structural Stability of Soil. *Australian Journal of Soil Research*. 29(6): pp.729-743.

Tisdall, J. M. and Oades, J. M. 1980. The Effect of Crop-Rotation on Aggregation in a Red-Brown Earth. *Australian Journal of Soil Research*. 18(4): pp.423-433.

Tisdall, J. M. and Oades, J. M. 1982. Organic-Matter and Water-Stable Aggregates in Soils. *Journal of Soil Science*. 33(2): pp.141-163.

Tisdall, J. M., Smith, S. E. and Rengasamy, P. 1997. Aggregation of soil by fungal hyphae. *Australian Journal of Soil Research*. 35(1): pp.55-60.

Toyota, K., Young, I. M. and Ritz, K. 1996. Effects of soil matric potential and bulk density on the growth of *Fusarium oxysporum* f sp *raphani*. *Soil Biology & Biochemistry*. 28(9): pp.1139-1145.

Tracy, S. R., Black, C. R., Roberts, J. A., Sturrock, C., Mairhofer, S., Craigon, J. and Mooney, S. 2012. Quantifying the impact of soil compaction on root system architecture in tomato (*Solanum lycopersicum*) by X-ray micro-computed tomography. *Annals of Botany*.

Tracy, S. R., Roberts, J. A., Black, C. R., McNeill, A., Davidson, R. and Mooney, S. J. 2010. The X-factor: visualizing undisturbed root architecture in soils using X-ray computed tomography. *Journal of Experimental Botany*. 61(2): pp.311-313.

Trevors, J. T. 1996. Sterilization and inhibition of microbial activity in soil. *Journal of Microbiological Methods*. 26(1-2): pp.53-59.

Van den Bulcke, J., Boone, M., Van Acker, J. and Van Hoorebeke, L. 2009. Three-Dimensional X-Ray Imaging and Analysis of Fungi on and in Wood. *Microscopy and Microanalysis*. 15(5): pp.395-402.

Vogel, H. J. 1997. Morphological determination of pore connectivity as a function of pore size using serial sections. *European Journal of Soil Science*. 48(3): pp.365-377.

Vogel, H. J. 2002. Topological characterization of porous media. *Morphology of Condensed Matter: Physics and Geometry of Spatially Complex Systems*. 600 pp.75-92.

Vogel, H. J. and Roth, K. 2001. Quantitative morphology and network representation of soil pore structure. *Advances in Water Resources*. 24(3-4): pp.233-242.

Vogel, H. J., Weller, U. and Schluter, S. 2010. Quantification of soil structure based on Minkowski functions. *Computers & Geosciences*. 36 pp.1236 - 1245.

Wallis, M. G. and Horne, D. J. 1992. Soil water repellency. *Advances in Soil Science*. 20 pp.91-146.

Wilkinson, S. C., Anderson, J. M., Scardelis, S. P., Tisiafouli, M., Taylor, A. and Wolters, V. 2002. PLFA profiles of microbial communities in decomposing conifer litters subject to moisture stress. *Soil Biology & Biochemistry*. 34(2): pp.189-200.

Witkowska-Walczak, B. 2000. Influence of aggregate size of Eutric Cambisol and Gleyic Phaeozem on evaporation. *International Agrophysics*. 14(4): pp.469-475.

Wojcik, E. 2005. The relationship between water content and suction pressure inMio-Pliocene silts in Stegny profile (Poland). *Przeglad Geograficzny*. 53(8): pp.699-702.

Wolf, R. E. 1994. Growth and Harvest Imbalance - Rely. *Journal of Forestry*. 92(7): pp.41-41.

Wright, S. F., Nichols, K. A. and Schmidt, W. F. 2006. Comparison of efficacy of three extractants to solubilise glomalin on hyphae and in soil. *Chemosphere*. 64(7): pp.1219-1224.

Wright, S. F., Starr, J. L. and Paltineanu, I. C. 1999. Changes in aggregate stability and concentration of glomalin during tillage management transition. *Soil Science Society of America Journal*. 63(6): pp.1825-1829.

Wright, S. F. and Upadhyaya, A. 1996. Extraction of an abundant and unusual protein from soil and comparison with hyphal protein of arbuscular mycorrhizal fungi. *Soil Science*. 161(9): pp.575-586.

Wright, S. F. and Upadhyaya, A. 1998. A survey of soils for aggregate stability and glomalin, a glycoprotein produced by hyphae of arbuscular mycorrhizal fungi. *Plant and Soil*. 198(1): pp.97-107.

Wright, S. F., Upadhyaya, A. and Buyer, J. S. 1998. Comparison of N-linked oligosaccharides of glomalin from arbuscular mycorrhizal fungi and soils by capillary electrophoresis. *Soil Biology & Biochemistry*. 30(13): pp.1853-1857.

Yao, S.-H., Zhang, B. and Hu, F. 2011. Soil biophysical controls over rice straw decomposition and sequestration in soil: The effects of drying intensity and frequency of drying and wetting cycles. *Soil Biology & Biochemistry*. 43(3): pp.590-599.

Young, I. M. and Crawford, J. W. 2004. Interactions and self-organization in the soil-microbe complex. *Science*. 304(5677): pp.1634-1637.

Young, I. M., Crawford, J. W., Nunan, N., Otten, W. and Spiers, A. eds. 2008. *Microbial Distribution in Soils: Physics and Scaling*.

Young, I. M., Crawford, J. W. and Rappoldt, C. 2001. New methods and models for characterising structural heterogeneity of soil. *Soil & Tillage Research*. 61(1-2): pp.33-45.

Young, I. M. and Ritz, K. 2000. Tillage, habitat space and function of soil microbes. *Soil & Tillage Research*. 53(3-4): pp.201-213.

Zhang, X., Deeks, L. K., Bengough, A. G., Crawford, J. W. and Young, I. M. 2005. A mass balance based numerical method for the fractional advection-dispersion equation: theory and application. *Journal of Hydrology*. 206 pp.59-79.

APPENDICES

Appendix 1 – individual measurements for water retention experiments in Chapter 3.

ploughed			not ploughed			not ploughed		
water outflow	matric head	water content	water outflow	matric head	water content	water outflow	matric head	water content
0	1	0.45	0.8	0.4	0.38	0	1	0.36
0	2	0.45	0	1.3	0.38	0	1.9	0.36
0.6	3.7	0.45	0.4	3.9	0.38	0.6	3.1	0.36
0.4	4.2	0.44	0.3	5	0.37	0.5	3.6	0.35
0.6	4.8	0.44	0	6	0.37	0	4.6	0.35
0	5.7	0.44	0	6.9	0.37	0	5.6	0.35
0.4	6.2	0.44	0	7.9	0.37	0	6.6	0.35
1.2	8.7	0.43	0	10	0.37	0	8.5	0.35
1	10	0.43	0	11.7	0.37	0.2	10.7	0.35
1.4	11.4	0.42	0	13.8	0.37	0.4	12.8	0.34
0.8	13.1	0.41	0.1	17.3	0.37	0	14.7	0.34
0.4	14.4	0.41	0	19.4	0.37	0	16.9	0.34
0.8	15.4	0.41	0	21.3	0.37	0.4	18.1	0.34
0.4	16.9	0.4	0	23.4	0.37	0	19.9	0.34
1.6	18.6	0.4	0.2	25.1	0.37	0.2	21.8	0.34
0	20.4	0.39	0	26.9	0.37	0	23.9	0.34
2.2	23.4	0.39	0.4	28.8	0.37	0.4	28.1	0.34
1.8	27.5	0.38	0.4	33.1	0.37	0.6	33.1	0.34
3	31.6	0.37	0.4	39.8	0.37	0.2	39.8	0.33
1	38.9	0.35	0.2	46.7	0.37	0	46.7	0.33
0.6	44.7	0.35	4.2	51.2	0.36	1.8	52.4	0.33
0.4	49	0.34	0.4	54.9	0.34	0.4	56.2	0.32
0	53.7	0.34	0	60.2	0.37	0	61.6	0.32
1.2	58.8	0.34	0.4	64.5	0.33	0.4	66	0.32
0	64.6	0.33	0	69.1	0.33	0	70.7	0.32
1.8	79.4	0.33	0	74.1	0.33	0.2	75.8	0.32
0.6	100	0.32	0	79.4	0.33	0	81.2	0.32
0	104.7	0.32	0	85.1	0.33	0	85.1	0.32

Appendix 1.1. Measurements of water outflow and a matric head for samples from different parts of JHI experimental site.

F17			F13	
Matric head	Volumetric water content	Weight	Volumetric water content	Weight
1	0.47	446.6	0.47	445.6
3.7	0.45	443.3	0.46	443.9
6.6	0.44	441.6	0.45	442.302
14.4	0.42	438	0.43	438.9
20.4	0.38	431.4	0.42	437.2
25.7	0.36	428	0.38	430.4
33.8	0.34	424.6	0.34	423.6
39.8	0.33	422.9	0.33	421.9
47.8	0.32	421.2	0.32	420.2
57.5	0.31	419.5	0.3	416.868
66	0.3	417.8	0.296	416.1
75.8	0.3	417.8	0.29	415.1
87.1	0.3	417.1		
F14			F15	
Matric head	Volumetric water content	Weight	Volumetric water content	Weight
1	0.45	446.4	0.47	439.3
5.1	0.45	446.4	0.46	437.9
8.7	0.44	444.5	0.45	435.6
17.7	0.41	439.6	0.4	427.4
23.4	0.38	434.5	0.36	421.3
30.9	0.34	428.5	0.32	415.2
39.8	0.34	427.2	0.31	412.5
46.7	0.31	422.8	0.29	409.1
54.9	0.3	420.4	0.28	407.4
64.5	0.28	418.4	0.27	405.9
75.8	0.27	415.8	0.26	404.1
85.1	0.27	415.8	0.26	404
95.4	0.27	415.8	0.26	404.1
104.7	0.26	414.6	0.26	404.1
114.8	0.26	414.1	0.25	402.39
C19			C21	
Matric head	Volumetric water content	Weight	Volumetric water content	Weight
1	0.49	448	0.49	449.1
3.7	0.47	444.6	0.47	445.6
6.6	0.45	441.3	0.46	443.9
14.4	0.42	436.2	0.44	440.6
20.4	0.39	431.1	0.42	437.2
25.7	0.36	425.8	0.38	430.4
33.8	0.34	422.6	0.37	428.7
39.8	0.31	417.5	0.35	425.3
47.8	0.29	414.1	0.33	421.9
57.5	0.29	414.1	0.32	420.2
66	0.28	412.4	0.31	418.5
75.8	0.28	412.4	0.31	418.5
87.1	0.27	411.9	0.31	418.5

Appendix 1.2 (continued on p. 192)

	C20		C22	
Matric head	Volumetric water content	Weight	Volumetric water content	Weight
1	0.45	443.1	0.46	448.9
5.1	0.44	442.1	0.44	445.6
8.7	0.43	440.3	0.43	443.9
17.7	0.4	434.9	0.41	440.5
23.4	0.37	430.5	0.38	435.4
30.9	0.34	424.1	0.35	430.3
39.8	0.32	422.2	0.33	426.9
46.7	0.3	417.9	0.3	421.8
54.9	0.28	415.2	0.29	420.1
64.5	0.27	413.5	0.27	417.6
75.8	0.26	411.8	0.27	417.6
85.1	0.26	411.3	0.27	417.6
95.4	0.26	411.3	0.26	415.9
104.7	0.26	411.2	0.26	415.5
114.8	0.26	411.2	0.26	415.1

Appendix 1.2. The measurements of weight and matric head values for microcosms inoculated with *R. solani* and controls in Experiment 1.

Set 1 Control			Set 2 Inoculated		
Matric Head	Volumetric water content	Weight	Matric Head	Volumetric water content	Weight
1	0.39	330.5	2.4	0.4	331.7
3.5	0.39	330.5	4.5	0.4	330.7
7	0.38	329.5	8.6	0.4	329.2
11.2	0.38	329.5	13.1	0.4	329.2
16.6	0.38	329.5	18.1	0.4	329.2
26.2	0.37	327.5	27.6	0.39	328.7
35.8	0.35	324.5	41.1	0.37	324.7
39.8	0.35	323.5	57.3	0.35	320.7
49.8	0.33	319.5	61.1	0.34	318.7
59.8	0.32	319.5	70.1	0.33	316.7
68.6	0.3	316.5	89.3	0.3	313.7
88.2	0.3	314.5	110.3	0.3	312.7
109.8	0.29	313.5	128.6	0.29	311.7
129.8	0.28	312.5			
Set 5 Control			Set 6 Control		
Matric Head	Volumetric water content	Weight	Matric Head	Volumetric water content	Weight
3.2	0.4	334.2	3.4	0.4	339.1
7	0.4	334.2	5.7	0.4	339.1
10.2	0.39	333.2	18.4	0.39	334.1
14.7	0.39	333.2	36.8	0.38	332.1
28.2	0.38	331.2	41.2	0.37	331.1
37.2	0.34	324.2	50.9	0.35	329.1
51.2	0.32	322.2	59.7	0.34	326.1
69.9	0.31	320.2	71.2	0.33	324.1
88.4	0.3	318.2	90	0.32	320.1
107.9	0.3	318.2	132.2	0.3	318.1
130	0.29	316.2			
Set 3 Inoculated			Set 3 Control		
Matric Head	Volumetric water content	Weight	Matric Head	Volumetric water content	Weight
3.2	0.4	166.7	3.2	0.4	166.6
14.6	0.4	166.3	14.6	0.39	164.9
19	0.39	163.9	19	0.37	164.1
28.2	0.37	162	28.2	0.35	160.3
37.2	0.3	161.4	37.2	0.33	159.7
41.8	0.3	160	41.8	0.33	158.8
51.8	0.3	159.5	51.8	0.31	157.9
69	0.3	158.6	69	0.3	157.2
88.1	0.29	157.8	88.1	0.29	156.4
108.1	0.28	156.8	108.1	0.28	155.6
127.3	0.27	156.3	127.3	0.27	155.2

Appendix 1.3 (Continued on p. 194). The measurements of weight and matric head values for microcosms inoculated with *R. solani* and controls in Experiment 2.

Set 7 Inoculated		
Matric Head	Volumetric water content	Weight
3	0.41	331.4
5.7	0.41	331.4
9.7	0.41	331.4
29.5	0.39	329.4
43.7	0.37	324.4
52.5	0.35	321.4
62	0.34	320.3
91.7	0.32	317.4
111.5	0.31	313.9
134.3	0.3	311.9

Appendix 1.3 (Continued from p.193). The measurements of weight and matric head values for microcosms inoculated with *R. solani* and controls in Experiment 2.

Samples inoculated with *R. solani*					
f2			f3		
weight (g)	Volumetric water content	Matric head	weight (g)	Volumetric water content	Matric head
82.5	0.4	1	83	0.39	1
82.5	0.4	5.8	83	0.39	5.8
82	0.39	10.9	82.8	0.38	10.9
81.3	0.37	14.9	82.4	0.37	15
81	0.37	19.4	82	0.36	19.5
80.5	0.35	23.4	81.6	0.35	23.4
80	0.34	26.9	81.2	0.34	26.9
79.2	0.32	30.1	80.6	0.33	30.2
79	0.32	34.9	80.4	0.32	34.9
78.7	0.31	39.8	80.3	0.32	39.8
78	0.3	48.9	80	0.31	48.9
77.9	0.29	58.2	79.8	0.31	58.2
77.6	0.29	62.2	79.3	0.3	62.2
f6			f7		
weight (g)	Volumetric water content	Matric head	weight (g)	Volumetric water content	Matric head
81.5	0.41	1	83.5	0.39	1
81.3	0.4	5.8	83.4	0.39	5.8
80.2	0.38	10.7	83.2	0.38	10.7
79.1	0.35	14.4	83	0.38	14.4
78.6	0.34	17.7	83	0.38	17.7
77.3	0.31	22.3	82.6	0.37	22.3
76.9	0.3	24.5	82.3	0.36	24.5
76.4	0.29	28.8	81.8	0.35	28.8
76.3	0.29	33.8	81.5	0.35	33.8
76.1	0.28	38	81.4	0.34	38
75.7	0.27	46.4	80.4	0.32	46.4
75.5	0.27	54.9	80.1	0.31	54.9
75.4	0.27	64.5	79.6	0.3	64.5
		F4			F5
weight (g)	Volumetric water content	Matric head	weight (g)	Volumetric water content	Matric head
82.9	0.39	1	83.3	0.39	1
82.9	0.39	5.8	83.3	0.39	5.8
82.7	0.38	10.9	82.8	0.38	10.7
82.1	0.37	14.9	82.3	0.37	14.4
81	0.34	19.4	82	0.36	17.7
80.6	0.33	23.4	81.2	0.34	22.3
80	0.32	26.9	80.8	0.33	24.5
79	0.3	39.8	80.2	0.32	28.8
78.5	0.29	48.9	80	0.31	33.8
78.3	0.28	58.2	79.7	0.31	38
77.9	0.27	62.2	79.2	0.3	46.4
			79.	0.3	54.9
			78.7	0.28	64.5

Appendix 1.4 a. Continued on pages 196 and 197.

		F8			F9
weight (g)	Volumetric water content	Matric head	weight (g)	Volumetric water content	Matric head
83.4	0.39	1	83.2	0.4	1
83.1	0.38	5.8	82.6	0.38	5.8
83	0.38	10.7	82.3	0.38	10.7
82.9	0.3	14.4	82.1	0.37	14.4
82.9	0.38	17.7	82	0.37	17.7
82.6	0.37	22.3	81.3	0.35	22.3
82.2	0.36	24.5	80.7	0.34	24.5
81.5	0.34	28.8	79.9	0.32	28.8
81.1	0.34	33.8	79.6	0.32	33.8
80.6	0.32	38.1	79.3	0.31	38.1
79.8	0.3	46.4	78.9	0.3	46.4
79.5	0.3	54.9	78.6	0.28	54.9
79.2	0.29	64.5	78.5	0.28	64.5
c2			c3		
weight (g)	Volumetric water content	Matric head	weight (g)	Volumetric water content	Matric head
82.6	0.39	1	82.9	0.39	1
81.9	0.37	4.8	82.4	0.37	4.8
81.8	0.37	9.3	82.1	0.37	9.3
81.5	0.36	13.4	82	0.36	13.4
81.2	0.35	18.1	81.8	0.36	18.1
81.1	0.35	22.9	81.4	0.35	22.9
81	0.35	26.9	81.1	0.34	26.9
80.5	0.34	29.5	80.5	0.33	29.5
80.3	0.33	34.9	80.3	0.32	34.9
80.1	0.33	38.9	80.1	0.32	38.9
79.4	0.31	47.4	79.4	0.3	47.4
79.3	0.31	56.2	79.2	0.3	56.2
78.7	0.29	63.1	78.7	0.29	63.1
		c4			c5
weight (g)	Volumetric water content	Matric head	weight (g)	Volumetric water content	Matric head
82.7	0.38	1	81.6	0.37	1
82.5	0.37	4.9	81.4	0.37	4.9
82	0.36	9.3	80.9	0.36	9.3
81.6	0.35	13.4	80.4	0.35	13.5
81.3	0.35	18.1	80.3	0.34	18.2
80.9	0.34	22.9	80.3	0.34	22.9
80.5	0.33	26.9	79.8	0.33	26.9
80.1	0.32	29.5	79.1	0.32	29.5
80	0.32	34.9	79	0.31	34.9
79.8	0.31	38.9	78.6	0.3	38.9
79.2	0.3	56.2	77.9	0.29	56.2
79	0.29	63.1	77.5	0.29	63.1

Appendix 1.4 a. (Continued)

		C6			C7
weight (g)	Volumetric water content	Matric head	weight (g)	Volumetric water content	Matric head
82.3	0.38	5.5	82.5	0.37	5.4
81.9	0.37	10.4	82.5	0.36	10.4
81.4	0.35	13.8	82.3	0.36	13.8
81.2	0.35	18.6	82.2	0.36	18.6
81	0.35	23.4	81.9	0.35	23.4
80.6	0.34	28.1	81.7	0.35	28.1
80	0.32	30.9	81.3	0.34	30.9
79.9	0.32	35.9	81.2	0.33	35.9
79.7	0.31	40.7	81	0.33	40.7
79.3	0.31	48.9	80	0.31	48.9
79	0.3	58.4	80	0.31	58.4
78.4	0.28	67.4	79.4	0.29	67.4
		c8			c9
weight (g)	Volumetric water content	Matric head	weight (g)	Volumetric water content	Matric head
82.5	0.38	1	82.3	0.38	1
82	0.37	5.5	82.1	0.38	5.5
82	0.37	10.4	80.1	0.33	28.2
81.9	0.36	13.8	79.3	0.31	30.9
81.7	0.36	30.9	79.1	0.31	35.9
81.4	0.35	35.9	78.9	0.3	40.7
81.2	0.35	40.7	78.4	0.29	48.9
80.5	0.33	48.9	78.3	0.29	58.4
80.3	0.33	58.4	77.8	0.28	67.4
79.6	0.31	67.4			

Appendix 1.4 a (Continued from pages 196 and 195). The records of weight and matric head values for microcosms inoculated with *R. solani* and controls in the first water retention measurement in Experiment 3.

Microcosms inoculated with *R. Solani*					
f2			f3		
weight (g)	Volumetric water content	Matric head	weight (g)	Volumetric water content	Matric head
82.1	0.39	1	82.7	0.38	1
82	0.35	5.6	82.7	0.32	5.6
80.9	0.36	12.5	81.9	0.36	12.5
79.7	0.34	19.9	80.9	0.34	19.9
78.4	0.31	26.9	80	0.31	26.9
78.4	0.31	35.4	79.3	0.3	35.3
77.1	0.28	43.6	78.9	0.29	43.6
76.7	0.27	52.4	78.1	0.27	52.4
76.4	0.26	61.6	77.7	0.26	61.6
76.1	0.25	72.4	77.5	0.26	72.4
76.1	0.25	81.2	77.5	0.26	81.2
75.9	0.25	91.2	77.3	0.25	91.2
f4			f5		
weight (g)	Volumetric water content	Matric head	weight (g)	Volumetric water content	Matric head
82.6	0.38	1	82.567	0.379	1
82.4	0.38	5.6	82.481	0.377	5.6
81.8	0.36	12.5	80.976	0.342	12.5
80.2	0.33	19.9	80.288	0.326	19.9
78.9	0.3	26.9	79.17	0.3	26.9
78.4	0.29	35.3	78.697	0.289	35.3
77.7	0.27	43.6	78.181	0.277	43.6
77.4	0.26	52.4	77.794	0.268	52.4
77.2	0.26	61.6	77.493	0.261	61.6
77.1	0.26	72.4	77.364	0.258	72.4
76.9	0.25	81.2	77.278	0.256	81.2
76.8	0.25	91.2	77.192	0.254	91.2
f6			f7		
weight (g)	Volumetric water content	Matric head	weight (g)	Volumetric water content	Matric head
80.9	0.4	1	82.7	0.37	1
80.7	0.39	6.4	82.6	0.37	6.4
78.2	0.33	13.9	82.3	0.36	13.9
76.6	0.3	20.9	81.8	0.35	20.9
75.9	0.28	28.4	80.6	0.32	28.4
75.5	0.27	36.3	79.8	0.31	36.3
74.9	0.26	44.6	79.1	0.29	44.6
74.4	0.25	53.7	78.4	0.27	53.7
74.3	0.24	61.6	78.2	0.27	61.6
74.2	0.24	70.7	78.1	0.27	70.7
74.1	0.24	81.2	77.9	0.26	81.2
73.9	0.23	91.2	76.9	0.24	91.2

Appendix 1.4 b (Continued on pages 199 and 200).

f8			f9		
weight (g)	Volumetric water content	Matric head	weight (g)	Volumetric water content	Matric head
82.6	0.37	1	82.1	0.38	1
82.4	0.37	6.4	82.1	0.37	6.4
82.3	0.36	13.9	81.5	0.36	13.9
81.8	0.35	20.9	80.3	0.33	20.9
80.6	0.32	28.4	79.1	0.30	28.4
80.1	0.31	36.3	78.6	0.29	36.3
79.1	0.29	44.6	78.3	0.29	44.6
78.8	0.28	53.7	77.4	0.27	53.7
78.8	0.28	61.6	77.2	0.26	61.6
78.1	0.27	70.7	77.1	0.26	70.7
77.9	0.26	81.2	76.7	0.25	81.2
77.8	0.26	91.2	76.8	0.25	91.2
Controls					
c2			c3		
weight (g)	Volumetric water content	Matric head	weight (g)	Volumetric water content	Matric head
81.4	0.36	1	81.7	0.36	1
81.2	0.35	4.8	81.5	0.35	4.8
80.9	0.35	12.3	81.2	0.35	12.3
80.4	0.34	20.4	80.2	0.32	20.4
79.4	0.31	28.4	79.5	0.31	28.4
78.8	0.3	37.4	78.9	0.29	37.4
78.1	0.28	45.7	78.3	0.28	45.7
77.5	0.27	54.9	77.8	0.27	54.9
77.1	0.26	63.1	77.4	0.26	63.1
76.9	0.26	72.4	77.3	0.26	72.4
76.7	0.25	81.2	77.1	0.25	81.2
76.6	0.25	91.2	76.9	0.25	91.2
c4			c5		
weight (g)	Volumetric water content	Matric head	weight (g)	Volumetric water content	Matric head
82.1	0.36	1	81.2	0.37	1
81.6	0.35	4.8	80.9	0.36	4.8
80.7	0.33	12.3	79.8	0.33	12.3
80	0.32	20.4	78.8	0.31	20.4
79.1	0.3	28.4	77.9	0.29	28.4
78.6	0.28	37.4	77.6	0.28	37.4
78.1	0.27	45.7	77.1	0.27	45.7
77.7	0.26	54.9	76.6	0.26	54.9
77.4	0.26	63.1	76.3	0.25	63.1
77.2	0.25	72.4	76.1	0.25	72.4
77.1	0.25	81.2	75.9	0.24	81.2
76.9	0.25	91.2	75.8	0.24	91.2

Appendix 1.4 b. (Continued)

c6			c7		
weight (g)	Volumetric water content	Matric head	weight (g)	Volumetric water content	Matric head
82.1	0.37	1	82.1	0.36	1
81.8	0.37	5.4	81.9	0.35	5.4
80.8	0.34	13.4	81.6	0.35	13.4
79.9	0.32	21.3	81.2	0.34	21.3
78.8	0.3	28.8	80.5	0.32	28.8
78.6	0.29	37.1	80.1	0.31	37.1
78.1	0.28	45.7	79.2	0.29	45.7
77.5	0.27	54.9	78.7	0.28	54.9
77.1	0.26	64.5	78.3	0.27	64.5
76.9	0.25	72.4	78.1	0.26	72.4
76.8	0.25	85.1	77.9	0.26	85.1
76.7	0.25	93.3	77.7	0.26	93.3
c8			c9		
weight (g)	Volumetric water content	Matric head	weight (g)	Volumetric water content	Matric head
81.7	0.36	1	81.9	0.38	1
81.5	0.36	5.4	81.7	0.37	5.4
81.1	0.35	13.4	80.9	0.35	13.4
80.3	0.33	21.3	79.5	0.32	21.3
79.3	0.31	28.8	78.5	0.3	28.8
78.8	0.29	37.1	77.9	0.28	37.1
78.2	0.28	45.7	77.3	0.27	45.7
77.8	0.27	54.9	76.9	0.26	54.9
77.5	0.26	64.5	76.6	0.25	64.5
77.3	0.26	72.4	76.5	0.25	72.4
77.1	0.25	85.1	76.3	0.25	85.1
76.9	0.25	93.3	76.1	0.24	93.3

Appendix 1.4 b (Continued). The records of weight and matric head values for microcosms inoculated with *R. solani* and controls in the second water retention measurement in Experiment 3 after the drying process.

Set1	f5		f3	
Matric head (cm)	Weight (g)	volumetric water content	Weight (g)	volumetric water content
0	81.4	0.38	81.7	0.4
1	81.4	0.38	81.7	0.4
11.5	80.9	0.36	81.2	0.39
24.5	79.1	0.32	79.5	0.35
37.5	77.7	0.29	78	0.31
52.5	77	0.27	77.2	0.29
72.5	76.3	0.26	76.5	0.28
97.5	76	0.25	76.2	0.27
Set1	f4		f8	
Matric head (cm)	Weight (g)	volumetric water content	Weight (g)	volumetric water content
0	82.7	0.4	81	0.37
1	82.7	0.4	81	0.37
11.5	81.9	0.38	80.9	0.37
24.5	79.7	0.35	79.4	0.34
37.5	78.3	0.3	77.9	0.3
52.5	77.6	0.28	77	0.28
72.5	76.6	0.26	76.1	0.26
97.5	76.2	0.25	76	0.26
Set2	c10		c6	
Matric head (cm)	Weight (g)	volumetric water content	Weight (g)	volumetric water content
0	80.5	0.37	82.2	0.4
1	80.5	0.37	82.2	0.4
10.5	79.5	0.35	81.7	0.38
24.5	77.1	0.3	79.6	0.33
37.5	76.2	0.28	78	0.3
52	75.7	0.26	77.3	0.28
72	75.2	0.25	76.7	0.27
97.5	75	0.25	76.3	0.26
Set2	c4		c7	
Matric head (cm)	Weight (g)	volumetric water content	Weight (g)	volumetric water content
0	81.4	0.39	82.1	0.39
1	81.4	0.39	82.1	0.39
10.5	80.6	0.37	81.5	0.37
24.5	78.2	0.31	79.8	0.33
37.5	77.2	0.29	78.4	0.3
52	76.5	0.27	77.6	0.28
72	76	0.26	77	0.27
97.5	75.6	0.25	76.5	0.26

Appendix 1.5 a. (Continued on p. 202) The records of weight and matric head values for microcosms inoculated with *R. solani* and controls in the first water retention measurement in Experiment 4.

Set3	f1		f7	
Matric head (cm)	Weight (g)	volumetric water content	Weight (g)	volumetric water content
0	82.1	0.4	81.7	0.39
1	82.1	0.4	81.7	0.39
10.5	80.5	0.36	80.3	0.36
23.5	78	0.3	78.2	0.31
37	77	0.28	77.1	0.28
51.5	76.5	0.26	76.4	0.26
72	75.9	0.25	75.9	0.25
98.5	75.7	0.25	75.6	0.25
Set3	f6		f2	
Matric head (cm)	Weight (g)	volumetric water content	Weight (g)	volumetric water content
0	82.7	0.4	82.1	0.39
1	82.7	0.4	82.1	0.39
10.5	81.7	0.38	80.8	0.36
23.5	79.6	0.33	78.4	0.3
37	78.1	0.3	77.4	0.28
51.5	77.3	0.28	76.7	0.26
72	76.5	0.26	76.3	0.25
98.5	76.2	0.25	76	0.25
Set4	c5		c1	
Matric head (cm)	Weight (g)	volumetric water content	Weight (g)	volumetric water content
0	81.7	0.39	81.1	0.39
1	81.7	0.39	81.1	0.39
11	81.1	0.37	79.8	0.36
23.5	78.5	0.31	77.3	0.31
38	77.3	0.29	76.4	0.28
53.5	76.5	0.27	75.4	0.26
74	75.9	0.25	75.2	0.26
101	75	0.23	75	0.25
Set4	C3		C2	
Matric head (cm)	Weight (g)	volumetric water content	Weight (g)	volumetric water content
0	81	0.37	81.8	0.4
1	81	0.37	81.8	0.4
11	79.7	0.34	80.2	0.36
23.5	77.9	0.3	77.9	0.31
38	76.9	0.28	76.8	0.29
53.5	76.3	0.26	76	0.27
74	75.6	0.25	75.7	0.26
101	75.4	0.24	75.5	0.26

Appendix 1.5 a. (Continued from p. 201) The records of weight and matric head values for microcosms inoculated with *R. solani* and controls in the first water retention measurement in Experiment 4.

Set1	f3		f5	
Matric head (cm)	Weight (g)	volumetric water content	Weight (g)	volumetric water content
0	80.7	0.37	81	0.37
1	80.7	0.37	81	0.37
18	77.9	0.31	79.1	0.32
32	76.7	0.28	77.3	0.28
52	76	0.26	76.5	0.26
71.5	75.5	0.25	75.8	0.25
91	75.2	0.25	75.5	0.24
Set1	f4		f8	
Matric head (cm)	Weight (g)	volumetric water content	Weight (g)	volumetric water content
0	81.7	0.37	81.4	0.38
1	81.7	0.37	81.4	0.38
18	78.9	0.31	78.5	0.32
32	77.4	0.28	77	0.28
52	76.7	0.26	76.5	0.27
71.5	76	0.24	75.6	0.25
91	75.9	0.24	75.5	0.25
Set2	c6		c10	
Matric head (cm)	Weight (g)	volumetric water content	Weight (g)	volumetric water content
0	81	0.37	80.3	0.37
1	81	0.37	80.3	0.37
17	79	0.32	77.1	0.3
31	77.5	0.29	76	0.27
50	76.6	0.26	75.4	0.26
68.5	76	0.25	74.9	0.24
90	75.7	0.24	74.7	0.24
Set2	c7		c4	
Matric head (cm)	Weight (g)	volumetric water content	Weight (g)	volumetric water content
0	81.1	0.36	80.7	0.37
1	81.1	0.36	80.5	0.36
17	79.5	0.33	77.7	0.3
31	77.7	0.29	76.5	0.27
50	76.9	0.27	75.9	0.26
68.5	76.3	0.25	75.3	0.24
90	75.9	0.24	75.1	0.24
Set3	f6			f2
Matric head (cm)	Weight (g)	volumetric water content	Weight (g)	volumetric water content
0	81.6	0.38	81.1	0.37
1	81.6	0.38	81.1	0.37
18	79.3	0.32	77.6	0.28
31	77.5	0.28	76.6	0.26
51.5	76.8	0.26	76.1	0.25
70.5	76.1	0.25	75.6	0.24
91	75.9	0.25	75.5	0.24

Appendix 1.5 b. Continued on p. 204.

Set3	f7		f1	
Matric head (cm)	Weight (g)	volumetric water content	Weight (g)	volumetric water content
0	80.8	0.37	80.8	0.36
1	80.8	0.37	80.8	0.36
18	77.5	0.29	77.3	0.28
31	76.5	0.27	76.5	0.26
51.5	75.8	0.25	75.8	0.25
70.5	75.4	0.24	75.3	0.24
91	75.25	0.24	75.1	0.23
Set4	c1		c2	
Matric head (cm)	Weight (g)	volumetric water content	Weight (g)	volumetric water content
0	81	0.39	80.6	0.37
1	81	0.39	80.6	0.37
21.5	77.2	0.3	77	0.29
30.5	76.1	0.28	76.1	0.27
50.5	75.4	0.26	75.4	0.25
69	75	0.25	75	0.24
88.5	74.8	0.25	74.8	0.24
Set4	c3			c5
Matric head (cm)	Weight (g)	volumetric water content	Weight (g)	volumetric water content
0	80.6	0.36	80.3	0.36
1	80.6	0.36	80.3	0.36
21.5	77.5	0.29	77.5	0.29
30.5	76.6	0.27	76.8	0.27
50.5	76	0.26	76	0.26
69	75.4	0.24	75.5	0.24
88.5	75.2	0.24	75.5	0.24

Appendix 1.5 b. The records of weight and matric head values for microcosms inoculated with *R. solani* and controls in the second water retention measurement in Experiment 4 after the drying process.

Appendix 2 – R source code

Appendix 2.1 – R code version 1

```
# file name: 1.R
# created: originally 1.R 11.03.09


#Porosity

in1 <- as.matrix(read.table("v1.txt"))

print(sum(in1))

# XY axes
xrange = c(0,9.2)
yrange = c(0,1)

# total porosity
print("total porosity:")
print(1-sum(in1)/(126^3))

no_segments = 9
segments = seq(1,9)
tpor = numeric()
tot_pores=numeric()

dim(in1) = c(126,126,126)

for(k in 1:no_segments) {
if (k==1)
{
  x = sum(in1[ , (((k-
1)*(126/no_segments)+2)):((k)*(126/no_segments)),])
}
else
{
 x = sum(in1[ , (((k-
1)*(126/no_segments)+1)):((k)*(126/no_segments)),])
}
print ("X");
print (x);

 tot_pores[k]=126*126*14 -x
      x=x/(126^2*14) ;
  tpor[k] =1- x
  print(tpor[k])

}

#Biomass

in2 <- as.matrix(read.table("s00.txt"))

# XY axes
xrange = c(0,9.2)
yrange = c(0,15)
```

```
# total biomass
print("total biomass:")
print(sum(in2))

no_segments = 9
segments = seq(1,9)
tr = numeric()
tbio = numeric()
fraction = numeric()

dim(in2) = c(126,126,126)
occupied_pores=numeric()
total_occupied_pores_per_volume=numeric()

total_occupied_pores_per_volume<-0
for(y in 1 : no_segments)
{
occupied_pores[y]<-0

}
            for(y in 1:9)
            {
            for(t in (((y-
1)*(126/no_segments)+1)):((y)*(126/no_segments)))
            {
            for (s in 1: 126)
            {
                  for(u in 1 : 126)
                  {

                  if(in2[s, t, u ]>0)
                  {
                        #print("PORE OCCUPIED")
                        #print(in2[u, s, t])
                        #print(u)
                        #print(s)
                        #print(t)
                        occupied_pores[y]<- occupied_pores[y]+ 1
                        total_occupied_pores_per_volume<-
total_occupied_pores_per_volume+1
                  }
                  }

                  }



      }
      print("OCCUPIED PORES PER SEGMENT")
      print(occupied_pores[y])
      print(y)

      }


print("OCCUPIED PORES PER VOLUME")
print(total_occupied_pores_per_volume)


no_voxels = 126*126*14
```

```
for(k in 1:no_segments) {
  if(k==1)
{
  x = sum(in2[ ,(((k-1)*(126/no_segments)+2)):((k)*(126/no_segments))
,])
}
else
{
  x = sum(in2[ ,(((k-1)*(126/no_segments)+1)):((k)*(126/no_segments))
,])

}
      x=x/no_segments ;
  tr[k] = x
  print(x)
  print((k-1)*(126/no_segments)+1)
  print((k)*(126/no_segments))


  tbio[k] = occupied_pores[k]/ tot_pores[k]
  fraction[k] = (occupied_pores[k]/no_voxels)

}

x<-cbind(tpor,tbio,tr,fraction)

x2<-data.frame(x)
 write.table(x2,"info00.txt",quote=FALSE)
```

Appendix 2.2 –R script version 2.

```
#
# file name: test_RP_100909.R
# created: 09.09.10
#



# number of time steps
no_timesteps = X



#--

doAnalysis<- function(no_timesteps, timestep){

  #--
  # porosity
  #

  # I/O processing - reading input (structure file)
  in1 <- as.matrix(read.table(paste(working_dir, "v1.txt", sep="")))

  print(sum(in1))

  # XY axes
  xrange = c(0,9.2)
  yrange = c(0,1)

  # total porosity
  porosity_t <- (1-sum(in1)/(126^3))
  cat(paste("total porosity: ", porosity_t, "\n"))

  no_segments = 9
  segments = seq(1,9)
  tot_pores = numeric()
  tpor = numeric()

  dim(in1) = c(126, 126, 126)

  for(k in 1:no_segments){

    if(k==1) {
      x = sum(in1[ , (((k-
1)*(126/no_segments)+2)):((k)*(126/no_segments)),])
    }
    else {
      x = sum(in1[ , (((k-
1)*(126/no_segments)+1)):((k)*(126/no_segments)),])
    }
    cat(paste("X: ", x, "\n"))

    tot_pores[k] = (126*126*14) - x
    x = x/(126^2*14)
    tpor[k] = 1 - x
    print(tpor[k])

  }
```

```
  #--
  # biomass
  #

  # I/O processing - reading input (biomass density file)
  in2 <- as.matrix(read.table(paste(working_dir, "s",
formatC(timestep, width=2, flag="0"), ".txt", sep="")))

  # XY axes
  xrange = c(0, 9.2)
  yrange = c(0, 15)

  # total biomass
  biomass_t<- sum(in2)
  cat(paste("total biomass: ", biomass_t, "\n"))

  no_segments = 9
  segments = seq(1, 9)
  tr = numeric()
  tbio = numeric()
  fraction = numeric()

  dim(in2) = c(126, 126, 126)
  occupied_pores = numeric()
  total_occupied_pores_per_volume = numeric()
  total_occupied_pores_per_volume = 0

  for(y in 1:no_segments){
    occupied_pores[y]<-0
  }

  for(y in 1:9){
    for(t in (((y-1)*(126/no_segments)+1)):((y)*(126/no_segments))){

      for (s in 1:126){
        for(u in 1:126){
        if(in2[s, t, u ]>0){
            #print("occupied pores: ")
            #print(in2[u, s, t])
            #print(u)
            #print(s)
            #print(t)
            occupied_pores[y]<- occupied_pores[y] + 1
            total_occupied_pores_per_volume<-
total_occupied_pores_per_volume + 1
        }
        }
      }
    }
    cat(paste("segment: ", y, "\n"))
    cat(paste("occupied pores per segment: ", occupied_pores[y],
"\n"))
  }

  cat(paste("occupied pores per volume: ",
total_occupied_pores_per_volume, "\n"))

  no_voxels = 126*126*14

  for(k in 1:no_segments){
```

```
    if(k==1){
      x = sum(in2[ ,(((k-
1)*(126/no_segments)+2)):((k)*(126/no_segments)) ,])
    }
    else {
      x = sum(in2[ ,(((k-
1)*(126/no_segments)+1)):((k)*(126/no_segments)) ,])
    }
    x = x/no_segments
    tr[k] = x
    print(x)
    print((k-1)*(126/no_segments)+1)
    print((k)*(126/no_segments))

    tbio[k] = occupied_pores[k]/tot_pores[k]
    fraction[k] = occupied_pores[k]/no_voxels

  }

  summary<- cbind(tpor, tbio, tr, fraction)
  out<- data.frame(summary)

  # I/O processing - reading output
  write.table(out, paste(working_dir, "info", formatC(timestep,
width=2, flag="0"), ".txt", sep=""), quote=FALSE)


}


#--

# time step (initial condition)
timestep = 0

for(i in 1:no_timesteps){
  doAnalysis(no_timesteps, timestep)
  timestep = timestep + 1
}
```

Appendix 3 – Publications as an outcome of the thesis, attached as follows:

- Pajor, R., Falconer, R. E., Hapca, S. and Otten, W. 2010. Modelling and quantifying the effect of heterogeneity in soil physical conditions on fungal growth. *Biogeosciences*. 7 pp.3731 - 3740.

- Otten, W., Pajor, R., Schmidt, S., Baveye, P. C., Hague, R. and Falconer, R. E. 2012. Combining X-ray CT and 3D printing technology to produce microcosms with replicable, complex pore geometries. *Soil Biology & Biochemistry*. 51 pp.53-55.

Appendix

Modelling and quantifying the effect of heterogeneity in soil physical conditions on fungal growth.

Radoslaw Pajor, Ruth Falconer, Simona Hapca and Wilfred Otten

The SIMBIOS Centre, University of Abertay Dundee, Kydd Building, Dundee, DD1 1HG, UK.

Correspondence to: W Otten (w.otten@abertay.ac.uk)

Abstract

Despite the importance of fungi in soil ecosystem services, a theoretical framework that links soil management strategies with fungal ecology is still lacking. One of the key challenges is to understand how the complex geometrical shape of pores in soil affects fungal spread and species interaction. Progress in this area has long been hampered by a lack of experimental techniques for quantification. In this paper we use X-ray computed tomography to quantify and characterize the pore geometry at microscopic scales (30 µm) that are relevant for fungal spread in soil. We analysed the pore geometry for replicated samples with bulk-densities ranging from 1.2-1.6 g/cm^3. The bulk-density of soils significantly affected the total volume, mean pore diameter and connectivity of the pore volume. A previously described fungal growth model comprising a minimal set of physiological processes required to produce a range of phenotypic responses was used to analyse the effect of these geometric descriptors on fungal invasion, and we showed that the degree and rate of fungal invasion was affected mainly by pore volume and pore connectivity. The presented experimental and theoretical framework is significant first step towards understanding how environmental change and soil management impact on fungal diversity in soils.

1 Introduction

The pivotal role of fungi in ecosystem functioning is now widely accepted, and soil management strategies that support fungal diversity are to be encouraged. Fungi are ubiquitous microorganisms in soil (0.8 – 16 km of hyphae per 1g of soil (Young *et al*. 2008; Finlay, 2006)) and they have a significant influence on aggregation and stabilisation of soil particles (Bossuyt et al., 2001;Tisdall, 1991), nutrient and carbon dynamics (Taylor et al., 2009), and many soil-borne diseases (Otten et al., 2004). Their unique mycelial form of growth makes them particularly suited for exploration of very heterogeneous environments such as soil (Boswell 2007, Otten 1999). Unlike for bacteria, colonisation of soil by fungi is not limited to water-filled volumes, and they can readily overcome locally less suitable growth conditions and patchy nutrient distributions. However, very little work has looked at how fungi colonize soil and how microscopic heterogeneity affects the colony morphology, and a theoretical framework of species interaction in a 3D heterogeneous soil environment is still lacking.

One of the challenges in studying species interactions in soil is that soils are heterogeneous at spatial scales ranging from the micrometer (reflecting the pores within which microbial interactions take place) to kilometres. Whereas the heterogeneity of soils at larger scales has received considerable attention (Lark, 2005), the microscopic heterogeneity has been largely ignored. The size of bacterial cells is less than 10 µm, fungal diameters range roughly from 1-50 µm and fungal colonies are of the order of cm, hence even at the scales of micro-organisms we already bridge 10^3 orders of magnitude (Finlay, 2006). The heterogeneity of soil structure at the micro scale (pore scale) controls the flow of water, the availability of nutrients, and the diffusion of oxygen to micro-organisms (Young and Crawford, 2004). At those scales, soil structure

creates spatially separate niches for various microorganisms (Or et al., 2007), and preferential pathways through which they can move either autonomously or via convective transport with water.

The opacity of soils and a lack of non-invasive quantitative techniques to study growth dynamics of fungi *in situ* make it difficult to understand how the microscopic heterogeneity of soils affects fungal dynamics and contributes to biodiversity. Conventional soil physical techniques to characterise soil structure have concentrated on bulk physical parameters where we quantify for example aggregate size distributions (after we exerted physical forces upon the soil) or bulk-density. While we can derive overall porosity values from these measures, they tell us very little about the geometry and connectivity of the pore space. Other methods for analysis of the pore space are based on destructive sampling such as thin sectioning (Harris et al., 2003;Nunan et al., 2001), or on information of pore size distribution derived from water retention curves (Dane et al., 2002). Neither of these methods accurately account for the 3-D structure and connectivity of the pore space. Only recently, the development of techniques such as X-ray micro-tomography allow for quantification and visualisation of the internal soil structure without destroying the sample. A soil sampling ring with 4 cm diameter can be readily scanned within 60 minutes at a resolution of approximately 30 µm. For smaller samples resolutions of <1µm can be obtained. However, current capabilities of X-ray micro-tomography systems still do not allow us to visualise and quantify the dynamics of fungi in soils. Neither are there currently other techniques that can quantify the spatial distribution of fungi within a 3-D heterogeneous structure at microscopic scales.

The use of mathematical modelling offers a way forward. With models we can study precisely the effect of the pore geometry on fungal growth, as conditions that are correlated in experimental systems can be controlled separately. There are a number of

fungal growth models which consider fungal growth dynamics at different spatial scales: the colony (cm's) or the hyphal scale (µm). The most recent models merge both scales which is important to predict colony dynamics from interactions between hyphae and the environment. Most models are based on earlier work by (Edelstein, 1982) and (Edelstein and Segel, 1983) who considered fungal spread at colony scales. Bosswel et al. (Boswell et al., 2002) extended these models by including directional growth and bidirectional translocation mechanisms. Stacey et al. (Stacey et al., 2001) developed a model to scale-up from hyphae to the colony level. This work was used to investigate transmission rates of plant pathogens. Vectorial-based models (Meskauskas et al., 2004) moved analysis from 2-D to 3-D with the possibility to model fruiting bodies. An ecologically important characteristic of fungi is that they can spread via hyphal growth and translocate nutrients over several cm's within a colony, making them particularly adapt for heterogeneous environments such as soil. Under nutrient pore conditions, biomass can be relocated within a colony and support further fungal growth. However most of these models do not include the ability of fungi to reuse their own biomass (hereafter referred to as recycling) hence they are less suitable for heterogeneous environments. The model we used in this work is a fungal growth model developed by Falconer (Falconer et al., 2005), and described below. Uniquely, this model can model fungal spread in 3-D, and can be combined with the X-ray CT data that describe the pore geometry. This is the first time that this model will be applied to a range of pore geometries that result from different bulk-densities.

The main aim of this work is to quantify and visualise the effect of the internal structure of soil on fungal growth dynamics and colonization efficiency in 3-D. First we will investigate how the pore geometry of microcosms prepared at a range of soil densities is affected at microscopic scales, and then we will use theoretical modelling to

test which of these descriptors of the pore geometry affect fungal colonization. We first conduct the simulations with a high C content in the soil sample to ensure fungal growth is not constrained, and then test if the same response of fungal spread to pore geometry is found in C-limited conditions.

2 Materials and methods

2.1 Preparation of soil microcosms

We used a sandy loam soil (organic matter 2.6%; sand, 71%; silt, 19%; clay, 10%; pH 6.2) sampled from an experimental site (Bullion field) of SCRI (Scottish Crop Research Institute UK). The soil was air-dried and sieved to obtain aggregates sized 1-2 mm. The soil was sterilized by double autoclaving (1h cycles with 48h intervals) prior to packing. Soil was packed into the PVC rings at densities of 1.2 g/cm^3 (n=3), 1.3 g/cm^3 (n=2), 1.4 g/cm^3 (n=3), 1.5 g/cm^3 (n=4) and 1.6g/cm^3 (n=2). These soils were used in a previous study where the invasion of fungi into soil was investigated in thin sections from these samples (Harris et al., 2003), for which the samples were resin impregnated. The aim was to produce samples that differ in physical characteristics of pore-space to test its effect on fungal colonization.

2.2 Quantification of soil structure

A Metris X-Tek X-ray micro-tomography system was used for quantification and visualisation of the inner pore space of the soil microcosms. All soil microcosms were scanned at 160 kV, 201 µA and 3003 angular projection, 4 frames per second and a 0.1 mm Al filter. Radiographs were reconstructed into a 3D volume using CT-Pro (Nikon), imported into VGStudiomax (http://www.volumegraphics.com/), and converted into 8-bit binary TIFF image stacks with voxel-thick slices. All soil samples were scanned and

reconstructed into 3D volumes at a resolution of 30 µm (voxel size). The reconstructed volumes were cropped to obtain equally sized volumes for all samples of 300 x 300 x 300 voxels (9 mm x 9 mm x 9 mm). Because the scanned, large volumes were not uniform these samples were not cropped around a fixed midpoint but cropped to avoid areas with ring artefacts and noise related to scanning, and predominantly occurring around the edges of each sample. A single global threshold value was set for each of these samples. Binary data sets were created by thresholding the greyscale image stacks in ImageJ. The choice of threshold value was based on the histogram region corresponding with the pore-solid interface, taking into account variation of grey scale values in pores of different shapes and sizes, and averaging over 5 randomly selected slices per sample using Image J (ImageJ, http://rsb.info.nih.gov/ij/). In a study comparing different thresholding methods it was shown that this methodology predicted porosity close to the mean value of all tested methods and agreed well with the overall porosity of the bulk soil sample (Baveye et al., 2010). To allow for analysis of the effect of pore geometry on fungal growth, the thresholded (binary) datasets were further divided in a consistent way into eight subsamples (pseudo replicates) with dimensions of 128 x 128 x 128 voxels (see Fig.1.). This division was necessary due to computational limitations of the fungal growth model in a 3-D space (see below). In this work replicates of each treatment (density, n=2-4) will be referred to as the samples, and datasets sized 128^3 will be called subsamples.

We quantified the following physical properties of the subsamples (Deurer et al., 2009):

- porosity– the total number of voxels defined as pores divided by total volume of the sample. This represents the maximum volume in a soil sample within which fungi can potentially spread,

- pore space connectivity – A voxel is considered to belong to the same cluster if one of the six directly neighbouring voxels was identified as pore space. We quantified the number of separate pore clusters and the percentage of the pore volume belonging to each of those clusters. For our analysis we focus on the percentage of the pore volume belonging to the largest cluster, as this was the only connected pore volume large enough to spread over the entire width of the soil sample.
- pore sizes distribution – We calculated the distribution of pore radii by simulating a growing sphere at every voxel of pore space till it reached a voxel with solid phase and we plotted the distribution of the radii of the spheres.

2.3 Fungal growth model

Fungal growth was modelled using the framework developed by Falconer et al. (2005). This model is parsimonious in construction and reduces the biological complexity capturing the minimal set of physiological processes required to reproduce observed ranges in phenotypic responses (Falconer et al., 2005). It was shown that the model can capture fungal growth dynamics in homogeneous as well as in nutritionally heterogeneous environments (Falconer et al., 2007). The model is based on five physiological processes**:** uptake, redistribution of biomass, remobilisation of biomass, inhibitor production, and growth. Spread of biomass in the model is effectively described by a diffusive process. All of physiological processes are known to be important for vegetative growth of fungi but have not been collectively included in any other modelling framework. For a detailed explanation of the model the reader is referred to Falconer et al. (2005). The model can simulate growth in a 3-D pore space. As the objective of this study is to analyse the effect of pore geometry, we used

parameters for one single fungal species only. In previous work the fungal trait set for effective invasion of heterogeneous environments was identified (Falconer et al., 2008). Simplified assumptions were made with respect to the nutritional heterogeneity of the soil environment: we assumed Carbon to be homogeneously distributed throughout the pore volume. We analysed the effect of a high (100, C units per voxel) and low (10, C units per voxel) carbon content on fungal growth dynamics to test if our results were dominated by the availability of resources. At the start of the simulation, fungal biomass was placed only in a unit-thick voxel vertical plane (Fig.1.). Fungal spread was initiated from this plane and followed throughout the sample. The simulations were terminated when a threshold value of total biomass (10^{-6}) reached the opposite edge of the subvolume (break through time).

2.4 Interpretation of output from the model

To enable for comparison of fungal invasion among treatments we captured the dynamics and spatial distribution of fungal invasion by dividing each subsample into segments that were perpendicular to the direction of fungal growth, and parallel to the plane of inoculation (Fig.1.). Following our analysis for the physical properties, we quantified the following characteristics:

- Biomass per segment: this quantifies at each time step the *amount of biomass* per segment at specified distances from the site of inoculation, as a measure of the ability of fungi to invade the soil structure.

- Fraction of pore volume occupied by fungal biomass – here we combine the data on the porosity within each segment with the biomass per segment to calculate for each time-step the fraction of pores that are filled with biomass. This measure enables characterization of the efficiency at which the pore volume is colonised by fungi.

2.5 Statistical Analysis

To test for the effect of the bulk density on soil porosity, medium pore size and measures of connectivity, a nested ANOVA model was used with bulk density as fixed factor (with levels 1.2, 1.3, 1.4, 1.5, 1.6) and the samples as nested factors within the different bulk density levels. Bonferroni post-hoc pair wise comparison tests were carried out to determine significant differences among means.

We used a Generalized Estimation Equations (GEEs) model with normal errors and first order autoregressive correlation structure to test for an effect of bulk-density and distance from the site of inoculation on fungal biomass densities within each subsample. The variables bulk density (with five levels), distance (with nine levels, (segments) corresponding to the distance from the inoculation point), and sub-samples that were nested with the different bulk density levels were used as explanatory variables in the model. More specifically, bulk density was introduced as a between subjects factor, while distance was treated either as within subject covariate or as a factor, as indicated by the Quasi Likelihood under Independence model selection criterion (QIC). An interaction term between factors bulk density and distance was also accommodated in the model and Bonferroni post-hoc pair wise comparison tests were carried out to determine significant differences among means of the different factor levels at a significant level of 0.05. All the statistical analyses were carried out in SPSS v.17 (Hardin and Hilbe, 2003).

3 Results

3.1 Effect of density on physical properties

The 3-D geometry of the pore space was substantially affected by the density at which the samples were packed (Fig.2.). Visual examination of the pore volumes in 3-D showed that the total pore space was less in the more densely packed soil. Whereas in the 2D transects pores within the pore volume appeared to be disconnected, this was no longer the case when the pore volume was examined in 3D. In 3-D the majority of the pores was connected and belonged to a single large cluster. In addition, for soil packed at higher densities the pore volume appeared to be connected via smaller valleys. As can be seen from Fig.2. (k-o) the largest connected cluster was in contact with all sides which in principle will allow for spread of fungi through the soil sample.

Porosity, which is the volume through which fungal growth was modelled, was calculated for each of the subsamples. In addition, porosity was also calculated for segments within the subsamples (see also Fig 1); the segments represent the smaller scale heterogeneity within each sample. No significant interaction between the different treatment densities and segments was found ($p=0.269$). The mean porosity was very strongly affected by the density ($p < 0.001$) ranging from 0.38 for density 1.3 g/cm^3 to 0.21 for samples at 1.6 g/cm^3 density (Table 1), while the differences between slices within each subsample (Fig.3.) were not significant ($p=0.15$).

There was a decline in the median pore size with bulk density (Table 1) but only the median pore diameter at a density of 1.6 was significantly different from those at 1.2 and 1.3 ($p < 0.04$). The changes in porosity and pore diameter show that when soils were packed at higher densities the overall pore volume declined and mainly the larger pores were reduced. However, for all samples the mean pore diameter remained an order of magnitude larger than a typical fungal diameter of 1-50 µm (Finlay, 2006). No significant differences were found for porosity and median pore diameter between replicated samples at this scale.

All subsamples had highly connected pore volumes with a minimum of 90% of the pore volume connected to a single large cluster for all densities. Fig.2. shows how the connected largest clusters and the remaining pore-space that did not belong to this cluster, is distributed throughout the soil sample. There were significant differences in connectivity between replicates at all densities ($p<0.001$) indicating a greater variability of this parameter at this scale. In particular, the connectivity was significantly lower for the samples at higher densities (95% for 1.5 ($p<0.015$) and 90% for 1.6, ($p<0.001$) as compared to lower densities (97% for 1.2, 1.3 and 1.4 soil bulk density).

3.2 Effect of the physical characteristics on fungal invasion

Due to the high connectivity of the pore space, the amount of biomass following fungal invasion displayed trends similar to those found for the porosity, with significant differences between treatments ($p<0.001$) (Fig. 3B). As expected, biomass content decreased as porosity decreased, with the sample with the highest porosity also having the highest biomass after fungal invasion. The soil with the lowest porosity had an average biomass after fungal invasion of only 54% of that of the sample with the highest porosity (Fig 3B, 4.13E5 for density 1.6 and 7.65E5 for density 1.3). This difference is comparable with the difference in the porosity which demonstrates the overriding importance of the total pore volume for fungal invasion. There was a noticeable drop ($p < 0.001$) in biomass content at distances further than approximately 2.5 mm from the site of inoculation (fig 3B). The drop in biomass content characterized the front of colony growth.

The amount of biomass per sample did not inform us about the spatial distribution of the biomass. To obtain a quantitative measure of the spatial colonization, we quantified the fraction of the pore space that became colonized. With increasing

distance from the site of inoculation, the fraction of pores occupied by biomass declined steeply (Fig.4.). At distance <2.5 mm, nearly all of the pore space was occupied by fungal biomass. This reflects the high connectivity of the pore space for all samples. The drop in biomass at larger distances coincided with a drop in the fraction of pores that were occupied (Fig.4.). Soil packed at a density of 1.6 g/cm^3 (the most densely packed material) showed an earlier decline in the fraction of pores colonized with distance (Fig.4., $p<0.001$). As the porosity did not change with distance for these samples (Fig.3A) it is most likely a consequence of the lower connectivity for this sample (Table.1.). As a fungal colony spread into a soil sample, the larger pores were colonized first (as they were typically well connected, Fig.5a) and this was followed by colonization of the smaller pores (Fig.5b), and the invasion typically followed a sharp colony front (Fig.5d and e).

3.3 Carbon level and dynamics of fungal invasion.

Differences in the dynamics of fungal invasion are shown in Fig.6., which shows how in the middle of the sample the biomass increased with time. All treatments had a similar characteristic shape for the dynamics. Initially, for $t<8$, the biomass was absent until the edge of a fungal colony had progressed sufficiently far into the soil sample. Once the edge of a colony reached a specified distance from the site of inoculation (here shown for 2.5 mm in Fig.6.) then the pore volume at that distance became rapidly colonized for all densities. However, the rate of colonization differed per treatment with the highest rates (sharpest increase) for the lower density samples. As expected, in a better connected sample (lower density soil) fungal biomass moved through the volume rapidly, almost as a steep front over time filling all available pore space. For the more

densely packed soil, fungal invasion progressed slower (shown by the lower rate of increase) and the final level of fungal biomass was lower (Fig.6.).

The dynamics of fungal invasion were also determined by the availability of Carbon in the soil (Fig.6B). Although the trends for fungal invasion were qualitatively similar for both resource levels, the limitation of carbon radically affected biomass content reducing the final level of biomass following invasion to 1%. As expected, this reduction reflects the lower amount of C available for fungal growth. Limitation of C level also affected the rate of invasion. With unlimited resources colonization at a distance of 2.5 mm from the site of inoculation started at t = 7, but the starting point for microcosms with limited resources was delayed to t =10. Overall it also took longer for soils with a lower resource level for the fungal colony to spread through the entire soil volume. At high resource levels this took on average (17 time units), whereas at lower resource levels this increased to 22 time units.

4 Discussion

One of the difficulties in studying fungal invasion is the lack of suitable quantitative techniques that enable monitoring of fungal spread through soil over time. Techniques used so far include plating out of aggregates to obtain colony forming units, ergosterol essay (Feeney et al., 2006), MAb-ELISA – for specific species (Otten et al., 1997) or quantification by PCR (Lopez-Mondejar et al. 2009). These techniques however only enable a single snap shot in time, and, perhaps more importantly, require the destruction of the physical environment which contributed to the growth dynamics. Hence we obtain quantitative information of fungal biomass in bulk-soil samples, but no information about the spatial location of the fungi within the soil environment at the microscopic scales where interactions and processes occur. To date, the only way by

which quantitative information about the spatial distribution of fungal mycelium in undisturbed soil samples can be obtained, is in biological thin sections (Tippkotter and Ritz, 1996), but even there the information is essentially constrained to a 2-D plane from the 3-D soil environment. It is therefore important to develop a novel method for analysis and visualisation of the effect of the heterogeneity of the pore volume on microbial processes in 3-D.

The simulations showed that for all soil samples a large percentage of the pore space was colonized by fungi. This is an inherent property of the model, which describes the fungal invasion as a diffusive process, as a result of which all connected pore space would be expected to be colonized eventually. As a result, for a well connected pore volume, the total porosity is the key determinant of the density of fungal biomass following invasion. Close to the site of inoculation, nearly all pore space became colonized for all treatments (Fig. 4). However, if the connectivity is less than 1 (e.g. with increasing bulk density), then progressively less pore space becomes colonized at distances further away from the site of inoculation as biomass spreads only through a connected network. In that case the connectivity of the pore space becomes an increasingly important factor.

In accordance with experimental data for the invasive spread of *R. solani* in the same soil samples (Harris *et al*., 2003) pore volumes with a larger diameter became colonized first. Behind the progressing colony front in the larger pores, the fungi subsequently colonize the pore volumes with smaller diameters. However, the model does appear to overestimate the colonization of smaller pores as experimental data showed that there was a greater preference for larger connected pores (Otten et al., 2004). This could be the result of a more heterogeneous distribution of Carbon in the soil compared to the simulations, or a result of blockage of pores by water, which means

that the connectivity of the pore volume in the simulations is overestimated as we assume all pores to be filled with air. Future work may need to address this in more detail where we can consider extending the modelling approach by including mechanisms that enhance spread through larger pores.

On nutrient rich agar plates, fungi typically form circular colonies, with a step change in biomass density at the advancing colony edge. In nutrient poor systems, colony spread is often more heterogeneous as fungi switch from an exploitative to an explorative mode (Boddy et al., 2009). In soil, we similarly expect this colony shape to be mediated by the heterogeneity of the pore volume with the advancing edge of a colony less clearly defined as the colony needs to negotiate a tortuous pathway of connected pores, resulting in a more gradual change in biomass density towards the growing edge of the colony. For all treatments, we observed nevertheless steep declines in biomass density and in the percentage of colonized pores at the colony growing front. For loosely packed soil the change in density at the front was steeper, characteristic of faster more homogeneous growth (Fig.3, 4). Fungi spreading though soil packed at higher densities had a smoother decay in density at the growing front. At these densities soil had a smaller amount of available pore space, which was less connected and had smaller median pore size (Table.1.). This trend in the effect of pore geometry on fungal colony development is in agreement with experimental results reported by Harris (Harris et al., 2004) and Ritz (Ritz and Young, 2004) where it was shown that fungi spread faster through large pores with a high percentage of air-filled spaces. Fungi in volumes with small, poorly connected pores grow slower but colonies tend to have denser biomass (Harris 2003, Ritz 2004). While the differences may appear to be small, it should be noted that such small differences can have a significant impact on larger

scale invasive spread of fungi and can make a fungal species switch from invasive to non-invasive spread (Bailey et al., 2000; Kleczkowski et al., 1997).

Current CT tomography systems have a number of limitations. One of the biggest challenges is the ratio between sample size and resolution (voxel size), with a smaller resolution for larger sample sizes. With our system, the maximum size of the sample which can be scanned is 25 x 20 cm, at a resolution of approximately 150 µm. The disadvantage of a lower resolution is that we loose information about micro-pores, and as a result can loose the connectivity in the pore network. Whereas with our system we could obtain resolutions (5 µm) smaller than typical fungal diameters, this would have required us to restrict the sample sizes to be too small to be meaningful for fungal colonies and the length scales at which heterogeneity in physical conditions is observed in these samples. The sample size we used in this paper is still small compared to sizes that ordinarily would be assumed representative for a field. However, the small sizes were representative for the relatively homogeneous samples used in this study, as they were obtained by repacking sieved soil. In our statistical analysis of the quantification of pore space, we allowed for variability within treatments (between sub-samples), as well as between treatments, and we showed that the difference between sub-samples within a treatment was not significant, but that difference between sub-samples from different treatments was significant. It is however not possible to extrapolate this result to soil samples from natural fields, and no extrapolation can be made towards the effect of management on fungal growth from these small samples. Young and Ritz (1999) reviewed the impact of tillage on colonies of microbes and argued that typical soil disturbance may not be significant for fungal colonies at small scales. The results in this study should be seen as a first step towards understanding the effect of soil management on fungal growth. Although the resolution of approximately 30 µm in the scans used in

this paper is larger than a typical hyphal diameter, it is smaller than typical internodes' length, and appropriate for fungal colonization which is typically determined by the ability of fungal hyphae to branch within a confined space (Otten and Gilligan, 1998). In addition, the resolution is identical to the approximate resolutions of thin sections, the only technique currently available to visualize fungi in soil, enabling a qualitative comparison with experimental data.

Another bias in the results can be caused by thresholding, which is one of the most crucial steps in image processing where an operator differentiates between solid material and pore-space. A single threshold value as used in this paper is known to overestimate large pores and underestimate small pores and thin valleys. However, it was also shown that for the type of samples in this study, a reasonable agreement with the overall porosity was found (Baveye et al 2010). Tarquis et al (2008; 2009) showed the impact of thresholding on various geometrical descriptors of pore geometry, but the consequences for soil functioning is still largely unknown, which can be explored with the modelling framework presented in this paper.

5. Conclusions

In this paper we showed how a combination of X-ray tomograpghy (to characterise the soil structure) and mathematical modelling (to model fungal invasion in 3-D structural heterogeneous environments) can be used to identify the effect of pore geometry on fungal spread. Such a analysis is an essential first step towards a theoretical basis for management decision taking that would aim to maintain or support biodiversity in soils, which is currently lacking. The theoretical approach enables separation of nutritional and structural effects on fungal growth, which is difficult to achieve by other means. We showed that both the dynamics and the degree of colonization are not just affected

by the porosity, but also depend on the connectivity of the pore volume. Further work is now required to identify how colonization efficacy relates to fungal traits and heterogeneity in the availability of carbon.

Acknowledgements

The authors wish the acknowledge support for this study from the University of Abertay Dundee and from the Scottish Alliance for Geosciences, Environment and Society (SAGES). The University of Abertay Dundee is a charity registered in Scotland, no: SC016040. We also thank Dr Grinev for discussions on the use of X-ray CT for quantifying soil structure.

References

Bailey, D. J., Otten, W., and Gilligan, C. A.: Saprotrophic invasion by the soil-borne fungal plant pathogen *Rhizoctonia solani* and percolation thresholds, New Phytologist, 146, 535-544, 2000.

Baveye, P. C., Laba, M., Otten, W., Bouckaert, L., Sterpaio, P. D., Goswami, R. R., Grinev, D., Houston, A., Hu, Y., Liu, J., Mooney, S., Pajor, R., Sleutel, S., Tarquis, A., Wang, W., Wei, Q., and Sezgin, M.: Observer - dependent variability o f the thresholding step in the quantitative analysis of soil images and X-ray microtomography data, Geoderma, 157, 51-63, 2010.

Boddy, L., Hynes, J., Bebber, D. P., and Fricker, M. D.: Saprotrophic cord systems: dispersal mechanisms in space and time, Mycoscience, 50, 9-19, 10.1007/s10267-008-0450-4, 2009.

Bossuyt, H., Denef, K., Six, J., Frey, S. D., Merckx, R., and Paustian, K.: Influence of microbial populations and residue quality on aggregate stability, Applied Soil Ecology, 16, 195-208, 2001.

Boswell, G. P., Jacobs, H., Davidson, F. A., Gadd, G. M., and Ritz, K.: Functional consequences of nutrient translocation in mycelial fungi, Journal of Theoretical Biology, 217, 459-477, 10.1006/yjtbi.3048, 2002.

Dane, J. H., Hopmans, J. W., Romano, N., Nimmo, J., and Winfield, K. A.: Soil water retention and storage - Introduction., in: Methods of Soil Analysis. Part 4. Physical Methods., edited by: Dane, J. H., Soil Science Society of America, 2002.

Deurer, M., Grinev, D., Young, I., Clothier, B. E., and Mueller, K.: The impact of soil carbon management on soil macropore structure: a comparison of two apple orchard systems in New Zealand, European Journal of Soil Science, 60, 945-955, :10.1111/j.1365-2389.2009.01164.x, 2009.

Edelstein, L.: The Propagation of Fungal Colonies - a Model for Tissue-Growth, Journal of Theoretical Biology, 98, 679-701, 1982.

Edelstein, L., and Segel, L. A.: Growth and Metabolism in Mycelial Fungi, Journal of Theoretical Biology, 104, 187-210, 1983.

Falconer, R. E., Bown, J. L., White, N. A., and Crawford, J. W.: Biomass recycling and the origin of phenotype in fungal mycelia, Proceedings of the Royal Society B-Biological Sciences, 272, 1727-1734, 10.1098/rspb.2005.3150, 2005.

Falconer, R. E., Bown, J. L., White, N. A., and Crawford, J. W.: Biomass recycling: a key to efficient foraging., Oikos, 9, 2007.

Falconer, R. E., Bown, J. L., White, N. A., and Crawford, J. W.: Fungal Interactions in Fungi, The Royal Society Interface, 5, 2008.

Feeney, D. S., Bengough, A. G., Hallett, P. D., Rodger, S., White, N., and Young, I. M.: Assessing the impact of biological exudates associated with soil water repellency, Soil Management for Sustainability, 38, 475-483, 2006.

Finlay, R. D.: The fungi in Soil, in: Modern soil microbiology., edited by: Van Elsas, J., Jansson, J. K., and Trevors, J. T., CRC Press, 2006.

Hardin, J. W., and Hilbe, J. M.: Generalized Estimating Equations, Stata Corporation, 2003.

Harris, K., Young, I. M., Gilligan, C. A., Otten, W., and Ritz, K.: Effect of bulk density on the spatial organisation of the fungus *Rhizoctonia solani* in soil, FEMS Microbiology Ecology, 44, 45-56, 2003.

Kleczkowski, A., Gilligan, C. A., and Bailey, D. J.: Scaling and spatial dynamics in plant-pathogen systems: From individuals to populations, Proceedings of the Royal Society of London Series B-Biological Sciences, 264, 979-984, 1997.

Lark, R. M.: Exploring scale-dependent correlation of soil properties by nested sampling, European Journal of Soil Science, 56, 307-317, 10.1111/j.1365-2389.2004.00672.x, 2005.

Lopez-Mondejar, R., Anton, A., Raidl, S., Ros, M., and Pascual, J. A.: Quantification of the biocontrol agent *Trichoderma harzianum* with real-time TaqMan PCR and its potential extrapolation to the hyphal biomass, Bioresource Technology, 101, 2888-2891, 2009.

Meskauskas, A., Fricker, M. D., and Moore, D.: Simulating colonial growth of fungi with the Neighbour-Sensing model of hyphal growth, Mycological Research, 108, 1241-1256, 10.1017/s0953756204001261, 2004.

Nunan, N., Ritz, K., Crabb, D., Harris, K., Wu, K. J., Crawford, J. W., and Young, I. M.: Quantification of the in situ distribution of soil bacteria by large-scale imaging of thin sections of undisturbed soil, Fems Microbiology Ecology, 37, 67-77, 2001.

Or, D., Smets, B. F., Wraith, J. M., Dechesne, A., and Friedman, S. P.: Physical constraints affecting microbial habitats and activity in unsaturated porous media - A review., Advances in Water Resources, 30, 2007.

Otten, W., and Gilligan, C. A.: Effect of physical conditions on the spatial and temporal dynamics of the soil-borne fungal pathogen *Rhizoctonia solani*, New Phytologist, 138, 629-637, 1998

Otten, W., Gilligan, C.A., and Thornton, C.R. Quantification of fungal antigens in soil with a monoclonal antibody-based ELISA: analysis and reduction of soil-specific bias. Phytopathology, 730-736, 1997

Otten, W., Harris, K., Young, I. M., Ritz, K., and Gilligan, C. A.: Preferential spread of the pathogenic fungus *Rhizoctonia solani* through structured soil, Soil Biology & Biochemistry, 36, 203-210, 2004.

Ritz, K., and Young, I. M.: Interactions between soil structure and fungi, Mycologist, 18, 52-59, 2004.

Stacey, A. J., Truscott, J. E., and Gilligan, C. A.: Soil-borne fungal pathogens: scaling-up from hyphal to colony behaviour and the probability of disease transmission, New Phytologist, 150, 169-177, 2001.

Tarquis, A.M., Heck, R.J., Andina, D., Alvarez, A., and Anton, J.M. Pore network complexity and thresholding of 3D soil images. Ecological complexity 6, 230-239, 2009.

Tarquis, A.M., Heck, R.J., Grau, J.B., Fabregat, J., Sanchez, M.E., and Anton, J.M. Influence of thresholding in mass and entropy dimension of 3-D soil images. Nonlinear Processes in geophysics, 15, 881-891, 2008.

Taylor, L. L., Leake, J. R., Quirk, J., Hardy, K., Banwart, S. A., and Beerling, D. J.: Biological weathering and the long-term carbon cycle: integrating mycorrhizal evolution and function into the current paradigm, Geobiology, 7, 171-191, 10.1111/j.1472-4669.2009.00194.x, 2009.

Tippkotter, R., and Ritz, K.: Evaluation of polyester, epoxy and acrylic resins for suitability in preparation of soil thin sections for in situ biological studies, Geoderma, 69, 31-57, 1996.

Tisdall, J. M.: Fungal Hyphae and Structural Stability of Soil, Australian Journal of Soil Research, 29, 729-743, 1991.

Young, I. M., and Crawford, J. W.: Interactions and self-organization in the soil-microbe complex, Science, 304, 1634-1637, 2004

Young, I. M., and Ritz, K.: Tillage, habitat space and function of soil microbes, Soil&Tillage Research, 53, 201-213, 2000.

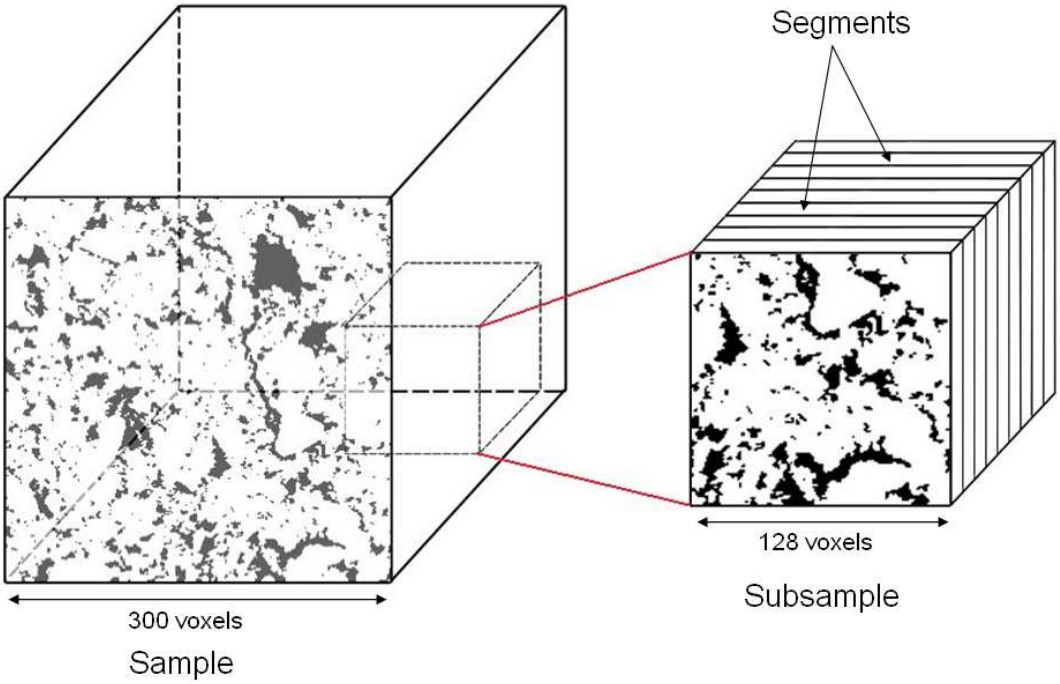

Fig.1. 3-D spatial arrangement of the data structure. Treatments were compared by comparing physical properties for cubed samples. Within each sample, subsamples were selected, which were divided in segments to enable quantification of fungal invasion. Fungal invasion was initiated from the first segment in each subsample.

1.2 g/cm^3

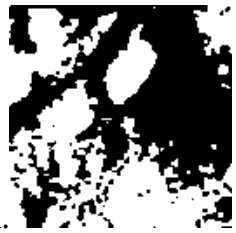
a.
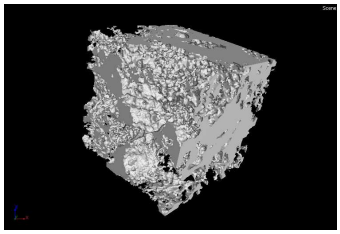
f.
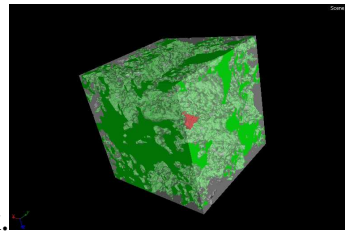
k.

1.3 g/cm^3

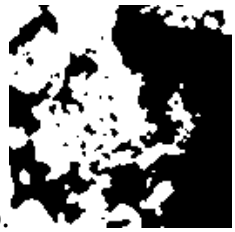
b.
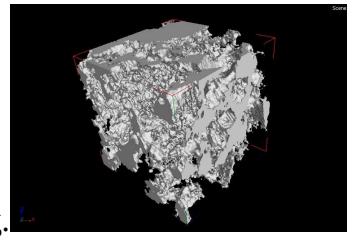
g.
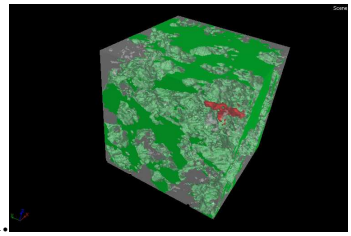
l.

1.4 g/cm^3

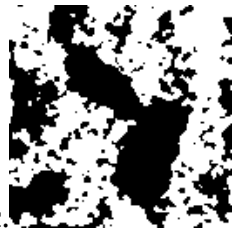
c.
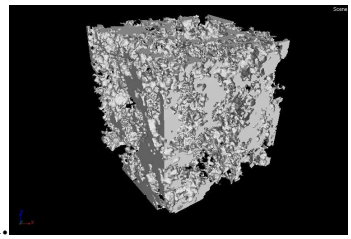
h.
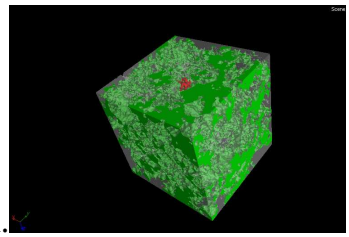
m.

1.5 g/cm^3


d.
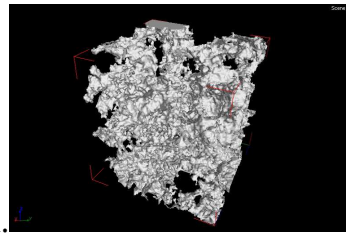
i.
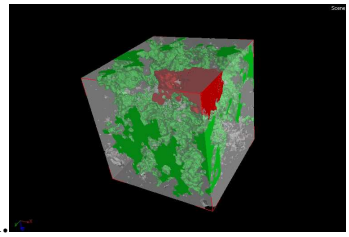
n.

1.6 g/cm^3


e.
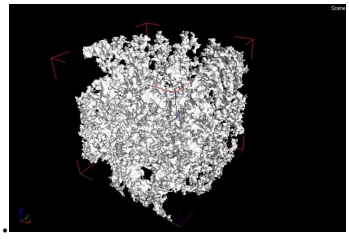
j.
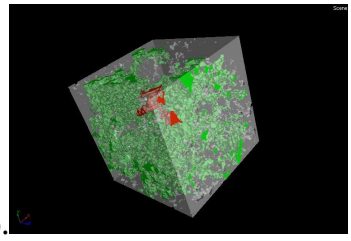
o.

Fig 2. Pore space visualisation – a-e: thresholded 2-D slices of subsamples (white-solid, black-pore), f-j: whole pore space in 3-D as visualized with X-ray CT, k-o) 3-D view of subsample with the largest connected pore (green), the second largest connected pore (red) and the remaining pore space (bright gray). One representative examples is shown for each of the density treatments (1.2 – 1.6).

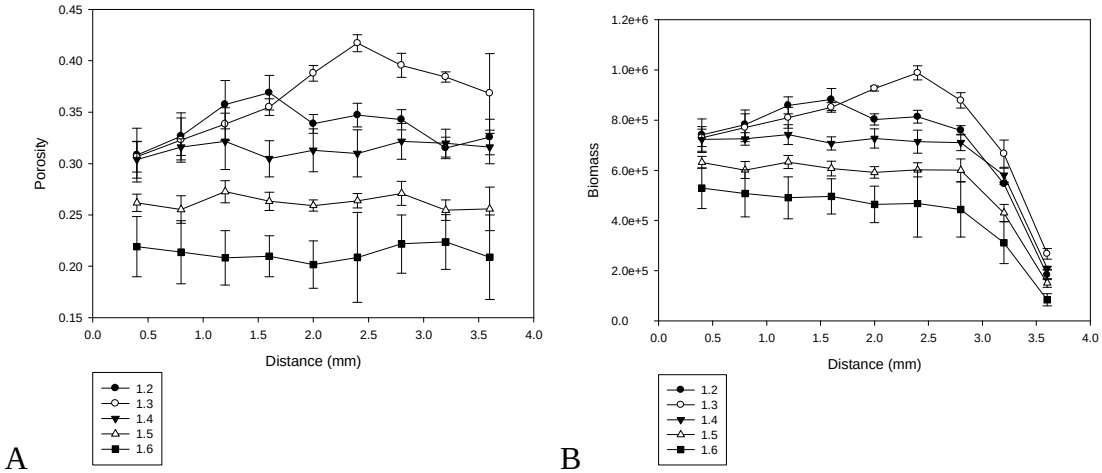

A B

Fig.3. Mean changes of porosity with distance from the site of inoculation (A), and the simulated biomass distribution in each segment (B), for soils at bulk-densities of 1.2, 1.3, 1.4, 1.5, and 1.6 g/cm^3.

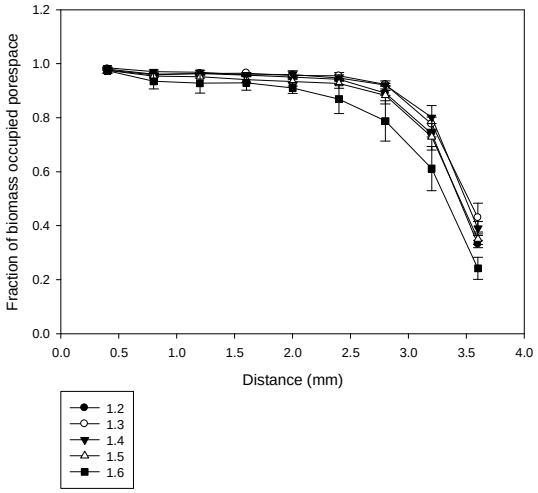

Fig.4. Mean changes in the fraction of pore space occupied by biomass in each segment with distance from the site of inoculation, for soils at bulk-densities of 1.2, 1.3, 1.4, 1.5, and 1.6 g/cm^3.

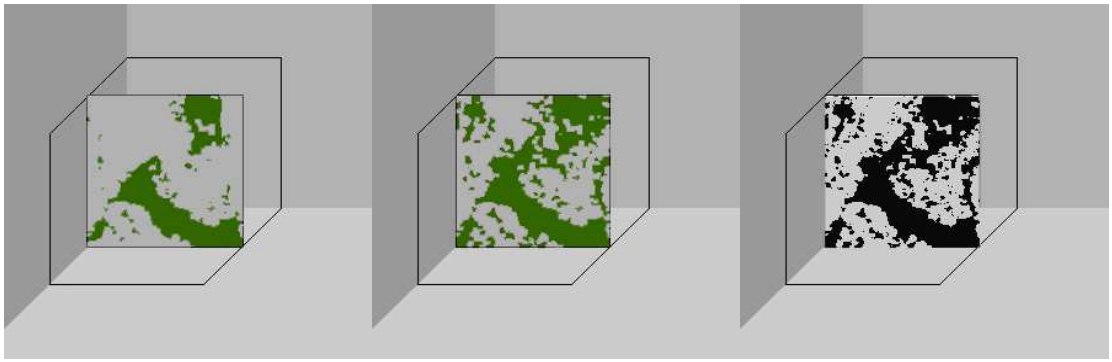

(a) (b) (c)

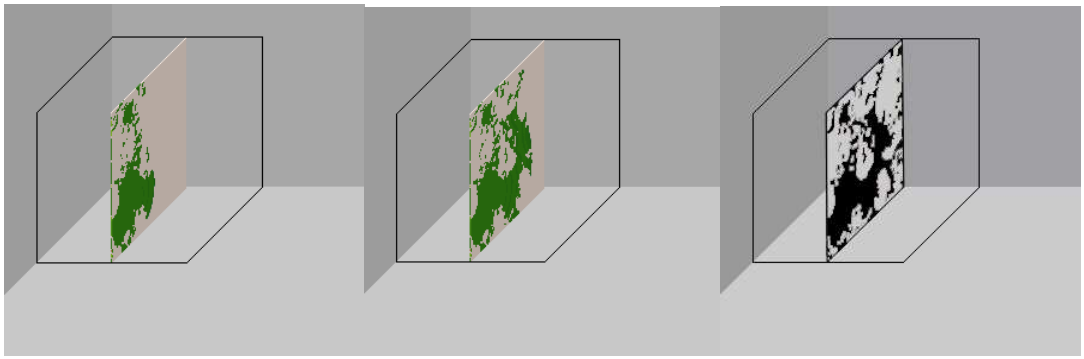

(d) (e) (f)

Fig.5. 2-D slices through the z axis (a-c, perpendicular to the direction of spread) and x axis (d-f, in the direction of spread) showing biomass occupancy at t=8 (a,d, halfway the time required to spread through the entire volume)), t=12 (b,e, at the time the colony had spread to the opposite side of the subsample), and corresponding pore space (c,f) where solid –brown, pore space – gray for a sample at a bulk density of 1.6 g/cm^3.

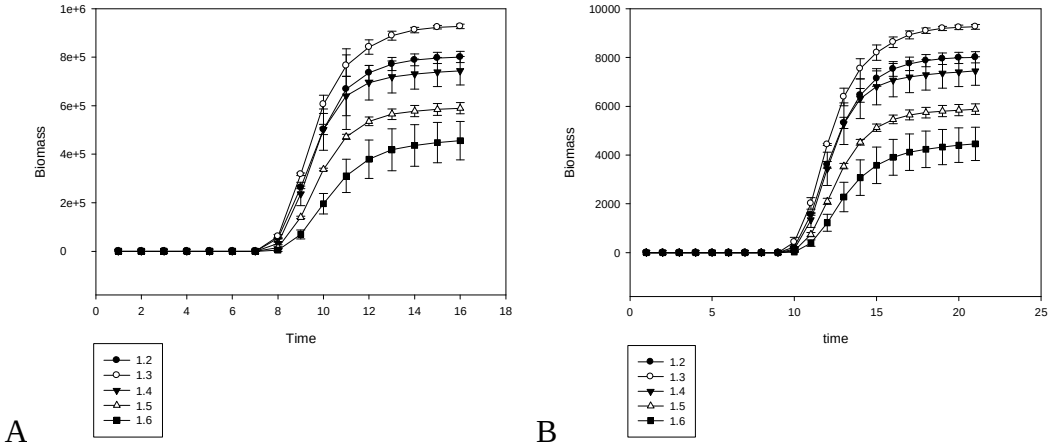

A B

Fig.6. Mean dynamics of biomass at the middle of each subsample (5th segment) with 'unlimited' (A) and limited (B) resource, for soils at bulk-densities of 1.2, 1.3, 1.4, 1.5, and 1.6 g/cm^3.

Appendix

Combining X-ray CT and 3D printing technology to produce microcosms with replicable, complex pore geometries.

W. Otten[1], R. Pajor[1], S. Schmidt[1], P. C. Baveye[1,3], R. Hague[2], and R. E. Falconer[1].

[1]The SIMBIOS Centre, University of Abertay Dundee, DD1 1HG Dundee, UK.

[2]Additive Manufacturing Research Group, Loughborough University, LE11 3TU, Loughborough, UK

[3] Department of Civil and Environmental Engineering, Rensselaer Polytechnic Institute, Troy, NY 12180, USA.

Keywords:

Soil structure, X-ray CT, additive manufacturing process

Corresponding author: W. Otten, The SIMBIOS Centre, University of Abertay Dundee, DD1 1HG Dundee, UK.

e-mail:w.otten@abertay.ac.uk

phone +44 (0)1382 308533

Combining X-ray CT and 3D printing technology to produce microcosms with replicable, complex pore geometries.

Abstract:

Measurements in soils have been traditionally used to demonstrate that soil architecture is one of the key drivers of soil processes. Major advances in the use of X-ray Computed Tomography (CT) afford significant insight into the pore geometry of soils, but until recently no experimental techniques were available to reproduce this complexity in microcosms. This article describes a 3D additive manufacturing technology that can print physical structures with pore geometries reflecting those of soils. The process enables printing of replicated structures, and the printing materials are suitable to study fungal growth. This technology is argued to open up a wealth of opportunities for soil biological studies.

Microcosms have played a central role in the development of ecology, leading to model-driven insights into habitat fragmentation, competitive exclusion, resource allocation, and succession (Drake et al., 1996). These conceptual advances could be relevant to soils, whose complex geometry and heterogeneity is widely recognized as the key driver in many ecological processes. In soil science, the development of ecological theories is nevertheless in its infancy and the discipline still stands to benefit from more hypothesis-driven research (Prosser et al, 2007). This requires the level of experimental control afforded by model systems (Jessup et al. 2004). To date, introduction of heterogeneity in microcosms has been limited due to the difficulty in

controlling and replicating the pore geometries of soil at scales relevant for microbial processes, and systematic study of the impact of soil structure on microbial invasions has been restricted to computer simulation studies (e.g., Falconer et al., 2005, 2012). There is therefore a pressing need to advance soil microcosms in ways that retain the control of laboratory-based studies, along with the heterogeneity encountered in the field (Baveye et al., 2011).

Engineers have been utilizing 3D printing or "additive manufacturing" for more than a decade. This technology is maturing and printing at small spatial scales is now possible even for complex stalactite like structures encountered in soil. Heterogeneous structures can be printed with a range of materials, including plastics, glass and ceramics. 3D printing technology is on the cusp of major exploitation in many areas (Marks, 2011). The latter tend to be at large spatial scales (> cm), but exploitation at the micron scale is an exciting opportunity, albeit with a few challenges. Here we demonstrate how micro X-ray CT imaging, which quantifies soil structure, can be combined with 3D printing to produce replicated static model microcosms that exhibit the physical heterogeneity found in soils. To produce microcosms, soil pore geometries can be quantified via X-ray CT or digitally designed to desired structures. The digital map is subsequently used in the 3D printing technique to produce replicated structures that can be used to explore for example the role of physical heterogeneity on fungal spread or transport processes. Soil samples including repacked sieved loam and undisturbed samples were scanned at a resolution of 29.3 um, with a Nikon HMX 225 X-ray micro-tomography system (Pajor et al., 2010). If required, these structures can subsequently be printed in different sizes to scale the porous medium (Fig 1). From the voxel data, the surface of pore network was extracted. The result of this process is a surface representation of the sample, with stereo lithography file format (STL). The

polygonal mesh consists of up to 10.5 million triangles. This retains the key characteristics of the pore volume but does introduce some smoothening of the surface walls compared to real soil. An EOS P390 polymeric Laser Sintering machine (Additive Manufacturing Research Group, Loughborough University) was used to print the 3D structures in Nylon 12. The P390 has a heated chamber which is filled with a thin layer (0.1mm) of polymeric powdered materials (typically semi-crystalline polymers such as Nylon 12). A 50W CO_2 Laser is used to selectively melt (print) the polymeric powder according to the digital map. The powder offers a supporting surface during the printing process enabling so called stalactite-like structures. The powder is removed from the pore space after the printing process. Other printers use two plastics, one of which (representing the pore space) is dissolved after the printing process. Nylon 12, used in this study, is a resistant material enabling autoclaving and re-use of the samples, is resistant to most chemicals and has a low water adsorption. Up to two hundred replicated soil-like microcosms, as in Fig.1, can be printed overnight at very low cost covering the price of polymers only. The final stage is removal of the unprinted powder from internal cavities using a variety of methods such as vibration, ultrasonication, vacuuming, boiling, brushing and rinsing. This currently restricts the printing process to structures with well and fully connected pore volumes.

Replicate printed structures need be similar and tolerated by microorganisms. To ascertain that these conditions are met, ten Nylon-12 model systems were printed from the same structure. The Nylon 12 structures were then rescanned as above and data were converted to binarized images in ImageJ v 43 using Li's method. The surface area of the pore-solid interface and the pore volume for each replicate were determined. The average pore volume fraction, which is the total volume within which all microbial and physical processes occur, was 0.66 and highly reproducible with a small standard error

(SE) of 0.0064. Similarly the volume of the solid phase (Nylon 12) was highly reproducible for each printed structure with an average of 10,985 mm^3 (SE = 223). The average solid-air interface of the structures was 38,320 mm^2 (SE = 1301). All standard errors were within 3% of the mean values showing a highly successful reproduction for complex geometries.

To assess whether the printed microcosms could host fungi, we introduced 3 poppy seeds that were previously colonised by *Rhizoctonia solani* into the 3D printed soil and incubated it at 23 ^{0}C for 3 days. The colonisation by this fungus was similar to that previously observed in bulk-soil (Harris et al., 2003) and in cracks (Otten et al., 2004), with preferential spread within larger pores and fungal hyphae bridging air gaps (Fig 2). This indicates that the soil-derived model systems are suited to study the effect of physical heterogeneity on fungal growth and species interactions (Fig 2).

In conclusion, 3D printing makes it possible to produce replicable static model systems possessing some of the physical complexity of soils. The current example is focused on relatively large pores, with the original structure scaled up three times to ensure all powder could be removed from the intricate pore network, and to produce pores with diameters in which we can study fungal invasion. Future work will address the limits of 3D printing technology in accurately replicating soil samples with more complicated geometries (lower porosities, high tortuosity) from which powder removal is a key challenge and to test the microscopic characteristics of the surface. Nevertheless, advancements can be made to comprehend interactions whilst explicitly considering structural heterogeneity, something hitherto not possible with alternative methods. Finally alternative polymers can be used to alter hydrophobicity of surface properties and determine its effect on hydrological properties of the structure. Many printers are available at prices of a few thousand pounds. Although the cheaper versions

may not be able to cope with the complexity of soil structures, it is likely that rapid advances will make this an accessible technology in the near future.

Acknowledgement: We thank Dr. Veronica Morales for valuable discussion and Mr. Mark East for printing the structures.

References.

Baveye, P.C., Rangel, D., Jacobson, A.R., Laba, M., Darnault, C., Otten, W., Radulovich, R., Camargo, F. A. O., 2011. From Dust Bowl to Dust Bowl: Soils are Still Very Much a Frontier of Science. Soil Science Society of America Journal, 75., 6, 2037-2048.

Drake, J.A., Huxel, G.R., Hewitt, C.L., 1996. Microcosms as models for generating and testing community theory. Ecology, 77, 670-677.

Falconer, R.E., Bown, J., White, N., Crawford, J., 2005. Biomass Recycling and the origin of phenotype in fungal mycelia. Proc. Roy. Soc B. Lond. 272, 1727-1734.

Falconer, R., Houston, A., Otten, W., Baveye, P.C., 2012. Emergent behaviour of fungal dynamics: Influence of soil architecture and water distribution. Soil Science (In Press).

Harris, K., Young, I.M., Gilligan, C.A., Otten, W., Ritz, K., 2003. Effect of bulk density on the spatial organisation of the fungus *Rhizoctonia solani* in soil. FEMS Microbial Ecology, 44, 45-56.

Jessup, C.M., Kassen, R., Forde, S E., Kerr, B., Buckling, A., Rainey, P. B., Bohannan, B.J.M., 2004. Big questions, small worlds: microbial model systems in ecology. Trends in Ecology and Evolution, 19,189-197.

Marks, P., 2011. 3D printing takes off with the world's first printed plane, New Scientist, 211, 17-18

Otten, W., Harris, K., Young, I.M., Ritz, K., Gilligan, C.A., 2004. Preferential spread of the pathogenic fungus *Rhizoctonia solani* through structured soil. Soil Biology & Biochemistry 36, 203-210.

Pajor, R., Falconer, R., Hapca, S., Otten, W., 2010. Modelling and quantifying the effect of heterogeneity in soil physical conditions on fungal growth. Biogeosciences 7, 3731-3740.

Prosser, J. I., Bohannan, B. J. M., Curtis, T. P., Ellis, R. J., Firestone, M. K., Freckleton, R. P., Green, J. L., Green, L. E., Killham, K., Lennon, J. J., Osborn, A. M., Solan, M., Van der Gast, C. J., Young, J. P. W., 2007. The role of ecological theory in microbial ecology. Nature Reviews Microbiology 5, 384-392.

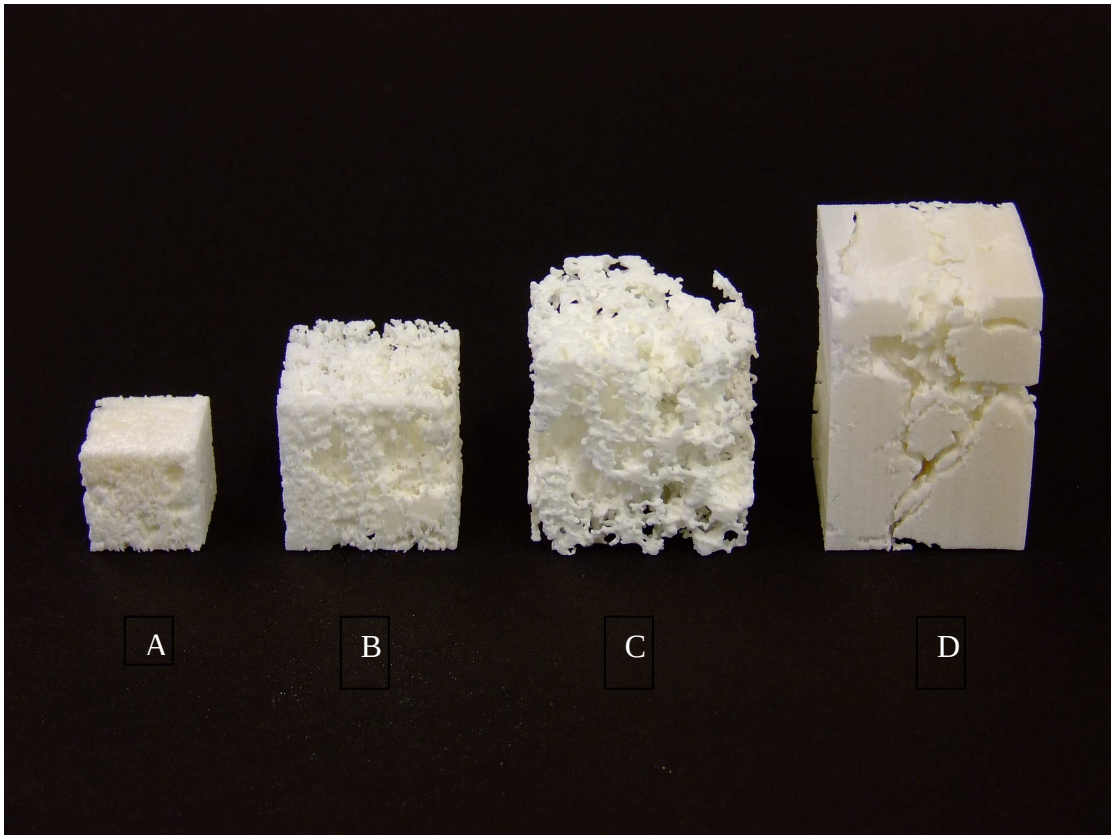

Fig 1 Soil-like structures demonstrating the range of microcosms that can be reproduced with 3D printing from a digital map. Printed structures from repacked sieved loamy sand (scaled to (A) 1.8 and (B) 2.7 cm wide), (C) the same sample but now with the pore space printed, and (D) an example of printed undisturbed soil sample with macro-pores.

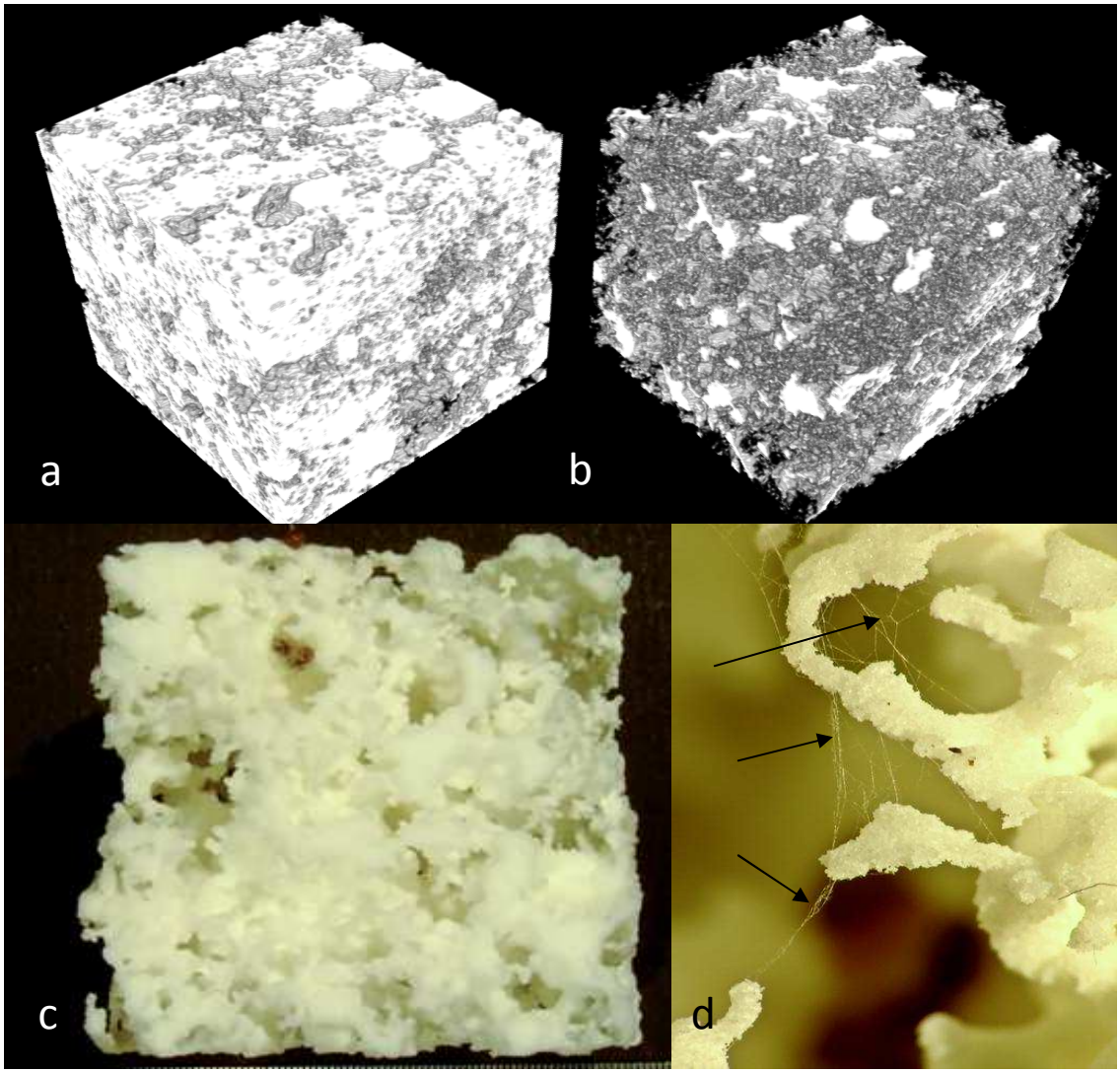

Figure 2. X-ray CT permits the visualization of the solid volume (a) and pore volume (b) at a spatial resolution of 30 µm. In the 3D printed Nylon 12 replica of the soil structure (c), fungal hyphae are easily visible in a close-up view (d; hypha indicated by an arrow).

Sample density [g/cm^3]	Mean porosity	Standard error	Mean connectivity [%]	Standard error	Median of pore size	Standard error
1.2	0.34	0.02	96.5	0.5	370	23
1.3	0.38	0.02	97.0	0.3	375	24
1.4	0.31	0.01	97.0	0.4	348	23
1.5	0.26	0.01	95.1	0.2	334	11
1.6	0.21	0.01	90.0	0.6	309	13

Table.1. Mean and standard error estimates of bulk physical characteristics for soil microcosms.